

TECHNISCHE UNIVERSITÄT MÜNCHEN

Lehrstuhl für Humanbiologie

# Functional analysis of cytosolic sensors of viral nucleic acids and their role for innate antiviral immune defense

Katharina Eisenächer

Vollständiger Abdruck der von der Fakultät Wissenschaftszentrum Weihenstephan für Ernährung, Landnutzung und Umwelt der Technischen Universität München zur Erlangung des akademischen Grades eines

## Doktors der Naturwissenschaften

genehmigten Dissertation.

Vorsitzende:	Univ.-Prof. Dr. H. Daniel
Prüfer der Dissertation:	1. Univ.-Prof. Dr. M. Schemann
	2. Priv.-Doz. Dr. A. Krug
	3. Prof. Dr. Adolfo García-Sastre, Ph.D. (Mount Sinai School of Medicine, New York, USA)

Die Dissertation wurde am 04.10.2010 bei der Technischen Universität München eingereicht und durch die Fakultät Wissenschaftszentrum Weihenstephan für Ernährung, Landnutzung und Umwelt am 10.02.2011 angenommen.

Here is my secret. It is very simple: It is only with the heart that one can see rightly; what is essential is invisible to the eye.

Antoine de Saint-Exupéry ★ *Le Petit Prince*

---

# TABLE OF CONTENTS

<b>Table of Contents</b> .....	<b>I</b>
<b>Index of Figures</b> .....	<b>VI</b>
<b>Index of Tables</b> .....	<b>VIII</b>
<b>Abbreviations</b> .....	<b>IX</b>
<b>1 Introduction</b> .....	<b>1</b>
<b>1.1 The innate immune system protects from invading pathogens</b> .....	<b>1</b>
<b>1.2 Pattern recognition receptors</b> .....	<b>2</b>
<b>1.3 RIG-I-like receptors are viral RNA sensors</b> .....	<b>2</b>
1.3.1 Identification of RIG-I and its function .....	<b>3</b>
1.3.2 MDA5 .....	<b>5</b>
1.3.3 Downstream signaling is mediated by the adaptor protein IPS-1 .....	<b>6</b>
1.3.4 LGP2 .....	<b>7</b>
1.3.5 Viral recognition by RIG-I-like receptors .....	<b>8</b>
1.3.6 RLRs are accurate sensors of virus invasion – discrimination between self and non-self .....	<b>11</b>
<b>1.4 RLR-mediated signal transduction</b> .....	<b>13</b>
<b>1.5 Regulation of RLR signaling by cellular proteins</b> .....	<b>17</b>
1.5.1 Role of ubiquitination for activation and degradation of RIG-I .....	<b>18</b>
1.5.2 RIG-I splice variant functions as off-switch regulator of its own pathway .....	<b>20</b>
1.5.3 Regulation of MDA5 .....	<b>20</b>
1.5.4 Regulation of RLR signaling at the level of IPS-1 .....	<b>21</b>
1.5.5 Other mechanisms involved in the regulation of RLR signaling .....	<b>22</b>
<b>1.6 Interaction between RLRs and viral proteins</b> .....	<b>24</b>
1.6.1 Viral escape from recognition by the RLR system .....	<b>24</b>
1.6.2 Disruption of the interaction of signaling molecules .....	<b>25</b>
1.6.3 Cleavage or degradation of signaling molecules .....	<b>27</b>
<b>1.7 Involvement of RLRs in autoimmunity</b> .....	<b>29</b>
<b>2 Aims of the study</b> .....	<b>33</b>
<b>3 Material &amp; Methods</b> .....	<b>35</b>

<b>3.1</b>	<b>Material</b> .....	<b>35</b>
3.1.1	Primers.....	35
3.1.2	Plasmids.....	35
3.1.2.1	<i>Commercially available and published plasmids</i> .....	35
3.1.2.2	<i>Plasmids constructed in this project</i> .....	36
3.1.3	Antibodies and protein standard for IFN- $\beta$ enzyme-linked immunosorbent assay .....	37
3.1.4	Antibodies.....	38
3.1.5	Cell lines, virus strains and bacterial strains .....	38
3.1.5.1	<i>Cell lines</i> .....	38
3.1.5.2	<i>Virus strains</i> .....	39
3.1.5.3	<i>Bacterial Strains</i> .....	39
3.1.6	Buffers, solutions and media .....	40
3.1.6.1	<i>Media for cell culture</i> .....	40
3.1.6.2	<i>Solutions for cell culture applications</i> .....	42
3.1.6.3	<i>Buffers for cytokine ELISA</i> .....	42
3.1.6.4	<i>Media for bacterial applications</i> .....	43
3.1.6.5	<i>Buffers and solutions for protein biochemistry</i> .....	44
3.1.6.6	<i>Buffers for molecular biology</i> .....	47
<b>3.2</b>	<b>Methods</b> .....	<b>48</b>
3.2.1	Mice.....	48
3.2.2	Tissue culture.....	48
3.2.2.1	<i>Cell lines</i> .....	48
3.2.2.2	<i>Cryopreservation of cells</i> .....	49
3.2.2.3	<i>Transient transfection of cell lines</i> .....	49
3.2.2.4	<i>Generation of murine bone marrow derived DCs</i> .....	50
3.2.3	Virus propagation and titer determination.....	50
3.2.3.1	<i>Propagation of VSV strains</i> .....	50
3.2.3.2	<i>EMCV stock preparation</i> .....	51
3.2.3.3	<i>Determination of virus titers by plaque assay</i> .....	51
3.2.4	Dual Luciferase reporter assay .....	52
3.2.5	Stimulation of DCs and determination of cytokine levels by ELISA .....	53
3.2.6	Molecular Biology.....	55
3.2.6.1	<i>Isolation and purification of DNA</i> .....	55
3.2.6.2	<i>Analysis and cloning of DNA</i> .....	57
3.2.6.3	<i>Site-directed mutagenesis</i> .....	59
3.2.6.4	<i>Synthesis of 5'-triphosphate RNA by in vitro transcription</i> .....	61
3.2.6.5	<i>Isolation of total RNA from virus-infected cells</i> .....	63
3.2.6.6	<i>Isolation of total RNA from stimulated DCs and expression analysis of cytokines and ISGs by quantitative real-time PCR</i> .....	63

3.2.6.7	<i>Isolation of RNA from bacteria</i> .....	65
3.2.7	Protein biochemistry.....	66
3.2.7.1	<i>Preparation of cell lysates</i> .....	66
3.2.7.2	<i>Determination of protein concentration</i> .....	67
3.2.7.3	<i>Immunoprecipitation</i> .....	67
3.2.7.4	<i>SDS polyacrylamide gel electrophoresis (PAGE)</i> .....	68
3.2.7.5	<i>Silver staining of SDS-PAGE gels</i> .....	69
3.2.7.6	<i>Mass spectrometry analysis</i> .....	70
3.2.7.7	<i>Immunoblotting</i> .....	70
3.2.7.8	<i>RNA binding assay</i> .....	71
<b>4</b>	<b>Results</b> .....	<b>73</b>
<b>4.1</b>	<b>Identification of a functional domain at the C-terminus of RIG-I</b> .....	<b>73</b>
4.1.1	AA 802 to 925 of RIG-I can be expressed as Flag-tagged protein.....	73
4.1.2	Overexpression of RIG-I (AA 802-925) inhibits RIG-I-mediated IFN induction.....	74
4.1.3	The C-terminal domain of RIG-I contains conserved cysteine residues which form a zinc-binding cluster.....	76
4.1.4	The role of C-terminal Cys residues for RIG-I-mediated IFN induction	79
4.1.4.1	<i>IFN-<math>\beta</math> promoter activation in response to virus infection and 5'-triphosphate RNA</i> .....	79
4.1.4.2	<i>Influence of the integrity of the zinc-binding site in the CTD of RIG-I on endogenous RIG-I signaling</i> .....	85
4.1.5	Involvement of the zinc-binding site in the CTD of RIG-I in the interaction with signaling adapter IPS-1 and binding of 5'-triphosphate RNA.....	87
4.1.6	5'-triphosphate RNA interacts with a positively charged conserved binding groove in the CTD of RIG-I.....	89
<b>4.2</b>	<b>The role of the cysteine rich C-terminal domain of MDA5</b> .....	<b>94</b>
4.2.1	Influence of the invariant Cys residues on MDA5-mediated IFN induction.....	94
4.2.2	Analysis of MDA5-mediated IFN induction in response to picornavirus infection.....	96
<b>4.3</b>	<b>RIG-I mediates TLR-independent recognition of <i>Helicobacter pylori</i> RNA</b> ..	<b>99</b>
<b>4.4</b>	<b>Identification of an interferon-inducible short form of human RIG-I</b> .....	<b>103</b>
4.4.1	Detection of an interferon-induced short variant of human RIG-I.....	103
4.4.2	RIG-I short form is upregulated in a time- and dose-dependent manner.....	104
4.4.3	Sequence analysis of RIG-I short form.....	105
4.4.4	Cloning and overexpression of RIG-I short form.....	108

4.4.5	Investigation of the function of RIG-I short form in RIG-I-mediated innate immune signaling.....	109
4.4.5.1	<i>RIG-I short form acts as inhibitor of RIG-I-mediated type I IFN induction</i> .....	110
4.4.5.2	<i>Ubiquitination of RIG-I short form</i> .....	112
<b>5</b>	<b>Discussion</b> .....	<b>115</b>
<b>5.1</b>	<b>The C-terminal domain is the RNA 5'-triphosphate sensor of RIG-I</b> .....	<b>115</b>
5.1.1	The C-terminal domain is another functional domain of RIG-I.....	116
5.1.2	The zinc-coordination site within the CTD is a key structural motif....	117
5.1.3	The RIG-I CTD is involved in ligand recognition .....	118
5.1.4	A conserved groove in the regulatory domain acts as 5'-triphosphate RNA-binding site .....	120
5.1.5	Model for activation of RIG-I by the regulatory domain.....	122
<b>5.2</b>	<b>The C-terminal cysteine-rich domain of MDA5 mediates ligand specificity</b>	<b>124</b>
<b>5.3</b>	<b><i>Helicobacter pylori</i> RNA is recognized by RIG-I</b> .....	<b>126</b>
5.3.1	<i>Rig-I</i> mRNA is upregulated in <i>H. pylori</i> -infected BMDCs.....	127
5.3.2	<i>H. pylori</i> RNA activates RIG-I in a 5'-triphosphate-dependent manner .....	128
5.3.3	<i>H. pylori</i> virulence factors might contribute to the recognition of its RNA in the cytosol.....	129
<b>5.4</b>	<b>A novel RIG-I variant negatively regulates its own pathway</b> .....	<b>131</b>
5.4.1	Type I IFN treatment and 5'-triphosphate RNA stimulation reveals the presence of three RIG-I variants.....	132
5.4.2	RIG-I short form acts as inhibitor of the RIG-I-mediated IFN response .....	134
5.4.3	Proposed mechanism of RIG-I regulation by RIG-I short form.....	135
<b>6</b>	<b>Summary</b> .....	<b>137</b>
<b>7</b>	<b>References</b> .....	<b>141</b>
<b>8</b>	<b>Appendix</b> .....	<b>151</b>
<b>8.1</b>	<b>Equipment</b> .....	<b>151</b>
<b>8.2</b>	<b>Consumables</b> .....	<b>153</b>
<b>8.3</b>	<b>Reagents</b> .....	<b>154</b>
<b>8.4</b>	<b>Kits and enzymes</b> .....	<b>159</b>
<b>8.5</b>	<b>Primers</b> .....	<b>160</b>
<b>8.6</b>	<b>Supplemental figures</b> .....	<b>169</b>

**Acknowledgement** ..... **174**

## INDEX OF FIGURES

<b>Figure 1.</b>	Schematic representation of the RLR family members: RIG-I, MDA5 and LGP2.....	<b>3</b>
<b>Figure 2.</b>	Organelle-specific IPS-1 signaling.....	<b>16</b>
<b>Figure 3.</b>	RLR-mediated signal transduction and its regulation.....	<b>19</b>
<b>Figure 4.</b>	Schematic representation of the steps involved in site-directed mutagenesis of plasmid DNA using the Quick Change Kit.....	<b>60</b>
<b>Figure 5.</b>	Generation of 5'-triphosphate RNA by <i>in vitro</i> transcription.....	<b>62</b>
<b>Figure 6.</b>	Overexpression of Flag-RIG-I (AA 802-925).....	<b>74</b>
<b>Figure 7.</b>	RIG-I (AA 802-925) acts as an inhibitor of RIG-I-mediated IFN induction.....	<b>76</b>
<b>Figure 8.</b>	Comparative sequence analysis of the C-terminal domain of RIG-I and the homologous regions of MDA5 and LGP2.....	<b>78</b>
<b>Figure 9.</b>	Ribbon model of the RIG-I C-terminal domain (AA 802-925).....	<b>79</b>
<b>Figure 10.</b>	Mutation of conserved Cys residues to arginine (C→R) within the RIG-I CTD abolishes activation of the IFN-β promoter in response to virus infection.....	<b>81</b>
<b>Figure 11.</b>	Mutation of the four zinc-coordinating Cys residues to alanine (C→A).....	<b>83</b>
<b>Figure 12.</b>	Mutation of the zinc-binding cluster in the RIG-I CTD impairs 5'-triphosphate RNA-mediated IFN induction.....	<b>84</b>
<b>Figure 13.</b>	Lack of dominant negative effect of RIG-I C→R mutants in Huh7.5 cells.....	<b>85</b>
<b>Figure 14.</b>	Lack of dominant-negative effect of RIG-I C→R point mutants in HEK293 cells.....	<b>86</b>
<b>Figure 15.</b>	Interaction of the RIG-I CTD with IPS-1 and 5'-triphosphate RNA.....	<b>88</b>
<b>Figure 16.</b>	Analysis of amino acid residues that might be involved in the formation of a triphosphate-binding site within the CTD of RIG-I.....	<b>92</b>
<b>Figure 17.</b>	Mutation of the putative triphosphate-binding site in RIG-I abolishes activation of the IFN-β promoter in response to 5'-triphosphate RNA and virus infection.....	<b>93</b>
<b>Figure 18.</b>	WT MDA5 induces IFN-β promoter activation after transfection of poly(I:C).....	<b>95</b>
<b>Figure 19.</b>	MDA5-mediated IFN-β promoter activation in response to EMCV.....	<b>97</b>
<b>Figure 20.</b>	<i>Trif</i> -independent type I IFN induction in BMDCs.....	<b>100</b>
<b>Figure 21.</b>	RIG-I-mediated type I IFN by <i>Helicobacter pylori</i> RNA.....	<b>102</b>
<b>Figure 22.</b>	Detection of endogenous human RIG-I by immunoblotting.....	<b>103</b>
<b>Figure 23.</b>	Induction of RIG-I short form is time- and dose-dependent.....	<b>104</b>

---

<b>Figure 24.</b>	Immunoprecipitation of RIG-I short form and mass spectrometry analysis .....	<b>106</b>
<b>Figure 25.</b>	Ectopic expression of Flag-tagged RIG-I short form .....	<b>108</b>
<b>Figure 26.</b>	Inhibition of RIG-I-mediated IFN- $\beta$ promoter activation by RIG-I short form .....	<b>112</b>
<b>Figure 27.</b>	Analysis of the ubiquitination state of RIG-I variants upon type I IFN treatment .....	<b>113</b>
<b>Figure 28.</b>	Proposed model for RIG-I activation by 5'-triphosphate RNA-induced dimer formation .....	<b>123</b>
<b>Figure 29.</b>	Biochemical analysis of RIG-I variants .....	<b>170</b>
<b>Figure 30.</b>	The RIG-I regulatory domain (RD) binds RNA 5'-triphosphates.....	<b>171</b>
<b>Figure 31.</b>	The regulatory domain promotes 5'-triphosphate RNA-dependent RIG-I dimerization .....	<b>172</b>
<b>Figure 32.</b>	Localization of the RNA 5'-triphosphate-binding site on the RIG-I CTD .....	<b>173</b>

---

## INDEX OF TABLES

<b>Table 1.</b>	Detection of RNA viruses by RIG-I and MDA5.....	<b>10</b>
<b>Table 2.</b>	Viral inhibitors of RLR signaling.....	<b>26</b>
<b>Table 3.</b>	Antibodies and standard for IFN- $\beta$ ELISA .....	<b>37</b>
<b>Table 4.</b>	Antibodies used for immunoprecipitation and immunoblotting .....	<b>38</b>
<b>Table 5.</b>	Index of cell lines .....	<b>39</b>
<b>Table 6.</b>	Index of competent cells used for DNA amplification.....	<b>40</b>
<b>Table 7.</b>	Composition of SDS-PAGE gels.....	<b>69</b>
<b>Table 8.</b>	Oligonucleotide primers for cloning .....	<b>161</b>
<b>Table 9.</b>	Oligonucleotide primers for analytical PCR and sequencing.....	<b>162</b>
<b>Table 10.</b>	Oligonucleotide primers for generation of PCR products comprising the leader RNA of VSV.....	<b>163</b>
<b>Table 11.</b>	Oligonucleotide primers for site-directed mutagenesis of the conserved RIG-I cysteines into arginine (C $\rightarrow$ R).....	<b>164</b>
<b>Table 12.</b>	Oligonucleotide primers for site-directed mutagenesis of conserved RIG-I cysteines residues into alanine (C $\rightarrow$ A).....	<b>165</b>
<b>Table 13.</b>	Oligonucleotide primers for site-directed mutagenesis of the triphosphate-binding groove in the CTD of RIG-I.....	<b>166</b>
<b>Table 14.</b>	Oligonucleotide primers for site-directed mutagenesis of conserved cysteines residues in MDA5 (C $\rightarrow$ R).....	<b>167</b>
<b>Table 15.</b>	Oligonucleotide primers for quantitative real time PCR.....	<b>168</b>

## ABBREVIATIONS

<b>a</b>	Anti	<b>DEAD</b>	Asp-Glu-Ala-Asp motif
<b>Å</b>	Angstrom	<b>ddH<sub>2</sub>O</b>	Double distilled water
<b>AA</b>	Amino acid	<b>DDX3</b>	DEAD box protein 3
<b>Ab</b>	Antibody	<b>DI</b>	Defective interfering particle
<b>ABTS</b>	2,2'-azino-bis(3-ethylbenzthiazoline-6-sulphonic acid)	<b>D-MEM</b>	Dulbecco's Modified Eagle's Medium
<b>AGS</b>	Aicardi-Goutières syndrome	<b>DMSO</b>	Dimethyl sulfoxide
<b>Amp</b>	Ampicillin	<b>DNA</b>	Dexoyribonucleic acid
<b>APS</b>	Ammonium persulphate	<b>DNase I</b>	Desoxyribonuclease I
<b>ATCC</b>	American Type Culture Collection	<b>dNTP</b>	Deoxyribonucleotide triphosphate
<b>Atg5/12</b>	Autophagy protein 5/12	<b>ds</b>	Double stranded
<b>ATP</b>	Adenosine 5'-triphosphate	<b>DSMZ</b>	German Collection of Microorganisms and Cell Cultures (Deutsche Sammlung von Mikroorganismen und Zellkulturen)
<b>bp</b>	Base pair	<b>DSS</b>	Dextran sulfate sodium
<b>BHK-21</b>	Baby hamster kidney cell line	<b>DTT</b>	Dithiothreitol
<b>BLAST</b>	Basic Local Alignment Search Tool	<b>DUBA</b>	Deubiquitinating enzyme A
<b>BM</b>	Bone marrow	<b>EBER</b>	EBV-encoded small RNAs
<b>BSA</b>	Bovine serum albumin	<b>EBV</b>	Epstein Barr Virus
<b>°C</b>	Centigrade	<b>E. coli</b>	<i>Escherichia coli</i>
<b>CARD</b>	Caspase recruitment domain	<b>EDTA</b>	Ethylenediaminetetraacetic acid
<b>CARDIF</b>	CARD adapter inducing IFN-β	<b>EGFP</b>	Enhanced green fluorescent protein
<b>cDC</b>	Conventional dendritic cell	<b>ELISA</b>	Enzyme-linked immunosorbent assay
<b>CIAP</b>	Calf intestinal alkaline phosphatase	<b>EMCV</b>	Encephalomyocarditis virus
<b>CLR</b>	C-type lectin receptor	<b>ER</b>	Endoplasmic reticulum
<b>cm<sup>2</sup></b>	Square centimeter	<b>EtOH</b>	Ethanol
<b>CPE</b>	Cytopathic effect	<b>EY4A</b>	Eyes absent 4
<b>CTD</b>	C-terminal domain	<b>FACS</b>	Fluorescence activated cell sorting
<b>CycA</b>	Cyclophilin A	<b>FADD</b>	Fas-associated death domain
<b>CYLD</b>	Cylindromatosis	<b>FCS</b>	Fetal Calf Serum
<b>DAI</b>	DNA dependent activator of IRFs	<b>FL</b>	Full length
<b>DAK</b>	Dihydroxyacetone kinase	<b>Fluc</b>	Firefly luciferase
<b>DAMP</b>	Damage-associated molecular pattern	<b>for</b>	Forward
<b>DC(s)</b>	Dendritic cell(s)		
<b>DD</b>	Death domain		

<b>GALT</b>	Gut-associated lymphatic tissue	<b>IUBMB</b>	International Union of Biochemistry and Molecular Biology
<b>gC1QR</b>	Globular domain of complement component	<b>ISG</b>	Interferon-stimulated gene
<b>GDP</b>	Guanosine diphosphate	<b>ISG15</b>	ISG15 ubiquitin-like modifier
<b>GFP</b>	Green fluorescent protein	<b>ISRE</b>	Interferon stimulated response element
<b>GM-CSF</b>	Granulocyte-macrophage colony-stimulating factor	<b>IVT</b>	<i>In vitro</i> transcription
<b>G-MEM</b>	Glasgow Minimal Essential Medium	<b>JAK</b>	Janus kinase
<b>G protein</b>	Glycoprotein	<b>JEV</b>	Japanese encephalitis virus
<b>GTP</b>	Guanosine triphosphate	<b>Kan</b>	Kanamycin
<b>h, hrs</b>	Hour(s)	<b>Kb</b>	Kilobase
<b>HA</b>	Hemagglutinin	<b>kDa</b>	Kilodalton
<b>HC</b>	Heavy chain	<b>KO</b>	Knockout
<b>HCV</b>	Hepatitis C virus	<b>LC</b>	Light chain
<b>HEK293</b>	Human embryonic kidney cells	<b>LB</b>	<i>Luria Bertani</i>
<b>Hela</b>	cervical cancer cells taken from Henrietta Lacks	<b>LGP2</b>	Laboratory of genetics and physiology-2
<b>Hepes</b>	4-(2-Hydroxyethyl)piperazine-1-ethanesulfonic acid	<b>M</b>	Molar
<b>HMGB1</b>	High-mobility group box protein 1	<b>mA</b>	Milliampere
<b>HRP</b>	Horseradish peroxidase	<b>mAb</b>	Monoclonal antibody
<b>HSP</b>	Heat shock protein	<b>MAPK</b>	Mitogen-activated protein kinases
<b>HSV-1/-2</b>	Herpes simplex virus-1/-2	<b>MAVS</b>	Mitochondrial antiviral signaling protein
<b>Huh</b>	Human hepatoma cell line	<b>MDA5</b>	Melanoma differentiation associated protein 5
<b>IB</b>	Immunoblot	<b>MEF(s)</b>	Mouse embryonic fibroblast(s)
<b>IBD</b>	Inflammatory bowel disease	<b>mFD</b>	Milli farad
<b>IFN</b>	Interferon	<b>µg</b>	Microgram
<b>IFN I</b>	Type I interferon	<b>mg</b>	Milligram
<b>IκB</b>	Inhibitor of NFκB	<b>min</b>	Minute(s)
<b>IKK</b>	Inhibitor of κB kinase	<b>miRNA</b>	Micro RNA
<b>IKK-i</b>	inducible IκB kinase	<b>MITA</b>	Mediator of IRF3 activation
<b>IL-1β</b>	Interleukin-1 β	<b>ml</b>	Milliliter
<b>IP</b>	Immunoprecipitation	<b>mm</b>	Millimeter
<b>IPS-1</b>	Interferon-β promoter stimulator protein 1	<b>mM</b>	Millimolar
<b>IPTG</b>	Isopropyl-β-D-thiogalactopyranoside	<b>MNV-1</b>	Murine norovirus-1
<b>IRAK</b>	IL-1 receptor-associated kinase	<b>MOI</b>	Multiplicity of infection
<b>IRF</b>	Interferon regulatory factor	<b>mRNA</b>	Messenger RNA
<b>ISD</b>	Immunostimulatory DNA	<b>MS</b>	Mass spectrometry
		<b>MSS4</b>	Mammalian suppressor of SEC4

<b>MuV</b>	Mumps virus	<b>p.t.</b>	Post transfection
<b>MW</b>	Molecular weight	<b>PVDF</b>	Polyvinyl difluoride
<b>MyD88</b>	Myeloid differentiation response protein 88	<b>RACE</b>	Rapid amplification of cDNA ends
<b>N</b>	Normal	<b>RD</b>	Regulatory domain
<b>NaOH</b>	Sodium hydroxide solution	<b>REUL</b>	RIG-I E3 ubiquitin ligase
<b>NDV</b>	Newcastle disease virus	<b>rev</b>	Reverse
<b>NEAA</b>	Non-essential amino acids	<b>RIG-I</b>	Retinoic acid-inducible gene 1
<b>NEMO</b>	NFκB essential modulator	<b>RIP-1</b>	Receptor interacting protein 1
<b>NF-κB</b>	Nuclear factor-κB	<b>RIPA</b>	Radioimmunoprecipitation assay
<b>ng</b>	Nanogram	<b>Riplet</b>	RING-finger protein leading to RIG-I activation
<b>NIH</b>	National Institute of Health	<b>RL</b>	Renilla luciferase
<b>NLR</b>	NOD-like receptor	<b>RLR</b>	Retinoic acid-inducible gene like receptors
<b>NLRX1</b>	NLR family member X1	<b>RLU</b>	Relative light unit
<b>N protein</b>	Nucleoprotein	<b>Rluc</b>	Renilla luciferase
<b>NOD</b>	Nucleotide oligomerization domain	<b>RNA</b>	Ribonucleic acid
<b>NOX2</b>	NADPH oxidase 2	<b>RNAi</b>	RNA interference
<b>NP-40</b>	Nonidet P-40	<b>rRNA</b>	Ribosomal RNA
<b>NS</b>	Non-structural protein	<b>RNase</b>	Ribonuclease
<b>nt</b>	Nucleotide	<b>RNaseH</b>	Ribonuclease H
<b>OD</b>	Optical density	<b>RNF</b>	RING-finger protein
<b>o/N</b>	Overnight	<b>ROS</b>	Reactive oxygen species
<b>PAGE</b>	Polyacrylamide gel electrophoresis	<b>rpm</b>	Revolutions per minute
<b>PAMP</b>	Pathogen-associated molecular pattern	<b>RT</b>	Room temperature
<b>PBS</b>	Phosphate buffered saline	<b>RT-PCR</b>	Reverse transcriptase PCR
<b>PCR</b>	Polymerase chain reaction	<b>SA</b>	Streptavidin
<b>PDB</b>	Protein data bank	<b>SAMHD1</b>	sterile alpha motif domain and HD domain-containing protein 1
<b>PFU</b>	Plaque forming units	<b>sc</b>	Subcloning
<b>PGS</b>	Protein G sepharose	<b>sec</b>	Second(s)
<b>p.i.</b>	Post infection	<b>SD</b>	Standard deviation
<b>PIFN-β</b>	Promoter IFF-β gene	<b>SDS</b>	Sodium dodecyl sulphate
<b>PIV</b>	Parainfluenza virus	<b>SeV</b>	Sendai virus
<b>PMSF</b>	Phenylmethylsulfonylfluorid	<b>SLE</b>	Systemic lupus erythematosus
<b>Pol-III</b>	RNA polymerase III	<b>ss</b>	Single stranded
<b>poly(dA:dT)</b>	Poly(deoxyadenylic:thymidilic) acid	<b>STAT</b>	Signal transducer and activator of transcription 3
<b>poly(I:C)</b>	Poly(inosinic:polycytidylic) acid	<b>STING</b>	Stimulator of interferon genes
<b>5'-ppp</b>	5'-triphosphate	<b>SV</b>	Splice variant
<b>PRR</b>	Pattern-recognition receptor		

<b>TAE</b>	Tris-acetate-EDTA	<b>TRIM25</b>	Tripartite motif 25
<b>TANK</b>	TRAF family member-associated NF $\kappa$ B activator	<b>U</b>	Unit(s)
<b>TBE</b>	Tris-borate-EDTA	<b>Ub</b>	Ubiquitin
<b>TBS-T</b>	Tris buffered saline with Tween-20	<b>UniProtKB</b>	Universal Protein Resource
<b>TBK1</b>	TANK binding kinase 1	<b>UTP</b>	Uridine 5'-triphosphate
<b>TEMED</b>	N,N,N',N'-Tetramethylethylenediamine	<b>UV</b>	Ultraviolet
<b>TK</b>	Thymidine kinase	<b>Vero</b>	Verda reno (green kidney)
<b>TLR</b>	Toll-like receptor	<b>VISA</b>	Virus-induced signaling adapter
<b>TM</b>	Transmembrane domain	<b>VSV</b>	Vesicular stomatitis virus
<b>TNF</b>	Tumor necrosis factor	<b>v/v</b>	Volume per volume
<b>TOM70</b>	Translocases of outer membrane	<b>WNV</b>	West Nile virus
<b>TRADD</b>	TNF receptor-associated death domain	<b>w/o</b>	Without
<b>TREX1</b>	Three prime repair exonuclease 1	<b>WT</b>	Wild-type
<b>Trif</b>	Toll/interleukin-1 receptor domain-containing adapter protein	<b>w/v</b>	Weight per volume

#### Amino Acids (AA)

<b>A, Ala</b>	Alanine	<b>M, Met</b>	Methionine
<b>C, Cys</b>	Cysteine	<b>N, Asn</b>	Asparagine
<b>D, Asp</b>	Aspartic acid	<b>P, Pro</b>	Proline
<b>E, Glu</b>	Glutamic acid	<b>Q, Gln</b>	Glutamine
<b>F, Phe</b>	Phenylalanine	<b>R, Arg</b>	Arginine
<b>G, Gly</b>	Glycine	<b>S, Ser</b>	Serine
<b>H, His</b>	Histidine	<b>T, Thr</b>	Threonine
<b>I, Ile</b>	Isoleucine	<b>V, Val</b>	Valine
<b>K, Lys</b>	Lysine	<b>W, Trp</b>	Tryptophan
<b>L, Leu</b>	Leucine	<b>Y, Tyr</b>	Tyrosine

# 1 INTRODUCTION

## 1.1 The innate immune system protects from invading pathogens

Vertebrates are constantly threatened by the invasion of pathogens like bacteria, fungi and parasites as well as viruses. To counteract the threat of pathogenic invasion, higher eukaryotes have evolved self-defense mechanisms: adaptive (acquired) and innate immunity. Innate immunity was considered to be the less complex and the less flexible system until 1996, when Toll was discovered in *Drosophila* species and its mammalian homologues, the Toll-like receptors (TLRs), were found to mediate recognition of pathogens by the innate immune system (Lemaitre *et al.*, 1996). These findings led to the discovery of pattern-recognition receptors (PRRs) and their role in the regulation of the entire immune system.

The innate immune system is the first line of defense against invading pathogens and is mediated by immune cells including macrophages, and dendritic cells (DCs) as well as non-hematopoietic cells such as epithelial cells, endothelial cells and fibroblasts. Acquired immunity in turn is involved in the elimination of pathogens in the late phase of infection and the generation of immunological memory. While acquired immunity is characterized by specificity and develops by clonal selection from a vast repertoire of lymphocytes bearing antigen specific receptors, the innate immune system recognizes pathogens via PRRs that discriminate between self and non-self. In contrast to the large repertoire of receptors generated by gene rearrangement, which are utilized by the acquired immune system, PRRs are germline-encoded and therefore limited in number. However, PRRs possess common characteristics. First, PRRs recognize structures that are conserved among microbial species, known as pathogen-associated molecular patterns (PAMPs) that are essential for the pathogen's survival and therefore difficult for the microorganism to alter. Bacteria and fungi have unique cell wall components, such as glycoproteins or lipodoglycans, which are not found in the host, and so the detection of these PAMPs might be relatively easy (Yoneyama and Fujita, 2010). However, major viral PAMPs are viral nucleic acids, which are structurally similar to cellular nucleic acids of the host. Moreover, PRRs are also responsible for recognizing

endogenous molecules released from damaged cells, termed damage-associated molecular patterns (DAMPs) (Takeuchi and Akira, 2010). Secondly, PRRs are constitutively expressed on all cells of a given type and completely independent of immunological memory (Akira *et al.*, 2006). Each PRR reacts with a specific PAMP, shows a distinct expression pattern and activates a specific signaling cascade to induce the expression of mediators such as type I interferon and proinflammatory cytokines, which limit expansion and dissemination of invading pathogens early on and simultaneously shape the adaptive immune response (Yoneyama and Fujita, 2009) to eradicate the pathogen and establish immunological memory.

## **1.2 Pattern recognition receptors**

Currently, four different PRR families have been identified. These include transmembrane proteins namely Toll-like receptors (TLRs) and C-type lectin receptors (CLRs), as well as cytoplasmic retinoic acid-inducible gene (RIG-I) like receptors (RLRs) and nucleotide oligomerization domain (NOD)-like receptors (NLRs). Among these, TLRs, RLRs and NLRs have been shown to be critically involved in the recognition of viral nucleic acids. TLRs and RLRs commonly induce type I IFNs in addition to proinflammatory cytokines via different signaling pathways, whereas NLRs are known to mediate interleukin-1  $\beta$  (IL-1 $\beta$ ) generation from pro-IL-1 $\beta$  through activation of caspase-1 (Kanneganti *et al.*, 2007; Petrilli *et al.*, 2007).

## **1.3 RIG-I-like receptors are viral RNA sensors**

The RLR family itself comprises a family of RNA helicases consisting of the three members RIG-I, melanoma differentiation-associated gene 5 (MDA5) and laboratory of genetics and physiology-2 (LGP2), that have been identified so far (Figure 1). RNA helicases are enzymes which possess the ability to unwind dsRNA molecules in an energy-dependent fashion through the hydrolysis of nucleoside triphosphates (NTPs), such as ATP (Tanner and Linder, 2001). However, recent studies showed that rather than being a processive RNA helicase that consistently unwinds RNA, several proteins act as RNA ‘chaperones’, promoting the formation of optimal RNA structures through local RNA unwinding or by mediating RNA-protein association/dissociation (Fairman

*et al.*, 2004; Lorsch, 2002). RNA helicases are localized in the cytoplasm, where they are involved in recognizing the genomic RNA of dsRNA viruses as well as dsRNA generated as replication intermediates of viruses bearing a ssRNA genome. In general, the expression of RLRs was demonstrated to be greatly enhanced in response to type I IFN stimulation or virus infection, hence they belong to the family of IFN-induced genes.

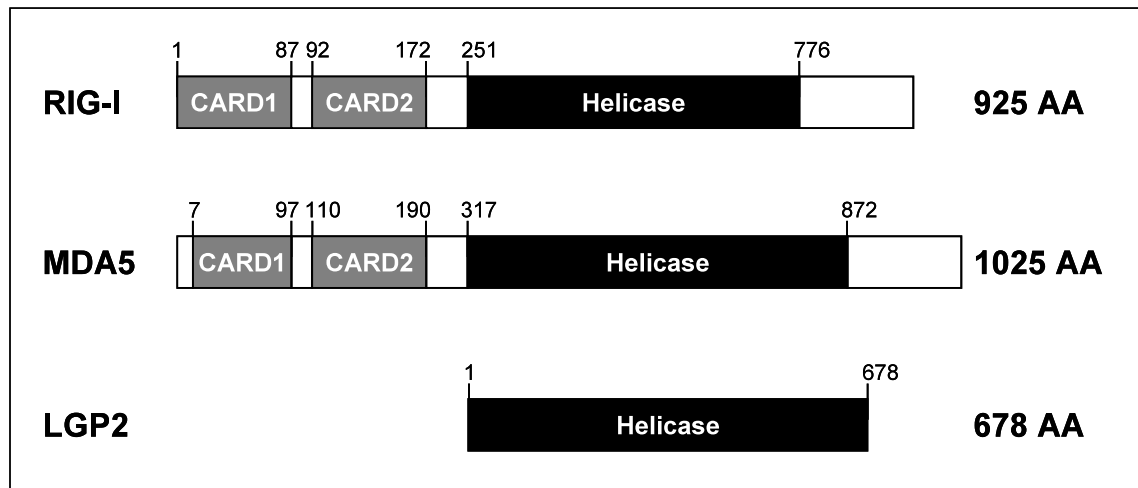


**Figure 1.** Schematic representation of the RLR family members: *RIG-I*, *MDA5* and *LGP2*

### 1.3.1 Identification of RIG-I and its function

*RIG-I*, also known as *DDX58*, was identified originally as a gene induced in retinoic acid-treated acute promyelocytic leukaemia cells (Sun, 1997). Subsequent identification of a porcine homolog of *RIG-I* as a porcine reproductive and respiratory syndrome virus-induced gene was the first line of evidence for the possible connection between *RIG-I* and viral infection (Zhang *et al.*, 2000). Finally, in 2004, Yoneyama *et al.* were able to functionally isolate *RIG-I* as a cDNA clone that can activate interferon regulatory factor 3 (IRF3) regulated reporter gene expression in response to transfection with synthetic dsRNA poly(I:C) (Yoneyama *et al.*, 2004), hence revealing that *RIG-I* is involved in type I IFN induction in response to foreign RNA in the cytosol.

*RIG-I* was demonstrated to belong to the family of DExD/H box containing RNA helicases, which is distinguished by the presence of several conserved motifs including the characteristic DExD/H sequence (where x can be any amino acid) within the helicase domain that is highly conserved in proteins from viruses and bacteria to

humans (Fuller-Pace, 2006; Linder *et al.*, 1989; Tanner and Linder, 2001). In addition to the helicase domain, located in the central part of the protein, the RNA helicase RIG-I contains two caspase recruitment domains (CARDs) at the N-terminus (Zhang *et al.*, 2000). CARDs were first identified as modules of 90 to 100 AA involved in apoptosis signaling pathways, with the CARDs mediating the association of adaptor proteins and procaspases through homodimerization of their respective CARDs (Vaughn *et al.*, 1999).

The functions of RIG-I have been analyzed in detail in the first publication by Yoneyama *et al.* (2004), using deletion constructs of the full-length RIG-I protein. Overexpression of the N-terminal region of RIG-I comprising the two tandem CARDs can act as a constitutive activator and was sufficient to induce IRF3 and nuclear factor  $\kappa$  B (NF- $\kappa$ B) activation even in the absence of a dsRNA stimulus or viral challenge. These results strongly suggested that the tandem CARDs act as an effector domain activating a downstream molecule, which has not been yet identified when RIG-I was discovered. Although full-length RIG-I showed no constitutive activity, a strong increase of IFN signaling was observed in response to infection with Newcastle disease virus (NDV) or dsRNA transfection, revealing that RIG-I must be activated upon stimulation with either virus or isolated RNA. Furthermore, treatment of cells with type I interferon increased the amount of endogenous RIG-I corresponding to its IFN-inducible nature. Moreover, a mutant lacking CARD1 and CARD2 was not capable of eliciting an antiviral response and had a dominant negative effect (Yoneyama *et al.*, 2004). Thus, the helicase domain of RIG-I strictly regulates RIG-I function in a virus- or dsRNA-dependent manner. In line with this, introduction of a point mutation (K270A) at the Walker-type ATP-binding site in the helicase domain (Walker *et al.*, 1982) of full length RIG-I also conferred dominant negative activity to RIG-I (Yoneyama *et al.*, 2004). Therefore, it was concluded that the helicase activity of RIG-I is indispensable for its function as signal transducer and that ATP hydrolysis is required for downstream signaling.

To investigate the functional role of RIG-I *in vivo*, *Rig-I* deficient mice were generated. Surprisingly, most embryos lacking *Rig-I* were lethal at embryonic days 12.5 to 14.0, only a few mice were born alive (Kato *et al.*, 2005). Nevertheless, these mice showed growth retardation and died within three weeks after birth. Histological analysis revealed massive liver degeneration (Kato *et al.*, 2005), suggesting that RIG-I seems to

be required for developmental processes in addition to virus recognition and signaling. Taken together these first studies described RIG-I as the prototypic member of the RLR family, which mediates the activation of IRF3 and NF- $\kappa$ B signaling pathways upon recognition of foreign dsRNA that has entered the cytosol, resulting in the induction of type I IFNs as well as proinflammatory cytokines.

### **1.3.2 MDA5**

Another DExD/H-box containing RNA helicase that is involved in the sensing of intracellular RNA and the induction of type I IFNs in response to RNA viruses is MDA5 (Andrejeva *et al.*, 2004). MDA5 reveals the same structure like its family member RIG-I, containing the N-terminal CARDs as well as the helicase domain in the central region of the protein. *MDA5* was originally isolated as a gene induced by the IFN- and protein kinase C-activating compound mezerein in a melanoma cell line (Kang *et al.*, 2002). Furthermore, Kovacsovics and colleagues reported in 2002 that MDA5, which was then called Helicard, is cleaved by caspases upon induction of apoptosis, thereby separating the CARDs from the helicase domain. The helicase domain then localizes to the nucleus, where it is involved in DNA degradation and nuclear remodelling during apoptotic cell death (Kovacsovics *et al.*, 2002).

MDA5, also designated as IFIH1, is the closest relative of RIG-I, exhibiting 23 and 35 % amino acid homology in the N-terminal tandem CARDs and the helicase domain, respectively (Yoneyama *et al.*, 2005). Functional analysis of MDA5 *in vitro* revealed that MDA5 functions as a positive regulator for the induction of type I IFNs and proinflammatory cytokines, similar to RIG-I. As RIG-I, MDA5 is ubiquitously expressed in low abundance and expression is induced upon virus infection or type I IFN treatment. The essential role of MDA5 in virus-induced innate immunity was shown by analysis of knockout (KO) mice upon picornavirus infection (Gitlin *et al.*, 2006; Kato *et al.*, 2006). Moreover, these studies revealed, that although MDA5 and RIG-I are closely related, they have unique roles in the innate immune response to RNA viruses. Hence, RIG-I and MDA5 have evolved to specifically recognize different types of RNA virus, but utilize a common mode of activation and trigger shared downstream signaling pathways that finally lead to protection of the threatened host.

### 1.3.3 Downstream signaling is mediated by the adaptor protein IPS-1

When RIG-I was discovered and its domains were analyzed by overexpression of deletion constructs, removal of the helicase domain was shown to render RIG-I constitutively active in the absence of both intracellular dsRNA and virus infection. Hence, it was speculated that the N-terminally located tandem CARDs of RIG-I might act as an effector domain that either directly activates a downstream molecule or is indirectly involved in the activation of this putative molecule. Moreover, it was already mentioned that during apoptosis, CARDs associate with adaptor proteins, suggesting that the CARDs of RIG-I might also be involved in the recruitment of accessory proteins.

Therefore, BLAST search was performed to identify proteins containing CARD-like domains (Meylan *et al.*, 2005; Seth *et al.*, 2005), which might interact with RIG-I or MDA5, respectively. In addition, different groups performed cDNA library screening to detect molecules that are able to activate the IFN- $\beta$  promoter (Kawai *et al.*, 2005) or the NF- $\kappa$ B pathway (Xu *et al.*, 2005) to understand the signaling pathways that are involved in the activation of IRF3 and NF- $\kappa$ B by viruses. Finally, the adaptor protein of the RLR pathway was identified by four independent groups and designated as IFN- $\beta$  promoter stimulator 1 (IPS-1) (Kawai *et al.*, 2005), mitochondrial antiviral signaling protein (MAVS) (Seth *et al.*, 2005), virus-induced signaling adapter (VISA) (Xu *et al.*, 2005) and CARD adapter inducing IFN- $\beta$  (CARDIF) (Meylan *et al.*, 2005), respectively. *In vitro* studies revealed that the RLR-triggered IFN response was significantly enhanced by overexpression of IPS-1 (Kawai *et al.*, 2005; Meylan *et al.*, 2005; Seth *et al.*, 2005; Xu *et al.*, 2005) and conversely impaired in cells lacking IPS-1 in response to either RIG-I or MDA5 specific stimulation (Kumar *et al.*, 2006; Sun *et al.*, 2006), indicating that IPS-1 is indispensable for RLR-mediated signaling. IPS-1 consists of a single N-terminal CARD, which was shown to interact with the tandem CARDs of RIG-I, and a proline-rich region in the middle of the protein. In addition, IPS-1 encodes a hydrophobic transmembrane (TM) domain at its C-terminus that localizes it to the outer mitochondrial membrane (Seth *et al.*, 2005). Deletion analyses have shown that both the CARDs and the transmembrane domain are essential for the function of IPS-1. Moreover, the mitochondrial localization is critical for its signaling activity since deletion or truncation of the TM domain leading to cytoplasmic expression of the

molecule, results in the failure of signal activation. Furthermore, the signaling function of IPS-1 is abolished when it is artificially mislocalized to the plasma membrane or the endoplasmic reticulum (Seth *et al.*, 2005). In a very recent publication, it was shown that IPS-1 in addition to the mitochondria also localizes to the peroxisomes in human and mouse cells (Dixit *et al.*, 2010). Thus, by expression of IPS-1, which was demonstrated to act as common adapter molecule in RLR-mediated signaling, mitochondria and peroxisomes serve as essential signaling platforms for innate immunity.

#### 1.3.4 LGP2

The third RLR family member is encoded by *LGP2/Lgp2* (*DHX58/Dhx58*), which was originally identified as the gene adjacent to the STAT3/5 locus (Cui *et al.*, 2001). LGP2 shows 31 and 41 % AA identities to the helicase domains of RIG-I and MDA5, respectively, but interestingly completely lacks N-terminal CARDs (Yoneyama *et al.*, 2005) suggesting that it not able interact with IPS-1 by CARD-CARD interaction as was shown for RIG-I and MDA5.

*LGP2* mRNA synthesis is rapidly induced in human cells by IFN- $\alpha$ , cytoplasmic dsRNA or virus infection (Komuro and Horvath, 2006), indicating that it belongs to the family of IFN-inducible genes, as well. However, overexpression studies indicate that LGP2 itself is not able to induce IFN- $\beta$  gene transcription, which is consistent with the lack of CARDs and the inability to associate with IPS-1 by CARD-CARD interactions. In contrast, *in vitro* experiments showed that LGP2 plays an inhibitory role in RIG-I-mediated antiviral signaling. Rothenfusser *et al.* (2005) were the first to demonstrate that LGP2 acts as a natural host-derived negative regulator of RIG-I signaling by binding to viral dsRNA, thereby preventing RIG-I-mediated recognition. Although LGP2 lacks the CARDs it was shown to interact with IPS-1 in a virus-independent manner that requires both mitochondrial localization and the C-terminal CARD of IPS-1. The CARD-independent interaction of LGP2 with IPS-1 was shown to be critically dependent on the mitochondrial TM domain and the region between AA 300 to 440 of IPS-1 (Komuro and Horvath, 2006). Thus, the CARD of IPS-1 is still free to engage upstream sensors RIG-I and MDA5. However, coimmunoprecipitation studies revealed that in addition to IPS-1, LGP2 associates with RIG-I and MDA5 (Komuro and Horvath, 2006). The inhibitory role of LGP2 was further explained by Yoneyama *et*

*al.* (2005), who proposed a model, in which LGP2 specifically masks the target RNA from recognition by RIG-I and MDA5. Yoneyama and colleagues observed that knockdown of LGP2 expression leads to enhanced ISRE gene induction in response to NDV infection, indicating that LGP2 is responsible for the negative feedback of IFN gene activation. It was hypothesized that LGP2 functions to prevent overproduction of IFNs, which, if left uncontrolled, could have negative consequences for the host. But, *in vivo* analysis of *Lgp2* lacking mice revealed a dichotomy of LGP2 function with respect to regulation of RIG-I and MDA5 activity. While *Lgp2* deficient mice showed reduced susceptibility to viruses recognized by RIG-I, these mice showed enhanced susceptibility to challenge with MDA5 specific viruses like encephalomyocarditis virus (EMCV) (Venkataraman *et al.*, 2007). However, a recent study using *Lgp2* KO mice demonstrated that LGP2 acts as a positive regulator of both MDA5- and RIG-I-mediated viral recognition, except for influenza virus (Satoh *et al.*, 2010). Taken together, at the moment the function LGP2 in the antiviral innate immune is not fully understood.

### 1.3.5 Viral recognition by RIG-I-like receptors

The RLR members RIG-I and MDA5 have been shown to interact with IPS-1 to activate IRF3 and NF- $\kappa$ B in response to stimulation, whereas the third member LGP2, which is suggested to function as a regulator of both RIG-I and MDA5, is not able to trigger an IFN response. Moreover, it was demonstrated that although activating a common downstream signaling mechanism, RIG-I and MDA5 exert differential roles in the recognition of RNA viruses (Kato *et al.*, 2006), suggesting that they are able to distinguish different RNA viruses.

While cells lacking RIG-I did not produce type I IFNs in response to various RNA viruses, including paramyxoviruses (such as NDV and Sendai virus), vesicular stomatitis virus (VSV) and influenza virus (Kato *et al.*, 2005; Kato *et al.*, 2006; Melchjorsen *et al.*, 2005), mice lacking *Mda5* did not produce type I IFNs in response to infection with picornaviruses like EMCV, Mengo virus and Theiler's virus (Gitlin *et al.*, 2006; Kato *et al.*, 2006). Mice lacking *Rig-I* or *Mda5* are highly susceptible to infection with VSV and EMCV, respectively, which is consistent with the failure to induce IFN (Kato *et al.*, 2006). Further investigation revealed that MDA5 is also required for the control of murine norovirus infection (McCartney *et al.*, 2008). Murine

norovirus-1 (MNV-1) is one of several murine noroviruses isolated from research mouse facilities and has been used as a model of human norovirus infection, since noroviruses are important pathogens causing viral epidemic gastroenteritis worldwide. There have been several further studies that identified RNA viruses that are specifically recognized in a RIG-I-dependent manner. Thus, RIG-I was demonstrated to be involved in the inhibition of Ebola virus replication (Spiropoulou *et al.*, 2009) as well as the sensing of members of the flavivirus family such as Japanese encephalitis virus (JEV) and hepatitis C virus (HCV) (Kato *et al.*, 2006; Sumpter *et al.*, 2005). HCV is the major cause for liver transplantation since establishment of an acute HCV infection often progresses to chronic infection with liver cirrhosis leading to liver failure. Thus, the innate immune response is an important component of the acute hepatic antiviral defenses that are triggered *in vivo* within days of exposure to HCV (Bartenschlager and Lohmann, 2001) and is therefore likely to contribute to the clearance of acute infection, thereby preventing the progression to chronic hepatitis. However, complete viral clearance is not achieved in all cases, since studies have shown that 20 % to 25 % of HCV infected patients develop a chronic infection (Rodger *et al.*, 2000). In line with this, in cultured hepatocytes it was shown that RIG-I plays an essential role as TLR-independent PAMP receptor that specifically binds dsRNA structured regions within the HCV genome to induce the innate immune cascade (Sumpter *et al.*, 2005). In contrast, human hepatoma cells bearing a point mutation (T55I) in CARD1 of RIG-I are highly permissive for HCV (Sumpter *et al.*, 2005). With this regard, recognition of GB virus, a surrogate mouse model virus for human HCV, is also mediated by RIG-I (Chen *et al.*, 2007).

However, recent studies revealed that some viruses are redundantly sensed by both RIG-I and MDA5. Interestingly, among the flavivirus family, although JEV and HCV are specifically detected by RIG-I, West Nile virus (WNV) and Dengue virus have been demonstrated to be sensed by both RIG-I and MDA5 (Fredericksen *et al.*, 2008; Loo *et al.*, 2007). Hence, cooperation of RIG-I and MDA5 in response to WNV infection was suggested to mediate an IFN amplification loop that supports immune effector gene expression during WNV infection, thereby establishing an antiviral state (Fredericksen *et al.*, 2008). Interestingly, vaccine strains of measles virus were also found to activate cells in a RIG-I/MDA5-dependent manner, whereas wild-type measles failed to induce type I IFN (Shingai *et al.*, 2007).

**Table 1. Detection of RNA viruses by RIG-I and MDA5**

Most of the RNA viruses, containing relatively short dsRNA with a 5'-triphosphate moiety, are recognized by RIG-I. In contrast, long dsRNA is detected by MDA5. Reovirus as well as West Nile virus and Dengue virus, members of the flavivirus family, are detected by both RIG-I and MDA5.

virus family	genome	virus species	ligand
<b>RIG-I</b>			
<i>Paramyxoviridae</i>	negative-sense ssRNA	Newcastle disease virus	5'-pppRNA
		Sendai virus	
		Sendai Virus DI particle	dsRNA
<i>Flaviviridae</i>	positive-sense ssRNA	Japanese encephalitis virus	5'-pppRNA
		Hepatitis C virus	
		GB virus	
<i>Rhabdoviridae</i>	negative-sense ssRNA	Vesicular stomatitis virus	5'-pppRNA or dsRNA
<i>Orthomyxoviridae</i>	negative-sense ssRNA	Influenza A virus	5'-pppRNA
<b>MDA5</b>			
<i>Picornaviridae</i>	positive-sense ssRNA, 5'-VPg	Encephalomyocarditis virus	dsRNA
		Theiler's virus	
		Mengo virus	
<i>Caliciviridae</i>	positive-sense ssRNA, 5'-VPg	Murine norovirus-1	dsRNA ?
<i>Coronaviridae</i>	positive-sense ssRNA	Murine hepatitis virus	dsRNA ?
<b>RIG-I and MDA5</b>			
<i>Reoviridae</i>	dsRNA	Reovirus	RIG-I: short segments MDA5: long segments
<i>Flaviviridae</i>	positive-sense ssRNA	West Nile virus	dsRNA ?
		Dengue virus	

Furthermore, innate immune recognition of reoviruses also seems to involve both RIG-I and MDA5. Loo *et al.* (2007) demonstrated that the reovirus dsRNA genome is detected by either RIG-I or MDA5 in a segment length-dependent manner.

However the exceptional role of RIG-I and MDA5 in the recognition of RNA viruses, was contradicted by a recent report that revealed the involvement of RIG-I in antiviral signaling to Epstein-Barr virus (EBV), which possesses a dsDNA genome (Samanta *et al.*, 2006). It was shown that in latently EBV-infected cells, EBV-encoded small RNAs (EBERs), were responsible for activation of the RIG-I-mediated induction of type I IFN. Additionally, MDA5 was reported to be involved in the IFN response to RNAs generated during Vaccinia virus infection (Pichlmair *et al.*, 2009). Vaccinia virus, which belongs to the poxvirus family, contains a linear dsDNA genome.

Taken together, RIG-I and MDA5 specifically recognize distinct virus species, but cooperation of both pathways in the recognition of some viruses results in a markedly enhanced antiviral immune response, providing maximum defense of the host cell to the invading viruses.

### **1.3.6 RLRs are accurate sensors of virus invasion – discrimination between self and non-self**

Virus sensing is highly discriminative, given that RLRs are localized in the cytoplasm, where host RNAs are abundant. Yet, RLR activation occurs only in infected cells. Thus, for the RLRs to be activated, they must detect RNA bearing a molecular pattern that is only present in virus-infected cells.

Differential virus recognition implicates that RIG-I and MDA5 are specific in their detection of RNA viruses, presumably through recognition of distinct structures of viral RNA. Initially, both RIG-I and MDA5 were implicated in the recognition of poly(I:C), which is a synthetic dsRNA analogue that mimics viral RNA (Rothenfusser *et al.*, 2005; Yoneyama *et al.*, 2004). However, analysis of KO mice revealed that MDA5, but not RIG-I, is responsible for eliciting the type I IFN response to poly(I:C) stimulation (Kato *et al.*, 2006). In 2006, two groups independently demonstrated that 5'-triphosphate (5'-ppp)-containing viral RNA, which is detectable in most RNA virus genomes as well as in *in vitro* transcribed RNA, is selectively recognized by RIG-I as non-self foreign RNA (Hornung *et al.*, 2006; Pichlmair *et al.*, 2006). Accordingly, the induction of

antiviral responses following infection with influenza A virus, which contains 5'-ppp structures but does not lead to detectable dsRNA accumulation, is controlled by RIG-I (Pichlmair *et al.*, 2006). Furthermore, it was demonstrated that RNA isolated from Rabies virus-infected cells activates RIG-I, whereas RNA from non-infected cells as well as dephosphorylated RNA fails to activate RIG-I. Therefore, single-stranded RNA (ssRNA) bearing a 5'-ppp is the specific ligand for RIG-I. Actually, RIG-I specifically binds RNA containing a 5'-triphosphate moiety, but not RNA bearing a 5'-di- or 5'-monophosphate (Hornung *et al.*, 2006). Thus, the 5'-triphosphate is the molecular pattern that enables discrimination between self and non-self RNA. Host RNA synthesis takes place in the nucleus. Like the viral transcript, cellular primary transcripts contain a 5'-triphosphate. Since the cellular RNAs undergo various processes such as 5'-modification of the mRNA with a 7-methylguanosine (m7Gppp) Cap structure, 5'-cleavage of tRNA and the complexation of rRNAs with ribosomal proteins, they are masked from detection by RIG-I.

However, the 5'-ppp structure is necessary but not sufficient for RIG-I recognition. Two recent studies showed that in addition to the 5'-triphosphate, base-pairing at the 5'-end of the RNA is required for RIG-I activation (Schlee *et al.*, 2009; Schmidt *et al.*, 2009). RIG-I can translocate on base-paired RNA and this might contribute to its signaling activity (Myong *et al.*, 2009). In addition to a panhandle structure at the 5'-ppp end, RIG-I activation is also influenced by other characteristics of the RNA. Together with the 5'-ppp end of the genome, activation of RIG-I by HCV is determined by a polyuridine motif in the 3'-nontranslated region of the HCV genome (Saito *et al.*, 2008). Furthermore, products of host RNA cleavage by ribonuclease (RNase) L, which are characterized by 5'-hydroxyl- and 3'-monophosphate ends, also seem to contribute to RIG-I activation (Malathi *et al.*, 2007). Recently, by applying biochemical and deep sequencing analysis, Baum and colleagues were able to pinpoint the exact nature of RNA molecules that interact with RIG-I under natural conditions, during the course of Sendai virus (SeV) and influenza virus infections (Baum *et al.*, 2010). They conclude that viral replicating RNA constitutes the majority of the viral immunostimulatory RNA associated with RIG-I. It was observed that shorter RNA molecules containing 5'-triphosphorylated ends as well as some dsRNA regions preferentially associate with RIG-I (Baum *et al.*, 2010).

Moreover, two groups independently demonstrated that RIG-I is involved in the sensing of AT-rich dsDNA (Ablasser *et al.*, 2009; Chiu *et al.*, 2009). The synthetic dsDNA mimetic poly(dA:dT) was converted by host RNA polymerase III (Pol-III) into a 5'-triphosphate RNA intermediate, which was in turn recognized by RIG-I in human and mouse cells (Ablasser *et al.*, 2009). It was also shown that in latently EBV-infected cells, EBER molecules are transcribed in large amounts by RNA polymerase III. RNA polymerase III-dependent activation of RIG-I/IPS-1-mediated type I IFN induction coincided with EBER expression (Ablasser *et al.*, 2009). This is in line with the finding that Pol-III inhibition leads to significantly reduced IFN- $\beta$  induction not only by DNA viruses but also by intracellular bacteria (Chiu *et al.*, 2009). Thus, recognition of dsDNA viruses by RIG-I is mediated by an intracellular transcription process that converts DNA into RNA ligands, rather than direct detection of cytoplasmic dsDNA by RIG-I.

Much less is known about the nature of the RNAs that are agonist for MDA5. RIG-I and MDA5 seem to directly discriminate the length of dsRNA. Since shortening of poly(I:C) to  $\leq 1000$  nt converts it into a RIG-I agonist, MDA5 is thought to recognize long dsRNA generated during infection (Kato *et al.*, 2008). Indeed, it was shown that activation of MDA5 requires higher-order RNA structures (Pichlmair *et al.*, 2009).

## 1.4 RLR-mediated signal transduction

RIG-I and MDA5 are able to discriminate their respective RNA ligands by length as well as distinct patterns such as the triphosphate moiety at the 5'-end of the RNA. In addition, both RIG-I and MDA5 are involved in the recognition of a variety of different viruses, which are characterized by differences in their genome complexity and different replication strategies. However, activation of RIG-I and MDA5 orchestrates a complex signaling cascade involving various signaling proteins that ultimately results in the activation of IRF3 and NF- $\kappa$ B to induce type I IFNs and proinflammatory cytokines.

IPS-1 was shown to play a central role in this pathway, since mouse embryonic fibroblasts (MEFs) and conventional DCs lacking *Ips-1* are defective in producing type I IFNs and proinflammatory cytokines in response to all RNA viruses recognized by RIG-I or MDA5 (Kumar *et al.*, 2006; Sun *et al.*, 2006). Taken together, these findings indicated that IPS-1 plays an essential role in RIG-I/MDA5 signaling. Hence, it was

shown that activated RIG-I and MDA5, respectively, interact with IPS-1 through homophilic interactions between CARD domains, leading to the recruitment of downstream signaling molecules. Finally, ligand binding to the RLRs leads to RLR-IPS-1 interaction, which in turn activates downstream signaling molecules such as NF- $\kappa$ B, mitogen-activated protein kinase (MAPK) and IRFs, subsequently resulting in the induction of type I IFNs and proinflammatory cytokines.

Since the first description of RIG-I in 2004, various studies to reveal the complex signaling mechanisms downstream of the RLRs have been performed. Tumor necrosis factor (TNF) receptor-associated factor (TRAF) family members have been demonstrated to be critically involved in this signaling cascade. It was shown that TRAF3, which is known to be an E3 ligase for Lys63-linked polyubiquitination, directly interacts with the TRAF-interacting motif (TIM) located within the proline-rich region of IPS-1 (Saha *et al.*, 2006). Cells lacking TRAF3 showed substantial impairment of the virus-induced signal, indicating the role of TRAF3 in RLR signaling. The function of TRAF3 in turn is regulated by the deubiquitinase DUBA (deubiquitinating enzyme A) (Kayagaki *et al.*, 2007), since an increased RLR-induced type I IFN response was observed when DUBA was absent, whereas DUBA overexpression resulted in a decreased IFN response. DUBA is able to interact with TRAF3, thereby selectively cleaving Lys63-linked polyubiquitin chains on TRAF3, which results in dissociation from the downstream signaling complex containing TBK1 (TRAF family member-associated NF- $\kappa$ B activator (TANK)-binding kinase 1). Therefore, DUBA acts as negative regulator of innate immune responses. In addition, two other TRAF family members, TRAF2 and TRAF6, are also able to interact with IPS-1 (Xu *et al.*, 2005). Subsequently, recruitment of TRAF proteins transmits signals to the downstream protein kinases, inhibitor of NF- $\kappa$ B (I $\kappa$ B) kinase (IKK) family members, which are essential for the activation of transcription factors IRF3, IRF7 and NF- $\kappa$ B, respectively, indicating the essential role of TRAF proteins in the RLR signaling cascade.

Activation of IRF3 and NF- $\kappa$ B by the RLR/IPS-1 complex is mediated by two different signaling pathways. There are two pathways known as the canonical (or classical) pathway and the non-canonical pathway that lead to the activation of NF- $\kappa$ B (Ghosh *et al.*, 1998; Karin, 1999; Zhao *et al.*, 2007). The common regulatory step in both of these cascades is the activation of an IKK complex consisting of catalytic kinase subunits

(Ikk $\alpha$  and/or IKK $\beta$ ) and the regulatory non-enzymatic scaffold protein NEMO (NF- $\kappa$ B essential modulator). On the one hand, the canonical IKK complex and NEMO mediate phosphorylation of I $\kappa$ B, which in turn leads to its subsequent proteasome-dependent degradation allowing functional NF- $\kappa$ B to translocate to the nucleus to activate target genes regulated by  $\kappa$ B sites (Karin and Ben-Neriah, 2000). In contrast, two IKK-related kinases, TBK1 and the inducible I $\kappa$ B kinase (IKK-i), regulate phosphorylation-mediated activation of IRF3 and IRF7 (Fitzgerald *et al.*, 2003; McWhirter *et al.*, 2004; Perry *et al.*, 2004; Sharma *et al.*, 2003). Upon phosphorylation, IRF3/7 form homo- and/or heterodimers that translocate into the nucleus, where they bind to IFN-sensitive responsive elements (ISREs), resulting in the expression of type I IFNs and a set of IFN-inducible genes (Honda *et al.*, 2006; Honda *et al.*, 2005). Cells lacking both IRF3 and IRF7 have been shown to fail to produce type I IFNs in response to viral infection. However, it was demonstrated that the regulatory subunit of the canonical pathway, NEMO, also plays a role in TBK1-IKK-i mediated activation of IRFs (Zhao *et al.*, 2007). In addition, in uninfected cells suppressor of IKK-i (SIKE) interacts with TBK1, sequestering TBK1 from IRF3, while this interaction is disrupted upon viral stimulation leading to TBK1 release and subsequent IRF3 phosphorylation (Huang *et al.*, 2005). Hence, SIKE might sequester TBK1/IKK-i in inactive forms under steady state conditions to avoid unnecessary activation of these kinases. Moreover, while interaction between IPS-1 and TRAF3 is essential for the recruitment of both IKK complexes, TRAF2/6 in contrast is likely to be responsible for NF- $\kappa$ B activation (Saha *et al.*, 2006; Xu *et al.*, 2005).

Furthermore, it was demonstrated that death domain (DD)-containing molecules such as Fas-associated death domain (FADD) and receptor interacting protein 1 (RIP1) contribute to the IPS-1 signaling complex (Balachandran *et al.*, 2004). These molecules activate the NF- $\kappa$ B branch of the signaling pathway via activation of caspase-8 and caspase-10 by interacting with the C-terminal part of IPS-1 (Takahashi *et al.*, 2006). Moreover, TRADD (TNFR-associated DD), another DD-containing protein, was demonstrated to form a complex with IPS-1, TRAF3, TANK and the DD proteins FADD and RIP, thereby activating both IRF3 and NF- $\kappa$ B (Michallet *et al.*, 2008).

STING, a protein designated as stimulator of interferon genes, was identified as regulator of RLR-mediated activation of both NF- $\kappa$ B as well as IRF3 transcription pathways (Ishikawa and Barber, 2008). It was observed that MEFs are highly

susceptible to VSV infection in the absence of STING. A second group independently identified a protein, then called mediator of IRF3 activation (MITA), that acts as adaptor protein to recruit TBK1 and IRF3 to IPS-1 (Zhong *et al.*, 2008). Virus-triggered activation of IRF3 was abolished when MITA was absent. However, MITA in turn is regulated by ring-finger protein 5 (RNF5) that catalyzes Lys48-linked ubiquitination of MITA after viral infection, thereby suppressing an excessive type I IFN response (Zhong *et al.*, 2009).

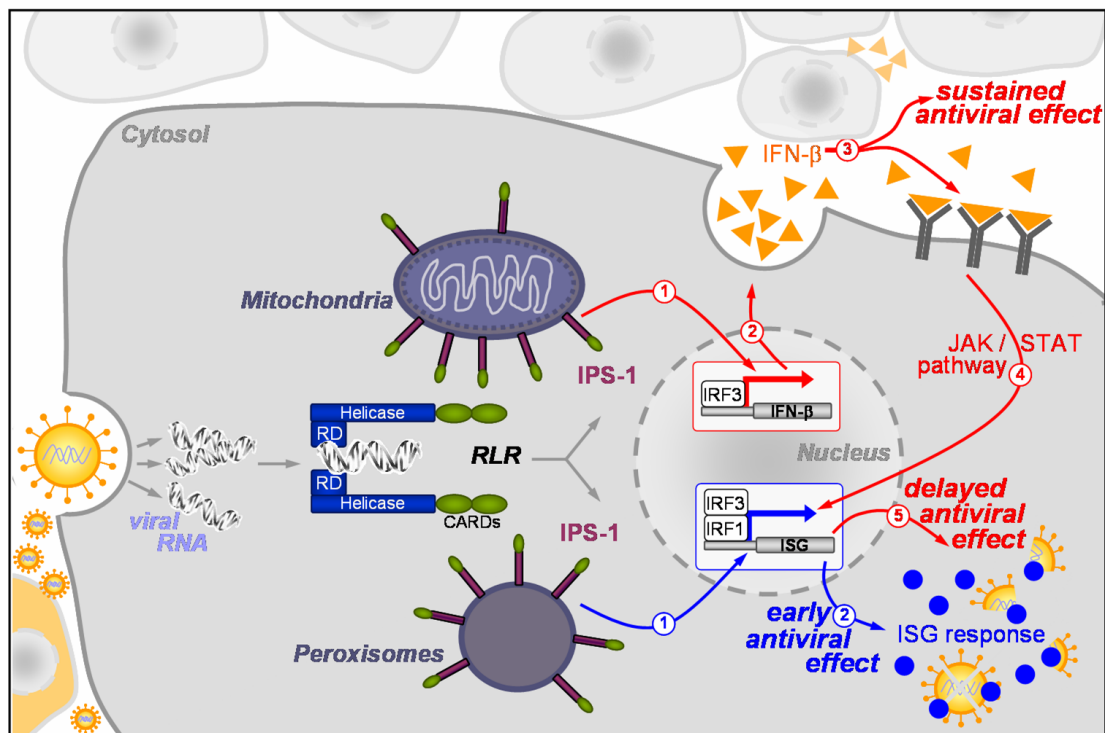


**Figure 2.** *Organelle-specific IPS-1 signaling*

Upon detection of viral RNA by the cytoplasmic RNA helicases, RIG-I and MDA5 interact with the signaling adaptor molecule IPS-1 leading to the induction of type I IFN expression. IPS-1 is expressed on mitochondria as well as peroxisomes. IPS-1 localized to the peroxisomes leads to rapid expression of interferon-stimulated genes (ISGs), which results in an early, but transient antiviral response that is independent of type I IFN. This early antiviral state limits the infection until enough IFN is produced to induce a complete panel of ISGs that can inhibit viral replication and induces an antiviral state. Type I IFN production is mediated by mitochondrial IPS-1. Thus, the mitochondrial IPS-1 establishes a sustained antiviral effect that subsequently initiates the general activation of ISGs via activation of the JAK/STAT pathway upon binding of secreted IFN to the type I IFN receptor. Cooperation between both IPS-1 signaling pathways is necessary for maximal containment of virus replication. (*modified from Dixit et al.*, 2010)

Recently, it was shown that the antiviral response, in which adaptor protein IPS-1 is one of the key players, is not just directly activated in an on- or off-manner. Hence, a recent study by Dixit *et al.* (2010) demonstrated that IPS-1 acts in a temporally and organelle-

specific regulated fashion. As already mentioned, IPS-1 was shown to constitutively associate with not only mitochondria but also peroxisomes. In their study, Dixit and colleagues created three different versions of IPS-1 that each localized exclusively to the cytosol, the mitochondrial membranes or peroxisomal membranes, respectively. Except for the cytosolic form, each IPS-1 variant induced the production of the IFN-induced antiviral protein viperin in response to infection with reovirus, a virus that was shown to trigger both RIG-I and MDA5 antiviral signaling. Interestingly, peroxisomal IPS-1 or wild-type IPS-1 produced viperin within 4 hrs of virus infection, whereas production of viperin by mitochondrial IPS-1 was significantly delayed (Dixit *et al.*, 2010). Thus, it is suggested that peroxisomal IPS-1 is essential for the rapid expression of antiviral genes resulting in an early but transient antiviral response that is independent of type I IFN. This early antiviral state curbs the infection until enough interferon is produced to induce the expression of a complete panel of interferon-stimulated genes (ISGs) and to halt viral replication permanently. In contrast, IPS-1 which is localized to the mitochondria activates the signaling pathway that finally results in the production of type I IFN, which in turn leads to the expression of ISGs inducing a sustained antiviral effect that is amplified by activation of the JAK/STAT pathway upon binding of secreted IFN to the type I IFN receptor. Taken together, the current understanding of RLR-mediated signaling transduction involves recruitment of the activated RLRs to both peroxisomal or mitochondrial IPS-1 to induce distinct signaling cascades leading to the activation of IRF3 and NF- $\kappa$ B and subsequently resulting in the induction of type I IFN and proinflammatory cytokines in an organelle- and time-dependent fashion.

## **1.5 Regulation of RLR signaling by cellular proteins**

PRR-mediated signaling is rapidly activated upon viral infection, leading to the production of type I IFNs and proinflammatory cytokines. However, the overproduction of type I IFNs can cause unwanted or excessive immune responses that may lead to allergy, necrosis, autoimmune diseases or other harmful effects (Theofilopoulos *et al.*, 2005). Thus, PRR-mediated type I IFN induction must be tightly regulated. Therefore, the host has evolved various mechanisms to prevent unnecessary activation in the steady state or excessive signaling under viral infection conditions.

### 1.5.1 Role of ubiquitination for activation and degradation of RIG-I

It was demonstrated that multiple steps in the signaling cascade, including activation of TBK1 and IKK, as well as nuclear import of NF- $\kappa$ B, are controlled by the ubiquitin system through both regulatory and degrading mechanisms (Bhoj and Chen, 2009). In addition, there are several reports demonstrating that post-translational modification of RLRs plays a critical role in their regulation.

Ubiquitination of RIG-I itself was demonstrated to be crucial for RIG-I-mediated antiviral activity (Gack *et al.*, 2007). The CARDs of RIG-I have been shown to specifically interact with the tripartite motif 25 (TRIM25) E3 ligase that delivers Lys63-linked ubiquitin to the Lys172 residue of RIG-I CARD2. The data clearly indicate that the ubiquitination of RIG-I CARD2 by TRIM25 is essential for IPS-1 binding as well as the ability of RIG-I to induce antiviral signal transduction. In a second study, Riplet/RNF135 was identified as alternative factor that promotes RIG-I activation independent of TRIM25 (Oshiumi *et al.*, 2008). RNF135 has also been identified as REUL in a study by Gao *et al.* (2009). In a recent report, the RIG-I signaling cascade was recreated in a cell-free system (Zeng *et al.*, 2010). Zeng and colleagues show that RIG-I activation by RNA promotes recruitment of unanchored Lys63-linked ubiquitin chains to the CARDs. Thus, it is suggested that unanchored ubiquitin chains together with RIG-I form a potent viral RNA sensor that directly communicates with IPS-1 to promote IRF3 activation ultimately resulting in an antiviral response (Zeng *et al.*, 2010).

However, ubiquitination of RIG-I can also lead to inhibition of RIG-I-mediated signaling. ISG15, one of the proteins strongly induced upon viral infection, is conjugated to RIG-I leading to its ubiquitination-mediated degradation by the proteasome (Kim *et al.*, 2008; Theofilopoulos *et al.*, 2005; Zhao *et al.*, 2005). Arimoto *et al.* (2007a) demonstrated that UbcH8 facilitates conjugation of ISG15 to RIG-I. RNF125 was reported to be involved in ubiquitination-mediated degradation of RIG-I, respectively (Arimoto *et al.*, 2007b). In addition, CYLD (cylindromatosis), a deubiquitinating enzyme, removes polyubiquitin chains from RIG-I and TBK1, which coincides with the inhibition of the IRF3 signaling pathway (Friedman *et al.*, 2008).

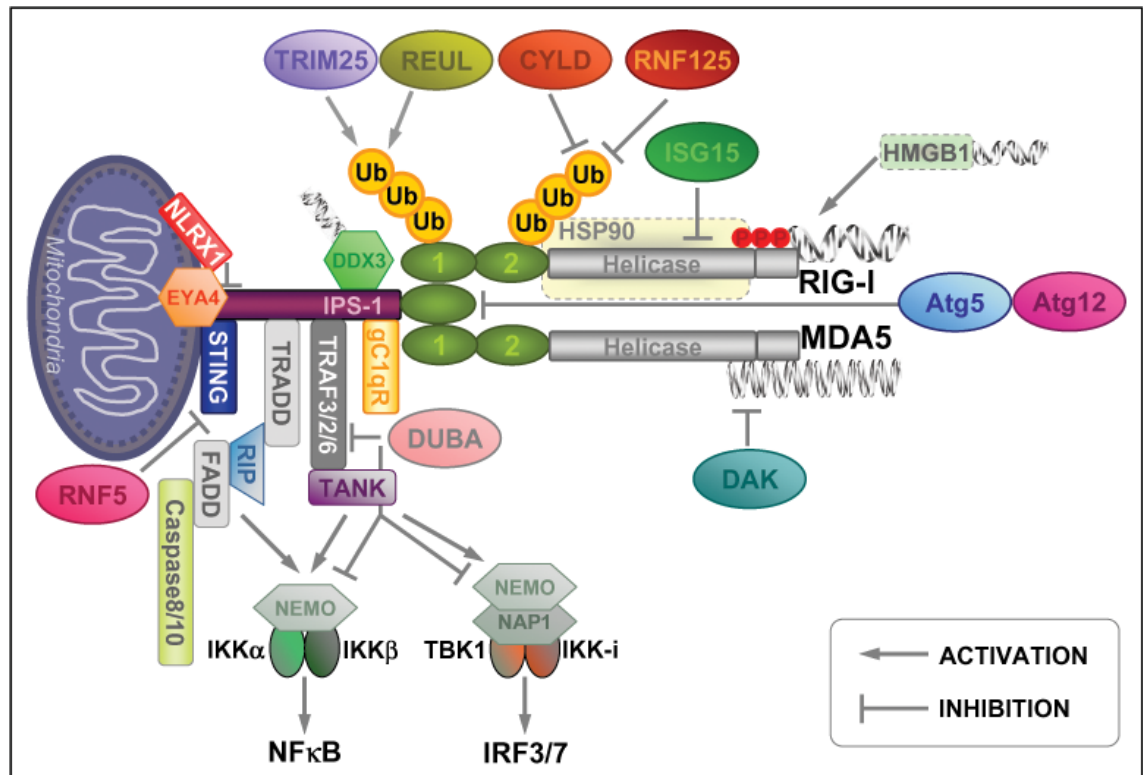


**Figure 3.** *RLR-mediated signal transduction and its regulation*

RIG-I and MDA5 are activated by different RNA ligands. RIG-I preferentially recognizes short dsRNA bearing a 5'-ppp moiety, whereas MDA5 responds to long dsRNA. Upon activation, RIG-I and MDA5 interact with IPS-1 and recruit signaling molecules, including TRAF2/3/6, TRADD, FADD and RIP as well as caspase-8 and -10, leading to activation of NF-κB and IRF3/7, respectively. Signaling is regulated by numerous kinds of regulatory molecules. The mitochondrial proteins NLRX1 and STING interact with IPS-1 and act as negative regulators. EYA4 associates with IPS-1, STING and NLRX1 acting as enhancer of the innate immune response. The function of STING is negatively regulated by RNF5-mediated Lys48-linked ubiquitination. Upon virus infection gC1qR is translocated to IPS-1, which results in inhibition of both IRF3 and NFκB activation. Complex formation between IPS-1 and DDX3 is important in the early response to virus infection by encountering viral RNA before RIG-I levels are upregulated. The Atg5-Atg12 complex, which plays a key role in autophagy, disrupts the CARD-CARD interactions of RIG-I and IPS-1. TRIM25 and REUL independently conjugate Lys63-linked ubiquitins to the RIG-I CARDS, thereby leading to full activation of RIG-I. CYLD is a negative regulator that removes polyubiquitin chains from RIG-I. In addition, RNF125 and conjugation of ISG15 negatively regulate the RIG-I pathway by ubiquitin-mediated degradation of RIG-I. Direct association of RIG-I and HSP90 is necessary for the stability of RIG-I since loss of this interaction leads to proteasomal degradation of RIG-I. HMGB1 proteins function as co-ligands in PRR signaling, allowing a more efficient and subsequent recognition of the ligand. DAK selectively inhibits MDA5 via direct interaction. DUBA interacts with TRAF3 to induce its deubiquitination, resulting in dissociation of TRAF3 from TBK1. (adapted from Yoneyama and Fujita, 2009)

Interestingly, in addition to the tightly regulated protein conjugation mechanisms, that control both the stability and signaling function of RIG-I, described above, RIG-I is

regulated by several other mechanisms. It was shown that RIG-I directly associates with heat shock protein (HSP) 90. Inhibition of this interaction leads to ubiquitination and proteasomal degradation of RIG-I (Matsumiya et al., 2009). In line with this, HMGB1 (high-mobility group box protein) has been described to interact with RIG-I as well as TLR9 (Yanai et al., 2009). It is suggested that binding of nucleic acids to HMGB1 is a prerequisite for the more efficient recognition by PRRs and subsequent activation of PRRs. Thus, HMGB1 functions as co-ligand in PRR signaling.

### **1.5.2 RIG-I splice variant functions as off-switch regulator of its own pathway**

In addition to ubiquitination, alternative splicing was shown to be involved in the regulation of RIG-I-mediated antiviral innate immune signaling (Gack *et al.*, 2008). In a second study, (Gack *et al.*, 2008) demonstrated the existence of a RIG-I splice variant whose expression is robustly upregulated upon viral infection and type I IFN treatment. The RIG-I splice variant lacks a short amino acid stretch within the CARD1 of RIG-I (AA 36-80) and thereby loses TRIM25 binding (Gack *et al.*, 2008). RIG-I splice variant is able to bind RNA and forms a complex with wild-type RIG-I. Hence, the formation of the RIG-I-WT/splice-variant complex abolishes interaction of RIG-I and IPS-1 and subsequently inhibits RIG-I-mediated IFN induction.

### **1.5.3 Regulation of MDA5**

MDA5-mediated signaling is controlled by DAK, a functionally unknown dihydroxyacetone kinase, which in coimmunoprecipitation experiments interacted with MDA5, but not RIG-I (Diao *et al.*, 2007). It was proposed that upon binding to dsRNA, the conformational change of MDA5 results in its higher affinity to IPS-1 compared to DAK. This was supported by the observation that MDA5 is disassociated with DAK upon viral infection. Thus, DAK seems to keep MDA5 inactive under steady state conditions (Diao *et al.*, 2007). Based on their findings, Diao and colleagues proposed a model for the action of DAK in which the terminal cyclase domain of DAK is able to sequester MDA5 in an inactive form upon binding to its N-terminal CARDS. Upon viral infection, MDA5 binds to viral RNA, causing a conformational change of the molecule that in turn leads to the release of DAK, allowing MDA5 to recruit the adapter protein IPS-1 and activating the type I IFN pathways.

### 1.5.4 Regulation of RLR signaling at the level of IPS-1

To prevent overproduction of type I IFN, the signaling cascade is not only regulated at the level of the RLRs. It has been demonstrated that the central adapter of the RLR-mediated innate immune signaling, IPS-1, is targeted by various proteins that mostly regulate IPS-1-RLR interaction, resulting in an either enhanced or reduced initiation of downstream signaling.

The first protein identified to act as regulator of IPS-1 is NLRX1, a highly conserved nucleotide-binding domain (NBD) and leucine rich repeat (LRR) containing family member (known as NLR). NLRX1 was shown to localize to the outer mitochondrial membrane, where it interacts with IPS-1 (Moore *et al.*, 2008). Ectopic expression of NLRX1 results in potent inhibition of RLR-IPS-1-mediated IFN activation and in the disruption of virus-induced RLR-IPS-1 interactions. NLRX1 and IPS-1 in turn are regulated by the threonine-phosphatase activity of a protein called Eyes absent 4 (EYA4) (Okabe *et al.*, 2009). EYA4 associates with IPS-1, STING and NLRX1 and acts as enhancer of the innate immune response by modulating the phosphorylation state of these signal transducers.

In addition, the interaction of RLRs and IPS-1 is blocked by the Atg5-Atg12 conjugate (Jounai *et al.*, 2007), that is known to be critically involved in autophagic processes. Autophagy has been implicated in the defense against infection with intracellular bacteria and viruses, respectively (Gutierrez *et al.*, 2004). Jounai and colleagues demonstrated that VSV infection induces higher levels of IRF3 phosphorylation as well as IFN- $\beta$  and IP10 in MEFs lacking Atg5 expression compared to wild-type cells. Further investigation revealed a direct interaction between the Atg5-Atg12 conjugate and RIG-I or MDA5, that is further enhanced by viral infection. Hence, Atg5-Atg12 disrupts the CARD-CARD interactions between the RLRs and IPS-1 (Jounai *et al.*, 2007), thereby suppressing RLR signaling. A recent study described designated receptor for globular domain of complement component (gC1qR) as another protein that interacts with IPS-1 (Xu *et al.*, 2009). SeV infection causes translocation of gC1qR to the mitochondria and enhances its association with IPS-1. Furthermore, overexpression of gC1qR inhibits RIG-I-mediated activation of IRF3 and NF $\kappa$ B. Conversely, RNAi knockdown of gC1qR enhanced the production of IFN- $\beta$  (Xu *et al.*, 2009). In addition,

mechanistic studies revealed a regulatory role for FLN29, which is an IFN-inducible gene, in the RLR pathway through interaction with IPS-1 (Sanada *et al.*, 2008).

In the early phase of viral infection, specific enhancement of the IPS-1 signaling pathway seems to play a key role. DDX3, which is a DEAD box helicase that is constitutively expressed, was reported to colocalize with IPS-1 around the mitochondria. Furthermore, Oshiumi *et al.* (2010) revealed that the C-terminal part of DDX3 directly binds to the IPS-1 CARD, and the whole DDX3 was also shown to associate with RIG-I. In the cytoplasm, there are large amounts of DDX3 and only trace amounts of RIG-I in resting cells. Therefore, when the virus initially infects human cells, the viral RNA seems to encounter DDX3 before RIG-I captures the viral RNA. It was demonstrated that the initial IPS-1 complex for RNA-sensing involves DDX3 in addition to trace RIG-I to cope with the early phase of infection. Thus, a minute amount of viral RNA is sufficient to activate IPS-1-mediated signaling (Oshiumi *et al.*, 2010). Recently, it was shown that Tom70 (translocase of outer membrane 70), a mitochondrial receptor, interacts with IPS-1 upon RNA virus infection. The clamp domain of Tom70 was shown to interact with HSP90, which also interacts with RIG-I, thereby recruiting TBK1/IRF3 to the mitochondria and boosting the antiviral response (Liu *et al.*, 2010).

Moreover, further characterization of IPS-1 revealed the existence of three splice variants (named IPS-1a, -1b and -1c) that display diverse biological activity (Lad *et al.*, 2008). Unlike IPS-1 that activates the IRF3 as well as the NF- $\kappa$ B pathway, variant 1b interacts with RIP1 and FADD, thereby selectively activating the IFN- $\beta$  promoter. In contrast, variant 1c represents a truncated form of IPS-1 which has no activity on either the IRF3 or NF- $\kappa$ B pathway, whereas IPS-1a does not share sequence homology with known proteins (Lad *et al.*, 2008).

### **1.5.5 Other mechanisms involved in the regulation of RLR signaling**

Recent studies revealed a new facet to the regulation of the innate host defense against viruses through identification of yet unrecognized functions of micro RNAs (miRNAs) as well as catabolic mechanisms in the regulation of RLRs.

miRNAs, an abundant class of highly conserved small (18-25 nt long) non-coding RNAs, are known to suppress gene expression by binding to the 3'-untranslational region of target mRNAs. miRNAs play key roles in the regulation of diverse biological processes, such as development, infection, immune response, inflammation and tumorigenesis (Bushati and Cohen, 2007). Hou *et al.* (2009) identified miRNA-146a as novel negative feedback regulator of RIG-I signaling and RIG-I-dependent antiviral pathways. miRNA-146 is upregulated by VSV infection, suggesting a new strategy of viral escape from the antiviral immune response (Hou *et al.*, 2009).

As already mentioned, autophagy was demonstrated to be utilized by cells of the innate and adaptive immune systems, respectively, to combat viral infections (Levine and Deretic, 2007). Tal *et al.* (2009) recently observed a link between the accumulation of reactive oxygen species (ROS) in cells defective in autophagy and a dysregulation of the RLR pathway. Cells lacking Atg5 expression show increased levels of IPS-1 protein and an increase in RLR signaling. Furthermore, these cells accumulate ROS localized to the mitochondria (Tal *et al.*, 2009). Depletion of ROS by antioxidant treatment significantly diminished the amplified RLR signaling phenotype in Atg5-deficient cells. Thus, such ROS-dependent activation of RLR, together with the increased IPS-1 levels, account for the functional augmentation of the RLR pathway and viral clearance in the absence of autophagy (Tal *et al.*, 2009). In line with this, the enzyme NOX2, a NADPH oxidase that is involved in the generation of high amounts of ROS, known as oxidative burst, in phagocytic cells, has been shown to be critical for the host cell to trigger an efficient RIG-I-mediated IRF3 activation in response to SeV infection (Soucy-Faulkner *et al.*, 2010).

Collectively, the RLR-mediated signaling pathway is regulated by multiple molecules, which exert their distinct functions not only at the level of the RLRs or IPS-1, but also regulate downstream signaling proteins. Notably, most of them function as negative regulators to prevent unwanted or prolonged activation of antiviral signaling which may be harmful for the host. Moreover, these regulators themselves are in turn controlled by other molecules.

## 1.6 Interaction between RLRs and viral proteins

Host and virus have exerted powerful selective pressure on each other throughout their evolution. The type I IFN system is the first line of defense against invading viruses. Therefore, it serves as a strong selective pressure for viral evolution (Akira and Takeda, 2004). On the other hand, the molecules involved in the signal transduction system are targeted by various viral components, which play a role in viral replication and assembly as well as pathogenesis, to evade host antiviral immunity (Bowie and Unterholzner, 2008).

### 1.6.1 Viral escape from recognition by the RLR system

Viruses seem to be smart in a way that they are aware of the mechanisms by which the host distinguishes self and non-self RNA (see chapter 1.3.6). They have evolved various mechanisms to evade the immune response of the host. A number of proteins encoded by viral genomes can process viral RNA and mimic the modifications of host RNA, thereby evading the detection by PRRs (Furuichi and Shatkin, 2000). For example, the 5'-terminus of picornavirus RNA such as the EMCV genome, which is selectively recognized by MDA5, was shown to be masked by the covalently linked viral peptide VPg (Flanegan *et al.*, 1977). It has also been reported that the viral genomes of Hantaan virus, Crimean-Congo hemorrhagic fever virus and Borna disease virus escape RIG-I signaling by selectively modifying their 5'-ppp structure into a 5'-monophosphate in infected cells (Habjan *et al.*, 2008; Schneider *et al.*, 2005). In line with this, formation of an m7Gppp cap structure at the 5'-end of viral RNAs also leads to viral immune escape (Chen *et al.*, 2009; von Grotthuss *et al.*, 2003). Poxviruses, which replicate in the cytoplasm, encode their own RNA capping machinery, thereby subverting the antiviral response of the infected host. Moreover, influenza A virus has evolved a strategy to mask its 5'-ppp structure by attaching capped 5'-fragments from cellular mRNA to its own genomic RNA (Plotch *et al.*, 1981), thereby actively exploiting the cellular mRNA of the infected host cell to evade from innate immune recognition.

However, many viruses produce dsRNA at some stage during their replication cycle, which is recognized by PRRs of the host cell. Therefore, some viral genomes encode dsRNA-binding proteins to avoid the innate antiviral immune response that is initiated by RLRs upon recognition of viral RNA. Vaccinia virus E3 protein (Chang *et al.*, 1992)

and Ebola virus VP35 (Cardenas *et al.*, 2006; Haasnoot *et al.*, 2007) have been shown to function as RNA-binding proteins. Furthermore, the non-structural protein 1 (NS1) of influenza A virus possesses RNA-binding capacity (Garcia-Sastre *et al.*, 1998), respectively. Thus, by expression of these proteins viruses actively shield their dsRNA structures generated during infection and viral replication from recognition by RLRs.

## **1.6.2 Disruption of the interaction of signaling molecules**

As already mentioned, virus-triggered induction of type I IFNs and proinflammatory cytokines depends on the interactions of various signaling molecules. To block the signaling cascades that lead to the establishment of an antiviral state and the restriction of virus replication, many viral proteins directly interact with the key signaling molecules to inhibit their function. Several viral proteins have been shown to be able to disrupt the RIG-I/MDA-5/IPS-1 signaling pathway by sequestering viral RNA from helicase binding and/or disrupting helicase interaction with downstream signaling molecules or by increasing protein degradation.

Influenza A NS1 protein employs the first two mechanisms to block RIG-I-mediated IFN induction (Wang *et al.*, 2002). Furthermore, it was shown that the influenza virus NS1 protein colocalizes with IPS-1 (Mibayashi *et al.*, 2007), suggesting the formation of a RIG-I/IPS-1 complex that subsequently leads to inhibition of downstream signaling. The G protein of human metapneumovirus directly interacts with RIG-I, thereby inhibiting IPS-1-mediated IFN I induction (Bao *et al.*, 2008), as well. In addition, Lu *et al.* (2008) observed that RIG-I/MDA5 signaling to IRF3 was inhibited by the V protein of human parainfluenza virus 2 (hPIV2), parainfluenza virus 5 (PIV5) and mumps virus (MuV), respectively. A recent study reported the involvement of rabies virus nucleoprotein (N) in the evasion of RIG-I activation by interfering with nuclear translocation of IRF3 (Masatani *et al.*, 2010).

Table 2. *Viral inhibitors of RLR signaling*

<b>virus species</b>	<b>inhibitors</b>	<b>target(s)</b>	<b>proposed mechanism</b>
<b>Viral escape from recognition by the RLR system</b>			
<b>Encephalomyocarditis virus</b>	5'-VPg		
<b>Poliovirus</b>		viral RNA	sequestration of RNA from RIG-I
<b>Vaccinia virus</b>	E3L		
<b>Influenza A virus</b>	NS1		
<b>Ebola virus</b>	VP35		
<b>Hantaan virus</b>			
<b>Crimean-Congo hemorrhagic fever</b>	phosphatase	viral RNA	monophosphorylation of 5'-end of viral RNA
<b>Borna disease virus</b>			
<b>SARS</b>	Nsp14, Nsp16	viral RNA	formation of a m7Gppp cap structure at the 5'-end of viral RNAs
<b>Poxviruses</b>			
<b>Influenza A virus</b>		viral RNA	snatching 5'-capped cellular mRNA to viral RNA
<b>Disruption of the interaction of signaling molecules</b>			
<b>Influenza A virus</b>	NS1	RIG-I	sequestration of RIG-I
<b>Human metapneumovirus</b>	G protein		
<b>parainfluenza virus 2</b>		TBK1/IKK-i	inhibition of IRF3 activation by acting as alternative substrates for TBK1/IKK-i
<b>parainfluenza virus 5</b>	V protein		
<b>mumps virus</b>			
<b>Rabies virus</b>	N protein	IRF3	inhibition of RIG-I downstream signaling
<b>Paramyxoviruses</b>	V protein	MDA5	sequestration of MDA5
<b>Hantavirus</b>	G protein	TBK1/ TRAF3	disruption of TBK1-TRAF3 interaction
<b>Cleavage or degradation of signaling molecules</b>			
<b>Poliovirus</b>	NS5A	MDA5	caspase- and proteasome-dependent cleavage of MDA5
<b>Picornaviruses</b>		RIG-I	cleavage of RIG-I
<b>Hepatitis C virus</b>	NS3/4A		
<b>GB virus</b>	NS3/4A		
<b>Hepatitis A virus</b>		IPS-1	cleavage of IPS-1
<b>Human rhinovirus 1</b>	viral protease		

Similarly, V proteins of paramyxoviruses have been shown to bind MDA5 resulting in inhibition of MDA5-mediated IFN- $\beta$  production (Andrejeva *et al.*, 2004; Childs *et al.*, 2007). As paramyxoviruses are sensed by RIG-I, the biological meaning of this specific MDA5 inhibition is not obvious, yet. However, it was reported that SeV defective interfering (DI) particles of the copy back type, which arise as mistakes of viral replication that occur when the viral polymerase releases from the genomic template and resumes synthesis at the nascent strand of template, could be detected by MDA5 (Yount *et al.*, 2008), while recognition of SeV is mediated by RIG-I. Hantavirus directly targets TRAF3, which is an essential part of the downstream signaling cascade, to inhibit RIG-I-mediated signal transduction. A study by Alff *et al.* (2006) revealed that ectopic expression of the cytoplasmic tail of Hantavirus G protein leads to inhibition of RIG-I and TBK-1 directed transcription of ISRE or IFN- $\beta$  promoters by interacting with TRAF3 that in turn disrupts the formation of TBK1-TRAF3 complexes which are required for downstream signaling responses (Alff *et al.*, 2008).

### **1.6.3 Cleavage or degradation of signaling molecules**

Viral proteins are rather efficient in the inhibition of innate immune signaling by employing the previously described evasion strategies, including active modification of the viral RNA, masking of RNA by formation of RNA-protein complexes as well as formation of inhibitory complexes either with RIG-I, MDA5 and IPS-1 or downstream signaling molecules such as TBK1. However, cleavage of signaling molecules seems to be the easiest way to stop RLR-mediated signal transduction immediately upon the onset of virus infection. In line with this, cleavage products of MDA5 have been observed in cells infected with poliovirus, a prototypic picornavirus (Barral *et al.*, 2007). It was shown that degradation of MDA5 in poliovirus-infected cells occurs in a proteasome- and caspase-dependent manner. Cleavage of MDA5 might be a mechanism to antagonize the production of type IFN in response to poliovirus infection allowing efficient viral replication without the pressure of elimination by the innate immune signaling. However, inhibition of MDA5 cleavage does not result in higher poliovirus titers (Barral *et al.*, 2007). Thus, the functional role of this mechanism needs to be further characterized. Infection with picornaviruses such as poliovirus, rhinovirus, echovirus and EMCV, also induces degradation of RIG-I (Barral *et al.*, 2009). In

contrast to MDA5, cleavage of RIG-I is not accomplished by cellular caspases or the proteasome. Rather, a proteinase encoded by the virus directly cleaves RIG-I.

The next level of RLR-mediated signaling is IPS-1 suggesting that cleavage of IPS-1 might be an easy way to circumvent RLR-mediated downstream signaling. Hence, cleavage of the shared RLR adapter molecule IPS-1 was demonstrated to be a regulatory mechanism utilized by the flaviviruses hepatitis C virus (HCV) (Li *et al.*, 2005; Meylan *et al.*, 2005) and GB virus B (GB-V) (Chen *et al.*, 2007) as well as the picornavirus family members hepatitis A virus (HAV) (Yang *et al.*, 2007a) and human rhinovirus (HRV1) (Drahoš and Racaniello, 2009). HCV encodes the non-structural protein NS3/4A that cleaves polypeptide precursors into mature and functional proteins during viral replication. In addition to its function in the viral replication cycle, the HCV NS3/4A protease specifically targets IPS-1 by cleaving it at position C508, thereby dislocating it from the outer mitochondrial membrane (Li *et al.*, 2005; Meylan *et al.*, 2005). Furthermore, virus-induced IKK- $\beta$  strongly colocalized with IPS-1 at the outer mitochondrial membrane, and the localization of both was disrupted by NS3/4A expression (Lin *et al.*, 2006). Mutation of the C508 residue to alanine was sufficient to maintain mitochondrial localization of IPS-1 and IKK- $\beta$  in the presence of NS3/4A. Interestingly, IPS-1 was also found to be localized to the cytosol in liver tissues of patients chronically infected with HCV (Loo *et al.*, 2006). Inhibitors of the HCV NS3/4A protease, which have originally been designed to inhibit HCV replication, are able to prevent IPS-1 cleavage, thereby restoring the RIG-I-mediated immune response to HCV (Johnson *et al.*, 2007). GB virus B is phylogenetically the closest relative to HCV and is used as a surrogate model for HCV. Like HCV, GB-V NS3/4A protease specifically cleaves IPS-1 and dislodges it from the mitochondria (Chen *et al.*, 2007). In contrast, upon hepatitis A virus infection the 3ABC precursor of its 3C<sup>pro</sup> protease is targeted to the mitochondria where it colocalizes with and subsequently cleaves IPS-1 (Yang *et al.*, 2007a). Thus, HAV disrupts host signaling by a mechanism that parallels that of the serine NS3/4A protease of hepatitis C virus, but differs in its use of a stable, catalytically active polyprotein processing intermediate. Moreover, in case of human rhinovirus 1 infection, cleavage of IPS-1 was demonstrated to be facilitated by two viral proteases (Drahoš and Racaniello, 2009).

## 1.7 Involvement of RLRs in autoimmunity

As already mentioned, *Rig-I* knockout mice that were generated to gain more information on the function of RIG-I *in vivo* are not viable (Kato *et al.*, 2005). Furthermore, it was observed that knockout of *Lgp2* leads to a defect in the development of the vagina of female mice homozygous for *Lgp2* KO and homozygous progeny was lower than the expected Mendelian ratio (Sato *et al.*, 2010). Therefore, it was speculated that RLRs also might play a role in processes other than antiviral signaling.

Interestingly, a point mutation in the *IFIH1* gene, encoding RLR family member MDA5, has been linked to a human autoimmune disease, type I diabetes (Nejentsev *et al.*, 2009). In this study, ten candidate genes in a pool of DNAs from patients suffering from type I diabetes were sequenced and their disease association was tested. This screen revealed four rare variants of *IFIH1* that lowered type I diabetes risk independently of each other (Nejentsev *et al.*, 2009). All four variants have predicted biological effects such as truncation of the protein or affecting essential splicing positions. The study suggested that variants, which are predicted to reduce the function of the IFIH1 (MDA5) protein, decrease the risk of type I diabetes, while normal IFIH1 function is associated with the disease (Nejentsev *et al.*, 2009). Interestingly, infection with enteroviruses, which belong to the picornavirus family, is more common among newly diagnosed type I diabetes patients and prediabetic subjects than in the general population and precedes the appearance of autoantibodies which are markers of prediabetes (Hyoty and Taylor, 2002).

The demonstration that MDA5 is linked to the development of type I diabetes, suggested that also RIG-I might play a role in this process. As described previously, so far *in vivo* studies to analyze RIG-I have been limited by the high lethality of *Rig-I* KO mice that suffered from fetal liver degeneration (Kato *et al.*, 2005), already indicating that there might be a link between RLRs and their involvement in processes other than antiviral signaling, such as mammalian development. To further study the biological function of RIG-I, Wang *et al.* (2007) generated *Rig-I* deficient mice taking a different strategy to the one previously reported by Kato *et al.* (2008). The disruption of the *Rig-I* locus was confirmed by northern blotting and western blotting, respectively. Surprisingly, these mice developed normally, were viable and fertile (Wang *et al.*,

2007). Thus, the different outcomes between the two different mutant mice likely result from targeting different regions of the *Rig-I* gene. However, the KO mice generated by Wang and colleagues displayed significant age-dependent loss of body weight. Extensive pathological analysis revealed that 70 % of adult *Rig-I* KO mice spontaneously developed a colitis-like phenotype with increased susceptibility to DSS-induced colitis (Wang *et al.*, 2007). Inflammatory bowel diseases (IBD), including Crohn's disease and ulcerative colitis, are considered to be associated with a breakdown of tolerance to the resident intestinal flora (Duchmann *et al.*, 1995) and immune activation in the gut-associated lymphatic tissue (GALT) consisting of Peyer's patches, mesenteric lymph nodes and immune cells in the lamina propria. Coinciding with this, mutant mice showed a dramatically decreased number of Peyer's patches. Furthermore, these *Rig-I* KO mice were characterized by an increase in effector T cells, whereas the naïve T cell population was decreased. In addition, RIG-I deficiency leads to the downregulation of G protein  $\alpha 2$  subunit (*G $\alpha$ i2*). In line with this, reporter assays demonstrated that RIG-I regulates the transcriptional activity of *G $\alpha$ i2*. Regulation of the *G $\alpha$ i2* promoter may be mediated by the activation of the NF- $\kappa$ B pathway (Arinze and Kawai, 2005). Thus, the development of colitis seems to be associated with downregulation of the *G $\alpha$ i2* gene and disturbed T cell homeostasis (Wang *et al.*, 2007). Another study reported the expression of RIG-I protein in renal biopsy specimens obtained from patients with lupus nephritis (Suzuki *et al.*, 2007). In line with this observation, high expression levels of *RIG-I* mRNA were detected in the urinary sediment of patients suffering from lupus nephritis (Tsugawa *et al.*, 2008). This study also showed decreased RIG-I expression levels following immunosuppressive treatment. Recently, IFN- $\gamma$  was found to induce expression of *RIG-I* in human mesangial cells (Imaizumi *et al.*, 2010), which are specialized cells that reside around blood vessels in the kidneys. As described previously, the IRF family of transcription factors plays important roles in the expression of genes involved in inflammatory and immune reactions. Among them IRF1 and IRF7 are known to be induced by IFNs (Steinberg *et al.*, 2009). Examination of the role of RIG-I in the expression of IRF1 and/or IRF7 induced by IFN- $\gamma$  revealed that knockdown of RIG-I expression inhibits IFN- $\gamma$  induced upregulation of IRF7, whereas it had no effect on IRF1 (Imaizumi *et al.*, 2010). Thus, Imaizumi and colleagues speculate that the expression of RIG-I in glomerular lesions reflects regional inflammatory processes, which may be involved in

the pathogenesis of lupus nephritis. However, it is currently still unclear how RLRs are activated by endogenous ligands in the situations described above.

Recently, several studies provided evidence that defects in the nucleic acid metabolism affecting the quantity or quality of nucleic acids or altering their spatial and temporal distribution within the cell can lead to inappropriate activation of nucleic acids sensors, thereby causing autoimmune disorders. It was shown that three prime repair exonuclease 1 (TREX1) deficiency results in intracellular accumulation of DNA and a type I IFN response that is independent of the TLR pathway (Yang *et al.*, 2007b). TREX1, also called DNase III, is responsible for the major 3'→5' DNA exonuclease activity in mammalian cells and polymorphisms of *TREX1* were described to be associated with Aicardi-Goutières syndrome (AGS) (Crow and Rehwinkel, 2009; Mazur and Perrino, 2001). AGS is a genetically determined encephalopathy demonstrating phenotypic overlap both with the complications of congenital viral infection, which are however not detected in this syndrome, and with systemic lupus erythematosus (SLE) (Crow and Rehwinkel, 2009). Interestingly, AGS is characterized by elevated IFN- $\alpha$  levels combined with increased numbers of lymphocytes in the cerebrospinal fluid (Goutieres, 2005; Lebon *et al.*, 1988). IFN- $\alpha$  seems to have a critical role for the pathogenesis of this disorder, since transgenic mice overexpressing IFN- $\alpha$  in astrocytes show similar pathology (Akwa *et al.*, 1998). In addition to *TREX1*, mutations in at least four more genes, the three subunits of ribonuclease H2 (*RNASEH2*) and the putative regulator of innate immune responses sterile alpha motif domain and HD domain-containing protein 1 (*SAMHD1*), are involved in the development of AGS (Crow *et al.*, 2006; Rice *et al.*, 2009). As TREX1 and RNASEH2 are nucleases, these proteins are involved in the removal of 'waste' nucleic acids (Alarcon-Riquelme, 2006; Stetson *et al.*, 2008; Yang *et al.*, 2007b). Taken together, these observations suggest that in the absence of TREX1, RNASEH2 and SAMHD1 activity, endogenous nucleic acids are accumulated and sensed as non-self, leading to the induction of an IFN-mediated immune response by cytosolic nucleic acid sensors such as RIG-I. Thus, defects in the regulation of the cellular nucleic acid metabolism define a novel cell-intrinsic, TLR-independent mechanism for the initiation of autoimmunity by stimulatory nucleic acids.

Taken together, these studies indicate that RLRs not only selectively protect the host cell by eliciting antiviral responses, but are also involved in the development of autoimmune and inflammatory diseases, either by direct modification of the RLR gene

or regulation of host cell factors, hence resulting in dysfunction of the cellular homeostasis.

## 2 AIMS OF THE STUDY

The current understanding of the recognition of RNA viruses independently of TLRs, involves the activation of the members of the RIG-I-like receptor family, RIG-I, MDA5 and LGP2. These molecules in the cytoplasm of the infected cell trigger a downstream signaling cascade, which finally results in the production of type I interferon and proinflammatory cytokines, subsequently leading to rapid virus elimination and the establishment of an antiviral state. Although it had been shown that RIG-I is specifically activated by a triphosphate group at the 5'-end of viral or synthetic RNA (Hornung *et al.*, 2006; Pichlmair *et al.*, 2006), the mechanisms involved in this specific ligand recognition were unknown when this study was started. At that time, it was established that initiation of downstream signaling by RIG-I involves CARD-CARD interactions with IPS-1 as well as the activity of the helicase domain, which is located in the central part of the RIG-I molecule and interacts with dsRNA unspecifically (Kumar *et al.*, 2006; Seth *et al.*, 2005; Sun *et al.*, 2006; Yoneyama *et al.*, 2004). However, it was unclear which part of the RIG-I molecule specifically interacts with the ligand 5'-triphosphate RNA. One publication by Saito *et al.* (2007) suggested that a repressor domain, which was mapped to the C-terminus of RIG-I, together with the helicase domain forms the functional unit that is sufficient to bind RNA.

**The central aim of the study was therefore to elucidate the structural and molecular mechanisms that are involved in the recognition of 5'-triphosphate RNA by RIG-I and to identify the molecular determinants of ligand specificity.**

So far, it had been shown that RLRs are activated by viral RNAs that arise in the cytoplasm of infected cells, whereas the role of RIG-I for recognition of bacterial RNA had not been investigated. The fact that the intracellular bacterium *Listeria monocytogenes* was shown to induce upregulation of RIG-I upon infection (Imaizumi *et al.*, 2006), suggested a possible cooperative role of RLRs in the innate immunity to bacteria in addition to other pattern recognition receptors such as TLRs.

**Therefore, the second aim of the study was to investigate the role of RLRs for bacterial recognition and activation of dendritic cells, which was studied for *Helicobacter pylori* infection.**

PRR-mediated signaling is rapidly upregulated upon viral infection, leading to the production of type I IFN and proinflammatory cytokines. To prevent excessive immune responses that might have deleterious effects, the host has evolved various mechanisms to tightly regulate these signaling cascades. It was shown that a RIG-I splice variant, which is generated by alternative splicing, acts as negative regulator of its own pathway (Gack *et al.*, 2008).

**The observation that a short variant of RIG-I, which is different from the RIG-I splice variant, could be detected in HEK293 cells upon type I IFN stimulation, led to the third aim of this study: the characterization of this novel short variant of RIG-I and its possible function for the regulation of RIG-I innate immune signaling at the level of the RIG-I protein itself.**

## 3 MATERIAL & METHODS

### 3.1 Material

For detailed information on equipment, consumable items and reagents as well as kits and enzymes please see the lists provided in chapter 8, sections 8.1 to 8.4.

#### 3.1.1 Primers

All oligonucleotide primers used in this study were synthesized by Metabion or MWG (Martiensried, Germany). For further information on the sequences see supplementary tables provided in chapter 8, section 8.5. Oligo(dT)15 primer was purchased from Promega (Mannheim, Germany).

#### 3.1.2 Plasmids

##### 3.1.2.1 *Commercially available and published plasmids*

<b>Ben2</b>	kind gift from Dr. Frank Schmitz (Institute for Systems Biology, Seattle, WA, USA)
<b>Flag-IPS-1-human</b>	kind gift from Dr. Frank Schmitz (Institute for Systems Biology, Seattle, WA, USA)
<b>Flag-LGP2</b>	Rothenfusser <i>et al.</i> (2005)
<b>Flag-RIG-I</b>	Yoneyama <i>et al.</i> (2004)
<b>MDA5</b>	Andrejeva <i>et al.</i> (2004)
<b>p125-Luc</b>	Sato <i>et al.</i> (2000)
<b>pEF-BOS</b>	BCCM/LMBP plasmid collection (Zwijnaarde, Belgium)
<b>pRL-TK</b>	Promega (Mannheim, Germany)
<b>pVSV-GFP</b>	kind gift from Dr. Oliver Ebert (Department of Internal Medicine, Klinikum rechts der Isar, Technical University Munich, Munich, Germany)

Ben2, generated by Dr. Frank Schmitz, is a modified pEF6V5His vector (available from Invitrogen) which was used for cloning as either N-terminal Flag- or HA-tagged variant, Ben2-Flag and Ben2-HA, respectively. Expression plasmids for RIG-I, MDA5 and

LGP2 encode the human form of the respective protein. Expression of RIG-I and LGP2 from these constructs, produces proteins that bear a N-terminal Flag-tag. p125-Luc was described previously (Sato *et al.*, 2000) and comprises the promoter region of the murine *IFN- $\beta$*  gene (-125 to +55), which is fused to the gene encoding the *Photinus pyralis* (firefly) luciferase reporter. pRL-TK expresses *Renilla reniformis* (seapansy) luciferase driven by the herpes simplex virus thymidine kinase (TK) promoter. pVSV-GFP encodes the full-length antigenomic VSV RNA under control of a T7 promoter, with insertion of a GFP transcription unit into the 3' noncoding region of the VSV-G gene.

### 3.1.2.2 Plasmids constructed in this project

#### HA-IPS-1-human

The coding sequence for human IPS-1 was PCR amplified from Flag-IPS-1-human using primers scIPS-1\_for and scIPS-1\_rev. The obtained PCR product was digested with *EcoRV* and *NotI* to generate DNA ends that were compatible with the *EcoRV/NotI* treated target vector Ben2-HA. Ligation of digested PCR product and Ben2-HA resulted in the generation of HA-IPS-1-human.

#### Flag-RIG-I (AA 802-925)

The sequence comprising AA 802 to 925 of human RIG-I was amplified by PCR from Flag-RIG-I. Restriction sites for *EcoRV* and *NotI* were introduced into the PCR product by the primers scRIG-I (AA 802-925)\_for and scRIG-I (AA802-925)\_rev, respectively. PCR product and Ben2-Flag vector were cleaved with *EcoRV* and *NotI* and subsequent ligation of insert and target vector resulted in the expression vector Flag-RIG-I (AA 802-925) with the Flag-tag located at the N-terminus

#### Flag-RIG-I mutants

Several RIG-I mutants were generated by site-directed mutagenesis using the Quick Change Site-directed Mutagenesis Kit. Detailed information on the site-directed mutagenesis method is provided in section 3.2.6.3. Primer sequences with annotated nucleotide exchanges are listed in Table 11 to Table 14.

### Flag-RIG-I short form

The sequence comprising AA 155 to 925 of human RIG-I was PCR amplified from Flag-RIG-I by the primer pair sc\_RIG-I short form\_for and sc\_RIG-I short form\_rev and subsequently digested with *EcoRV* and *NotI*. The digested PCR product was ligated to Ben2-Flag, which has been treated equally, to generate the Flag-RIG-I short form construct (tag located at N-terminus).

Detailed information on the primers used for cloning is provided in Table 8. All newly generated constructs were verified with regard to the correct nucleotide sequence and in frame ligation by DNA sequencing, which was performed by Eurofins MWG Operon (Martensried, Germany). Sequencing primers are listed in Table 9.

### 3.1.3 Antibodies and protein standard for IFN- $\beta$ enzyme-linked immunosorbent assay (ELISA)

Table 3. *Antibodies (Ab) and standard for IFN- $\beta$  ELISA*

Antibodies and Cytokines	Species-Isotype	Function	Company
<b>IFN-<math>\beta</math></b>			
<b>anti-mouse IFN-<math>\beta</math> neutralizing</b>	rat IgG1	capture Ab	US Biologicals
<b>anti-mouse IFN-<math>\beta</math></b>	rabbit	detection Ab	PBL
<b>Recombinant IFN-<math>\beta</math></b>	mouse	standard	PBL
<b>Conjugate</b>			
<b>anti-rabbit HRP</b>	donkey		Jackson Immuno Research

### 3.1.4 Antibodies

Table 4. *Antibodies used for immunoprecipitation (\*) and immunoblotting (\*\*)*

<b>PRIMARY ANTIBODIES</b>				
<b>Antigen</b>	<b>Species</b>	<b>Dilution</b>	<b>Blocking</b>	<b>Company</b>
<b>β-Actin</b>	rabbit	1:5000 <sup>**</sup>		Abcam
<b>Flag M2 (clone M2)</b>	mouse	1:1000 <sup>**</sup>	3 % milk	Sigma-Aldrich
<b>HA-POX (High Affinity, 3F10)</b>	rat	1:2000 <sup>**</sup>		Roche
<b>RIG-I (clone Alme-1)</b>	mouse	1:100 <sup>*</sup> 1:1000 <sup>**</sup>	5% milk	Enzo Life Sciences
<b>RIG-I (clone 8G7-12)</b>	rat	1:2 <sup>**</sup>	5% milk	IMI
<b>Ubiquitin (P4D1)</b>	mouse	1:100 <sup>*</sup>		Santa Cruz Biotechnology
<b>SECONDARY ANTIBODIES</b>				
<b>Antigen</b>	<b>Conjugate</b>	<b>Source</b>	<b>Dilution</b>	<b>Company</b>
<b>Mouse IgG (H+L)</b>	HRP	goat	1:7500	Dianova
<b>Rabbit IgG (H+L)</b>	HRP	goat	1:7500	Dianova
<b>Rat IgG (H+L)</b>	HRP	goat	1:10000	Amersham GE

The RIG-I monoclonal antibody (clone 8G7-12) was used as hybridoma supernatant, which was kindly provided by Dr. Elisabeth Kremmer from the Institute for Molecular Immunology (IMI), Service Unit Monoclonal Antibodies, at the Helmholtz Zentrum München.

### 3.1.5 Cell lines, virus strains and bacterial strains

#### 3.1.5.1 Cell lines

Cell lines were obtained as frozen cultures from either ATCC (Manassas, VA, USA) or DSMZ (Braunschweig, Germany) as indicated in Table 5. Huh 7.0 and Huh 7.5 cell lines that have been previously described (Bartenschlager and Pietschmann, 2005; Foy *et al.*, 2005) were kindly provided by Prof. Karl-Klaus Conzelmann (Max von

Pettenkofer Institute and Gene Center, Ludwig-Maximilians-University Munich, Munich, Germany). Further information on the cell lines is provided in Table 5.

**Table 5.** *Index of cell lines*

<b>Designation</b>	<b>Source_Cat.No</b>	<b>Origin</b>	<b>Morphology</b>
<b>HEK293</b>	DSMZ_ACC305	human	fibroblast
<b>BHK-21</b>	ATCC_CCL-10	Syrian golden hamster	fibroblast
<b>Hela</b>	DSMZ_ACC57	human	epithelial
<b>HEp-2</b>	ATCC_CCL-23	human	epithelial
<b>Vero</b>	ATCC_CCL-81	African green monkey	epithelial
<b>Huh 7.0/7.5</b>		human	epithelial

### **3.1.5.2 Virus strains**

Recombinant wild-type VSV (Schnell *et al.*, 1996) and the attenuated strain VSV-M51R were described previously (Ebert *et al.*, 2005; Ebert *et al.*, 2003) and kindly provided by Dr. Oliver Ebert (Department of Internal Medicine, Klinikum rechts der Isar, Technical University Munich, Munich, Germany). Wild-type VSV is known to block host mRNA export from the nucleus and thereby inhibits IFN induction in infected cells. In contrast, VSV-M51R with a mutation of methionine 51 (M51) to arginine lacks this shutoff function (Publicover *et al.*, 2006). EMCV was a kind gift from Prof. Otto Haller (Department of Virology, University of Freiburg, Freiburg, Germany).

### **3.1.5.3 Bacterial Strains**

Competent *Escherichia coli* strains for different applications were purchased either from Invitrogen (Karlsruhe, Germany), Promega (Mannheim, Germany) or Stratagene (La Jolla, CA, USA) as shown in Table 6.

**Table 6.** *Index of competent cells used for DNA amplification*

Strain	Application	Source
<i>E. coli</i> K12 DH5 $\alpha$	retransformation	Invitrogen
<i>E. coli</i> K12 JM109	retransformation	Promega
XL10-Gold ultracompetent cells	transformation of ligated DNA	Stratagene
XL1-Blue supercompetent cells	transformation of DNA generated by site-directed mutagenesis	Stratagene

In addition to retransformation, *E. coli* K12 strain DH5 $\alpha$  was used for isolation of bacterial RNA. *Helicobacter pylori* strain SS1 was obtained from Dr. Petra Voland (formerly at the Department of Internal Medicine, Klinikum rechts der Isar, Technical University Munich, Munich, Germany) and cultured as described previously (Rad *et al.*, 2007). Isolation of RNA from *E. coli* K12 DH5 $\alpha$  and *H. pylori* SS1 is described in detail in section 3.2.6.7.

### 3.1.6 Buffers, solutions and media

#### 3.1.6.1 Media for cell culture

<b>BHK-21</b>	G-MEM	
	containing L-Glutamine	
	10 % (v/v)	FCS (heat inactivated)
	1 % (v/v)	Tryptose broth
	1 % (v/v)	Penicillin/Streptomycin
<b>DCs</b>	RMPI 1640	
	10 % (v/v)	FCS (heat inactivated)
	1 % (v/v)	Glutamax-I
	1 % (v/v)	Sodium pyruvate
	1 % (v/v)	NEAA
	1 % (v/v)	Penicillin/Streptomycin
	0.05 mM	$\beta$ -Mercaptoethanol

---

<b>Flushing medium</b>	RPMI 1640 5 % (v/v) FCS (heat inactivated)
<b>HEK293</b>	D-MEM (ATCC) containing L-Glutamine 10 % (v/v) FCS (heat inactivated) 1 % (v/v) Penicillin/Streptomycin
<b>Hela</b>	D-MEM (Invitrogen) containing L-Glutamine and 4.5 g/l glucose 10 % (v/v) FCS (heat inactivated) 1 % (v/v) Penicillin/Streptomycin
<b>HEp-2</b>	MEM- $\alpha$ containing L-Glutamine 5 % (v/v) FCS (heat inactivated) 1 % (v/v) Penicillin/Streptomycin
<b>Huh7.0/7.5</b>	D-MEM (Invitrogen) containing L-Glutamine and 4.5 g/l glucose 10 % (v/v) FCS (heat inactivated) 1 % (v/v) Penicillin/Streptomycin
<b>Vero</b>	D-MEM (Invitrogen) containing L-Glutamine and 4.5 g/l glucose 10 % (v/v) FCS (heat inactivated) 1 % (v/v) Penicillin/Streptomycin
<b>Freezing medium</b>	70 % (v/v) complete culture medium of the respective cell line 10 % (v/v) DMSO 20 % (v/v) FCS (heat inactivated)

### 3.1.6.2 Solutions for cell culture applications

<b>Crystal Violet</b>	12.25 mM	Crystal violet
	137 mM	Sodium chloride
	5 % (v/v)	Formaldehyde (37 %)
	50 % (v/v)	Ethanol
	in ddH <sub>2</sub> O	
<b>Agarose Overlay</b>	1.5 % (w/v)	Agarose
	in PBS	
	heat in microwave and store at 4 °C as aliquots	

### 3.1.6.3 Buffers for cytokine ELISA

<b>Coating Buffer</b>	0.1 M	Disodium phosphate
	in ddH <sub>2</sub> O	
	pH 9.0 with Sodium dihydrogen phosphate	
<b>Blocking Buffer</b>	PBS	
	10 % (v/v)	FCS
<b>Dilution Buffer</b>	10 % (v/v)	FCS
	0.5 % (v/v)	Tween-20
	in PBS	
<b>Washing Buffer</b>	PBS	
	0.5 % (v/v)	Tween-20
<b>ELISA Substrate</b>	0.1 M	Citric acid pH 4.0
	0.02 % (v/v)	ABTS (50 mg/ml)
	1:1000	30 % hydrogen peroxide
<b>Stop Solution</b>	1 % (w/v)	SDS
	in ddH <sub>2</sub> O	

### 3.1.6.4 Media for bacterial applications

All media were autoclaved for 20 min at 121 °C prior to use.

**LB medium**                      1 % (w/v)      Bacto Tryptone  
    0.5 % (w/v)      Yeast Extract  
    171 mM          Sodium chloride  
    in ddH<sub>2</sub>O  
    pH 7.3 with 1 N NaOH

**LB agar**                         4 % (w/v)      LB Agar  
    in ddH<sub>2</sub>O

For bacterial selection, LB medium and LB agar were supplemented with antibiotics in the following final concentrations: ampicillin 100 µg/ml or kanamycin 50 µg/ml.

**NZY Broth**                      1 % (w/v)      N-Z-Amine A  
    0.5 % (w/v)      Yeast Extract  
    90 mM          Sodium chloride  
    in ddH<sub>2</sub>O  
    pH 7.5 with 1 N NaOH

*the following filter-sterilized supplements were added prior to use:*

**NZY<sup>+</sup> Broth**                      1.25 % (v/v)    1 M Magnesium chloride  
    1.25 % (v/v)    1 M Magnesium sulphate  
    1 % (v/v)        2 M D-(+)-Glucose

**SOC**                                2 % (w/v)      Bacto Tryptone  
    0.5 % (w/v)      Yeast Extract  
    10 mM          Sodium chloride  
    2.5 mM         Potassium chloride  
    10 mM          Magnesium chloride  
    10 mM          Magnesium sulphate  
    20 mM         D-(+)-Glucose  
    in ddH<sub>2</sub>O

### 3.1.6.5 Buffers and solutions for protein biochemistry

<b>4 x Stacking Gel Buffer</b>	0.5 M	Tris
	0.4 % (v/v)	SDS
	in ddH <sub>2</sub> O	
	pH 6.8 with HCl	
<b>4 x Resolving Gel Buffer</b>	1.5 M	Tris
	0.4 % (v/v)	SDS
	in dd H <sub>2</sub> O	
	pH 8.8 with HCl	
<b>10 % APS</b>	10 % (w/v)	APS in ddH <sub>2</sub> O
<b>10 x Running Buffer</b>	1.9 M	Glycin
	250 mM	Tris
	171 mM	SDS
	in ddH <sub>2</sub> O	
<b>1 x Blotting Buffer (semi dry method)</b>	21 mM	Tris
	192 mM	Glycin
	0.2 % (v/v)	Methanol
	in ddH <sub>2</sub> O	
<b>10 x Blotting Buffer (tank blotting method)</b>	1.9 M	Glycin
	250 mM	Tris
	in ddH <sub>2</sub> O	
<b>1 x Blotting Buffer (tank blotting method)</b>	100 ml	10 x Blotting Buffer
	200 ml	Ethanol absolute
	700 ml	ddH <sub>2</sub> O

---

<b>TBS-T</b>	1 M	Tris-HCl pH 8.0
	150 mM	Sodium chloride
	0.05 % (v/v)	Tween-20
	in ddH <sub>2</sub> O	
<b>Blocking Buffer</b>	5 % (w/v)	Skim Milk Powder in TBS-T
<b>Buffer A</b>	10 mM	Hepes pH 7.0
	1.5 mM	Magnesium chloride
	10 mM	Potassium chloride
	0.2 mM	DTT
	in ddH <sub>2</sub> O	
<b>10 x Cytoplasmic Extract Buffer</b>	300 mM	Hepes pH 7.9
	30 mM	Magnesium chloride
	1.4 M	KCl
	in ddH <sub>2</sub> O	
<b>Dialysis Buffer</b>	20 mM	Hepes pH 7.8
	100 mM	Potassium chloride
	2 mM	Magnesium chloride
	20 % (v/v)	Glycerol
	0.2 mM	EDTA
	0.5 mM	DTT
	in ddH <sub>2</sub> O	

---

<b>IP Lysis Buffer</b>	10 %	Glycerol
	20 mM	Tris-HCl pH 7.0
	137 mM	Sodium chloride
	2 mM	EDTA
	1 %	NP-40
	in ddH <sub>2</sub> O	
<i>the following supplements were added freshly prior to use:</i>		
1 tablet	Complete Protease Inhibitor Mix	
100 µl	100 mM PMSF (in Methanol)	
20 µl	500 mM Sodium orthovanadate (in ddH <sub>2</sub> O)	
in 10 ml IP lysis buffer		
<b>Flag-IP Lysis Buffer</b>	50 mM	Tris-HCl pH 7.4
	150 mM	Sodium chloride
	1 mM	EDTA
	1 % (v/v)	Triton X-100
	in ddH <sub>2</sub> O	
<b>Fixer</b>	50 % (v/v)	Methanol
	12 % (v/v)	Acetic acid
	0.05 % (v/v)	Formaldehyde (37 %)
	in ddH <sub>2</sub> O	
<b>Sensitizer</b>	12.7 mM	Sodium thiosulphate
in ddH <sub>2</sub> O		
<b>Staining solution</b>	11.8 mM	Silver nitrate
	0.075 %	Formaldehyde (37 %)
	in ddH <sub>2</sub> O	
<b>Developer</b>	565 mM	Sodium carbonate
	0.03 mM	Sodium thiosulphate
	0.05 % (v/v)	Formaldehyde (37 %)
	in ddH <sub>2</sub> O	

---

<b>Stop solution</b>	50 % (v/v)	Methanol
	12 % (v/v)	Acetic acid
	in ddH <sub>2</sub> O	

<b>Preserver</b>	20 % (v/v)	Ethanol
	2 % (v/v)	Glycerol
	in ddH <sub>2</sub> O	

### 3.1.6.6 *Buffers for molecular biology*

<b>50 x TAE</b>	2 M	Tris
	100 mM	EDTA
	5.71 % (v/v)	Glacial acetic acid
	in ddH <sub>2</sub> O	
pH 8.5 with 1 N NaOH		

<b>6 x Loading Dye</b>	25 % (v/v)	Glycerol
	0.05 M	EDTA pH 7.5 to 8.0
	0.25 % (w/v)	Bromophenolblue
	in ddH <sub>2</sub> O	

<b>DNA Ladder</b>	100 µl	Ladder
	180 µl	6 x Loading Dye
	720 µl	TE buffer

<b>TE Buffer</b>	10 mM	Tris-Cl pH 7.5
	1 mM	EDTA
	in ddH <sub>2</sub> O	

<b>3 M Na-Acetate</b>	3 M	Sodium acetate
	in ddH <sub>2</sub> O	
	pH 5.4 with glacial acetic acid	

## 3.2 Methods

If not specifically mentioned, the methods applied in this work are according to the protocols published in Molecular Cloning by Sambrook and Russell (Sambrook and Russel, 2001). If commercially available kits were used, the instructions provided by the manufacturer were followed.

### 3.2.1 Mice

Wild-type C57BL/6 mice were obtained from Harlan Winkelmann (Borchen, Germany). *Trif* mutant mice (*Lps2*), kindly provided by Bruce Beutler (The Scripps Institute, Department of Genetics, La Jolla, CA, USA), were described previously (Hoebe *et al.*, 2003). All mice were used on a C57BL/6 genetic background. Mice were kept under specific pathogen-free conditions at the animal facility of the Klinikum rechts der Isar at the Technical University Munich. Animal husbandry and experiments were approved by the local government authority. Experiments were performed with 6 to 8 week old female mice.

### 3.2.2 Tissue culture

#### 3.2.2.1 Cell lines

All cell cultures were maintained at 37 °C in a humified incubator with 5 % CO<sub>2</sub> atmosphere with the media listed in section 3.1.6.1. Cells were split every 3 to 5 days in a ratio ranging from 1:3 to 1:10 depending on the respective cell line. To passage cell lines that possess adherent growth properties, the medium was discarded, cells were washed with PBS and subsequently detached from the culture surface by incubation with 1 x trypsin/EDTA solution for 1 to 2 min at 37 °C. To inactivate the trypsin, cells were resuspended in the adequate medium and plated at an appropriate density in new tissue culture ware. In case of HEK293, the culture medium was removed and cells were rinsed with fresh culture medium to detach them from the culture surface without using trypsin digestion.

Cell lines were tested to be negative for mycoplasma contamination at regular intervals. Therefore, cell culture supernatants were subjected to PCR using mycoplasma specific oligonucleotide primers MycA and MycB (for sequences see Table 9).

### **3.2.2.2 Cryopreservation of cells**

To keep a stock of cells with a low passage number, cells were frozen as permanent cultures in liquid nitrogen. Cells were grown to a confluency of 95 % and detached from the culture surface by either incubation with 1 x trypsin/EDTA solution or flushing with culture medium. After counting and centrifugation at 1500 rpm for 5 min and 4 °C,  $1 \times 10^6$  cells were resuspended in 1 ml freezing medium, transferred to cryotubes and kept at  $-80$  °C for 72 hrs before storage in liquid nitrogen. Isopropanol isolated cryoboxes allowed gentle freezing of the cells (1 °C per hour).

For reconstitution of the frozen cultures, cells were thawed very quickly in a 37 °C waterbath and then transferred into 10 ml of the respective precooled culture medium. After 5 min centrifugation at 1500 rpm and 4 °C, cells were resuspended in the appropriate volume of culture medium and seeded into tissue culture plates.

### **3.2.2.3 Transient transfection of cell lines**

Transfection of cell lines was performed using Lipofectamine2000 and the serum-free medium Opti-MEM. In general, cells were seeded in the appropriate culture plates the day before transfection (about 90 % confluency at day of transfection). If not otherwise indicated, for transfection in 6-well plates  $1 \times 10^6$  cells were plated in 2 ml culture medium, whereas  $2 \times 10^5$  cells were seeded in 24-well plates in a total volume of 1 ml.  $3 \times 10^8$  cells were plated in 10 cm dishes in 10 ml culture medium. Transfection was carried out according to the protocol provided by the manufacturer. Briefly, Lipofectamine2000 was diluted in Opti-MEM and incubated for 5 min at RT. Then, DNA or RNA, diluted in Opti-MEM, was added to the pre-incubated Lipofectamine2000 and incubated for 20 min at RT to form transfection complexes. Ultimately, the culture medium was removed from the cells, replaced by the respective amount of Opti-MEM and the transfection complexes were added dropwise to the cells. Then, culture plates were gently rocked back and forth to administer transfection complexes evenly across the culture surface. After 4 to 6 hrs of incubation at 37 °C in a humidified incubator, the transfection mixture was removed and fresh pre-warmed culture medium was added to the cells, which were further cultured until they were subjected to lysis for western blot analysis or immunoprecipitation as well as luciferase assay.

### **3.2.2.4 Generation of murine bone marrow derived DCs**

Bone marrow derived DCs (BMDCs) were generated from wild-type C57BL/6 mice or *Trif* mutant mice (*Lgp2*) by a method modified from Inaba *et al.* (1992). Mice were euthanized by isofluran inhalation and the body was disinfected with 70 % EtOH. To obtain bone marrow cells, the hind legs were removed and cleaned from fur and muscle tissue. *Femora* and *tibiae* were flushed with flushing medium into a 10 cm petri dish using a 27 G needle under sterile conditions. After centrifugation at 1500 rpm and 4 °C for 5 min the cell pellet was resuspended in red blood cell lysis buffer and incubated for 3 min at RT to lyse erythrocytes. Lysis was blocked by adding 50 ml flushing medium to the cells and centrifugation for 5 min at 1500 rpm and 4 °C. The cell pellet was then resuspended in DC medium and the cell number was determined using a Neubauer counting chamber.

$5 \times 10^6$  bone marrow cells were seeded in 10 cm petri dishes in a total volume of 10 ml DC medium supplemented with 4 % (v/v) of supernatant containing murine granulocyte macrophage colony-stimulating factor (mGM-CSF) and incubated at 37 °C for 7 days. On day 3, 10 ml fresh DC medium containing 4 % mGM-CSF supernatant was added. The cells were subsequently split in a ratio of 1:2 at day 5 and cultured for 2 more days in a total volume of 20 ml supplemented with 4 % (v/v) mGM-CSF supernatant. mGM-CSF supernatant was obtained from the mGMCSF secreting plasmacytoma cell line J588L, which is stably transfected with a mGM-CSF expression plasmid.

## **3.2.3 Virus propagation and titer determination**

### **3.2.3.1 Propagation of VSV strains**

For production of VSV and VSV-M51R stocks, BHK-21 cells grown in 10 cm tissue culture dishes to approximately 90 % confluency, were infected with the respective virus strain diluted in serum-free G-MEM supplemented with 1 % (v/v) Penicillin/Streptomycin at a MOI of 0.1 and incubated at 37 °C in a humidified incubator until a strong cytopathic effect was visible (2 days). Then, the virus containing supernatant was harvested and subsequently clarified by centrifugation at 2000 rpm and 4 °C for 10 min. The VSV containing supernatant was aliquoted and stored at – 80 °C.

### **3.2.3.2 *EMCV stock preparation***

BHK-21 cells were grown in 10 cm tissue culture dishes to a confluency of about 70 % and infected with EMCV at a MOI of 0.01 at 37 °C in a humidified incubator under serum-free conditions using G-MEM containing 1 % (v/v) Penicillin/Streptomycin. After 1 h of virus adsorption, the inoculum was removed and BHK-21 culture medium was added. 72 hrs after infection, infectious supernatants were collected and cell debris was removed by centrifugation for 10 min at 1500 rpm and 4 °C. The cell culture supernatant, containing EMCV virus particles, was aliquoted and stored at – 80 °C.

### **3.2.3.3 *Determination of virus titers by plaque assay***

The virus concentration in the supernatants obtained from VSV and EMCV-infected BHK-21 cells, was determined by plaque assay. Therefore, susceptible cell monolayers were seeded in 6-well plates with a density of  $1 \times 10^6$  cells/well the day before infection. BHK-21 cells were used for measuring the titers of VSV strains, while EMCV titers were determined using Vero cells. To perform the plaque assay, 10-fold serial dilutions of the respective infectious supernatants were prepared in serum-free Opti-MEM. Then, the culture medium was removed, cells were washed once with PBS to remove residual medium containing FCS that might inhibit virus infection, and subsequently 2 ml of each dilution were added onto the susceptible cell monolayers. After incubation at 37 °C for 1 h, to allow the virus to attach to the target cells, the inoculum was removed, cells were rinsed with PBS to remove residual virus and the monolayers were covered with 2 ml agarose overlay. The viscous agarose overlay inhibits diffusion of released progeny virus from infected cells to cells that remained uninfected during the initial phase of infection. Consequently, each infectious particle that was contained in the 10-fold dilution infects a given cell in the monolayer and spreads to neighboring cells, thereby causing cytopathic effect and cell death that can be visualized as plaque. To determine the virus concentration in the infectious supernatants, 24 hrs to 36 hrs after infection the agarose overlay was carefully removed and cells were stained and fixed with 1 ml crystal violet solution per well for 30 min at RT. The crystal violet was discarded and plates were rinsed with tap water several times to remove the staining solution. Crystal violet selectively stains living cells and thus enhances the contrast between the living cells and the plaques, which appear as clear spots in a purple coloured cell layer.

Finally, the plaques were counted and the virus titer was determined by the following equation:

$$\text{virus titer (PFU/ml)} = \frac{\text{(counted plaques x dilution factor)}}{\text{volume of inoculum}}$$

To minimize error, titrations were always done in duplicates and only wells containing 1 to 20 plaques were counted.

### 3.2.4 Dual Luciferase reporter assay

Luciferase reporter assay was established to study RLR-mediated type I IFN induction. A dual reporter system was used to improve experimental accuracy, utilizing the simultaneous expression and measurement of two individual reporter enzymes, namely Firefly luciferase and Renilla luciferase, within a single system. In this assay, the so-called experimental reporter is correlated with the effect of specific experimental conditions, i.e. type I IFN induction, while cotransfection of the control reporter that is constitutively active, functions as internal control for the baseline response. Normalizing the activity of the experimental reporter to the internal control was used to minimize experimental variability caused by different transfection efficiencies and cell viability, for example in response to a viral stimulus.

To perform the luciferase reporter assay, cells were seeded in 24-well plates with a density of  $2 \times 10^5$  cells/well the day before transfection. Cells were transiently transfected with 100 ng experimental reporter plasmid expressing the firefly luciferase gene under control of the IFN- $\beta$  promoter (p125-Luc) and 10 ng of internal control plasmid pRL-TK together with 100 ng empty vector control (pEF-BOS) as well as, depending on the individual experiment, different amounts of RIG-I, MDA5 or LGP2 expression vectors. 18 hrs after primary transfection, cells were either infected with VSV-M51R or transfected with poly(I:C), RNA isolated from VSV or EMCV-infected cells and 5'-triphosphate RNA generated by *in vitro* transcription as well as RNA isolated from *Helicobacter pylori* SS1, respectively. The corresponding MOIs and RNA concentrations used for stimulation are indicated in chapter 4 in the respective figure legends. For reporter assays involving VSV-M51R infection, the virus stock was diluted

in serum-free Opti-MEM and cells were inoculated with virus at an MOI of 5. 1 h p.i., the inoculum was removed and replaced by fresh culture medium. In case of RNA transfection, cells were incubated with the transfection complexes for 4 hrs. 18 hrs after either transfection or infection, cell extracts were prepared using Passive Lysis Buffer supplied with the Dual Luciferase Reporter System and assayed according to the manufacturer's instructions using a Turner Luminometer. All transfections were performed using Lipofectamine2000 according to the protocol supplied by the manufacturer. Luciferase activities were measured as relative light units (RLU). For each sample Firefly activity (Fluc) was normalized to Renilla luciferase (Rluc) activity and calculated as fold induction by the following equation:

<b>1. Mock</b>	=	$\frac{\text{RLU Rluc (mock-treated sample)}}{\text{RLU Fluc (mock-treated sample)}}$
<b>2. Renilla factor</b>	=	Mock/RLU Rluc
<b>3. Fold induction</b>	=	Renilla factor x RLU Fluc

### 3.2.5 Stimulation of DCs and determination of cytokine levels by ELISA

GM-CSF derived DCs were stimulated with live *Helicobacter pylori* SS1, RNA isolated from *H. pylori* SS1 and *in vitro* transcribed 5'-triphosphate RNA comprising the VSV leader RNA (see section 3.2.6.4). For this purpose, GM-CSF derived DCs (for generation see section 3.2.2.4) were harvested on day 7 using PBS/0.05 mM EDTA. Cells were resuspended in DC culture medium at a density of  $1 \times 10^6$  cells/ml and 100  $\mu$ l ( $1 \times 10^5$  cells) of the cell suspension were subsequently seeded per well on a 96-well plate in duplicates.

Stimuli were prediluted in DC medium and added to the cells (100  $\mu$ l/well). Cells were infected with live *H. pylori* at an MOI of 50. *H. pylori* RNA and 5'-triphosphate RNA were complexed with the cationic liposome DOTAP (final concentration 12.5  $\mu$ g/ml) and added to the cells at a final concentration of 20  $\mu$ g/ml. Cell free culture supernatants were harvested 24 hrs after stimulation and stored at  $-20$  °C.

ELISA was used to determine the concentration of IFN- $\beta$  in cell culture supernatants after DC stimulation. Antibodies and IFN- $\beta$  standard used for ELISA are listed in Table 3. Plastic microwell plates were coated with anti-mouse IFN- $\beta$  Ab (capture Ab), diluted in coating buffer, for 3 hrs at RT. 50  $\mu$ l capture antibody were added to each well. Plates were washed 3 times with washing buffer to remove unbound antibody from the wells. To block non-specific binding, 200  $\mu$ l blocking buffer were applied to each well and plates were incubated for 30 min at RT. In the next step, blocking buffer was flicked off and 50  $\mu$ l samples and standards, respectively, were added. Dilutions of samples and standards were prepared in dilution buffer. Plates were incubated overnight at 4 °C. On day 2, plates were washed 4 times with washing buffer to remove unbound antigen. Next, 50  $\mu$ l of the anti-mouse IFN- $\beta$  detection Ab dilution (prepared in dilution buffer) were added to each well to detect the captured cytokines. After incubation for 2 hrs at RT, plates were washed 4 times and 50  $\mu$ l of the HRP conjugate were added per well and incubated for another 1 h at RT. Then, plates were washed 5 times and subsequently 100  $\mu$ l of the ELISA substrate were added to each well. Plates were incubated for approximately 10 min depending on the color intensity of the enzymatic reaction. HRP mediates oxidation of ABTS in the presence of hydrogen peroxide, which are contained in the ELISA substrate. The enzymatic reaction was stopped by addition of 100  $\mu$ l stop solution per well. To determine the concentration of bound antigen, the OD of the samples was measured at 405 nm and 495 nm.

Data analysis was performed with the Ascent 2.6 software. The IFN- $\beta$  concentration of the samples was calculated using a point-to-point standard curve ranging from 1000 U/ml to 1.95 U/ml recombinant IFN- $\beta$ . The lower detection limit of this ELISA was 1.95 U/ml.

## 3.2.6 Molecular Biology

### 3.2.6.1 Isolation and purification of DNA

#### 3.2.6.1.1 Recovery of plasmid DNA from filter paper

Plasmid DNA kindly provided by collaborators was recovered from whatman filter paper. The circle containing a high concentration of the respective plasmid DNA was cut out and transferred into a 1.5 ml tube. An appropriate volume of TE buffer was added and the filter paper was rehydrated overnight at 4 °C to dissolve plasmid DNA. After brief centrifugation, the supernatant was directly used for transformation of competent bacteria.

#### 3.2.6.1.2 Transformation of competent *E. coli*

Chemically competent *E. coli* K12 strains DH5 $\alpha$  and JM109 were used for retransformation of plasmid DNA. 20  $\mu$ l bacteria were thawed on ice and about 10 ng of DNA were added. After mixing by gentle swirling of the tube, bacteria were incubated on ice for 30 min. The tube was then transferred into a 42 °C waterbath, heat-shocked for 45 sec and rapidly returned to ice for 2 min. 200  $\mu$ l SOC medium were added and cultures were incubated for 1 h at 350 rpm in a thermomixer to induce bacterial recovery and growth. 80  $\mu$ l to 150  $\mu$ l of the transformation reaction were spread onto LB agar plates containing the appropriate antibiotic for bacterial selection. Plates were incubated for approximately 16 hrs at 37 °C until single bacterial colonies were clearly visible.

To recover newly generated plasmid DNA from ligation reactions, XL10-Gold ultracompetent cells were used for transformation. Cells were gently thawed on ice and 100  $\mu$ l were transferred into 14 ml round bottom tubes. 4  $\mu$ l of the  $\beta$ -Mercaptoethanol mix provided with the cells were added to each aliquot. Cells were incubated on ice for 10 min and swirled gently every 2 min. 2  $\mu$ l to 10  $\mu$ l of the ligation reaction were added to the competent cells. After 30 min incubation on ice, cells were heat-pulsed at 42 °C for 30 sec and rapidly transferred on ice for 2 min. Then, 900  $\mu$ l preheated NZY<sup>+</sup> broth were added to the transformation reaction and bacteria were incubated at 37 °C for 1 h with shaking at 250 rpm. 200  $\mu$ l of the transformation reaction were plated on LB agar plates containing the appropriate antibiotic. Plates were incubated overnight at 37 °C.

XL1-Blue supercompetent cells were exclusively used for propagation of DNA generated by site-directed mutagenesis. For a detailed transformation protocol see section 3.2.6.3.

#### **3.2.6.1.3 Glycerol cultures of bacteria**

To keep bacteria bearing plasmids of interest in a permanent culture, glycerol stocks were prepared by adding 400  $\mu$ l of 50 % sterile glycerol to 600  $\mu$ l fresh bacterial overnight culture. After mixing by vortexing, cultures were stored at  $-80$  °C.

#### **3.2.6.1.4 Isolation of plasmid DNA**

Small scale (miniprep) and large scale (maxiprep) isolation of plasmid DNA were performed using the respective kits from Qiagen following the manufacturer's instructions.

For small scale isolation, 4 ml LB medium supplemented with the respective antibiotic for bacterial selection, were either inoculated with a single colony picked from LB agar plates or bacterial glycerol stock. Cultures were maintained at 37 °C with shaking at 250 rpm. Overnight cultures were directly used for minipreps. As a modification of the protocol given by the manufacturer, plasmid DNA was recovered from the binding column by elution with 40  $\mu$ l ddH<sub>2</sub>O. 500 ng up to 1  $\mu$ g were then analyzed by restriction digestion (section 3.2.6.2.2).

To isolate large amounts of plasmid DNA, 250 ml LB medium containing the respective antibiotic were inoculated with 250  $\mu$ l of fresh bacterial culture and incubated for 16 hrs at 37 °C with constant agitation at 250 rpm. Bacteria were harvested by centrifugation of the cultures for 45 min at 4000 rpm and 4 °C. DNA isolation was then performed according to the protocol supplied by the manufacturer with the modification that DNA was precipitated by centrifugation at 4 °C and 4000 rpm for 1 h. To dissolve the dried DNA precipitate, 100 to 200  $\mu$ l of buffer TE were added to the tube and DNA was subsequently rehydrated overnight at 4 °C.

#### **3.2.6.1.5 Determination of DNA concentration and purity**

To determine the concentration and purity of plasmid DNA after DNA isolation, the optical density (OD) at 260 nm and 280 nm was measured using a spectrophotometer. The OD<sub>260</sub> allowed the calculation of nucleic acid concentrations of the samples, taking the OD of 1 equal to a concentration of 50  $\mu$ g/ml double stranded DNA. The ratio

between the two measurements ( $OD_{260}/OD_{280}$ ) provided an estimation of the sample purity. Plasmid DNA in the range of 1.7 and 1.8 was used for all experiments.

### 3.2.6.2 *Analysis and cloning of DNA*

#### 3.2.6.2.1 **PCR amplification of DNA inserts for cloning**

PCR amplification of DNA that was used for cloning, was performed using *Pfu* Ultra DNA polymerase. PCR reactions and cycling parameters were set up according to the protocol provided by the manufacturer.

##### CYCLING PARAMETERS

1. 95 °C	2 min
2. 95 °C	30 sec
3. Primer $T_m - 5$ °C	30 sec
4. 72 °C	1 min per Kb
5. go to 2., 30 x	
6. 72 °C	10 min
7. 4 °C	Pause

##### REACTION CONDITIONS

10 x reaction buffer	5 $\mu$ l
dsDNA template (20 ng/ $\mu$ l)	5 $\mu$ l
Primer for (10 $\mu$ M)	2.5 $\mu$ l
Primer rev (10 $\mu$ M)	2.5 $\mu$ l
dNTP Mix (10 mM)	1 $\mu$ l
ddH <sub>2</sub> O	ad 50 $\mu$ l
<i>Pfu</i> Ultra DNA polymerase	1 $\mu$ l

In general, amplification occurred using this protocol. If amplification failed or was insufficient, DMSO was added to the PCR reaction to a final concentration of 5 %.

#### 3.2.6.2.2 **Restriction enzyme digestion**

Restriction digests of plasmids or PCR products were performed in a total volume of 20  $\mu$ l to 50  $\mu$ l depending on the amount of DNA according to the protocol supplied by the manufacturer, using the recommended buffer and 10 U of the appropriate enzyme for each microgram of DNA. If necessary, 2  $\mu$ l of 10 x BSA were added. Digestion was performed for 2 to 4 hrs in a 37 °C waterbath.

### **3.2.6.2.3 Agarose gel electrophoresis**

DNA fragments obtained by restriction digest or PCR were separated and analyzed by agarose gel electrophoresis. All agarose gels were prepared in 1 x TAE buffer with the agarose concentration depending on the size of the expected fragments. To stain DNA fragments, ethidium bromide was added to a final concentration of 100 ng/ml before pouring the gel into the gel preparation tray. Samples were mixed with loading dye in a ratio of 6:1 and separated at 80 V to 100 V for 30 min to 1 h depending on the agarose concentration as well as the size of the expected fragments. All gels were run in 1 x TAE buffer. For size determination 8 µl of either a 100 bp or 1 Kb DNA ladder were also loaded onto the gel. Stained bands were visualized with UV light (254 nm) in a gel documentation system.

### **3.2.6.2.4 Extraction of DNA fragments from agarose gels**

If separated DNA fragments were to be used for further cloning steps, the respective band was recovered by gel excision. DNA was purified using the QIAquick gel extraction kit following the supplier's manual. To prevent UV-induced DNA damage, weak UV light was applied for visualization of the fragments during excision of the gel fragment.

### **3.2.6.2.5 Dephosphorylation of free DNA ends**

To avoid re-circularization of digested, linearized vector DNA, 5'-ends of the DNA fragments were dephosphorylated using calf intestinal alkaline phosphatase (CIAP). Vector DNA was treated with CIAP according to the instructions given by the supplier. The enzyme was added to the DNA of interest, which was recovered by gel extraction, and incubated for 1 h at 37 °C. Enzymatically treated DNA fragments were subsequently purified using the QIAquick PCR purification kit according to the respective protocol to remove all traces of salts and enzymes, which might interfere with downstream applications such as ligation.

### **3.2.6.2.6 Phenol/chloroform extraction and ethanol precipitation**

Phenol/chloroform extraction was used to remove proteins from DNA preparations or enzymatic reactions. 1 volume of phenol/chloroform mixed in the ratio 1:1 was added to the sample and mixed by vigorous vortexing for 10 s. After centrifugation at 14000 rpm for 10 sec the upper DNA containing phase was removed and transferred to a fresh 1.5 ml tube. Then, DNA was precipitated by ethanol precipitation. Briefly, 3 volumes of 100 % cold ethanol and 0.1 volume of 3 M Na-acetate (pH 5.4) were added to the DNA

containing phase. Samples were incubated at  $-80\text{ }^{\circ}\text{C}$  for 30 min and the precipitated DNA was centrifuged at 14000 rpm and  $4\text{ }^{\circ}\text{C}$  for 30 min. The supernatant was discarded and the pellet was washed once with 70 % cold ethanol. After another centrifugation step at 14000 rpm for 15 min the ethanol supernatant was carefully removed, the pellet air-dried at RT and finally resuspended in an appropriate volume of water.

### 3.2.6.3 *Site-directed mutagenesis*

Flag-RIG-I and MDA5 bearing point mutations in the C-terminal region of the respective protein were generated using the Quick Change Site-Directed Mutagenesis Kit. The basic procedure utilizes a supercoiled dsDNA vector with an insert of interest to be mutated and two synthetic oligonucleotide primers containing the desired mutation (Figure 4). The oligonucleotide primers that are complementary to the opposite strands of the plasmid, are extended during thermal cycling by *Pfu* Turbo DNA polymerase leading to the generation of a mutated plasmid containing nicks. Following thermal cycling, the sample is treated with the restriction endonuclease *DpnI*, which is specific for methylated DNA. Methylation of DNA occurs naturally during DNA replication in almost all competent bacteria that are *dam*<sup>+</sup>. Therefore, *DpnI* is used to digest the parental DNA template and to specifically select synthesized DNA that contains the desired mutation. The mutated vector DNA is then transformed into competent cells.

20 ng of either RIG-I or MDA5 plasmid DNA were used as template for the mutagenesis reaction with the following cycling parameters and reaction conditions:

#### CYCLING PARAMETERS

- |                                 |        |
|---------------------------------|--------|
| 1. $95\text{ }^{\circ}\text{C}$ | 30 sec |
| 2. $95\text{ }^{\circ}\text{C}$ | 30 sec |
| 3. $55\text{ }^{\circ}\text{C}$ | 1 min  |
| 4. $68\text{ }^{\circ}\text{C}$ | 9 min  |
| 5. go to 2., 11x                |        |

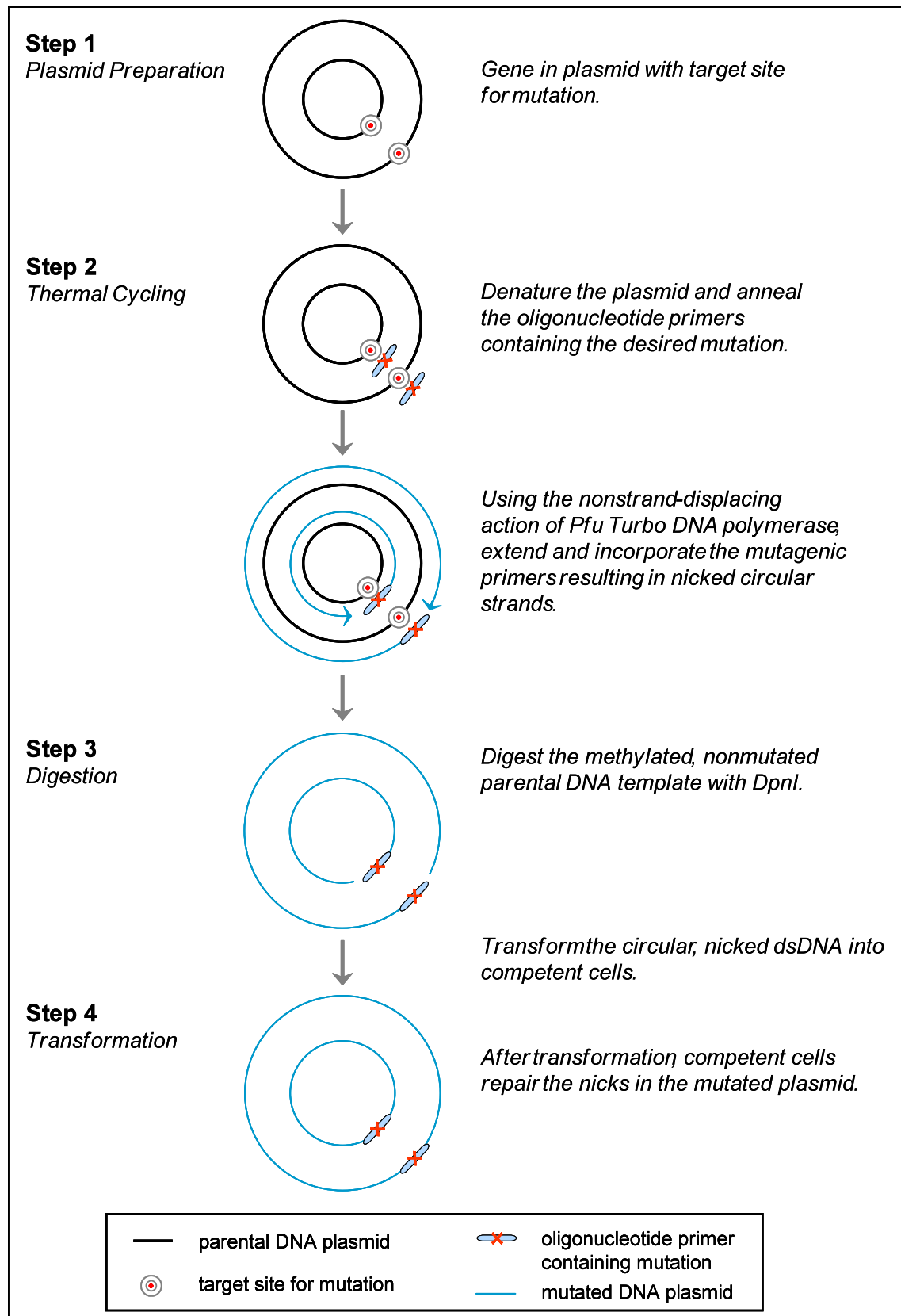


**Figure 4.** Schematic representation of the steps involved in site-directed mutagenesis of plasmid DNA using the Quick Change Kit (adapted from the manual included in the kit)

REACTION CONDITIONS

10 x reaction buffer	5 $\mu$ l
dsDNA template (5 ng/ $\mu$ l)	4 $\mu$ l
DMSO	2 $\mu$ l
Primer for (100 ng/ $\mu$ l)	1.25 $\mu$ l
Primer rev (100 ng/ $\mu$ l)	1.25 $\mu$ l
dNTP Mix	1 $\mu$ l
ddH <sub>2</sub> O	ad 50 $\mu$ l
<i>Pfu</i> Turbo DNA polymerase	1 $\mu$ l

Sequences of oligonucleotide primers used for the respective mutagenesis reactions are shown in chapter 8, section 8.5, Table 11 to Table 14. All mutations were performed according to UniProtKB/Swiss-Prot accession numbers O95786 (human RIG-I) or Q9BYX4 (human MDA5), respectively. 1  $\mu$ l *DpnI* was added to 50  $\mu$ l of the mutagenesis reaction. After 1 h incubation at 37 °C, 2  $\mu$ l of the digestion reaction were used to transform XL1-Blue supercompetent cells. 50  $\mu$ l of XL1-Blue cells were aliquoted to a prechilled 14 ml round bottom tube. 2  $\mu$ l of *DpnI* treated DNA were added to the competent cells. The transformation reactions were swirled gently to mix and incubated on ice for 30 min. After a heat pulse for 45 sec at 42 °C, reactions were placed on ice for 2 min. Then, 500  $\mu$ l NZY<sup>+</sup> broth preheated to 42 °C were added and samples were incubated at 37 °C and 250 rpm. 250  $\mu$ l of the transformation reaction were spread on LB agar plates containing the appropriate antibiotic.

Mutations were confirmed by DNA sequencing (performed by Eurofins MWG Operon, Martinsried, Germany).

#### **3.2.6.4 Synthesis of 5'-triphosphate RNA by *in vitro* transcription (IVT)**

5'-triphosphate RNA encompassing the VSV leader RNA sequence (pppVSVL) was generated by *in vitro* transcription (Figure 5). First, template DNA was amplified by PCR from pVSV-GFP, a full-length VSV cDNA clone. The 3' leader region of non-segmented negative-strand viruses does not encode a protein and has multiple functions for transcription and virus replication (Mink *et al.*, 1991). To generate leader RNAs of different length, four reverse primers (VSV-R1 to VSV-R4) binding to different regions of the VSV-N gene, which is adjacent to the leader RNA stretch, were used together

with a T7 promoter-specific forward primer (for primer sequences see Table 10). Thus, the obtained PCR products contained a T7 RNA polymerase consensus promoter followed by the sequence of interest to be transcribed. PCR products were concentrated by ethanol precipitation (described in section 3.2.6.2.6) and purified using the PCR Purification Kit according to the manufacturer's instructions.

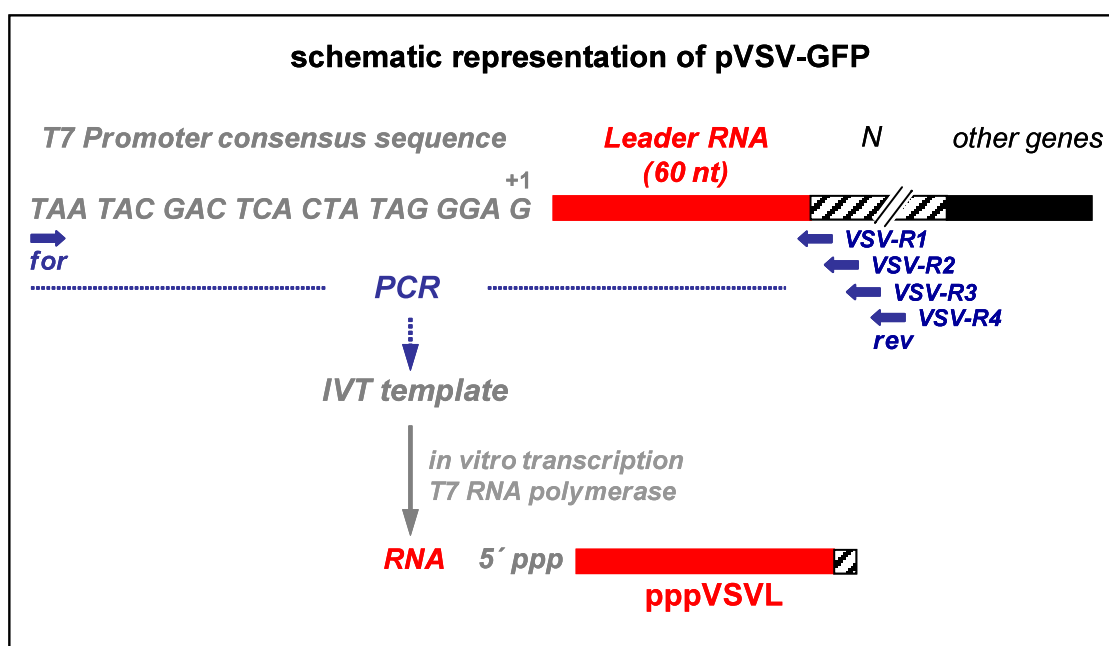


**Figure 5. Generation of 5'-triphosphate RNA by in vitro transcription**

pVSV-GFP, which is a cDNA clone that comprises full-length antigenomic VSV RNA under control of a T7 promoter, was used as PCR template to generate a PCR product that contains the T7 promoter and subsequently can be used for the generation of VSV-specific triphosphate RNA by *in vitro* transcription with T7 RNA polymerase. Initially, four different reverse primers (VSV-R1 to VSV-R4) were used in combination with the T7 promoter-specific forward primer, to produce a set of PCR products, which in turn serve as templates for IVT. All PCR products were efficiently transcribed into RNA and the length of the RNA did not influence its stimulatory potential. Thus, for all subsequent IVT reactions, VSV-R4 was used in combination with the forward primer.

*In vitro* transcription was carried out for 2 hrs at 42 °C using the Ampliscribe Flash T7 Kit in accordance with the protocol given by the supplier. The DNA template was removed by DNase I treatment and *in vitro* transcribed RNA was subsequently purified using the RNeasy Mini Kit. Removal of 5'-triphosphates was carried out by CIAP treatment. Therefore, 20 µg of *in vitro* transcribed RNA were treated with 30 U CIAP for 2 hrs at 37 °C in the buffer supplied with the enzyme, in the presence of 10 U RNase inhibitor. Following dephosphorylation, RNA clean up was performed using the RNeasy Mini Kit to obtain dephosphorylated RNA of high purity that can be used for

stimulation. Biotinylated VSV RNA, which was used for immunoprecipitation studies was also transcribed from the PCR product described above, by using a mixture of unlabeled UTP (6,5 mM final concentration) and Biotin-16-uridine-5'-triphosphate (3,5 mM final concentration) in the IVT reaction.

### ***3.2.6.5 Isolation of total RNA from virus-infected cells***

For isolation of total RNA from virus-infected cells, cells were seeded in 6-well plates at a density of  $1 \times 10^6$  cells/well 18 hrs prior to infection. HEp-2 cells and Hela cells were either infected with VSV wild-type and EMCV at an MOI of 1, respectively, or left untreated. After 16 hrs, total RNA was isolated using the RNeasy Mini Kit. RNA was eluted from the column with 30  $\mu$ l RNase free water. To remove residual contaminating genomic DNA from the RNA preparations, DNase I digestion was performed. To this end, 1  $\mu$ g RNA was diluted in the  $MgCl_2$  containing buffer supplied with the enzyme and treated with 20 U DNase I in the presence of 20 U RNase inhibitor. After 1 h incubation at 37 °C, 1  $\mu$ l RNase-free EDTA was added and the reaction was further incubated at 65 °C for 10 min to inhibit DNase I. Ultimately, the RNA was purified using the RNA cleanup protocol provided with the RNeasy Mini Kit to obtain a highly pure nucleic acid that can be used for subsequent stimulation of eukaryotic cells. RNA concentration was determined using the Nanodrop spectrophotometer.

### ***3.2.6.6 Isolation of total RNA from stimulated DCs and expression analysis of cytokines and ISGs by quantitative real-time PCR***

#### **3.2.6.6.1 Isolation of total RNA from stimulated GM-CSF derived DCs**

For isolation of total RNA from GM-CSF DCs derived from either WT C57BL/6 or *Trif* mutant mice, cells were directly stimulated with live *H. pylori* SS1 in 10 cm dishes at an MOI of 50 on day 7. 6 hrs after stimulation, cells in suspension were collected by pipetting. The remaining cells that attached to the culture surface were collected by incubation with 10 ml PBS/0.05mM EDTA for 1 min at 37 °C and subsequent pipetting. Cells were collected by centrifugation for 5 min at 1500 rpm and 4 °C. The supernatant was discarded and the cell pellet was carefully resuspended in 500  $\mu$ l Trizol reagent to lyse the cells.

The cell lysate was then passed through a 20 G needle to homogenize the sample. Subsequently, isolation of total RNA from stimulated GM-CSF DCs using Trizol reagent was performed. Briefly, 200  $\mu$ l chloroform were added and tubes were vigorously shaken for 15 s. After 3 min incubation at RT, samples were centrifuged for 15 min at 13000 rpm and 4 °C in a tabletop centrifuge to separate samples into a lower phenol phase, an interphase and an upper RNA containing aqueous phase. The aqueous phase was transferred to a fresh 1.5 ml tube and mixed with 250  $\mu$ l 2-Propanol. To precipitate RNA, the samples were incubated at RT for 10 min followed by centrifugation for 10 min at 13000 rpm and 4 °C. Finally, the pellet was washed once with 70 % Ethanol (13000 rpm, 4 °C, 5 min), the supernatant was carefully removed and the RNA pellet was dried at RT. The pellet was subsequently dissolved in 30  $\mu$ l RNase-free water by incubation at 55 °C for 10 min in a thermomixer.

To remove residual contaminating genomic DNA from the RNA preparation, DNase I digestion was performed. To this end, 1  $\mu$ g RNA was treated with 20 U DNase I and the MgCl<sub>2</sub> containing buffer supplied with the enzyme in the presence of 20 U RNase inhibitor. After 1 h incubation at 37 °C, 1  $\mu$ l RNase-free EDTA was added and the reaction was further incubated for 10 min at 65 °C to inhibit DNase I. RNA purity, integrity and concentration were determined using the Nanodrop spectrophotometer. RNA was stored at – 80 °C until used for cDNA synthesis.

#### **3.2.6.6.2 First strand cDNA synthesis**

cDNA, which was subsequently used for quantitative real-time PCR, was synthesized using Superscript II reverse transcriptase and the following protocol:

- (I) 11  $\mu$ l RNA  
1  $\mu$ l Oligo(dT)15 primer  
1  $\mu$ l dNTP Mix  
Incubation at 65 °C for 5 min, followed by 2 min on ice.
  
- (II) *addition of*  
4  $\mu$ l 5 x Reverse transcription buffer  
1  $\mu$ l 0.1 M DTT  
1  $\mu$ l RNase inhibitor  
1  $\mu$ l Superscript II (200 U)

Incubation at 50 °C for 1 h, followed by 10 min at 70 °C to inactivate Superscript II.

### 3.2.6.6.3 Quantitative real-time PCR

Expression of cytokines and ISGs upon stimulation of GM-CSF DCs with live *H. pylori* SS1 was analyzed by quantitative real-time PCR using the following reaction conditions:

2 x SYBR Green Mastermix	12.5 µl
Primer for (10 µM)	2.25 µl
Primer rev (10 µM)	2.25 µl
ddH <sub>2</sub> O	ad 20 µl
cDNA (diluted 1:5 in ddH <sub>2</sub> O)	5 µl

Primer sequences used for SYBR Green Taqman PCR are listed in chapter 8, section 8.5, Table 15.

Quantitative analysis was performed using the  $2^{-\Delta\Delta CT}$  method (Livak and Schmittgen, 2001), which is a convenient way to analyze relative changes in gene expression. This method is based on the comparison of the fluorescence signals of a given target gene and an unregulated housekeeping gene, such as the Cyclophilin A gene (*Ppia*). The difference in the signal intensities of target gene and housekeeping gene results in the  $\Delta CT$  value. The obtained  $\Delta CT$  values of all samples to be analyzed are normalized to a reference condition (i.e. an untreated control), which depends on the individual experiment, generating the respective  $\Delta\Delta CT$  values. For the treated samples, evaluation of  $2^{-\Delta\Delta CT}$  indicates the fold change in gene expression relative to the untreated control.

Since the gene encoding IFN- $\beta$  does not contain introns, quantitative real time PCR was also performed with RNA instead of cDNA to control for residual contaminating DNA. Amplification of a PCR product was never observed in the RNA control reaction, confirming that the RNA does not contain relevant amounts of genomic DNA after DNase I treatment.

### 3.2.6.7 Isolation of RNA from bacteria

For isolation of RNA from *H. pylori* SS1 and *E.coli* K12 strains, bacteria were grown to an OD<sub>590</sub> of 1 which was considered to contain about 10<sup>9</sup> organisms/ml. *H. pylori* SS1

was grown as described (Rad *et al.*, 2007). *E. coli* K12 strains were grown in LB medium without antibiotics. Bacteria were centrifuged for 10 min at 7500 rpm and 4 °C to collect bacteria. The bacterial pellet was then resuspended in 300 µl RNeasy Protect Cell Reagent to stabilize the RNA and centrifuged at 6900 rpm for 5 min at 4 °C. The supernatant was removed and the pellet was subsequently resuspended in 600 µl RNeasy Lysis Buffer provided with the RNeasy Mini Kit, which was used for all further isolation steps according to the protocol given by the manufacturer. RNA was eluted from the column using 50 µl RNase-free water.

Next, the RNA was treated with 20 U DNase I for 2 hrs at 37 °C in the MgCl<sub>2</sub> containing buffer supplied with the enzyme. To prevent RNA degradation, 20 U RNase inhibitor were added to the reaction. DNase I was subsequently inhibited by incubation for 10 min at 65 °C together with 2 µl RNase-free EDTA. Finally, all traces of enzymes were removed by RNA purification using the RNA cleanup protocol provided with the RNeasy Mini Kit. RNA concentration and integrity were determined using the Nanodrop spectrophotometer.

### **3.2.7 Protein biochemistry**

#### ***3.2.7.1 Preparation of cell lysates***

Cell lysis was always carried out on ice. Cells were lysed at different time points indicated in the respective figure legends in chapter 4. Depending on the application, different buffers were applied to prepare cell lysates.

For preparation of total lysates using M-PER lysis buffer, the cells were removed from the incubator and resuspended in culture medium. After centrifugation at 4 °C and 1500 rpm for 5 min, the cell pellet was washed twice with ice-cold PBS and then lysed with 300 µl to 500 µl M-PER lysis buffer depending on the pellet size. The lysate was transferred into a 1.5 ml tube and subsequently centrifuged at 13000 rpm for 15 min in a tabletop centrifuge to remove cell debris and nuclei. The cleared supernatant was transferred into new precooled 1.5 ml tubes and stored at – 80 °C.

Cells that were lysed with IP lysis buffer, were lysed directly in the culture plates. The culture medium was removed, cells were rinsed once with ice-cold PBS, the PBS was then discarded and depending on the size of the tissue culture plate, 150 µl (6-well plate) to 500 µl (10 cm dish) IP lysis buffer were directly added to the cell monolayers.

The plates were swirled gently to completely cover the cells with lysis buffer and incubated on ice. After 5 min, cells were scraped and incubated on ice for additional 15 min to allow complete lysis. The lysate was then homogenized by carefully pipetting up and down. Finally, the lysate was transferred to a prechilled 1.5 ml tube and centrifuged for 15 min at 14000 rpm and 4 °C to remove cell debris and nuclei. Then, the clear supernatant was transferred into a new tube and stored at – 80 °C.

### ***3.2.7.2 Determination of protein concentration***

The protein concentration of the obtained cell lysates was determined by Bradford assay. The method of Bradford is based on a shift of the absorption maximum of Coomassie Brilliant blue from 465 nm to 595 nm upon binding to proteins that can be easily measured by photometric analysis. The Bradford Reagent was diluted according to the instructions given by the supplier and 2 µl of the cell lysate were subsequently added to 1 ml of the diluted reagent in a photometer cuvette. After 5 min incubation in the dark, the OD<sub>595</sub> was determined. The protein concentration was calculated using a bovine serum albumin (BSA) standard curve.

### ***3.2.7.3 Immunoprecipitation***

Immunoprecipitation (IP) was performed using either Flag-agarose beads or protein G sepharose (PGS).

For immunoprecipitation experiments using Flag-agarose beads, cells were lysed in RIPA buffer according to the manufacturer's protocol with the modification that Flag-IP lysis buffer was used for all washing steps. 40 µl of the Flag-agarose gel suspension were washed twice with Flag-IP lysis buffer (500 µl for each washing step) and subsequently recovered at the bottom of the tube by centrifugation for 1 min at 6000 rpm and 4 °C. Next, protein lysates were added to the Flag-beads and the mixture was incubated for 2 hrs at 4 °C on a roller wheel. Then, Flag-beads were collected by centrifugation for 5 min at 6000 rpm and 4 °C, the supernatant containing unbound protein was removed, the beads were carefully resuspended in 1 ml Flag-IP lysis buffer and subsequently centrifuged for 1 min at 6000 rpm and 4 °C. This was repeated two more times to completely remove all non-specific proteins. Ultimately, the protein complexes were eluted from the beads by boiling at 95 °C for 5 min using 2 x Laemmli sample buffer containing β-Mercaptoethanol. The sample was centrifuged at 6000 rpm

for 5 min to collect the beads and finally the cleared supernatant, containing the protein fraction of interest, was removed and stored at  $-20\text{ }^{\circ}\text{C}$  until immunoblot analysis.

Protein G sepharose was used to perform IPs with either RIG-I- or Ubiquitin-specific antibodies. Briefly, the cells to be analyzed were lysed with IP lysis buffer as described previously (section 3.2.7.1). Protein G sepharose was washed three times with  $500\text{ }\mu\text{l}$  IP lysis buffer prior to use by centrifugation for 5 min at 6000 rpm and  $4\text{ }^{\circ}\text{C}$ . First, protein G sepharose was added to the lysate ( $100\text{ }\mu\text{l}$  PGS/ml lysate) and the lysates were precleared for 1 h at  $4\text{ }^{\circ}\text{C}$ . Next, the samples were centrifuged for 5 min at 6000 rpm and  $4\text{ }^{\circ}\text{C}$  to recover the lysate, which contained the proteins of interest. The cleared lysate was then incubated with the respective antibody at  $4\text{ }^{\circ}\text{C}$  overnight to promote formation of antibody-protein complexes. To recover the proteins of interest, protein G sepharose ( $200\text{ }\mu\text{l}$  PGS/ml lysate) was added to the lysate-antibody mixture to bind the antibody with high affinity. After an incubation of 2 hrs at  $4\text{ }^{\circ}\text{C}$ , samples were centrifuged for 5 min at 6000 rpm and  $4\text{ }^{\circ}\text{C}$  to collect PGS-antibody-protein complexes. The supernatant was carefully removed, the PGS beads were resuspended in 1 ml IP lysis buffer and subsequently centrifuged for 5 min at 6000 rpm and  $4\text{ }^{\circ}\text{C}$ . This washing step was repeated three times. The proteins were finally recovered from the beads by incubating the samples at  $95\text{ }^{\circ}\text{C}$  for 5 min followed by a 5 min centrifugation step at 6000 rpm. The clear supernatant containing proteins that have been recovered by IP, was transferred to a fresh tube and stored at  $-20\text{ }^{\circ}\text{C}$ . All incubation steps involving PGS and antibody were performed on a roller wheel.

#### ***3.2.7.4 SDS polyacrylamide gel electrophoresis (PAGE)***

Proteins were separated by size using SDS polyacrylamide gel electrophoresis under denaturing conditions. SDS-PAGE was performed using gels of 1.5 mm thickness. First, the 10 % resolving gel was poured and immediately covered with 2 ml 2-Propanol. After polymerization, the 2-Propanol was decanted and the gels rinsed several times with  $\text{ddH}_2\text{O}$ . Finally, the stacking gel (4 %) was poured and the comb (10 lanes) inserted. For gel composition see Table 7.

Before running the gels, the running cassette was assembled and the gels were completely overlaid with 1 x running buffer. Then, the combs were removed and the lanes flushed with running buffer using a 20 G needle to remove residual acrylamide. To analyze expression of RLRs,  $60\text{ }\mu\text{g}$  total lysate were loaded onto the gel. Therefore,

the corresponding volume of the protein sample was mixed with 2 x Laemmli sample buffer containing  $\beta$ -Mercaptoethanol and incubated for 5 min at 95 °C prior to loading. After cooling to RT, samples were loaded on the gel. For estimation of the protein size, 8  $\mu$ l of a protein standard were loaded onto the gel. Gels were run in 1 x running buffer at 120 V until the bromophenol running front left the separating gel at the bottom (about 60 to 90 min). Large gels (14 x 15 cm), which were used when more than 50  $\mu$ l of protein lysates had to be analyzed, were prepared with the same formulation, but using the fourfold volume. In case of these gels, the stacking gel was run at 20 mA until the samples entered the resolving gel, which was then run at 40 mA for 3 to 4 hrs until the running front reached the bottom of the gel.

**Table 7.** *Composition of SDS-PAGE gels*

The indicated amounts are sufficient to prepare 1 gel (size 6 x 9 cm) that is compatible with the Mini Protean II vertical electrophoresis system.

\*Rotiphorese gel 30, which is a ready to use 30 % acrylamide-bisacrylamide stock solution (ratio 37,5:1)

	<i>Resolving Gel</i>	<i>Stacking Gel</i>
	10 %	4 %
<b>Acrylamide solution *</b>	3.3 ml	2.5 ml
<b>4 x Resolving Gel Buffer</b>	2.5 ml	—
<b>4 x Stacking Gel Buffer</b>	—	3.75 ml
<b>ddH<sub>2</sub>O</b>	4.1 ml	9.75 ml
<b>10 % (w/v) APS</b>	100 $\mu$ l	100 $\mu$ l
<b>TEMED</b>	3.3 $\mu$ l	20 $\mu$ l

### 3.2.7.5 *Silver staining of SDS-PAGE gels*

Silver staining was performed to obtain distinct protein bands that can be submitted for mass spectrometry (MS) analysis. Thus, a silver staining protocol compatible with MS analysis was chosen (Winkler *et al.*, 2007). Silver staining is a highly sensitive method for directly detecting proteins in the polyacrylamide gels without the need of antibody incubation and autoradiography. Silver staining methods are about 10 to 100 times more sensitive than Coomassie Blue staining techniques. Thus, silver staining is the method of choice, when the amount of protein to be analyzed is limited.

For subsequent visualization of proteins, large gels were run as described previously. Before performing the silver stain, the stacking gels were removed and gels were shortly rinsed in ddH<sub>2</sub>O to remove residual running buffer. Then, gels were incubated in fixer for 15 min for three times in total. After washing (3 x 10 min) in 50 % EtOH, gels were incubated in sensitizer for 30 sec, rinsed with ddH<sub>2</sub>O, subsequently stained with silver nitrate for 20 min and again shortly rinsed with ddH<sub>2</sub>O. Next, the gels were incubated with developer and maintained in this solution until the proteins appeared as brown bands without an increased background stain. The staining reaction was blocked by immediately transferring the gels to stop solution when protein bands were clearly visible. Finally, bands of interest were cut out using a sterile scalpel, transferred into 1.5 ml tubes, stored in ddH<sub>2</sub>O and submitted for mass spectrometry analysis.

#### **3.2.7.6 *Mass spectrometry analysis***

Mass spectrometry analysis was performed at the Core Facility Proteomics of the Helmholtz Zentrum München using the Orbitrap XL mass spectrometer. Samples were processed (trypsin digestion) and prepared for analysis at the Helmholtz Zentrum. The Orbitrap XL is a mass spectrometer that combines two flexible and high-resolution analyzer systems, a linear ion trap and an Orbitrap mass analyzer. Briefly, with this system free ions are generated in the gas phase by electrospray ionisation (ESI). These ions are subsequently collected in the linear ion trap and stabilized by helium gas in the storage trap. In the next step ions are vertically transferred to the orbitrap analyzer and ion packages are positioned in the center of the analyzer. Finally, Orbitrap signals are amplified and transformed (Fast Fourier Transform, FFT), leading to the generation of a FFT frequency spectrum (detection). The last step is the conversion of the FFT spectrum into a mass spectrum that is analyzed.

#### **3.2.7.7 *Immunoblotting***

After the separation of the proteins by SDS-PAGE using the Mini Protean II system (small gels), proteins were transferred from the gels to a PVDF membrane by semidry blotting. To this end, the PVDF membrane was activated by incubation in methanol for 5 min at RT, followed by brief washing in ddH<sub>2</sub>O and a short equilibration in blotting buffer. Three sheets of Whatman blotting paper of the same size as the gel were soaked in blotting buffer and placed on the bottom electrode. The gel and the PVDF membrane were placed exactly on the bottom paper and covered with additional three sheets of

blotting paper that had also been equilibrated in blotting buffer. Before placing the upper electrode on the sandwich, bubbles were removed and the bottom electrode was dried from residual blotting buffer. Blotting was performed at 320 mA for 2 hrs. In case of large gels, proteins were transferred to nitrocellulose membrane using the tank blotting method at 25 V and 4 °C for 16 to 18 hrs.

For protein detection, the membranes were subsequently incubated with specific antibodies (Table 4). First, the membranes were blocked in blocking buffer for 1 h at 4 °C to avoid unspecific antibody binding. Then, the membranes were washed three times for 10 min in TBS-T and subsequently incubated overnight with the respective primary antibody at 4 °C. On the next day, the membranes were extensively washed with TBS-T for 90 min (each washing step 15 min) and incubated with the appropriate HRP-conjugated secondary antibody for 1 h at RT. Then, membranes were washed again in TBS-T for 90 min, incubated with Super Signal West Pico Chemiluminescent detection reagent and subjected to autoradiography to visualize protein bands. All antibody incubations and washing steps were carried out on a shaking platform.

If the membrane was subjected to incubation with a second different antibody, previous antibodies were removed from the membrane by stripping. Briefly, the membrane was rinsed in ddH<sub>2</sub>O for 10 min, followed by incubation in Restore Western Blot Stripping Buffer at 37 °C for 1 h with gentle agitation. After washing in ddH<sub>2</sub>O for 10 min at RT, stripped membranes were incubated again in blocking buffer at 4 °C overnight and subsequently subjected to a second round of protein detection.

### **3.2.7.8 RNA binding assay**

To analyze whether activation of RIG-I by 5'-triphosphate RNA is caused by direct RNA-protein interaction, a RNA binding assay was established. For this purpose,  $3 \times 10^8$  HEK293 cells (thirty 10 cm dishes) in total were transfected with either wild-type RIG-I or RIG-I C→R mutant expression plasmids using Lipofectamine2000 (6 µg plasmid DNA per dish). 24 hrs post transfection, cytoplasmic extracts were prepared as described by Saito *et al.* (2007) with minor modifications.

Briefly, cells were harvested, centrifuged for 5 min at 1500 rpm and 4 °C and the pooled cell pellet was washed with ice-cold PBS. Again, the cells were collected by centrifugation for 5 min at 1500 rpm and 4 °C. The pellet was then resuspended in five

packed cell volumes of buffer A (5 ml), followed by an incubation on ice for 5 min. After centrifugation for 10 min at 2000 x g and 4 °C, the cells were resuspended in two packed cell volumes of buffer A (2 ml) and subsequently homogenized using a glass homogenizer. The homogenate was centrifuged for 10 min at 2000 x g and 4 °C and the supernatant was recovered. Finally, the cytoplasmic extract was prepared by adding an additional 10 % volume of 10 x cytoplasmic extract buffer (300 µl) to this supernatant. Next, the mixture was centrifuged at 100000 x g in a Beckman 100 Ti ultracentrifuge rotor for 60 min at 4 °C. Then, the supernatant was subjected to dialysis using Slide-A-Lyzer dialysis cassettes against dialysis buffer for 7 hrs at 4 °C. The dialyzed material was centrifuged at 55000 x g for 20 min, the supernatant was collected and protein concentration was determined using Bradford assay (section 3.2.7.2). Samples were aliquoted and stored at – 80 °C until used in RNA binding studies.

Biotinylated 5'-triphosphate RNA encompassing the VSV leader RNA sequence (bio-pppVSVL) was generated by IVT as described previously (section 3.2.6.4). The RNA binding assay was performed according to Saito *et al.* (2007). 1 µg of bio-pppVSVL was mixed with 10 µg of the respective cytoplasmic extract in a total volume of 10 µl and this binding reaction was incubated for 1 h at 25 °C in a thermal cycler. Given that RNA is directly interacting with RIG-I, the resulting RNA-protein complexes consisting of bio-pppVSVL and Flag-RIG-I can be specifically recovered by pulldown assay using streptavidin (SA) agarose, which binds to the biotin tag of the RNA. Thus, the SA agarose slurry was washed five times with PBS at 13000 rpm for 1 min. Then, the binding reaction, in which RNA-protein complexes might have formed, was transferred to 25 µl SA agarose diluted in 400 µl dialysis buffer. Samples were incubated at 4 °C for 2 hrs on a roller wheel. Next, the SA agarose beads were collected by centrifugation for 1 min at 13000 rpm and 4 °C. The supernatant, containing unbound protein, was discarded and the SA agarose pellet was washed twice with 400 µl dialysis buffer. Finally, the samples were resuspended in 2 x sample buffer containing β-Mercaptoethanol and incubated in a boiling bath for 5 min at 95 °C. Samples were analyzed by SDS-PAGE and immunoblotting using anti-Flag M2 antibody to detect WT or mutant RIG-I proteins, respectively.

## 4 RESULTS

### 4.1 Identification of a functional domain at the C-terminus of RIG-I

Although the specific ligand of RIG-I was identified by two independent groups (Hornung *et al.*, 2006; Pichlmair *et al.*, 2006) as dsRNA bearing a triphosphate moiety at the 5'-end, the mode of RNA sensing by RIG-I remained elusive.

To gain further insight into the function of RIG-I and the molecular mechanisms by which RIG-I recognizes 5'-triphosphate RNA, we analyzed the RIG-I molecule at the level of the amino acid sequence and the predicted protein structure in collaboration with the Structural Biology Group of Prof. Karl-Peter Hopfner (Department of Biochemistry, Gene Center Munich). A putative domain at the C-terminus of RIG-I was mapped to the region spanning AA 802 to 925 of human RIG-I using database search, structure prediction software and limited proteolysis, which was performed by Sheng Cui in the group of Prof. Karl-Peter Hopfner.

#### 4.1.1 AA 802 to 925 of RIG-I can be expressed as Flag-tagged protein

To define the functional role of this putative domain, an expression construct bearing an N-terminal Flag-tag comprising this region was cloned. The construct will be referred to as RIG-I (AA 802-925) in this study. To verify the expression of this protein with an approximate MW of 15 kDa, 10 µg of plasmids encoding Flag-RIG-I (AA 802-925) or RIG-I full length were transfected into HEK293, respectively. Whole cell lysates (WCLs) were prepared 18 hrs after transfection and subsequently analyzed by SDS PAGE and immunoblotting using a Flag-specific antibody. Integrity of the lysates was confirmed with an actin-specific antibody. As depicted in Figure 6, the putative domain comprising AA 802 to 925 of human RIG-I was artificially expressed in HEK293 cells.

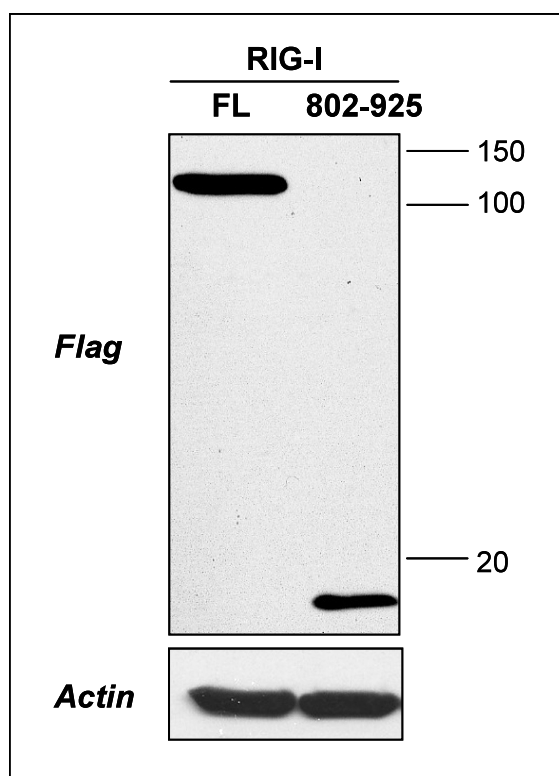


**Figure 6. Overexpression of Flag-RIG-I (AA 802-925)**

60  $\mu$ g of whole cell lysate from HEK293 cells that were transfected with either 10  $\mu$ g of RIG-I full length (FL) or RIG-I (AA 802 to 925) plasmid was subjected to SDS-PAGE and subsequent western blotting using a Flag- or  $\beta$ -Actin specific antibody, respectively. Molecular weight of the proteins is indicated in kDa.

#### 4.1.2 Overexpression of RIG-I (AA 802-925) inhibits RIG-I-mediated IFN induction

To explore the effects of the putative RIG-I C-terminal domain on RIG-I-mediated signal transduction, IFN- $\beta$  promoter reporter assay was performed. HEK293 cells were cotransfected with an IFN- $\beta$  promoter luciferase reporter plasmid, the pRL-TK internal control vector and either RIG-I full-length, RIG-I (AA 802-925) or RIG-I full-length together with an increasing amount of RIG-I (AA 802-925). 18 hrs after transfection, cells were subsequently transfected with *in vitro* transcribed 5'-triphosphate RNA (pppVSVL, for generation see section 3.2.6.4) or infected with VSV-M51R, which was already described in section 3.1.5.2. Overexpression of the putative C-terminal domain of human RIG-I potently inhibited RIG-I-mediated IFN- $\beta$  promoter activation upon both 5'-triphosphate RNA stimulation and VSV-M51R infection (Figure 7A and B).

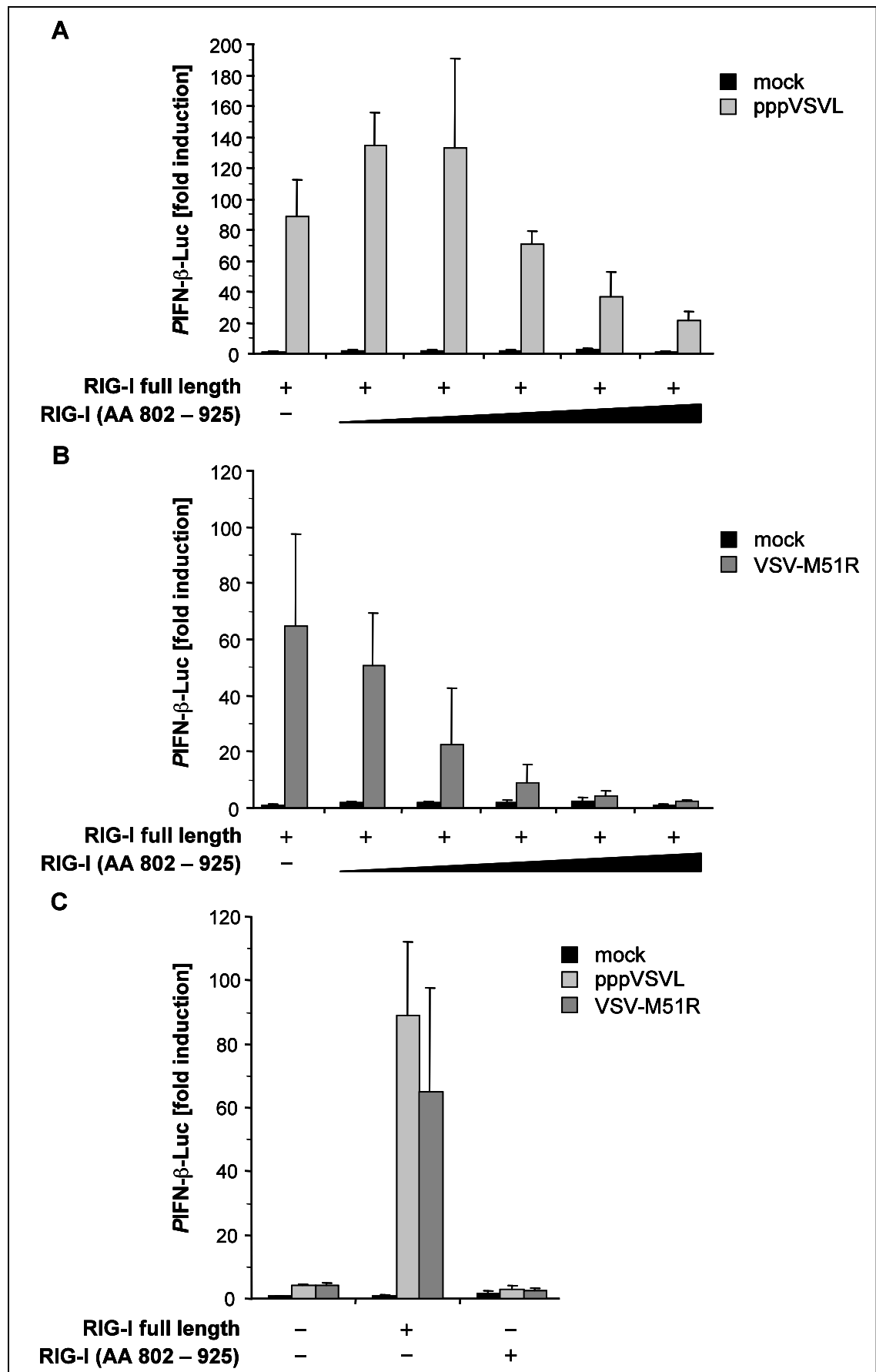


**Figure 7. RIG-I (AA 802-925) acts as an inhibitor of RIG-I-mediated IFN induction**

(A) and (B) HEK293 cells were either transfected with a RIG-I full length construct alone (2.5 ng) or RIG-I full-length together with increasing amounts of the plasmid encoding RIG-I (AA 802-925) (1 ng, 5 ng, 10 ng, 50 ng and 100 ng), respectively, together with an IFN- $\beta$  promoter luciferase construct (100 ng) as well as the internal control vector pRL-TK (10 ng). After 18 hrs, cells were subsequently stimulated by transfection with *in vitro* transcribed VSV leader RNA (pppVSVL, 1  $\mu$ g/ml) (A) or VSV-M51R infection (10 MOI) (B). IFN- $\beta$  promoter activity was measured by dual luciferase assay after 18 hrs.

(C) HEK293 cells were transfected with empty vector (100 ng), RIG-I full length (2.5 ng) and RIG-I (AA 802-925) (100 ng), respectively, together with the above described luciferase constructs. Subsequent stimulation and luciferase assay were performed as already described. IFN- $\beta$  promoter activity is shown as fold induction compared to mock-treated empty vector control. Data represent the mean  $\pm$  SD ( $n = 3$ ).

The suppression of the RIG-I-mediated IFN response by RIG-I (AA 802-925) was stronger in virus-infected cells (Figure 7B) compared to cells that have been stimulated with *in vitro* transcribed 5'-triphosphate RNA pppVSVL. RIG-I (AA 802-925) itself was not able to activate the IFN- $\beta$  promoter upon stimulation with both pppVSVL transfection and VSV-M51R infection. Even at a high concentration of 100 ng plasmid, which was demonstrated to have a strong suppressive effect on RIG-I-mediated IFN induction, activation of the IFN- $\beta$  promoter remained at the level of the empty vector control (Figure 7C). Thus, the C-terminal domain (CTD) of RIG-I, comprising AA 802 to 925, has repressor function and represents another functional domain in addition to the CARDs and the helicase domain.

### 4.1.3 The C-terminal domain of RIG-I contains conserved cysteine residues which form a zinc-binding cluster

Our hypothesis was, that the C-terminal domain apart from inhibiting constitutive signaling of RIG-I might be involved in specific RNA ligand recognition.

To further investigate this, comparative sequence analysis was performed, aligning the corresponding C-terminal regions of the RLR family members RIG-I, MDA5 and LGP2 (Figure 8).

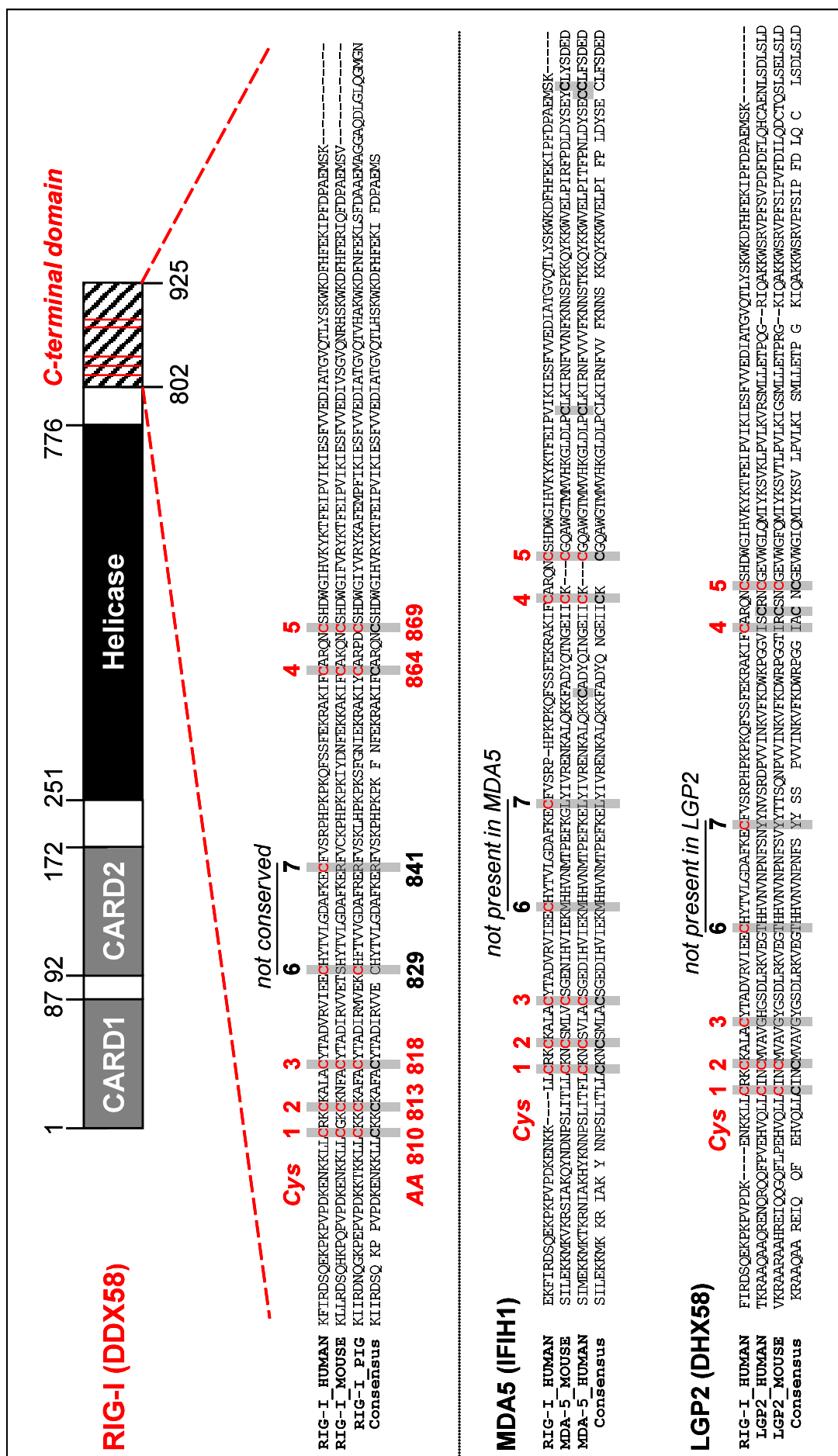


**Figure 8. Comparative sequence analysis of the C-terminal domain of RIG-I and the homologous regions of MDA5 and LGP2**

The C-terminal domain of human RIG-I, comprising AA 802 to 925, contains five conserved cysteine residues (Cys) that are conserved between species (indicated in red). In contrast, the Cys residues at AA position 829 and 841 (indicated in black) are not conserved between human, mouse and pig RIG-I. The homologous regions of MDA5 and LGP2 also possess these invariant Cys residues.

The alignment revealed that the CTD of human RIG-I contains five conserved cysteine residues at AA position 810, 813, 818, 864 and 869, respectively, that are indicated in red as Cys1 to Cys5. Furthermore, these residues are conserved between species as depicted in the sequences of RIG-I from mouse and pig, respectively (Figure 8, upper part, highlighted in grey). Human RIG-I contains two other Cys residues within this region at AA residue 829 and 841 (indicated in black as Cys6 and Cys7), which are not conserved between species. Interestingly, sequence comparison of human RIG-I and both mouse and human MDA5 as well as human and mouse LGP2, respectively, revealed that the homologous regions of MDA5 and LGP2 also contain these five invariant cysteine residues (Figure 8, lower part). The C-terminal cysteine rich domain therefore is a shared feature among the RLRs.

To learn more about the structure of the RIG-I CTD, a protein data bank (PDB) search (using the DALI domain dictionary, which is a numerical taxonomy of all known structures in the PDB; (Holm and Sander, 1993)) for structural relatives of the C-terminal domain was performed (Sheng Cui and Prof. Karl-Peter Hopfner). The search resulted in two significant hits, the C-terminal methionine sulfoxide reductase domain of PilB (PDB entry 1L1D) and the GDP/GTP exchange factor MSS4 (PDB entry 2FU5).

In line with this, further structural analysis (crystallography, 2.7 Å resolution by Sheng Cui and Karl-Peter Hopfner) revealed a zinc-binding site in the C-terminal region of RIG-I (Figure 9). Together, the four invariant Cys residues located at AA position 810, 813, 864 and 869 (Figure 9, green sticks) coordinate the zinc ion (Figure 9, depicted as magenta sphere). Although the Cys residue located at position 818 is conserved, it is not directly involved in the cluster formation. It was demonstrated to be closely located to the zinc-binding site, but does not bind the metal ion directly. In summary, the C-terminal domain of RIG-I spans AA 802 to 925, has a dominant negative effect on RIG-I-mediated IFN induction when overexpressed and contains a zinc-binding cluster

that is coordinated by four conserved Cys residues located at AA position 810, 813, 864 and 869, respectively.

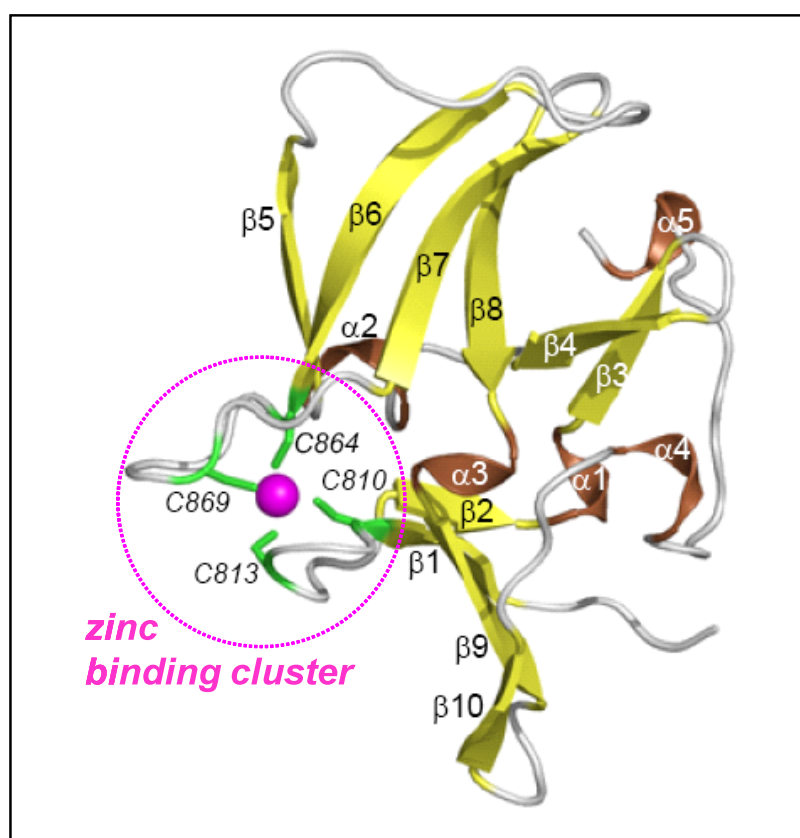


**Figure 9.** *Ribbon model of the RIG-I C-terminal domain (AA 802-925)*

The CTD is structurally organized in three leaves, consisting of two four-stranded ( $\beta 1$ ,  $\beta 2$ ,  $\beta 9$ ,  $\beta 10$  and  $\beta 5$ ,  $\beta 6$ ,  $\beta 7$ ,  $\beta 8$ ) and two one-stranded ( $\beta 3$ ,  $\beta 4$ ) antiparallel  $\beta$  sheets. Small helical turns connect the three  $\beta$  sheets. The two four-stranded  $\beta$  sheets are laterally connected by two protruding loops, each containing two highly conserved cysteine residues (C810, C813 and C864, C869). Together, the four invariant Cys residues (annotated as green sticks) coordinate the zinc ion (depicted as magenta sphere). The model was generated by Karl-Peter Hopfner and Sheng Cui (Structural Biology Group, Department of Biochemistry, Gene Center Munich).

#### 4.1.4 The role of C-terminal Cys residues for RIG-I-mediated IFN induction

##### 4.1.4.1 *IFN- $\beta$ promoter activation in response to virus infection and 5'-triphosphate RNA*

To analyze the functional relevance of the CTD, site-directed mutagenesis was performed to generate full-length RIG-I mutants, in which the conserved and non-conserved Cys residues are replaced by arginine (Arg) (C $\rightarrow$ R mutation). As already described, the CTD of RIG-I contains seven cysteines. Residues C810, C813, C864 and

C869 are conserved in all RLR family members, RIG-I, MDA5 and LGP2 (Figure 8), and form the identified zinc-binding cluster (Figure 9). C818, which was shown to be closely located to the zinc-binding site but not involved in binding the zinc ion itself, is conserved between RIG-I and MDA5 but not LGP2 (Figure 8). Mutation of the two non-conserved Cys residues (C829 and C841) served as control.

Wild-type and mutant RIG-I were tested for their ability to induce IFN- $\beta$  promoter activation in response to VSV-M51R infection using luciferase reporter assay (Figure 10A). Overexpression of WT RIG-I confers a low level of constitutive IFN- $\beta$  promoter activation in the absence of virus infection (15-fold induction compared to empty vector control). Infection with VSV-M51R results in a strong induction of IFN- $\beta$  promoter activity (32-fold compared to mock-infected cells expressing WT RIG-I). Activation of the IFN- $\beta$  promoter is also observed in RIG-I harbouring mutations of the non-conserved Cys residues, C829R and C841R, respectively. Interestingly, C841R showed a strong induction of the IFN- $\beta$  promoter, which was comparable to activation levels that have been observed with RIG-I WT, whereas lower IFN- $\beta$  promoter activation was achieved with the C829R mutant. However, mutation of any of one of the four invariant cysteines that form the zinc-binding cluster (C810, C813, C864 and C869) and the closely located C818 to arginine completely abolished the response to VSV-M51R.

To exclude, that these defects in IFN signaling are due to insufficient protein levels caused by reduced expression of mutant RIG-I compared to wild-type RIG-I, expression of the RIG-I cysteine mutants was monitored by immunoblotting using a Flag-specific antibody (Figure 10B). All mutants, except C818R were detected, indicating that the dramatically reduced IFN inducing activity is not due to a lack of protein expression. Since RIG-I C869R seemed to be expressed at lower levels compared to WT RIG-I, the IFN- $\beta$  promoter reporter assay was repeated using 400 ng of the respective RIG-I cysteine mutant plasmids for transfection (Figure 10A, insert). Again, RIG-I cysteine mutants were not able to efficiently induce IFN- $\beta$  promoter activity in response to VSV-M51R infection. However, transfection of these higher amounts of expression plasmids suggested intact constitutive signaling of RIG-I invariant Cys mutants since the IFN- $\beta$  promoter was activated by overexpression in the absence of virus infection.

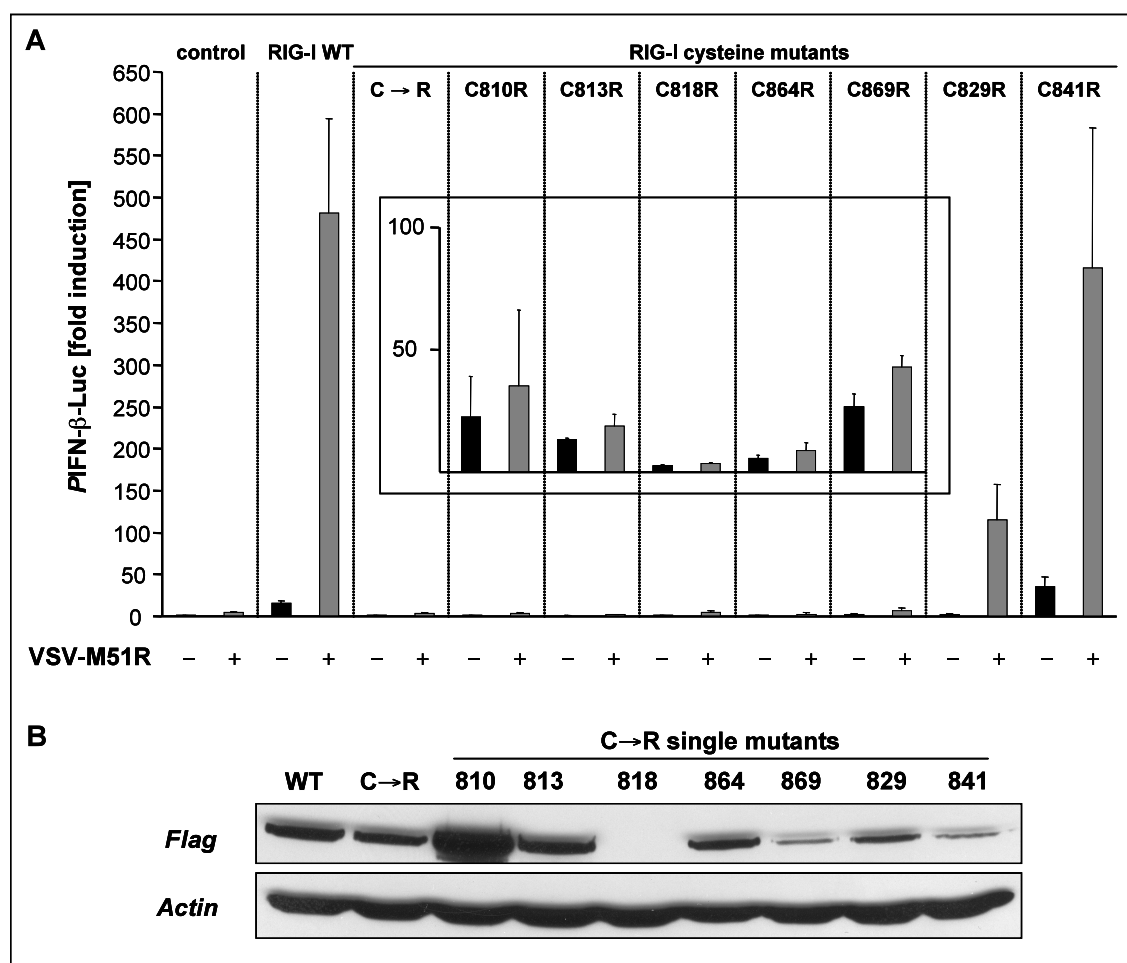


**Figure 10.** Mutation of conserved Cys residues to arginine (C→R) within the RIG-I CTD abolishes activation of the IFN-β promoter in response to virus infection

(A) HEK293 cells were either transfected with empty vector control, RIG-I WT or RIG-I full-length Cys mutants (100 ng each) together with an IFN-β promoter luciferase construct (100 ng) as well as the internal control vector pRL-TK (10 ng). In the RIG-I C→R mutant, all five invariant Cys residues were mutated to Arg. C810R, C813R, C818R, C864R and C869R mutants correspond to the conserved Cys residues, whereas in C829R and C841R the non-conserved Cys residues have been mutated. After 18 hrs, cells were subsequently infected with VSV-M51R (10 MOI). IFN-β promoter activity was measured by dual luciferase assay 18 hrs p.i.

(A, insert) HEK293 cells were treated as described above, with the modification that 400 ng of each RIG-I Cys single mutant was used for transfection. IFN-β promoter activity is shown as fold induction compared to mock-treated empty vector control. Data represent the mean ± SD ( $n = 5$ ).

(B) 60 μg whole cell lysates obtained from HEK293 cells transfected with 10 μg of either Flag-tagged WT RIG-I or RIG-I containing the respective cysteine (C) to arginine (R) mutations were analyzed by SDS-PAGE and immunoblotting with anti-Flag and anti-β-Actin antibody.

Although, expression of RIG-I containing point mutations of the conserved cysteine residues was confirmed by immunoblotting (Figure 10B), I wanted to prove the role of the zinc-binding cluster within the CTD for RIG-I-mediated IFN induction with a second, less disruptive strategy. Mutation of Cys to Arg is established, but considered to be relatively harsh since cysteine and arginine are highly different. The side chain on cysteine is thiol, which is nonpolar and thus cysteine is usually classified as a hydrophobic amino acid. Furthermore, the thiol is susceptible to oxidization generating the disulfide derivative cystine, which serves an important structural function in many proteins. In contrast, arginine is classified as polar amino acid. The guanidinium group of the arginine side-chain confers basic chemical properties to arginine (IUBMB, 1992). Thus, to exclude that the loss of IFN induction by mutant RIG-I is a consequence of disrupting the zinc-binding cluster by cysteine to arginine mutation (C→R), a second series of RIG-I mutants bearing alanine (Ala, A) instead of cysteine (C→A) was generated. Alanine is neutrally charged and thus should have less influence on protein structure and protein stability compared to arginine.

Again, wild-type and RIG-I mutants with the four invariant zinc-binding cysteines changed to alanine were tested for their ability to induce IFN- $\beta$  promoter activation in response to pppVSVL transfection and VSV-M51R infection (Figure 11A). Immunoblotting revealed that the expression level of the Ala mutants is similar to WT RIG-I and less influenced by the introduced mutations as in the case of Arg mutation (Figure 11B and Figure 10B). However, mutation of the conserved Cys residues to Ala also abrogated RIG-I-mediated IFN- $\beta$  promoter activation in response to either stimulus confirming the results obtained with the Arg mutants. As for the arginine mutants, mutation of the non-conserved Cys829 served as control. Infection with VSV-M51R resulted in a 301-fold induction of the IFN- $\beta$  promoter by RIG-I C829A (Figure 11A), which is higher than the IFN- $\beta$  promoter activation induced by the respective arginine mutant C829R. This difference may be due to reduced expression or stability of the arginine mutant. In conclusion, site-directed mutagenesis clearly demonstrated that the integrity of the zinc-binding site in the CTD is essential for RIG-I-mediated IFN induction in response to viral infection and transfection with 5'-triphosphate RNA.

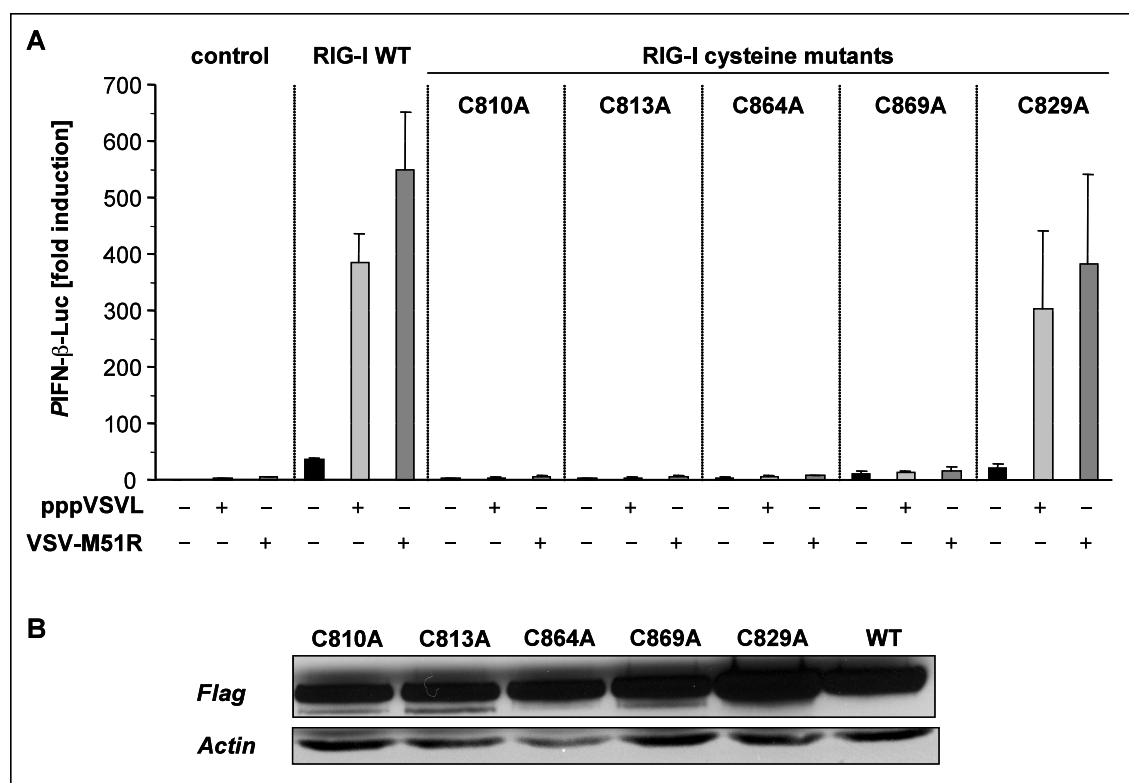


**Figure 11. Mutation of the four zinc-coordinating Cys residues to alanine (C→A)**

(A) Analysis of indicated RIG-I mutants using IFN-β promoter luciferase reporter assay. The same approach was used as described in detail for RIG-I Cys to Arg mutations (Figure 10A). Data represent the mean ± SD ( $n = 3$ ).

(B) Immunoblotting of lysates obtained from HEK293 cells transfected with the indicated RIG-I variants. Analysis was performed as described in Figure 10B.

Cysteine at AA position 818 was not mutated to alanine since it is not directly involved in formation of the zinc-binding cluster.

Since RIG-I is specifically activated by 5'-triphosphate RNA, luciferase reporter assay using two different RNA types, *in vitro* transcribed RNA comprising the leader RNA of VSV and total RNA isolated from VSV-infected HepG2 cells, was performed (Figure 12). WT RIG-I-mediated IFN-β promoter activation was markedly induced by *in vitro* transcribed RNA (6-fold compared to RNA from mock-infected cells) and total RNA isolated from VSV-infected cells (3.4-fold compared to RNA from mock-infected cells). In contrast, RIG-I C→R, in which all five invariant Cys residues are mutated to arginine, did not respond to either of the ligands tested.

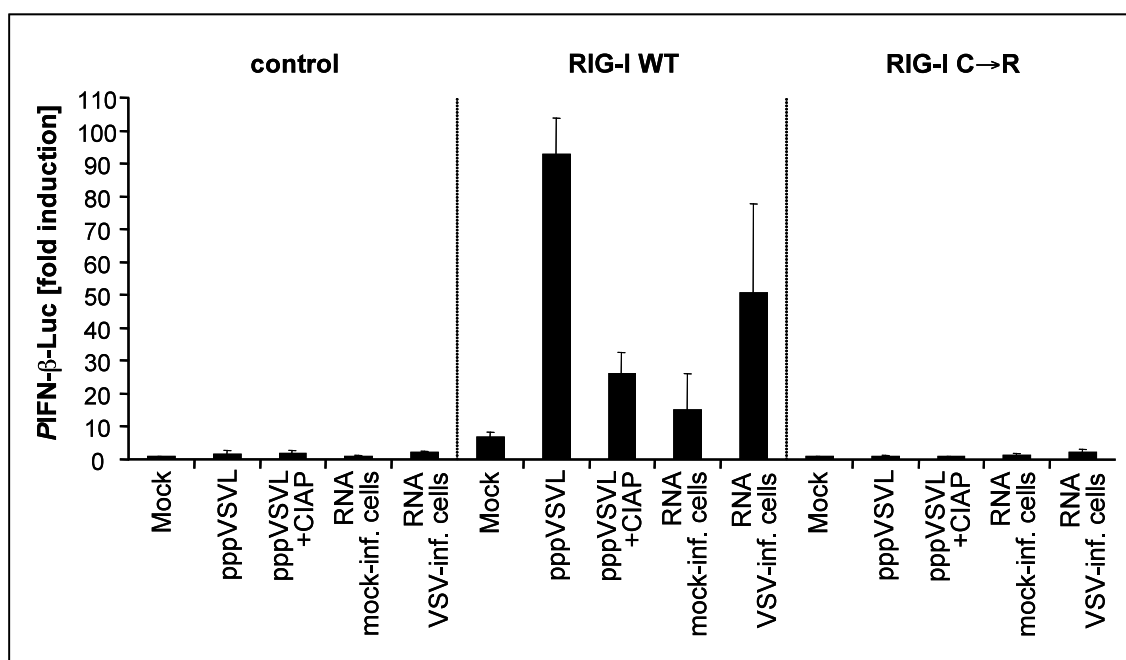


**Figure 12.** *Mutation of the zinc-binding cluster in the RIG-I CTD impairs 5'-triphosphate RNA-mediated IFN induction*

HEK293 cells were either transfected with empty vector control, RIG-I WT or RIG-I C→R mutant (all five invariant Cys mutated) (100 ng each) together with an IFN-β promoter luciferase construct (100 ng) as well as the internal control vector pRL-TK (10 ng). After 18 hrs, cells were subsequently stimulated with *in vitro* transcribed RNA (pppVSVL ± dephosphorylation with CIAP) or RNA from mock-infected and VSV-infected HepG2 cells (1 μg/each). IFN-β promoter activity was measured by dual luciferase assay after 18 hrs. IFN-β promoter activity is shown as fold induction compared to mock-treated empty vector control. Data represent the mean ± SD ( $n = 4$ ).

As expected, removal of the 5'-triphosphate moiety by CIAP (calf intestinal alkaline phosphatase) treatment strongly decreased the RIG-I-mediated IFN-β promoter activation. The low level IFN-β promoter induction upon transfection of dephosphorylated pppVSVL probably results from incomplete triphosphate removal, whereas IFN induction after transfection of RNA from uninfected cells might reflect the activation of RIG-I by short dsRNA. Thus, mutation of the zinc-binding site in the CTD of RIG-I abolishes RIG-I-mediated IFN activation in response to both, virus infection and RNA stimulation.

#### 4.1.4.2 Influence of the integrity of the zinc-binding site in the CTD of RIG-I on endogenous RIG-I signaling

The inability of RIG-I bearing mutations of the zinc-coordinating cysteines to induce IFN upon stimulation with 5'-triphosphate RNA or virus can be due to a dominant-negative inhibition of endogenous RIG-I similar to what has been described for RIG-I C (Yoneyama *et al.*, 2004), a construct that lacks the CARDs. To investigate this, IFN- $\beta$  promoter luciferase reporter assay was performed in Huh7.5 cells (Figure 13).

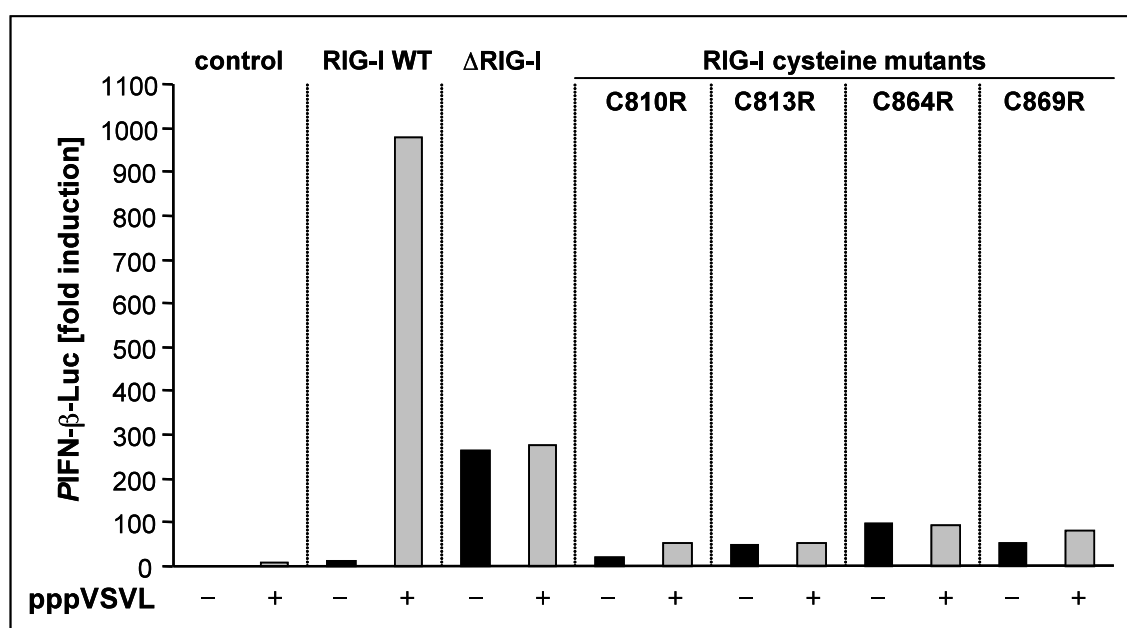


**Figure 13.** *Lack of dominant negative effect of RIG-I C $\rightarrow$ R mutants in Huh7.5 cells*

Huh7.5 cells were transfected with plasmids for empty vector control, RIG-I C (100 ng), RIG-I WT (10 ng) and 400 ng of RIG-I C $\rightarrow$ R single mutants (400 ng) together with IFN- $\beta$  promoter luciferase plasmid (100 ng) and internal control vector pRL-TK (10 ng). 16 hrs p.t., cells were transfected with pppVSVL (1  $\mu$ g/ml) and stimulated for 18 hrs. IFN- $\beta$  promoter activation (fold induction compared to mock-treated empty vector control) was measured by dual luciferase assay. (one of two representative experiments is shown)

Huh7.5 is a human hepatocellular carcinoma cell line that is not able to activate RIG-I-mediated downstream signaling and subsequent IFN induction due to a point mutation in the first CARD of RIG-I, that abrogates CARD-CARD interaction of RIG-I and IPS-1 (Sumpter *et al.*, 2005). Thus, Huh7.5 cells are an appropriate tool to study the effect of ectopic, overexpressed RIG-I variants in the absence of functional endogenous RIG-I. In line with the signaling defect of endogenous RIG-I, IFN- $\beta$  promoter activation in response to 5'-pppRNA was only induced when wild-type RIG-I was artificially expressed (Figure 13). Overexpression of the artificial RIG-I variant  $\Delta$ RIG-I, which contains only CARDs, resulted in constitutive IFN induction as described by Yoneyama

*et al.* (2004). Mutation of the zinc-coordinating cysteine residues in the RIG-I CTD abrogated RIG-I signaling also in the absence of signaling competent endogenous RIG-I (Figure 13). Thus, the loss of activity of the mutants is not due to a dominant-negative effect on endogenous RIG-I.

Next, the RIG-I C→R mutants were used in an experimental setting, where the IFN response of endogenous RIG-I to 5'-triphosphate RNA was measured. It was already demonstrated that the HEK293 cells used in these experiments barely respond to 5'-triphosphate RNA or virus infection when RIG-I is not expressed ectopically (Figure 10A). Thus, the HEK293 cells, which have been used throughout this study are characterized by very low expression of endogenous RIG-I.

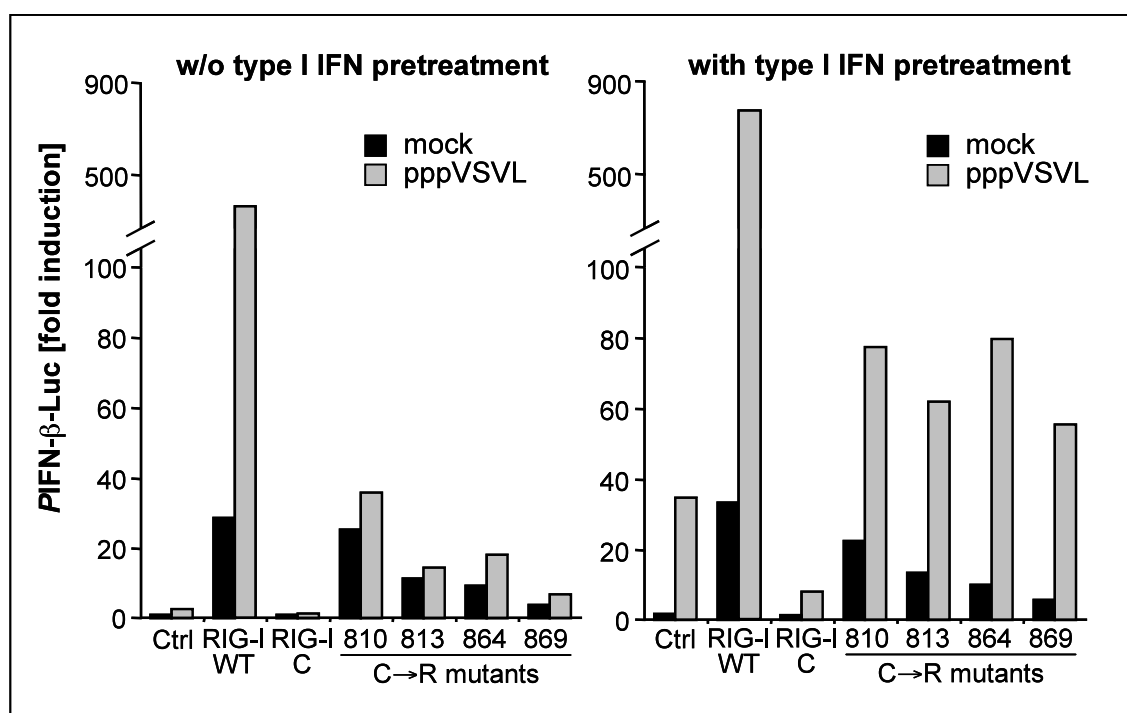


**Figure 14.** *Lack of dominant-negative effect of RIG-I C→R point mutants in HEK293 cells*

HEK293 cells were transfected with empty vector control plasmid (Ctrl), Flag-RIG-I WT, Flag RIG-I C (100 ng each) or Flag-tagged RIG-I C→R mutants (400 ng each) together with IFN- $\beta$  promoter luciferase plasmid (100 ng) and pRL-TK internal control (10 ng). Cells were transfected for 6 hrs and then either cultured in medium (left panel) or pretreated with 1000 U/ml type I IFN (right panel) to upregulate endogenous RIG-I. After 16 hrs, cells were then mock-treated (black columns) or transfected with *in vitro* transcribed RNA (pppVSVL, grey columns), respectively. IFN- $\beta$  promoter activity was measured 18 hrs after stimulation. IFN- $\beta$  promoter activity is shown as fold induction compared to mock-treated empty vector control. (one representative of two experiments is shown)

Since RIG-I expression was shown to be IFN-inducible (Yoneyama *et al.*, 2004), HEK293 cells were either pretreated with type I IFN to upregulate endogenous RIG-I or left untreated (Figure 14). HEK293 cells only responded to the RIG-I ligand pppVSVL when pretreated with type I IFN indicating very low expression of endogenous RIG-I in these cells in our experimental conditions (Figure 14, right panel, control). Ectopic expression of RIG-I WT and RIG-I C→R single mutants (C810R, C813R, C864R and C869R) in the absence of pppVSVL induced similar constitutive IFN- $\beta$  promoter activation in untreated cells and cells pretreated with type I IFN. Type I IFN pretreatment markedly enhanced the response of WT RIG-I to 5'-triphosphate RNA.

Whereas transfection of the CARD-lacking construct RIG-I C had the previously described dominant negative effect on the response of endogenous RIG-I to pppVSVL described by Yoneyama *et al.* (2004), constitutive activity of RIG-I C→R mutants and endogenous RIG-I activity were additive in cells pretreated with type I IFN. Thus, the activity of endogenous RIG-I is preserved in the presence of RIG-I C→R mutants. Taken together, these results confirm that the disruption of the zinc-binding cluster in the CTD of RIG-I leads to abrogation of RIG-I-induced IFN- $\beta$  promoter activation, but this is not due to a dominant negative effect of the mutants on the response of endogenous RIG-I to 5'-triphosphate RNA.

#### **4.1.5 Involvement of the zinc-binding site in the CTD of RIG-I in the interaction with signaling adapter IPS-1 and binding of 5'-triphosphate RNA**

The obtained results, that ectopic expression of the RIG-I CTD (AA 802-925) leads to suppression of RIG-I-mediated IFN induction upon stimulation with 5'-triphosphate RNA or virus infection (Figure 7) and that the integrity of the newly identified zinc-binding cluster is essential for inducing an IFN response (Figure 10, Figure 12), suggested that the C-terminal domain might be involved in the interaction of RIG-I with IPS-1 or in the binding of 5'-triphosphate RNA.

To investigate, if mutation of the zinc-coordination site in the CTD has an influence on the CARD-CARD-mediated protein interaction of RIG-I with IPS-1, immunoprecipitation was performed. Lysates were obtained from HEK293 cells cotransfected with HA-tagged IPS-1 and Flag-tagged RIG-I WT or Flag-RIG-I C→R

mutant, respectively (Figure 15A). Immunoprecipitation using Flag-antibody coupled to agarose beads followed by immunoblotting with an HA-specific antibody indicated that overexpressed WT RIG-I interacted with IPS-1, which is consistent with constitutive activity of WT RIG-I in the luciferase assay (Figure 10). The RIG-I C→R mutant similarly interacted with IPS-1 in the absence of RIG-I ligands – even stronger than WT RIG-I. Therefore, the ability of the RIG-I CARDS to bind to IPS-1 is not lost, but rather enhanced in the presence of mutations that might affect structure and function of the C-terminal domain.

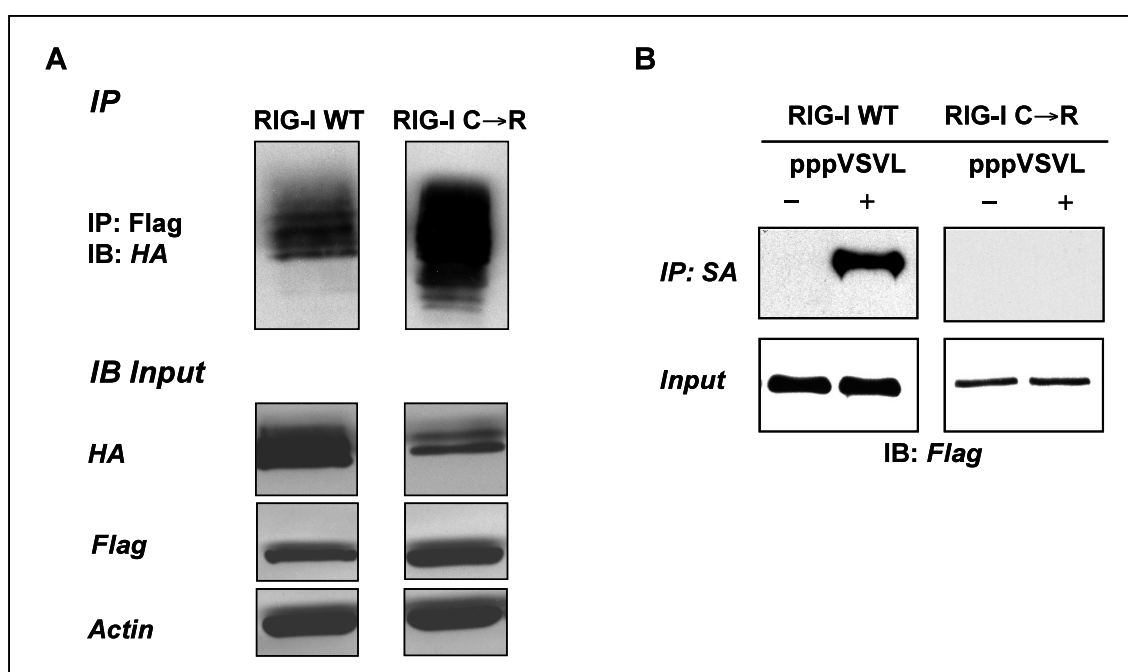


**Figure 15.** *Interaction of the RIG-I CTD with IPS-1 and 5'-triphosphate RNA*

(A) HEK293 cells were transfected with either Flag-RIG-I WT or Flag-RIG-I C→R mutant and HA-IPS-1 (ratio 1:1.5). 18 hrs after transfection, lysates were subjected to immunoprecipitation (IP) using Flag-agarose beads to recover RIG-I-IPS-1 complexes and analyzed by SDS-PAGE and immunoblotting using an anti-HA antibody. To check the integrity of the lysates with regard to expression of the interaction partners Flag-RIG-I and HA-IPS-1, 6 % of the input fraction were analyzed by immunoblotting (IB) with a Flag- or HA-specific antibody, respectively. Detection of  $\beta$ -Actin served as loading control.

(B) The cytoplasmic fraction of HEK293 cells transfected with Flag-tagged WT RIG-I or RIG-I C→R mutant was incubated with *in vitro* transcribed biotinylated pppVSVL. RNA-protein complexes were recovered by immunoprecipitation using streptavidin affinity beads. Input and pull-down samples were analyzed by SDS-PAGE and immunoblotting using anti-Flag antibody (one representative of two experiments is shown).

Furthermore, this is in line with the constitutive activity of RIG-I Cys single mutants C810R, C813R, C864R and C869R, which was observed after transfection of higher amounts of expression plasmids in the luciferase reporter assay (Figure 10A, insert), indicating that the interaction with the CARD of IPS-1 is enhanced when the CTD is dysfunctional due to disruption of the zinc-binding cluster, reflecting a repressor function of the C-terminal domain.

As described in the introduction, binding of 5'-triphosphate RNA by RIG-I is a prerequisite for its activation and subsequent interaction with IPS-1. Thus, it was analyzed whether mutations in the zinc-binding site disrupt 5'-triphosphate RNA binding. For this purpose, an *in vitro* RNA binding assay was performed. Cytoplasmic extracts prepared from HEK293 cells transfected with WT RIG-I or RIG-I C→R mutant were incubated with pppVSVL that had been labelled with biotinylated UTP during *in vitro* transcription. Samples were subsequently subjected to immunoprecipitation using streptavidin beads to recover RIG-I-RNA complexes. pppVSVL bound strongly to WT RIG-I, but not to mutated RIG-I in which all five invariant cysteine residues of the CTD had been changed to arginine (Figure 15B). Therefore, the integrity of the zinc-binding site of the RIG-I C-terminal domain is essential for binding of the specific ligand 5'-triphosphate RNA.

#### **4.1.6 5'-triphosphate RNA interacts with a positively charged conserved binding groove in the CTD of RIG-I**

The data obtained so far demonstrate that the zinc-coordination site is a key structural motif of the RIG-I C-terminal domain. Furthermore, the RNA binding assay revealed that disruption of the zinc-binding site by site-directed mutagenesis of the invariant cysteines to arginine renders RIG-I unable to interact with its specific ligand 5'-pppRNA suggesting that the CTD is involved in ligand binding. In line with the reports of Hornung *et al.* (2006) and Pichlmair *et al.* (2006), luciferase reporter assay indicated that RIG-I-mediated IFN induction in response to pppVSVL specifically depends on the 5'-triphosphate moiety since dephosphorylated VSV leader RNA was not able to induce activation of the IFN- $\beta$  promoter (Figure 12). This suggested that the CTD of RIG-I contains a structural motif that mediates binding of triphosphates.

Protein sites that bind triphosphates with high affinity, such as the active site of ATPases, often contain a positively charged patch to compensate the negative charge of the triphosphate chain (Sazinsky *et al.*, 2006; Wu *et al.*, 2005; Yagi *et al.*, 2007). Furthermore the binding sites are often highly sequence conserved. To obtain information whether the CTD of RIG-I contains a potential triphosphate-binding site, analysis of the sequence conservation and electrostatic potential, the hallmarks of triphosphate-binding sites, was performed (Sheng Cui and Karl-Peter Hopfner, see supplemental figures in section 8.6, Figure 32).

With regard to these criteria, the sequence conservation and the electrostatic potential at the solvent-accessible surface was analyzed. Sequence analysis revealed 14 AA residues that might be involved in the formation of a triphosphate-binding site in the CTD of RIG-I (Figure 16A). To obtain information on the putative triphosphate-binding site, candidate residues were mutated to either alanine or serine (C829S) and analyzed in terms of their potential to activate the IFN- $\beta$  promoter in response to 5'-triphosphate RNA and virus infection (Figure 16B). RIG-I WT induced strong activation of the IFN- $\beta$  promoter in response to pppVSVL (186-fold compared to mock-treated empty vector control) and VSV-M51R (325-fold compared to mock-treated empty vector control), whereas mutation of AA K858 and K888 led to markedly decreased activation of the IFN- $\beta$  promoter in response to both pppVSVL transfection (K858A: 115-fold, K888A: 72-fold compared to mock-treated empty vector control) and VSV-M51R infection (K858A: 6-fold, K888A: 65-fold compared to mock-treated empty vector control). Mutation of AA residues K849 and H830 in RIG-I resulted in a decreased activation of the IFN- $\beta$  promoter in response to infection with VSV-M51R (K849: 79-fold, H830: 140-fold compared to mock-treated empty vector control), while IFN- $\beta$  promoter induction upon stimulation with pppVSVL was comparable to RIG-I WT. In contrast, mutation of AA K907 to alanine nearly abrogated the activation of the IFN- $\beta$  promoter in response to 5'-triphosphate RNA (48-fold compared to mock-treated empty vector control), while the response to virus infection was comparable to RIG-I WT.

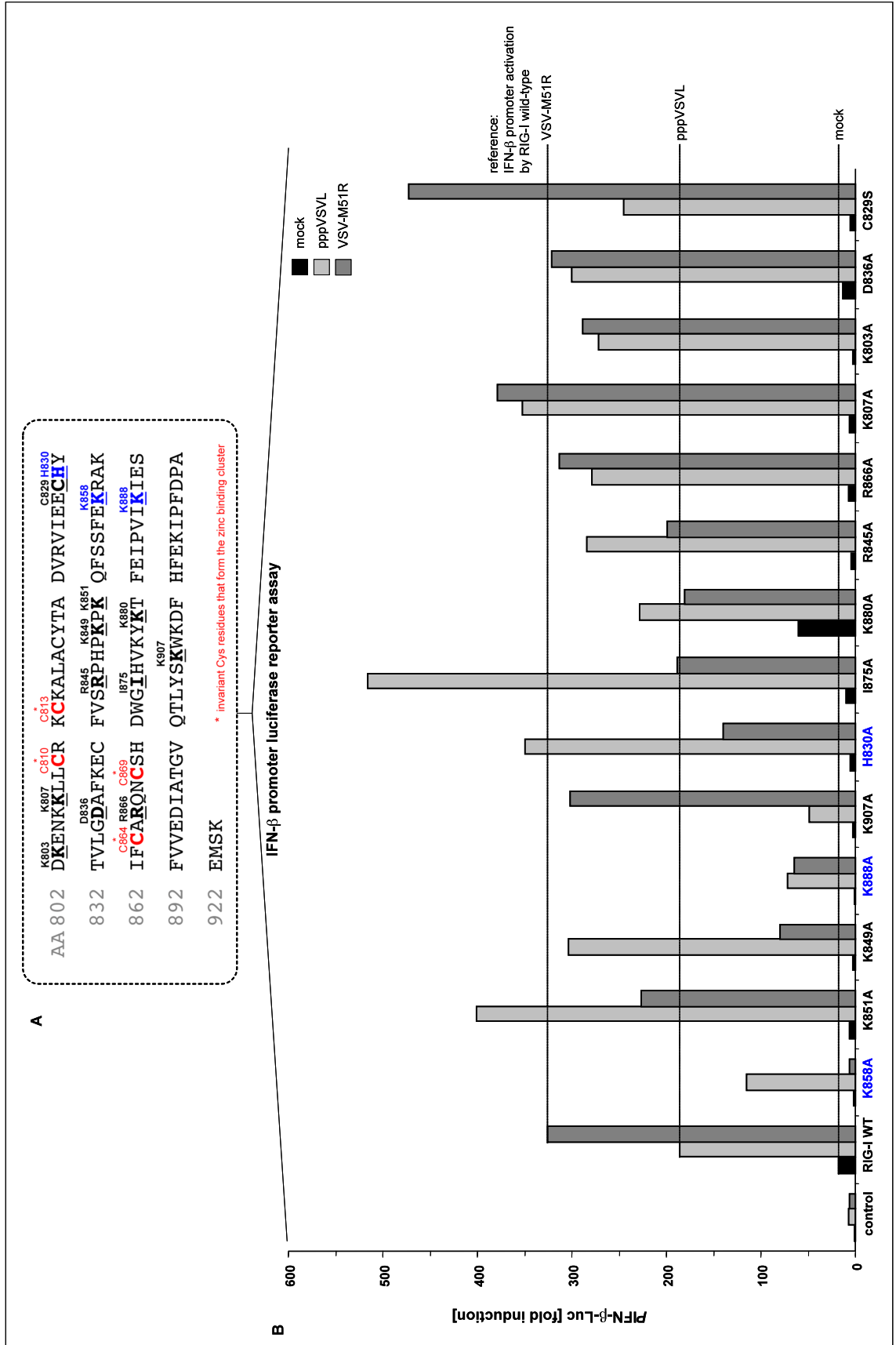


**Figure 16.** *Analysis of amino acid residues that might be involved in the formation of a triphosphate-binding site within the CTD of RIG-I*

(A) In consideration of the hallmarks of triphosphate-binding sites, sequence analysis revealed 14 AA residues that might be involved in the formation of a triphosphate-binding site in the CTD (AA 802 – 925) of RIG-I (highlighted in bold and underlined letters). Shown in blue are AA residues that were further analyzed (H830, K858 and K888). Invariant Cys residues that form the newly identified zinc-binding cluster are indicated in red.

(B) AA residues predicted to be directly involved in binding of 5'-triphosphate RNA were analyzed by IFN- $\beta$  promoter luciferase assay in comparison to wild-type RIG-I. HEK293 cells were transfected with either empty vector control, RIG-I WT or the indicated mutants (100 ng each) together with the IFN- $\beta$  promoter reporter plasmid (100 ng) and internal control vector pRL-TK (10 ng). 18 hrs after transfection, cells were transfected with *in vitro* transcribed pppVSVL (1  $\mu$ g/ml) or infected with VSV-M51R (5 MOI). 18 hrs after stimulation, IFN- $\beta$  promoter activation, shown as fold induction compared to mock-treated empty vector control, was analyzed. (one representative of two experiments is shown)

In addition to luciferase reporter assay, a fluorescence anisotropy assay was performed (Sheng Cui and Karl-Peter Hopfner, see Cui *et al.*, 2008) to test these 14 RIG-I mutants for their ability to interact with 5'-triphosphate RNA. With this assay it was revealed that mutations at positions H830 and K888 in the CTD of RIG-I significantly reduced the binding affinity, which is in line with the results obtained from IFN- $\beta$  promoter luciferase reporter assay. The mutation of AA K858 even dramatically reduced the binding of pppVSVL, which was also observed with the reporter assay. Interestingly, mutation of AA I875 to alanine, which was rather unremarkable in the IFN- $\beta$  promoter reporter assay, also resulted in a significantly reduced binding affinity of RIG-I to 5'-triphosphate RNA. Taken together, two different approaches, IFN- $\beta$  promoter luciferase assay and fluorescence anisotropy assay revealed that substitution of H830, K858, I875 and K888 within the CTD of RIG-I to alanine decreased both the IFN- $\beta$  promoter activation of RIG-I in response to 5'-triphosphate RNA as well as the binding affinity to this ligand.

Analysis of the electrostatic surface potential revealed that amino acid residues H830, K858, I875 and K888 are located within a prominent positively charged groove in the C-terminal domain of RIG-I indicating the presence of a triphosphate-binding site (see Figure 32 in section 8.6). Thus, RIG-I mutants H830, K858 and K888, which were identified to be involved in binding of triphosphate RNA by both luciferase reporter assay and fluorescence anisotropy assay, were further analyzed in terms of their ability to induce IFN- $\beta$  promoter activation upon stimulation with specific ligands. In addition to the more conservative alanine mutation where the surface charge was changed from

positive to neutral, site-directed mutagenesis to introduce glutamate (E) was performed, which is accompanied by a complete reversal of the surface charge from positive to negative. Analysis of RIG-I alanine mutants H830A, K858A and K888A indicated that IFN- $\beta$  promoter activity induced by transfection with pppVSVL or infection with VSV-M51R was significantly reduced, but not completely abrogated compared to RIG-I WT (Figure 17A).

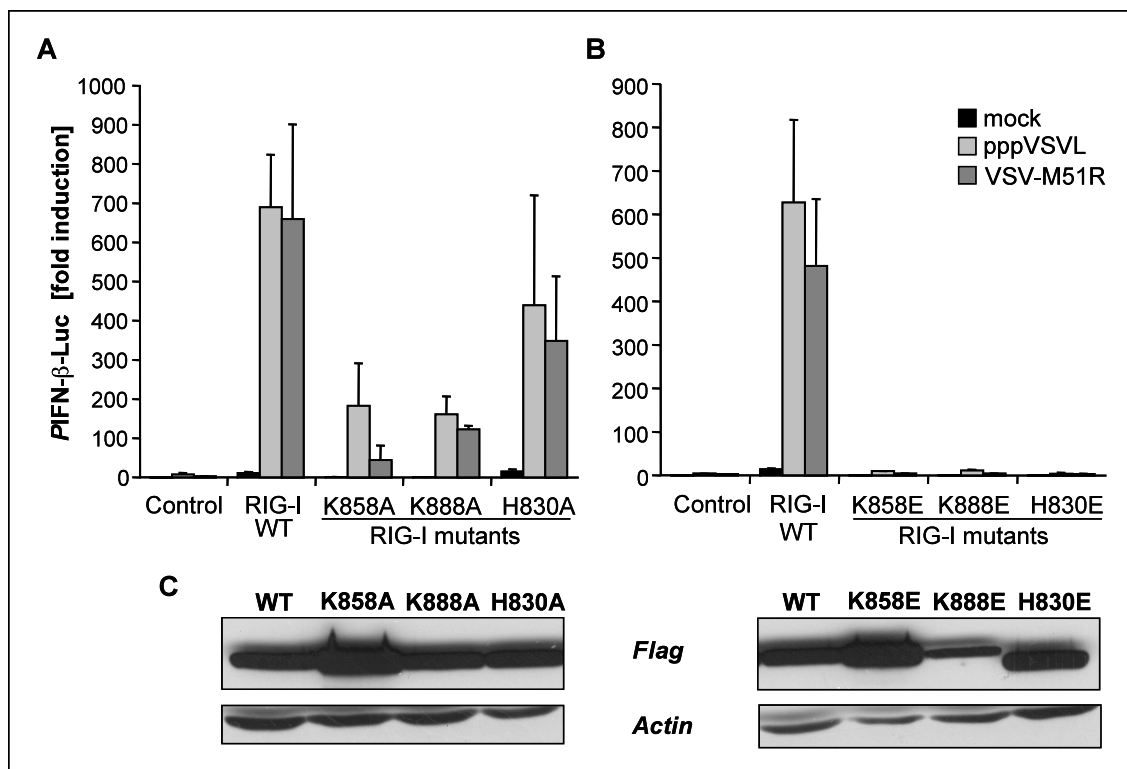


**Figure 17. Mutation of the putative triphosphate-binding site in RIG-I abolishes activation of the IFN- $\beta$  promoter in response to 5'-triphosphate RNA and virus infection**

HEK293 cells were transfected with plasmids encoding empty vector control (100 ng), RIG-I WT (10 ng) and the respective RIG-I mutants bearing either alanine (A) or glutamate (B) (100 ng each). 16 hrs after transfection, cells were transfected with pppVSVL (1  $\mu$ g/ml) or infected with VSV-M51R (10 MOI) and stimulated for further 18 hrs. IFN- $\beta$  promoter activity was measured by dual luciferase assay, shown as fold induction compared to mock-treated empty vector control. Data represent the mean  $\pm$  SD ( $n = 3$ ).

(C) To confirm expression of the mutants, HEK293 cells were transfected with 10  $\mu$ g of the respective expression plasmids. 18 hrs p.t., cells were lysed and WCLs were analyzed by SDS-PAGE and immunoblotting using a Flag-specific antibody. Detection of  $\beta$ -Actin served as loading control.

However, mutations to negatively charged glutamates in the same positions (H830E, K858E and K888E) entirely abrogated the response to both pppVSVL and VSV-M51R (Figure 17B). To exclude that the diminished IFN response is due to an expression defect of the mutated proteins, expression of all mutants was confirmed by

immunoblotting using a Flag-specific antibody (Figure 17C). Taken together, these results indicate that in addition to the newly identified zinc-coordination site, which was demonstrated to be a key structural motif of the CTD of RIG-I, at least three conserved residues, H830, K858 and K888, within a conserved positively charged binding groove of the C-terminal domain, are involved in the direct interaction with 5'-triphosphate RNA.

## **4.2 The role of the cysteine rich C-terminal domain of MDA5**

### **4.2.1 Influence of the invariant Cys residues on MDA5-mediated IFN induction**

RNA recognition by MDA5 is far less characterized compared to RIG-I. It was shown that MDA5 preferentially recognizes long dsRNA (Kato *et al.*, 2008). The synthetic dsRNA analogue poly(I:C) acts as agonist for MDA5 in its long form ( $\geq 1$  Kb) and can be converted into a RIG-I agonist by shortening the length to less than 1 Kb. *In vivo* experiments demonstrated that MDA5 is essential for the induction of an antiviral response upon infection with picornaviruses (Gitlin *et al.*, 2006; Hornung *et al.*, 2006; Kato *et al.*, 2006), murine norovirus-1 (McCartney *et al.*, 2008) and murine hepatitis virus. Furthermore, MDA5 was shown to be involved in the recognition of reovirus long dsRNA segments (Loo *et al.*, 2007) (Table 1). However, until now the distinct molecular feature that is recognized by MDA5 is not known.

As described in Figure 8, comparative sequence analysis revealed that the region of MDA5 homologous to the CTD of RIG-I (AA 802-925) is characterized by the presence of invariant cysteine residues (Figure 8). The corresponding C-terminal domain in MDA5 was mapped to AA 897 to 1025. Within the MDA5 CTD, the invariant Cys residues that form the newly identified zinc-coordination site in RIG-I, are located at AA positions C907, C910, C915, C962 and C964 (annotated as Cys1-Cys5 in Figure 8), respectively. To investigate the role of the invariant Cys residues, site-directed mutagenesis was performed and as for RIG-I, all conserved Cys residues were changed to arginine (MDA5 C $\rightarrow$ R). WT and mutant MDA5 were tested for their ability to trigger IFN- $\beta$  promoter activation in response to transfected poly(I:C), which is known to activate MDA5 (Figure 18). Transfection of poly(I:C) at different doses led to strong

activation of the IFN- $\beta$  promoter by overexpressed WT MDA5 (38-fold to 49-fold compared to empty vector control), whereas mutation of the invariant cysteines in MDA5 completely abrogated this response. Thus, similar to RIG-I, mutation of the invariant Cys residues in MDA5 leads to abrogation of IFN- $\beta$  promoter activation in response to poly(I:C) suggesting that the C-terminal domain confers ligand specificity of the RLRs.

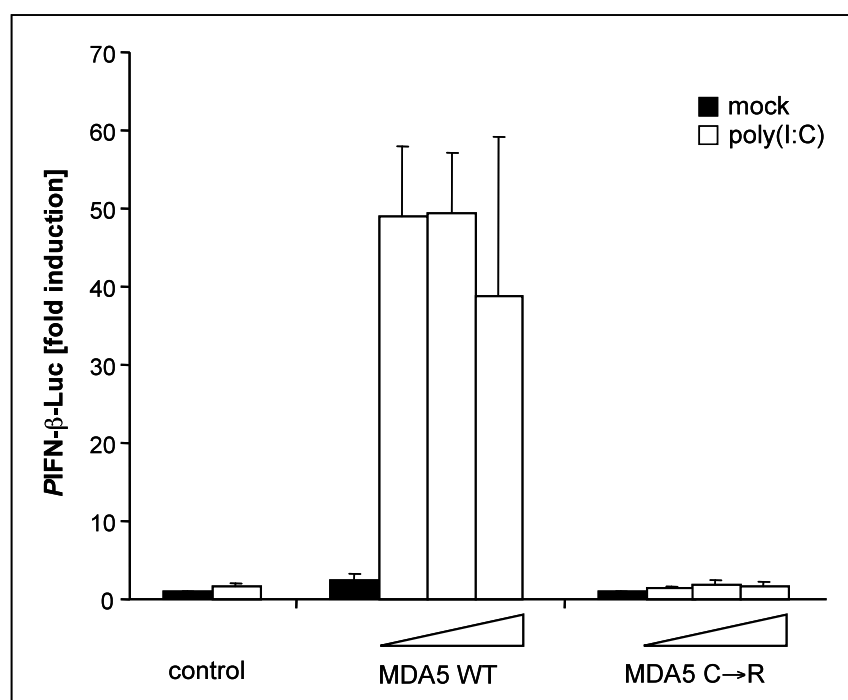


**Figure 18.** *WT MDA5 induces IFN- $\beta$  promoter activation after transfection of poly(I:C)* HEK293 cells were transfected with empty vector control (100 ng) and MDA5 WT or MDA5 C $\rightarrow$ R mutant (20 ng each) together with IFN- $\beta$  promoter luciferase reporter (100 ng) and pRL-TK internal control (10 ng). After 16 hrs, cells were stimulated with increasing amounts of poly(I:C) (2, 5 and 10  $\mu$ g/ml). IFN- $\beta$  promoter activity was measured by dual luciferase assay, shown as fold induction compared to mock-treated empty vector control. Data represent the mean  $\pm$  SD ( $n = 3$ ).

#### 4.2.2 Analysis of MDA5-mediated IFN induction in response to picornavirus infection

Due to the lack of information on the molecular pattern within viral RNA that is recognized by MDA5, *in vitro* characterization of MDA5 using reporter assays was limited to poly(I:C). I therefore investigated the MDA5-mediated IFN response to EMCV infection, which is the prototypic picornavirus, and transfection of total RNA isolated from EMCV-infected cells (Figure 19). It was already demonstrated that RNA isolated from VSV-infected cells is able to trigger RIG-I-mediated IFN induction (Figure 12), indicating that it contains RNA types bearing 5'-triphosphates generated during VSV replication. HEK293 cells were transfected with wild-type MDA5 alone, MDA5 together with LGP2 or WT RIG-I as control. As expected, WT RIG-I did not respond to EMCV infection, whereas infection with VSV-M51R led to a strong induction of IFN- $\beta$  promoter activation (Figure 19A). Furthermore, RNA from EMCV-infected cells failed to elicit an IFN response in RIG-I expressing cells, indicating that EMCV virus replication does not lead to the generation of RNAs that bear the distinct molecular pattern recognized by RIG-I, as was the case for VSV infection.

Interestingly, stimulation of RIG-I with poly(I:C) also induced IFN- $\beta$  promoter activation (39-fold compared to empty vector control) (Figure 19A), suggesting that the poly(I:C) which was used for this study contains a mixture of long and short dsRNA strands, that are able to activate both RIG-I and MDA5.

Overexpression of MDA5 constitutively induced IFN- $\beta$  promoter activation in the absence of ligand (11-fold compared to vector control) (Figure 19B). Subsequent stimulation with poly(I:C) led to further induction of IFN- $\beta$  promoter activity (51-fold compared to empty vector control) (Figure 19B). In addition, MDA5 also weakly responded to infection with EMCV (20-fold induction compared to control vector, 2-fold compared to mock-treated MDA5 expressing cells), but not to VSV-M51R. EMCV-infected cells showed a strong cytopathic effect that indicates active viral replication. But, activation of the IFN- $\beta$  promoter was much lower compared to the induction observed with VSV-M51R in RIG-I expressing cells. However, no increase in IFN- $\beta$  promoter activity was observed when MDA5 expressing cells were stimulated with RNA from EMCV-infected cells (8-fold induction compared to control vector

which is below the constitutive activity of MDA5 that was observed in the absence of ligand) (Figure 19B).

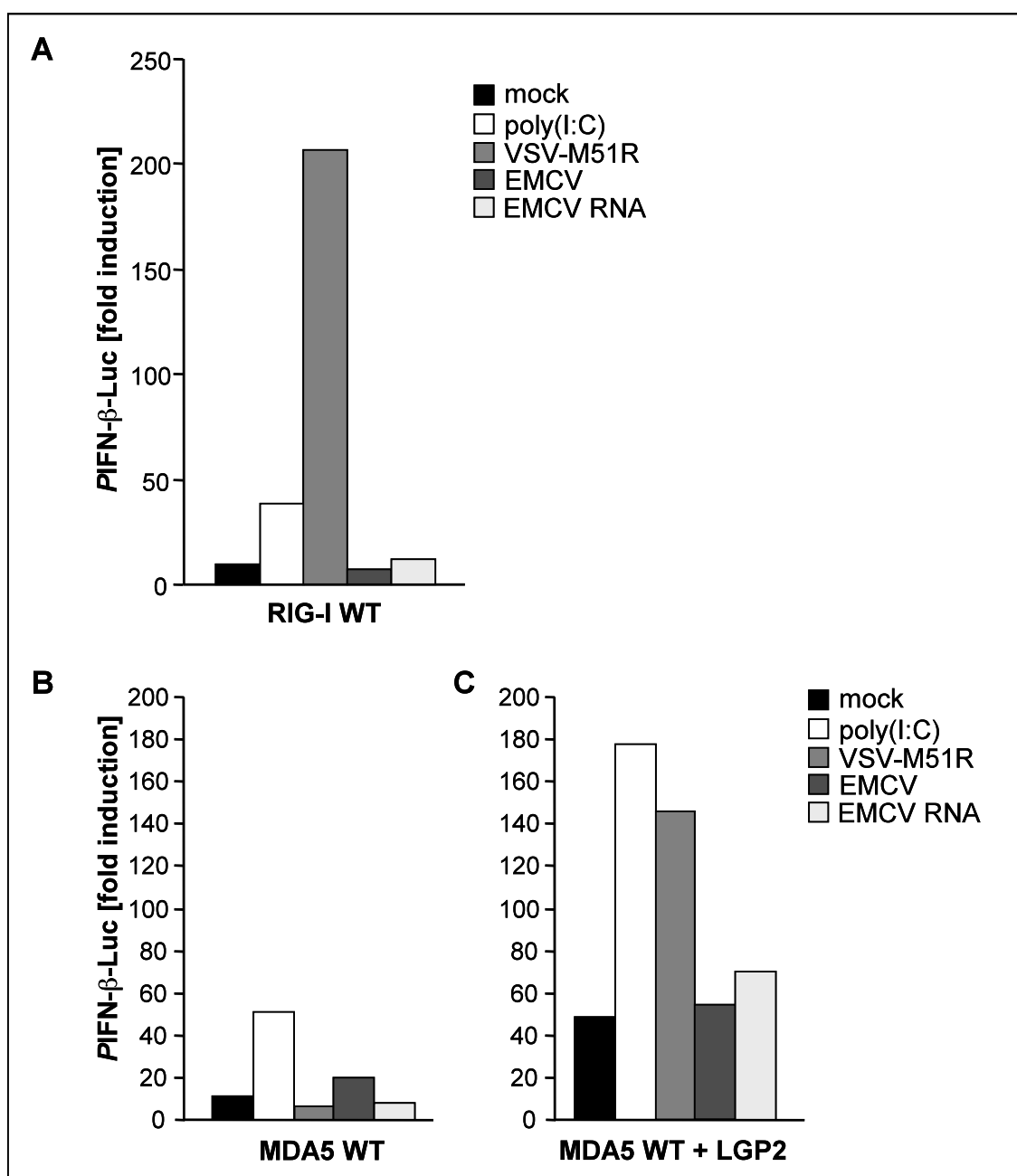


**Figure 19.** *MDA5-mediated IFN- $\beta$  promoter activation in response to EMCV*

HEK293 cells were transfected with plasmids encoding empty vector control (100 ng), RIG-I WT (10 ng) and MDA5 WT (20 ng) either alone or together with LGP2 (400 ng) as well as IFN- $\beta$  promoter luciferase (100 ng) and pRL-TK internal control (10 ng). 16 hrs p.t., cells were transfected with pppVSVL (2  $\mu$ g/ml), poly(I:C) (50  $\mu$ g/ml) and EMCV RNA (2  $\mu$ g/ml) or infected with VSV-M51R or EMCV (5 MOI each). After 16 hrs, IFN- $\beta$  promoter activation was measured by dual luciferase assay. IFN- $\beta$  promoter activation is shown as fold induction compared to empty vector control. (one of two representative experiments is shown)

---

Due to the comparably weak IFN response of MDA5, it was assumed that the MDA5-mediated signal transduction *in vivo* is facilitated not only by MDA5 but also accessory proteins. One candidate is LGP2, which was reported to act as positive regulator of MDA5-mediated antiviral signaling (Sato *et al.*, 2010). Thus, cotransfection of MDA5 and LGP2 was performed (Figure 19C). Cotransfection of MDA5 and LGP2 resulted in a much higher level of constitutive IFN- $\beta$  promoter induction (5-fold compared to transfection of MDA5 alone). IFN- $\beta$  promoter activation in response to poly(I:C) was 3.5-fold higher compared to MDA5 transfection alone. Interestingly, coexpression of LGP2 also led to unexpected IFN- $\beta$  promoter activation in response to VSV-M51R infection. However, cotransfection of LGP2 failed to markedly induce IFN- $\beta$  promoter activation in EMCV-infected cells or cells that had been stimulated with EMCV RNA (Figure 19C). Thus, total RNA from cells infected with picornavirus does not contain the specific molecular pattern or cofactor that is required to induce IFN- $\beta$  promoter activation by MDA5. It cannot be ruled out that the *in vitro* conditions lack a factor that participates in the MDA5 ligand recognition and signaling in primary cells or *in vivo*. Cotransfection of LGP2, which seemed a good candidate, alone, was not sufficient to complement the MDA5 pathway.

### 4.3 RIG-I mediates TLR-independent recognition of *Helicobacter pylori* RNA

Structural and molecular characterization of PRRs is fundamental for the understanding of how the immune system senses and discriminates invading pathogens to finally generate an appropriate adaptive immune response (Akira *et al.*, 2006). However, defining the roles played by individual PRRs in pathogen recognition is complicated by the fact that different PRRs trigger common pathways and therefore the lack of one PRR can often be compensated by others.

Characterization of the role of individual TLRs revealed that the cytokine response of bone marrow derived DCs (BMDCs) to *Helicobacter pylori* is mediated by TLR-dependent as well as TLR- and MyD88/Trif-independent mechanisms. Infection of BMDCs derived from wild-type C57BL/6 mice or *Trif* mutant mice with live *H. pylori* SS1 and analysis of the expression of IFN- $\beta$  (*Ifnb1*) and several type I IFN induced genes on mRNA level, revealed that the Trif pathway, that operates downstream of TLR3 and TLR4, was not essential for the type I IFN response to *H. pylori* infection (Figure 20A). However, transfection of DCs with RNA isolated from *H. pylori* and *in vitro* transcribed 5'-triphosphate RNA induced IFN- $\beta$  production, which was measured in the cell culture supernatants by ELISA (Figure 20B). *Ifnb1* mRNA as well as the mRNAs of the IFN responsive genes *Ifi204*, *Isg15* and *Rig-I* were induced to comparable levels in response to infection with *H. pylori* SS1 in *Trif* mutant and wild-type BMDCs. This raised the question, whether non-TLR PRRs are able to induce the type I IFN in response to *H. pylori*. Since RNA isolated from *H. pylori* was able to activate endosomal TLRs in DCs, *H. pylori* RNA in contrast might trigger one of the RLRs that recognize viral RNA to induce type I IFN.

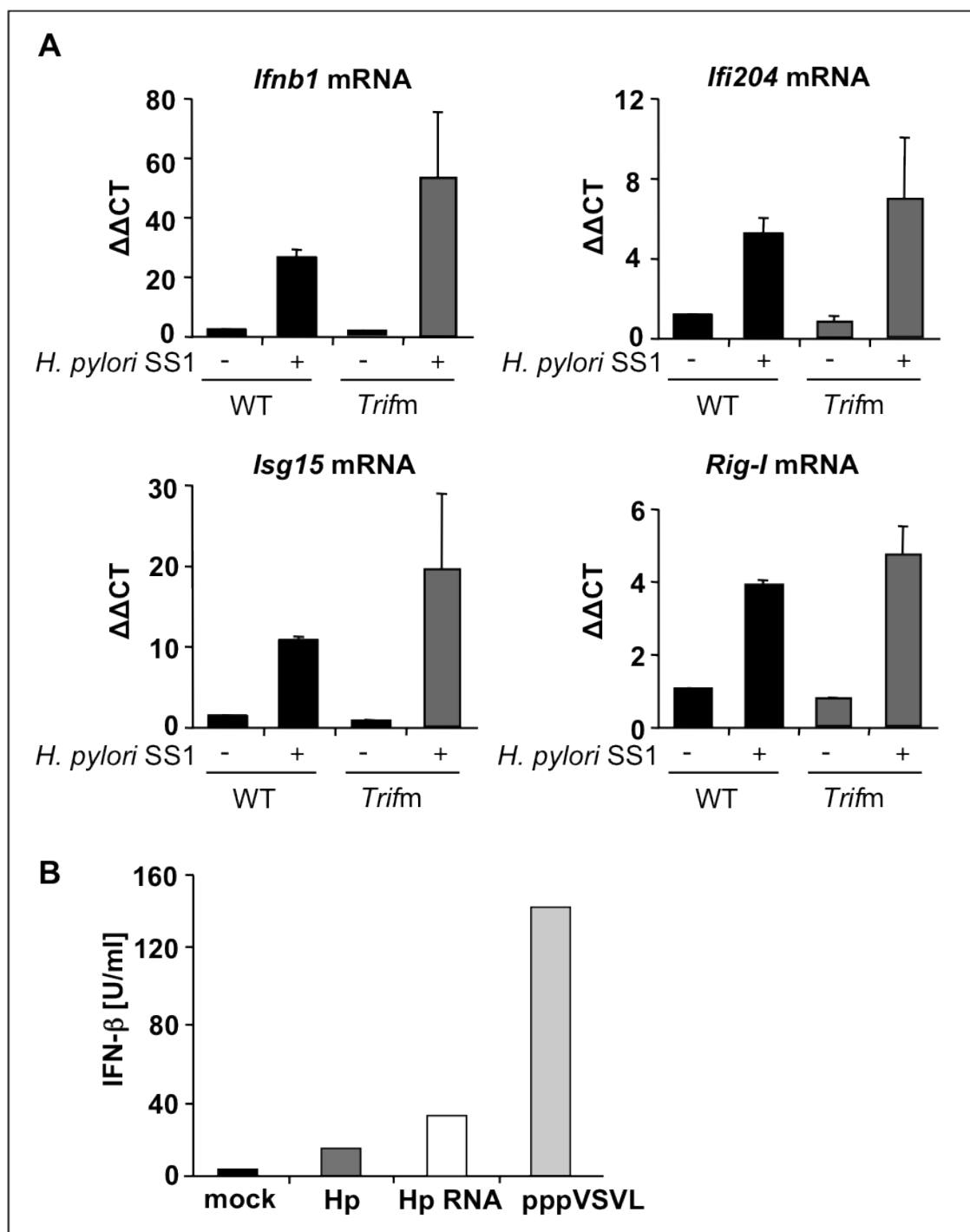


**Figure 20. *Trif*-independent type I IFN induction in BMDCs**

(A) BMDCs derived from either WT C57BL/6 mice or *Trif* mutant (*Trifm*) mice were infected with live *H. pylori* SS1 (50 MOI) or mock-infected. 6 hrs after infection, RNA was isolated and mRNA expression levels of IFN- $\beta$  (*Ifnb1*) and IFN-inducible genes (*Ifi204*, *Isg15*, *Rig-I*) were analyzed by quantitative real-time PCR using SYBR green. Mean  $\pm$  SD values ( $n = 4$ ) are shown.

(B) WT BMDCs were either infected with live *H. pylori* SS1 (Hp, 50 MOI) or transfected with RNA isolated from *H. pylori* (Hp RNA) or *in vitro* transcribed 5'-triphosphate RNA (pppVSVL, 20  $\mu$ g/ml each). 24 hrs after stimulation, cell culture supernatants were harvested and IFN- $\beta$  levels were determined by ELISA.

Therefore, HEK293 cells were transfected with RIG-I or MDA5 expression plasmids, respectively, and subsequently stimulated with *H. pylori* RNA to measure IFN- $\beta$  promoter activation (Figure 21). HEK293 cells transfected with RIG-I, were able to respond with IFN- $\beta$  promoter activation to *H. pylori* RNA (96-fold induction compared to mock-treated empty vector control) as well as to the specific ligands *in vitro* transcribed 5'-triphosphate RNA (pppVSVL, 158-fold induction compared to control) and VSV-M51R infection (106-fold compared to empty vector control), whereas MDA5 was not able to induce IFN- $\beta$  promoter activation in response to stimulation with *H. pylori* RNA (Figure 21A). Furthermore, RIG-I-mediated type I IFN induction by RNA isolated from *H. pylori* was abrogated when the RNA was pretreated with alkaline phosphatase, suggesting that *H. pylori* RNA contains 5'-triphosphates and activates RIG-I in a triphosphate-dependent manner. Cotransfection of RIG-I and LGP2 was performed, to investigate if LGP2 acts as a negative regulator of RIG-I-mediated IFN signaling also in the context of bacterial stimulation. Cotransfection dramatically decreased RIG-I-mediated IFN- $\beta$  promoter activation in response to all ligands tested (Figure 21A).

For comparison, another bacterial RNA, isolated from *E. coli*, was analyzed for its ability to trigger a RIG-I-dependent IFN response (Figure 21B and C). In contrast to *H. pylori* RNA, RNA isolated from *E. coli* was not able to induce IFN- $\beta$  promoter activation more than 2-fold compared to cells that were transfected with RIG-I but left untreated.

Furthermore, it was analyzed if *H. pylori* RNA interacts with the newly identified triphosphate RNA binding region in the CTD of RIG-I. The RIG-I mutant K858E was already shown to be unable to respond to stimulation with 5'-triphosphate RNA (Figure 17B). Indeed, K858E was also not significantly activated by *H. pylori* RNA (Figure 21B). Thus, *H. pylori* RNA can act as a specific RIG-I ligand and may thereby contribute to the induction of TLR- and MyD88-independent type I IFN and ISG expression in response to *Helicobacter pylori* infection.

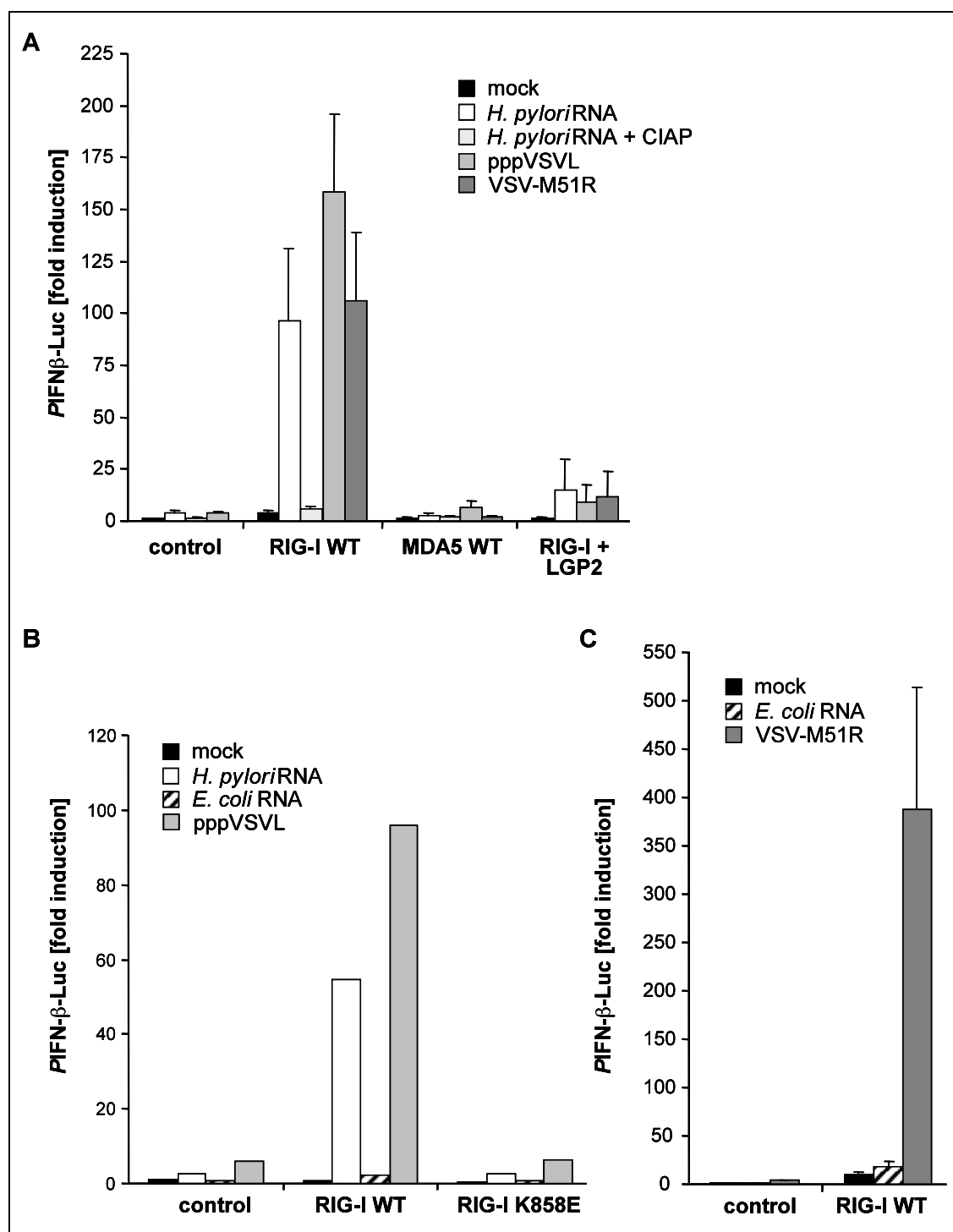


**Figure 21.** *RIG-I-mediated type I IFN by Helicobacter pylori RNA*

HEK 293 cells were transfected with IFN- $\beta$  promoter firefly luciferase reporter plasmid (100 ng) and pRL-TK control plasmid (10 ng) as well as plasmids encoding RIG-I WT (panel A 10 ng, panel B,C 100 ng), MDA5 WT (10 ng), LGP2 (400 ng), RIG-I mutant K858E (100 ng) or empty vector control (100 ng). Cells were either stimulated with *H. pylori* RNA (with or without CIAP treatment) (2,5  $\mu$ g/ml) or *E. coli* RNA (2  $\mu$ g/ml) and *in vitro* transcribed RNA pppVSVL (1 $\mu$ g/ml) or infected with VSV-M51R (5 MOI). IFN- $\beta$  promoter activity was measured by dual luciferase assay after 18 hours. Data are shown as fold induction compared to mock-treated empty vector control. (A) mean  $\pm$  SD ( $n = 4$ ), (B) one representative of two experiments, (C) mean  $\pm$  SD ( $n = 5$ ).

## 4.4 Identification of an interferon-inducible short form of human RIG-I

### 4.4.1 Detection of an interferon-induced short variant of human RIG-I

Detection of endogenous RIG-I in whole cell lysates of HEK293 cells pretreated with type I IFN revealed a yet unknown short form of human RIG-I with an approximate size of 95 kDa (Figure 22).

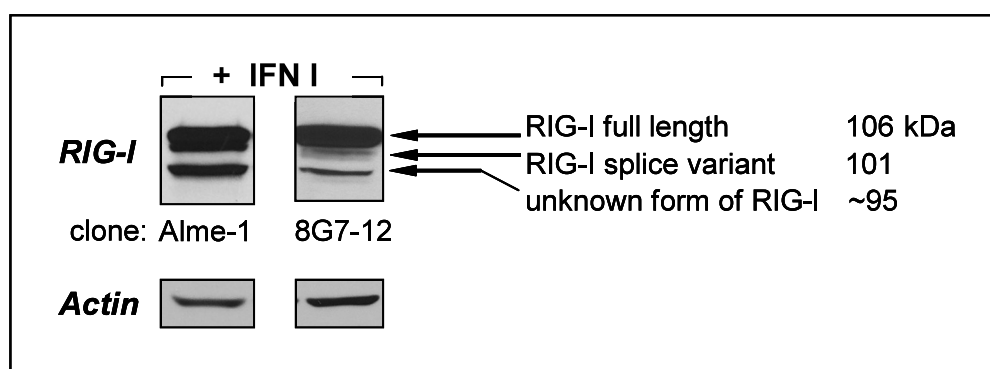


**Figure 22.** *Detection of endogenous human RIG-I by immunoblotting*

HEK293 cells were incubated with type I IFN (1000 U) for 18 hrs to induce expression of endogenous RIG-I. Cells were lysed and lysates were analyzed by SDS-PAGE and immunoblotting using two different RIG-I-specific antibodies, mouse mAb clone Alme-1 (left panel) and rat hybridoma supernatant (clone 8G7-12) (right panel). Detection of  $\beta$ -Actin served as loading control.

In addition to full-length human RIG-I and RIG-I splice variant (DDX58 isoform 2, UniProt entry O95786-2), the short form of RIG-I was specifically detected using two different antibodies, both recognizing different regions of the RIG-I protein. The RIG-I-specific mouse monoclonal antibody clone Alme-1 (used in the left panel, Figure 22) was raised against AA 201 to 713 of recombinant human RIG-I, whereas the region comprising AA 905 to 925 was used to generate the RIG-I-specific antibody clone 8G7-12 (used in the right panel, Figure 22). Although Alme-1 recognizes the helicase domain of RIG-I, whereas clone 8G7-12 is specific for the CTD of RIG-I, immunoblotting with both antibodies revealed a 95 kDa RIG-I-specific band suggesting that the RIG-I short form is N-terminally truncated. Data base search confirmed that a 95 kDa protein short form of RIG-I had not been identified and characterized so far.

#### 4.4.2 RIG-I short form is upregulated in a time- and dose-dependent manner

To further analyze the expression of the putative RIG-I short form in response to type I IFN with regard to the time point of its induction and its expression level compared to RIG-I full-length as well as RIG-I splice variant, HEK293 cells were either treated with 1000 U type I IFN for different time points or different doses of type I IFN for 18 hrs (Figure 23A and B).

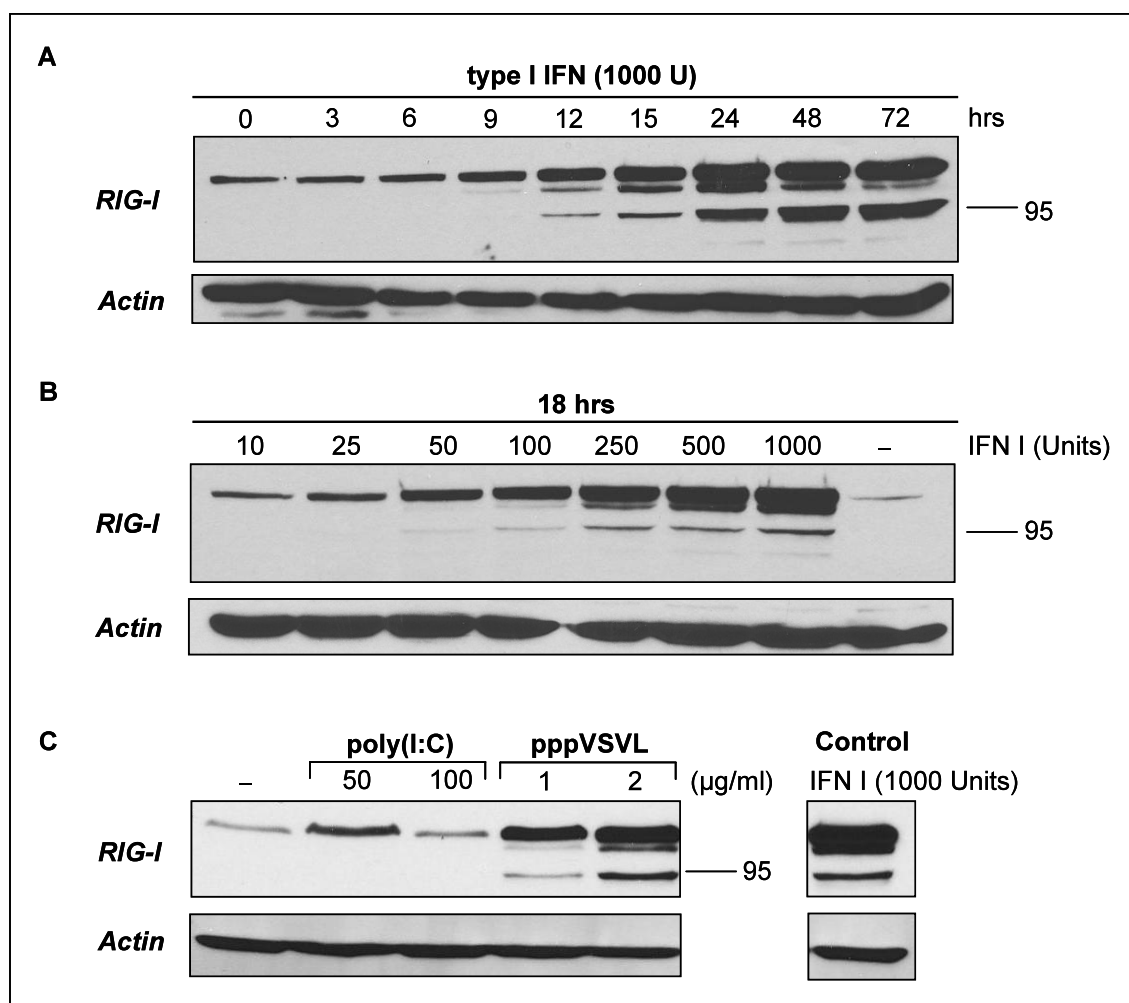


**Figure 23. Induction of RIG-I short form is time- and dose-dependent**

(A) HEK293 cells were treated with 1000 U type I IFN for the indicated time points. (B) Treatment of HEK293 cells with the indicated doses of type I IFN for 18 hrs. (C) HEK293 cells were transfected with either poly(I:C) or pppVSVL for 18 hrs. Treatment with 1000 U type I IFN for 18 hrs served as control. In all conditions, cells were lysed and lysates were analyzed by SDS-PAGE and immunoblotting using the RIG-I-specific antibody Alme-1. Detection of  $\beta$ -Actin served as loading control.

Neither RIG-I splice variant nor the putative RIG-I short form is detectable under steady state conditions. Detectable levels of RIG-I short form appeared within 12 hrs after type I IFN stimulation and the expression level further increased until 72 hrs after stimulation. Full-length RIG-I was upregulated in parallel. Interestingly, RIG-I short form was induced with a different kinetics compared to RIG-I splice variant, which appeared after 9 hrs (Figure 23A). 18 hrs after stimulation with 50 U type I IFN, a faint band corresponding to the putative short form was already visible. This was further increased when higher IFN doses were applied (Figure 23B).

Furthermore, induction of the putative short form of RIG-I was examined in response to transfection of specific RNA ligands. As depicted in Figure 23C, transfection of HEK293 cells with pppVSVL, which is a strong IFN inducer (Figure 11A), led to a dose-dependent induction of the 95 kDa protein, whereas the MDA5 ligand poly(I:C) failed to induce expression of the putative RIG-I short form, presumably due to its lower IFN inducing capacity. Thus, the putative RIG-I short form cannot be detected in the steady state, but is induced in a time- and dose-dependent manner after stimulation with type I IFN as well as the RIG-I-specific ligand 5'-triphosphate RNA.

#### 4.4.3 Sequence analysis of RIG-I short form

Mass spectrometry analysis was performed to obtain information on the amino acid sequence that encodes RIG-I short form. To obtain protein bands that can be submitted for mass spectrometry analysis, whole cell lysates of HEK293 cells treated with type I IFN were prepared, pooled and 10 mg total protein was subjected to immunoprecipitation using the RIG-I-specific antibody Alme-1 bound to protein G sepharose to recover RIG-I protein as well as proteins that interact with RIG-I. To control IP efficiency and to check, if this method is sufficient to recover RIG-I short form from whole cell lysates, 3 % of the IP were analyzed by SDS PAGE and subsequent immunoblotting using Alme-1. As depicted in Figure 24A (left panel, protein size is indicated in kDa), all three forms of RIG-I including the short form were recovered by immunoprecipitation with Alme-1. The remaining immunoprecipitated sample was then separated by SDS PAGE and the gel was subsequently stained with silver nitrate (Figure 24A, right panel).

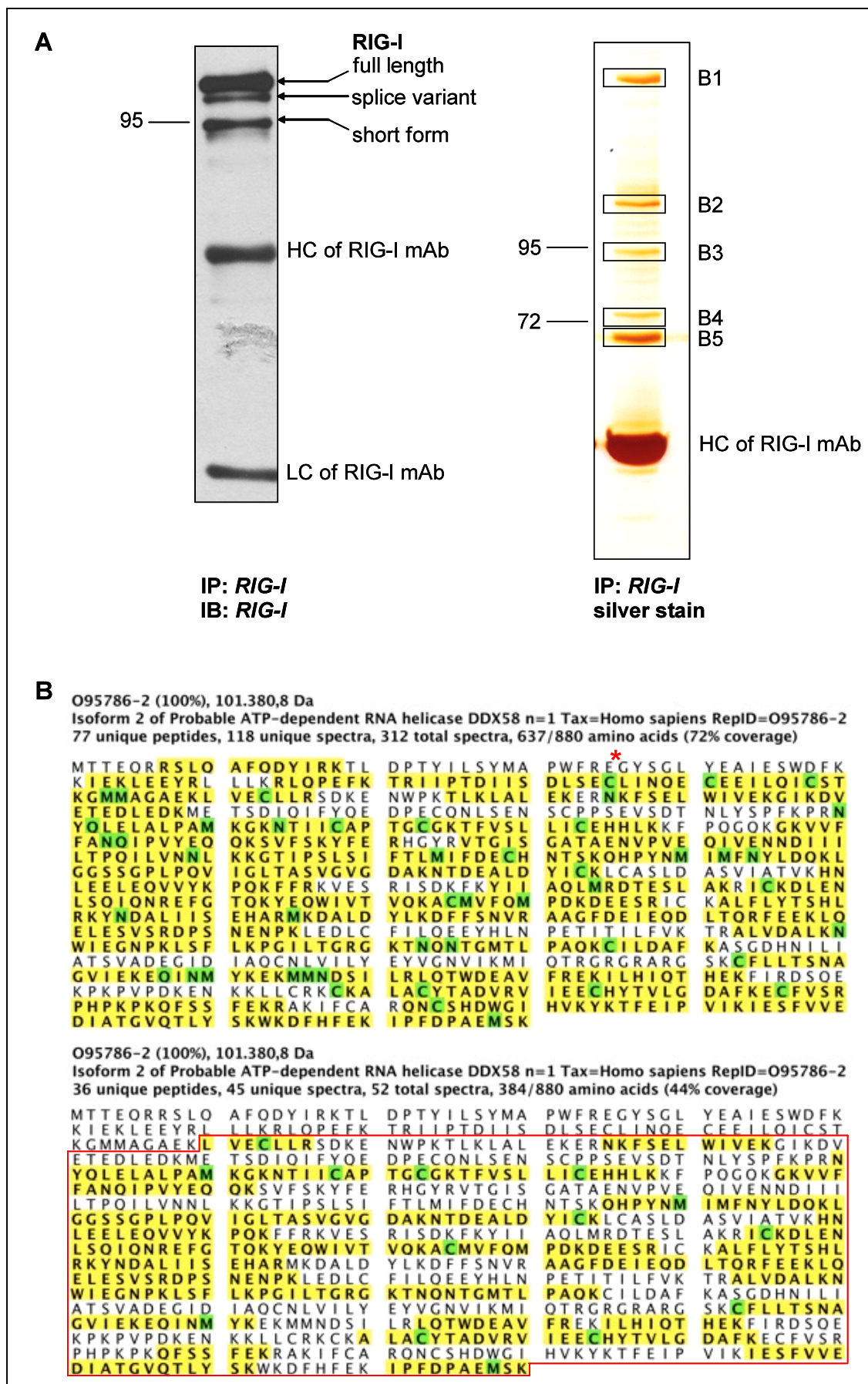


Figure 24. Immunoprecipitation of RIG-I short form and mass spectrometry analysis

Silver staining revealed five prominent bands (B1-B5) that were cut out and submitted for mass spectrometry analysis using the OrbiTrap XL, which was performed by our collaborator Hakan Sarioglu at the Core Facility Proteomics of the Helmholtz Zentrum München. The identified peptides were analyzed by MASCOT software and subsequently aligned to the UniProt database to determine the respective proteins. Analysis of the peptides obtained in each of the five bands by comparative sequence analysis clearly revealed the presence of RIG-I isoform 2, also designated as splice variant lacking AA residues 36 to 80, in band 3 (Figure 24B, upper sequence, alternative splicing site is indicated by red asterisk). In addition, band 3, which runs at the approximate size of the putative short form of RIG-I (95 kDa), contained a protein that was designated as RIG-I short form of isoform 2 with regard to sequence alignment (Figure 24B, lower sequence, indicated by red rectangle). RIG-I short form was identified by 36 unique peptides, which is consistent with 44 % peptide coverage. Detection of 2 peptides by mass spectrometry is sufficient to reliably identify a protein. Analysing the amino acid sequence revealed that the immunoprecipitated RIG-I short form lacks more than the AA region 36 to 80, that is removed in the splice variant.

Further analysis of the peptide spectra confirmed that the identified RIG-I short form of isoform 2 does not result from degradation of RIG-I isoform 2 by proteases during mass spectrometry analysis or a general poor sample quality leading to a shorter protein lacking more than AA 36 to 80 (analysis of the peptide spectra was performed by Hakan Sarioglu). However, it cannot be excluded that the start codon of the RIG-I short form is located further upstream of the leucine that was predicted by peptide alignment. In line with this, two candidate methionine residues are located in close proximity to L155 at AA position 148 and 149, respectively (Figure 24B, lower sequence).

Thus, RIG-I short form, which was demonstrated to be induced in HEK293 cells stimulated with type I IFN or 5'-triphosphate RNA in a time- and dose-dependent manner is a yet unknown variant of RIG-I probably comprising AA 155 to 925 of full-length RIG-I. RIG-I short form completely lacks CARD1 but possesses the C-terminal 18 amino acid residues of CARD2 and the complete helicase domain as well as the newly identified CTD. However, further analysis of the N-terminus is necessary to accurately map the location of the translational start site of RIG-I short form.

#### 4.4.4 Cloning and overexpression of RIG-I short form

In addition to RIG-I splice variant, which has been described as off-switch regulator of its own pathway by Gack *et al.* (2008), RIG-I short form is also endogenously upregulated by stimulation of HEK293 cells with type I IFN and 5'-triphosphate RNA at even later time points. To analyze, which function RIG-I short might have in RIG-I-mediated antiviral signal transduction, the sequence encoding RIG-I short form (AA 155-925 corresponding to bp 463-2778 of the RIG-I coding sequence) was cloned as Flag-tag bearing fusion construct into a mammalian expression vector. Thus, transient expression of Flag-RIG-I-short form in eukaryotic cells can be used to delineate its mode of action and its function in the tightly regulated RIG-I pathway.

First, expression of cloned RIG-I short form in HEK293 cells was monitored by immunoblotting using either a Flag-specific antibody or the RIG-I-specific antibody clone Alme-1 (Figure 25). A protein band of approximately 95 kDa in size that corresponds to RIG-I short form was clearly detected with both antibodies. Transfection of Flag-tagged RIG-I full-length served as control. Interestingly, lysates from RIG-I full-length expressing cells also revealed protein bands of approximately 95 kDa with the RIG-I-specific antibody Alme-1 (Figure 25, right panel). Thus, it needs to be elucidated whether overexpression of RIG-I full length *per se* leads to the induction of RIG-I short form.

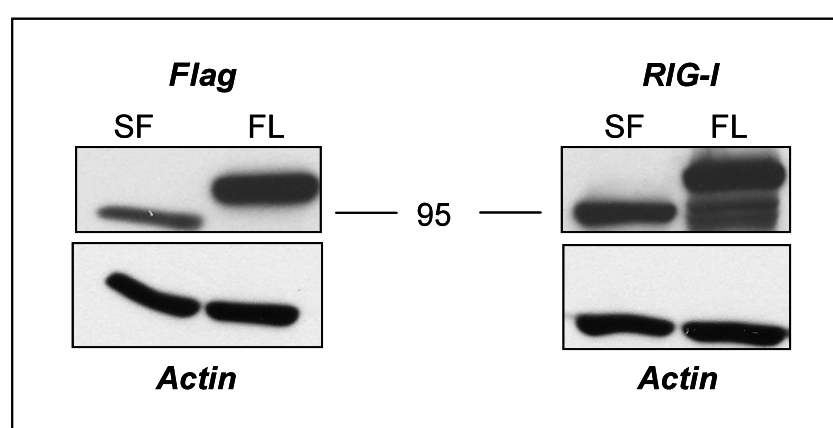


**Figure 25.** *Ectopic expression of Flag-tagged RIG-I short form*

HEK293 cells were transfected with 10  $\mu$ g of Flag-tagged RIG-I full-length (FL) and RIG-I short form (SF), respectively. 18 hrs after transfection, cells were lysed and whole cell lysates were analyzed by SDS-PAGE and immunoblotting using either a Flag-specific (left panel) or RIG-I-specific (clone Alme-1, right panel) antibody. Detection of  $\beta$ -Actin served as loading control.

Taken together, overexpression of RIG-I short form in HEK293 cells can be detected with a Flag- and RIG-I-specific antibody, indicating that the mammalian expression construct is functional.

#### **4.4.5 Investigation of the function of RIG-I short form in RIG-I-mediated innate immune signaling**

Mass spectrometry analysis confirmed the existence of RIG-I short form, which was shown to be endogenously induced by type I IFN and 5'-triphosphate RNA (Figure 23). Comparative sequence analysis of the peptides identified by mass spectrometry revealed that RIG-I short form comprises AA 155 to 925 of human RIG-I, which corresponds to an intact helicase domain as well as intact CTD and a partially lacking CARD2, whereas CARD1 is completely absent. This is in contrast to RIG-I splice variant that carries a short deletion in CARD1. Hence, RIG-I short form resembles RIG-I C, an artificial RIG-I construct containing the RIG-I helicase domain and CTD but completely lacking the CARDS, which has been utilized by Yoneyama *et al.* (2004) to delineate the function of the helicase domain in the RIG-I-mediated IFN response. Due to the lack of CARDS RIG-I C is not able to induce downstream signaling by CARD-CARD interactions of RIG-I and IPS-1. It therefore acts as dominant negative inhibitor of RIG-I-induced antiviral signaling.

Thus, several hypotheses were raised on the role of RIG-I short form in the context of RIG-I signaling. First, due to the complete lack of CARD1, RIG-I short form itself should not be able to interact with IPS-1 and to induce type I IFN upon stimulation with specific ligands. Secondly, since RIG-I short form is similar to RIG-I C, it might act as an endogenous inhibitor of RIG-I-mediated IFN signaling, for example by competing with RIG-I ligand binding. And last, RIG-I short form might function to control the levels of endogenous RIG-I in activated cells by promoting its degradation, thereby balancing the innate immune response and preventing overexpression of type I IFN that might be harmful to the host.

To elucidate the possible function of RIG-I short form in RLR-mediated signal transduction, IFN- $\beta$  promoter reporter assay and immunoprecipitation was performed to validate the previously described hypotheses.

#### ***4.4.5.1 RIG-I short form acts as inhibitor of RIG-I-mediated type I IFN induction***

It was hypothesized that RIG-I short form itself is not able to induce type I IFN upon stimulation with RIG-I-specific ligands, rather acting as inhibitor of RIG-I-mediated IFN signaling. To investigate this issue, IFN- $\beta$  promoter reporter assay was performed. HEK293 cells were cotransfected with an IFN- $\beta$  promoter luciferase reporter plasmid, pRL-TK internal control vector and RIG-I full-length, RIG-I short form or RIG-I full-length together with different doses of RIG-I short form. 18 hrs after transfection, cells were subsequently stimulated by transfection of 5'-triphosphate RNA (Figure 26A) or infection with VSV-M51R (Figure 26B).

Stimulation of RIG-I full-length expressing cells with 5'-triphosphate RNA led to a 226-fold activation of the IFN- $\beta$  promoter compared to mock-treated empty vector control. Cotransfection of RIG-I full-length and RIG-I short form at the same ratio had no influence on the induction of IFN- $\beta$  promoter activation (206-fold compared to mock-treated empty vector control). However, increasing the amount of RIG-I short form in the cotransfection with RIG-I full-length dramatically decreased the activation of the IFN- $\beta$  promoter. A 2.5-fold excess of RIG-I short form already decreased the induction of the IFN- $\beta$  promoter to 102-fold. Using a 10-fold (100 ng) and 40-fold (400 ng) excess of RIG-I short form in the cotransfection with RIG-I full-length, the induction of IFN- $\beta$  promoter activation (100 ng: 4.2-fold, 400 ng: 1.5-fold compared to mock-treated empty vector control) remained at the activation levels observed with the 5'-triphosphate RNA treated empty vector control (2.2-fold compared to mock-treated empty vector control) (Figure 26A).

Infection of cells transfected with 10 ng of RIG-I full-length with VSV-M51R resulted in a strong induction of IFN- $\beta$  promoter activity (355-fold compared to mock-treated empty vector control). Cotransfection of RIG-I full-length and RIG-I short form at an ratio of 1:1 and subsequent infection with VSV-M51R already markedly reduced the activation of the IFN- $\beta$  promoter (154-fold compared to mock-treated empty vector control) (Figure 26B), which was not the case in cells that had been transfected with the same amount of RIG-I full-length and RIG-I short form followed by transfection with 5'-triphosphate RNA (Figure 26A).

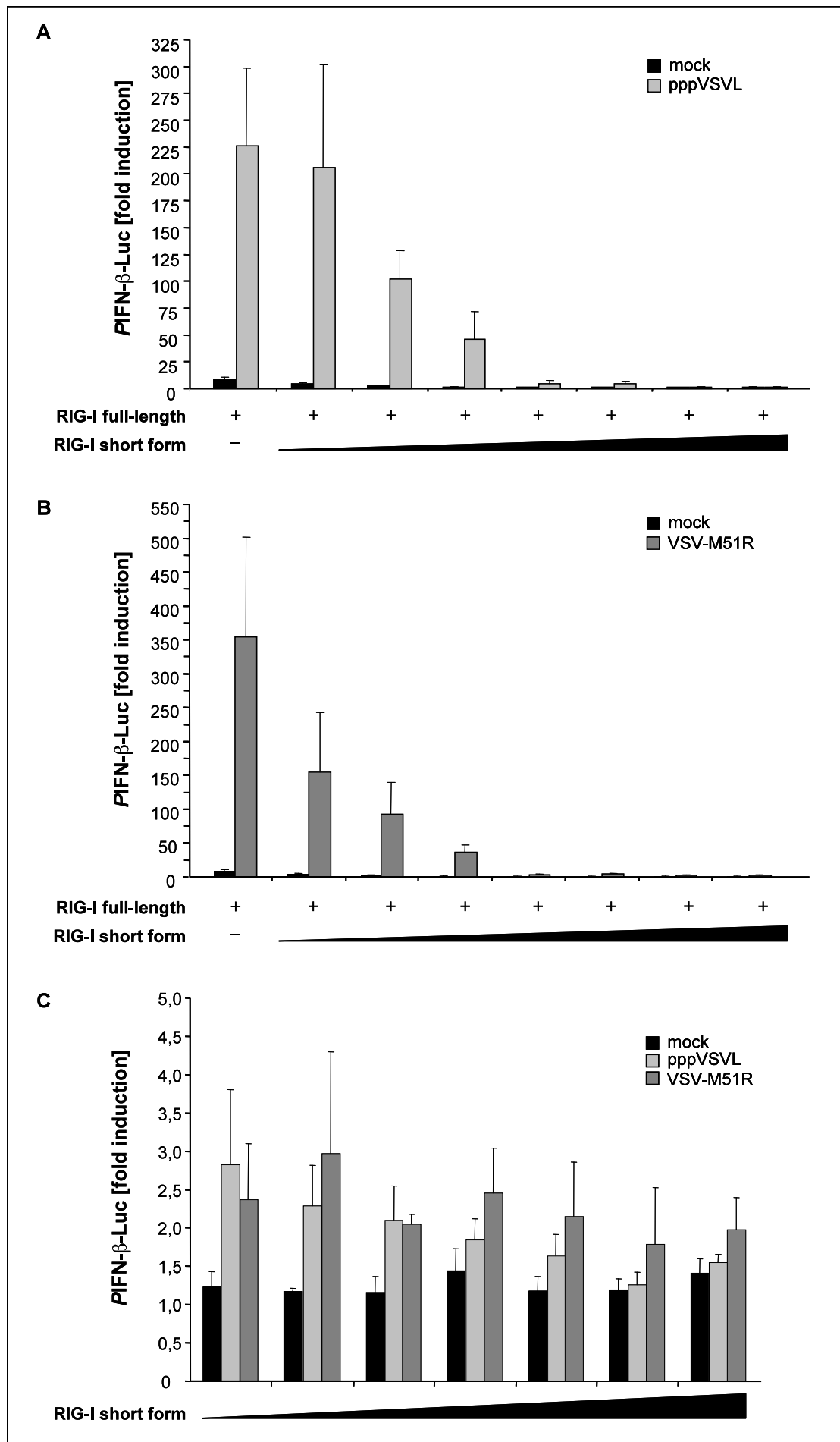


**Figure 26. Inhibition of RIG-I-mediated IFN- $\beta$  promoter activation by RIG-I short form**  
(A) and (B) HEK293 cells were either transfected with RIG-I full-length alone (10 ng) or cotransfected with RIG-I full-length (10 ng) and RIG-I short form (10 ng, 25 ng, 50 ng, 100 ng, 200 ng, 400 ng, 1000 ng) together with an IFN- $\beta$  promoter luciferase reporter construct (100 ng) and the internal control vector pRL-TK (10 ng). 18 hrs p.t., cells were transfected with 5'-triphosphate RNA (pppVSVL, 2  $\mu$ g/ml) (A) or infected with VSV-M51R (5 MOI) (B). IFN- $\beta$  promoter activity was measured by dual luciferase assay after 18 hrs.  
(C) HEK293 cells were transfected with different doses of RIG-I short form (10 ng, 25 ng, 50 ng, 100 ng, 200 ng, 400 ng, 1000 ng) together with the IFN- $\beta$  promoter reporter construct (100 ng) and pRL-TK internal control (10 ng). After 18 hrs, cells were either transfected with 5'-triphosphate RNA (pppVSVL, 2  $\mu$ g/ml) or infected with VSV-M51R (5 MOI). IFN- $\beta$  promoter activity was measured by dual luciferase assay 18 hrs after stimulation.  
Data represent the mean  $\pm$  SD ( $n = 3$ ).

Further increasing the amount of RIG-I short form dramatically reduced IFN- $\beta$  promoter activation upon VSV-M51R infection (25 ng: 93-fold, 50 ng: 37-fold) compared to the induction that was observed in VSV-M51R infected cells expressing only RIG-I full-length.

As expected, overexpression of RIG-I short form alone even when using high doses of plasmid did not result in the induction of IFN- $\beta$  promoter activation in response to either of the ligands tested (Figure 26C).

Thus, in contrast to RIG-I full-length, RIG-I short form *per se* is not able to induce IFN- $\beta$  promoter activation in response to both 5'-triphosphate RNA transfection and VSV-M51R infection, rather overexpression of RIG-I short form leads to an efficient suppression of the RIG-I-mediated IFN response to these ligands.

#### 4.4.5.2 Ubiquitination of RIG-I short form

RIG-I short form might be involved in balancing the levels of endogenous RIG-I in activated cells to prevent uncontrolled IFN signaling. If induction of RIG-I short form leads to degradation of RIG-I full length, one possible scenario is the formation of a multimeric RIG-I full-length/short-form complex that is degraded in a proteasome-dependent manner by Lys48-linked ubiquitination, thereby regulating the levels of endogenous RIG-I.

It was shown that the previously identified RIG-I splice variant (RIG-I  $\Delta$ AA 36-80) lacks the ability to interact with TRIM25, resulting in the loss of CARD ubiquitination and the inability to induce downstream signaling (Gack *et al.*, 2008). Furthermore, RIG-

I splice variant acts as inhibitor of RIG-I-mediated IFN signal transduction, which was also observed for the newly identified RIG-I short form (Figure 26A and B). Different studies revealed that ubiquitination plays a dual role in RIG-I-mediated signaling by inducing an active signaling conformation of RIG-I on the one hand, but also inhibiting RIG-I-mediated signaling on the other hand (Arimoto *et al.*, 2007a; Arimoto *et al.*, 2007b; Friedman *et al.*, 2008; Gack *et al.*, 2008; Gack *et al.*, 2007; Gao *et al.*, 2009; Zeng *et al.*, 2010). Thus, it was investigated whether RIG-I short form is ubiquitinated upon upregulation by type I IFN.

To assess ubiquitination of RIG-I short form, coimmunoprecipitation of lysates prepared from either mock-treated HEK293 cells or cells treated with type I IFN using an ubiquitin-specific antibody coupled to protein G sepharose was performed.

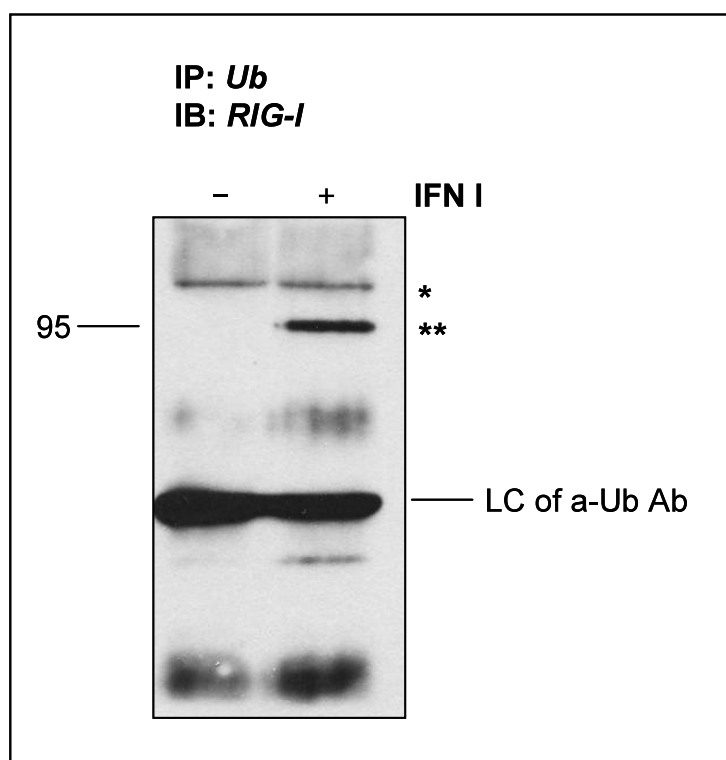


**Figure 27.** *Analysis of the ubiquitination state of RIG-I variants upon type I IFN treatment*

HEK293 cells were either treated with 1000 U type I IFN or left untreated. Cells were lysed after 24 hrs and lysates were subjected to coimmunoprecipitation using an antibody specific for all types of ubiquitin (Ub, clone P4D1) to recover proteins that bear ubiquitin chains. Proteins were subsequently analyzed by SDS-PAGE and immunoblotting using the RIG-I-specific antibody Alme-1. \* indicates RIG-I full-length, whereas \*\* corresponds to RIG-I short form. LC refers to the light chain of the Ub antibody that was coupled to protein G sepharose.

---

IP samples were subsequently analyzed by SDS-PAGE and immunoblotting using the RIG-I-specific antibody Alme-1 (Figure 27). Ubiquitin-specific immunoprecipitation revealed that RIG-I short form is absent in untreated cells, which is consistent with the previous finding that RIG-I short form is only detectable upon activation of the cells by IFN I or pppVSVL stimulation (Figure 23). While in untreated cells only RIG-I full-length was detected by RIG-I-specific immunoblotting, pre-treatment of HEK293 cells with type I IFN revealed that both RIG-I full-length and RIG-I short form are ubiquitinated (Figure 27). In line with the report of Gack *et al.* (2008), that RIG-I splice variant lacks ubiquitination, the RIG-I splice variant was not detected in this assay. Taken together this result indicates that the induction of endogenous RIG-I short form by type I IFN is accompanied by ubiquitination of the protein. Hence, ubiquitination, which was already shown to be critically involved in the regulation of RIG-I as well as downstream molecules, also seems to be critically involved in the suppression of RIG-I-mediated IFN activation by the newly identified RIG-I short form.

## 5 DISCUSSION

### 5.1 The C-terminal domain is the RNA 5'-triphosphate sensor of RIG-I

Since the discovery of the cytoplasmic DExD/H boxRNA helicase RIG-I in 2004 (Yoneyama *et al.*, 2004), major advances have been made in the understanding of TLR-independent virus recognition. To date, it is known that three different RLRs, namely RIG-I, MDA5 and LGP2, mediate recognition of viruses independently of the TLR system. Structural analysis revealed that RIG-I contains N-terminal tandem CARDs as well as a helicase domain in the central part of the protein (Yoneyama *et al.*, 2004). Functional characterization of RIG-I using deletion constructs of full-length RIG-I revealed that the CARDs act as an effector domain that activates a downstream molecule. IPS-1 (also known as MAVS, VISA or CARDIF) was then identified as adapter protein of the RLR pathway, transmitting signals from RIG-I and MDA5 to activate downstream molecules that finally induce the production of type I IFN and proinflammatory cytokines (Kawai *et al.*, 2005; Meylan *et al.*, 2005; Seth *et al.*, 2005; Xu *et al.*, 2005). Analysis of a construct comprising the RIG-I helicase domain but lacking the CARDs provided evidence that the helicase domain is essential for the signal-transducing function of RIG-I and that ATP hydrolysis is required for its activity (Yoneyama *et al.*, 2004). *In vivo* studies using the respective RLR knockout mice revealed that RIG-I is involved in the recognition of viral RNA that is generated during replication of various RNA viruses such as NDV, SeV, VSV, Influenza A virus, Japanese encephalitis virus and HCV (Kato *et al.*, 2006). Finally, the molecular pattern, which specifically activates RIG-I was described as RNA bearing a 5'-triphosphate moiety and it was suggested that 5'-triphosphate ssRNA is the primary ligand of RIG-I (Hornung *et al.*, 2006; Pichlmair *et al.*, 2006). However, recent studies demonstrated that dsRNAs with 5'-triphosphates are potent activators of RIG-I (Schlee *et al.*, 2009; Schmidt *et al.*, 2009). Furthermore, it was demonstrated that the genomic RNA of Influenza A virus and SeV represent the physiological agonists of RIG-I (Rehwinkel *et al.*, 2010). It was proposed that the panhandle structure formed by 5' and 3' ends of the viral RNA is likely a structural feature recognized by RIG-I (Fujita, 2009; Rehwinkel *et*

*al.*, 2010; Schlee *et al.*, 2009). However, the structural and molecular mechanisms involved in the recognition of 5'-triphosphate RNA remained elusive.

### **5.1.1 The C-terminal domain is another functional domain of RIG-I**

During the investigation of the structural and molecular mechanisms that might be involved in the recognition of 5'-triphosphate RNA, a study by Saito and colleagues provided evidence that an internal repressor domain, which is located at the C-terminus, controls RIG-I signaling. Overexpression of this domain inhibited RIG-I-mediated IFN- $\beta$  promoter activation in response to SeV infection (Saito *et al.*, 2007). Thus, Saito *et al.* proposed a model of RIG-I autoregulation and signaling, predicting that in resting cells, the repressor domain mediates a conformational state that masks the CARDS from signaling. Virus infection then leads to RIG-I activation and signaling by induction of conformational changes that demask the CARDS for signaling through IPS-1 interaction. However, the mode of this activation had not been elucidated.

To reveal domain functions in RNA-stimulated RIG-I activation, the *in vitro* biochemical properties of human RIG-I were analyzed together with a variety of truncation variants and isolated domains, which were produced as recombinant proteins, by Sheng Cui and Karl-Peter Hopfner. Analysis of the RIG-I molecule at the level of the amino acid sequence and by protein structure prediction as well as limited proteolysis indicated the presence of a putative domain at the C-terminus comprising AA 802 to 925 of RIG-I. This localization differs from the region comprising the repressor domain, which was mapped to AA 742 to 925 by Saito *et al.* (2007), which was not suited for structural analysis in our study. Overexpression of the putative C-terminal domain (AA 802-925) potently inhibited RIG-I-mediated IFN- $\beta$  promoter activation in response to both 5'-triphosphate RNA stimulation and VSV-M51R infection, which is in line with the observation of Saito *et al.* (2007). Thus, RIG-I (AA 802-925) has repressor function and represents another functional domain in addition to the CARDS and the helicase domain. Although the CTD identified in this study differs from the repressor domain described by Saito *et al.* (2007) with regard to the localization, it exerts the same inhibitory function on RIG-I signaling.

The finding that the identified CTD represents another functional domain that has important functions in RIG-I-mediated signaling was further supported by biochemical

analysis of a variant that contains the tandem CARDS and the helicase domain, but lacks the CTD (RIG-I $\Delta$ RD). While both RIG-I full-length and a variant that consisted of a functional helicase domain and CTD ( $\Delta$ CARD-RIG-I) were efficiently stimulated by either 5'-triphosphate RNA (RIG-I full-length) or 5'-triphosphate RNA and nonphosphorylated dsRNA ( $\Delta$ CARD-RIG-I), this variant was essentially inactive for both RNAs (section 8.6, Figure 29). This suggested that the CTD, besides its repressor function in RIG-I-mediated innate immune signaling, might be required either for RNA binding or that it stimulates the ATPase activity of the helicase domain by other means.

### **5.1.2 The zinc-coordination site within the CTD is a key structural motif**

Comparative sequence analysis revealed that the CTD contains five invariant cysteine residues that are located at AA position 810, 813, 818, 864 and 869, respectively. Cysteine residues have been described to play a major role in the formation of zinc fingers, small protein structural motifs that contribute to the stability of a given domain. Furthermore, zinc fingers are involved in the binding of nucleic acids, proteins or small molecules (Krishna *et al.*, 2003). Zinc fingers are structurally diverse and are present among proteins that perform a broad range of functions in various cellular processes, such as replication (Dong *et al.*, 1999; Lin *et al.*, 2005; Muller *et al.*, 2007) and repair (Ahel *et al.*, 2008; Alwin *et al.*, 2005; Park *et al.*, 1999), transcription (Laudes *et al.*, 2004; Nieto, 2002; Wang *et al.*, 2008; Wang *et al.*, 2006; Zhang *et al.*, 2010) and translation (Bick *et al.*, 2003; Fu *et al.*, 1996; Schiff *et al.*, 1988; Tijms *et al.*, 2001), metabolism (Bouchard *et al.*, 2007; Laudes *et al.*, 2004; Schmitz *et al.*, 2004; Wagner *et al.*, 2000) and signaling (Heyninck and Beyaert, 1999; Heyninck *et al.*, 1999; Minoda *et al.*, 2006; Saitoh *et al.*, 2005; Sharif-Askari *et al.*, 2010) as well as cell proliferation (Cayrol *et al.*, 2007; Liu *et al.*, 2007; Regl *et al.*, 2004; Remington *et al.*, 1997; Shiraishi *et al.*, 2007) and apoptosis (Chang *et al.*, 2000; Inoue *et al.*, 2002; Lademann *et al.*, 2001). Crystallization of the CTD, which was performed by Sheng Cui and Karl-Peter Hopfner, revealed that the crystals grew in the presence of zinc, confirming that the invariant cysteine residues are in fact involved in the binding of a metal ion. Structural analysis of the CTD illuminated that cysteine residues at AA positions 810, 813, 864 and 869 coordinate the zinc ion, whereas C818 does not bind the metal ion directly. Due to the multiple functions of zinc finger structures, it seemed likely that the zinc-coordination site in the CTD of RIG-I exerts other functions apart from stabilizing

this small domain. Disruption of the zinc-binding cluster in the CTD by site-directed mutagenesis of the invariant cysteine residues to arginine completely abolished the ability of RIG-I to induce IFN- $\beta$  promoter activity in response to its specific ligand 5'-triphosphate RNA or virus infection, whereas mutation of two non-conserved cysteine residues (C829 and C841) did not influence this response. These results confirmed that the CTD plays a major role in RIG-I-mediated IFN induction.

The zinc-coordinating cysteines are invariant not only among RIG-I from different species, but also in all available MDA5 and LGP2 sequences, providing further evidence that this motif is a central functional and structural element in the entire RLR family.

### 5.1.3 The RIG-I CTD is involved in ligand recognition

Because  $\Delta$ CARD-RIG-I was able to respond to 5'-triphosphate RNA, whereas the helicase domain was preferentially activated by nonphosphorylated dsRNA in the ATPase assay, it was unlikely that the CARDS or the helicase domain contain the specificity site for the recognition of RNA 5'-triphosphate moieties. Rather an intact CTD seems to be essential for ligand recognition, constituting a new aspect of the RIG-I C-terminal domain to the properties that have been attributed to the corresponding region described earlier by Saito *et al.* (2007).

Fluorescence anisotropy assay using a Alexa-Fluor 488-5-UTP-labelled 5'-triphosphate RNA demonstrated that much, but not all of the binding affinity of RIG-I for 5'-triphosphate RNA resides in the CTD, because the CTD itself interacted with this ligand (Figure 30A, see appendix, section 8.6). Conversely, dephosphorylated RNA did not bind with significant affinity to the CTD, which is consistent with the inability of RNA lacking the 5'-triphosphate to induce RIG-I-dependent IFN signaling. Additionally, the information obtained from *in vitro* RNA binding assay further corroborated the observation that there is a direct interaction between the RIG-I CTD and 5'-triphosphate RNA, since RIG-I containing mutations of the invariant cysteines that lead to disruption of the zinc-binding cluster failed to interact with 5'-triphosphate RNA. In the study of Saito and colleagues the C-terminal domain acts as repressor of RIG-I-mediated IFN signaling, but the mechanism of this inhibition remained unclear. With regard to our findings that the CTD directly interacts with the RNA ligand, the

CTD might exert its inhibitory role on RIG-I by competing for 5'-triphosphate RNA. Titration of increasing amounts of recombinant CTD together with either 5'-triphosphate RNA or nonphosphorylated dsRNA into a solution containing recombinant  $\Delta$ CARD-RIG-I indeed substantially reduced the capability of 5'-triphosphate RNA to activate  $\Delta$ CARD-RIG-I (Figure 30B, see appendix, section 8.6). Interestingly, the CTD also interfered somewhat with the ability of  $\Delta$ CARD-RIG-I to respond to nonphosphorylated dsRNA, albeit at a much lower level. These effects point out that the RIG-I CTD has two properties. First, the much more pronounced inhibition of 5'-triphosphate stimulation than dsRNA stimulation is due to competition for 5'-triphosphate RNA. Secondly, the CTD interferes with the activation of the helicase domain since the inhibition of dsRNA stimulation was much weaker compared to inhibition observed upon stimulation with RNA bearing 5'-triphosphates. One possible explanation for the latter characteristics is that the CTD has an impact in proper multimer formation of RIG-I, which was suggested to be essential for the signaling conformation of RIG-I (Saito *et al.*, 2007).

Saito *et al.* (2007) suggested that the C-terminal repressor domain regulates the conformation of RIG-I to prevent constitutive activation of the molecule in the absence of virus infection. Furthermore, their data supported a signaling mechanism in which RIG-I signals at least as dimeric unit. However, we were able to demonstrate that the CTD itself is a 5'-triphosphate RNA-dependent multimerization domain. In the absence of 5'-triphosphate RNA, the CTD remained as monomer, while multimerization occurred in the presence of RNA (Figure 31C and E, section 8.6). The same was observed for RIG-I, whereas for the RIG-I variant lacking the CTD no multimerization could be observed (Figure 31A, B and E, section 8.6). In contrast, synthetic ssRNA was not able to induce dimerization of RIG-I, indicating that the CTD is essentially required for 5'-triphosphate RNA-dependent dimer formation of RIG-I. In conjunction with the information obtained from ATPase assay and 5'-triphosphate binding, these data further support that the RIG-I CTD instead of acting as repressor domain (Saito *et al.*, 2007), exhibits a dual mechanistic role: first, the CTD is the recognition domain for 5'-triphosphate RNA and secondly, it triggers a structural switch that induces dimerization of RIG-I. With regard to its role as regulator of RIG-I conformation, it was observed that RIG-I bearing mutations of the invariant cysteine residues interacted with IPS-1 in the absence of virus infection much stronger than wild-type RIG-I, indicating the impact of the CTD on the intramolecular structure of RIG-I.

Taken together, our findings support the model of Saito and colleagues in which RIG-I resides in a signaling-inactive conformation in the steady state, which is regulated by the CTD to prevent interaction with IPS-1 and induction of downstream signaling. By illuminating the dual role of the CTD, we demonstrate that multimerization is in fact the critical step required to induce RIG-I signaling. Thus, due to the dual function of the CTD, which is essential for RIG-I activation and downstream signaling to induce an antiviral state, we suggest to designate the RIG-I CTD as regulatory domain (RD) instead of repressor domain.

#### **5.1.4 A conserved groove in the regulatory domain acts as 5'-triphosphate RNA-binding site**

It was demonstrated that the integrity of the regulatory domain is essential for the activation of RIG-I as well as the induction of RIG-I-mediated IFN induction by specifically recognizing 5'-triphosphate RNA. In summary, all assays revealed that the CTD is exclusively stimulated by RNA bearing a 5'-triphosphate moiety, indicating that the regulatory domain itself contains a structural motif, which specifically binds the 5'-triphosphate. Such triphosphate-binding sites are characterized by a positively charged patch, which compensates the negative charge of the triphosphate chain (Sazinsky *et al.*, 2006; Wu *et al.*, 2005; Yagi *et al.*, 2007). In line with this, analysis of the sequence conservation and electrostatic potential revealed the presence of a positively charged groove, which is rich in leucine residues, that colocalizes with a region of high sequence conservation (Figure 32, see appendix, section 8.6). Mutation of AA residues that are localized within this groove to alanine significantly altered the binding affinity of RIG-I to 5'-triphosphate RNA *in vitro*, as well as the induction of IFN- $\beta$  promoter activation in response to stimulation with 5'-triphosphate RNA and virus infection. Furthermore, site-directed mutagenesis of the respective residues to glutamate, which causes a complete reversal of the surface charge from positive to negative, even completely abolished the RIG-I-mediated IFN induction in response to both ligands tested, indicating that interaction of the viral RNA with the positively charged patch of the groove is a prerequisite for full activation of RIG-I.

Several groups tried to elucidate the structural requirements that in addition to the 5'-triphosphate are necessary to activate RIG-I. While the results by Hornung and Pichlmair suggested that 5'-triphosphate ssRNA is the primary ligand for RIG-I, several

studies revealed that dsRNA with 5'-triphosphate structure is required for RIG-I activation, whereas purely single stranded RNA bearing a 5'-triphosphate is not sufficient (Schlee *et al.*, 2009; Schmidt *et al.*, 2009). Furthermore, blunt-ended dsRNA rather than dsRNA with 5' and 3' overhangs binds to and stimulates RIG-I (Li *et al.*, 2009b; Marques *et al.*, 2006). Schlee *et al.* (2009) observed, that although blunt-ended dsRNA with 5'-triphosphates potentially triggers the activation of RIG-I, 5'-triphosphate dsRNA with 5' overhangs does not stimulate the activation of RIG-I effectively. Furthermore it was suggested that the panhandle structure formed by 5' and 3' ends of the viral RNA is recognized by RIG-I (Rehwinkel *et al.*, 2010; Schlee *et al.*, 2009).

A recent study investigated the structural basis of 5'-triphosphate dsRNA recognition by the RIG-I CTD and revealed that the CTD binds 5'-triphosphate dsRNA and ssRNA as well as blunt-ended dsRNA, with the highest affinity for 5'-triphosphate dsRNA (Lu *et al.*, 2010). Furthermore, IFN- $\beta$  promoter reporter assay demonstrated that all three forms of RNA stimulate RIG-I signaling. In addition to our observation that the positively charged groove within the CTD specifically recognizes 5'-triphosphate RNA, RIG-I recognizes the termini of RNA and interacts with the 5'-triphosphate as well as the backbone phosphodiester of the RNA (Lu *et al.*, 2010). Specific recognition of the termini of dsRNA has already been described for LGP2 (Li *et al.*, 2009b). In addition, the experiments performed by Lu and colleagues completed the overall picture of RIG-I-mediated 5'-triphosphate RNA recognition by demonstrating that the CTD primarily interacts with the 5' four nucleotides of the dsRNA, while the complementary strand only makes limited contributions to RNA binding, explaining how the CTD can bind both types of dsRNA and ssRNA containing a 5'-triphosphate structure. Furthermore, this study finally revealed which AA residues are involved in binding of distinct regions of the RNA. First, they confirmed that K858 and K888, which were identified to be localized in the conserved positively charged groove within the CTD in our study, recognize the 5'-triphosphate. However, K861 and H847, which were unremarkable in our study, also contribute to this recognition. The role of these residues was further confirmed in a second study, demonstrating that the side chains of K861 and K888 form a hydrogen-bond to the  $\alpha$  5'-phosphate, whereas the side chains of H847 and L858 form a hydrogen-bond to the  $\beta$  5'-phosphate (Wang *et al.*, 2010). A second group of residues interacted with the phosphate backbone, whereas the third group of residues interacts with the exposed bases at the termini of the RNA or with the RNA backbone (Lu *et al.*, 2010). Thus, the first two groups of residues mediate

5'-triphosphate RNA binding by multiple electrostatic interactions, whereas the last two groups contribute primarily to the binding of dsRNA lacking a 5'-triphosphate. Thus, the previously described amino acid residues in the C-terminal regulatory domain are exclusively involved in 5'-triphosphate RNA recognition. In contrast, the role of the helicase domain, which is also required for RIG-I activity, in the interaction with the ligand is less clear. A study by Myong *et al.* (2009) described a first mechanism by which the helicase domain could contribute to RIG-I activation. They observed that binding of 5'-triphosphate RNA to the RD stimulates the ATPase activity of the helicase domain, thereby triggering RIG-I to translocate on dsRNA *in cis*. Although the helicase domain is not directly involved in RNA binding, cooperative activity of the RD and the activated helicase domain seems to be essential to induce an active signaling conformation in RIG-I, in which the CARDS are exposed to the adapter protein IPS-1. However, to elucidate the detailed mechanism of how RNA binding activates RIG-I, the determination of high-resolution structures of full-length RIG-I bound to 5'-triphosphate RNA will be needed. However, with regard to the structural information of RIG-I available to date, the findings discussed above explain how RIG-I is able to recognize such a broad range of RNA ligands.

### 5.1.5 Model for activation of RIG-I by the regulatory domain

In summary, the data obtained throughout this study suggest a step-wise model of RIG-I activation that includes the following structurally and temporally regulated events (Figure 28).

As suggested in the study of Saito *et al.* (2007), in the steady state where 5'-triphosphate containing RNA ligands and other recently identified RNA signatures are absent, RIG-I resides in a monomeric and inactive form that possesses a conformation in which the CARDS mask an RNA-binding site in the helicase domain to prevent subsequent stimulation by dsRNA species. Since mutation of the zinc-coordination site in the C-terminal regulatory domain led to a much stronger interaction with IPS-1 compared to wild-type RIG-I, the RIG-I CARDS seem to be autoinhibited by the regulatory domain to prevent constitutive activation of RIG-I. Ligand binding to the 5'-triphosphate binding groove within the regulatory domain then induces a conformational change that results in the exposure of the CARDS, dimerization and stimulation of the helicase domain. It is likely that these macromolecular changes are

triggered by the binding energy of RNA 5'-triphosphates as it was described for ATP binding-dependent structural switches in ATPases (Hopfner and Tainer, 2003). Furthermore, the helicase domain is now free to interact with dsRNA. In conjunction with RNA-stimulated ATPase activity, these structural changes generate a signaling-active conformation of RIG-I. Activated RIG-I now presumably translocates on dsRNA in an ATP-dependent manner (Myong *et al.*, 2009), thereby exposing the CARDS for interaction with the downstream signaling adapter IPS-1.

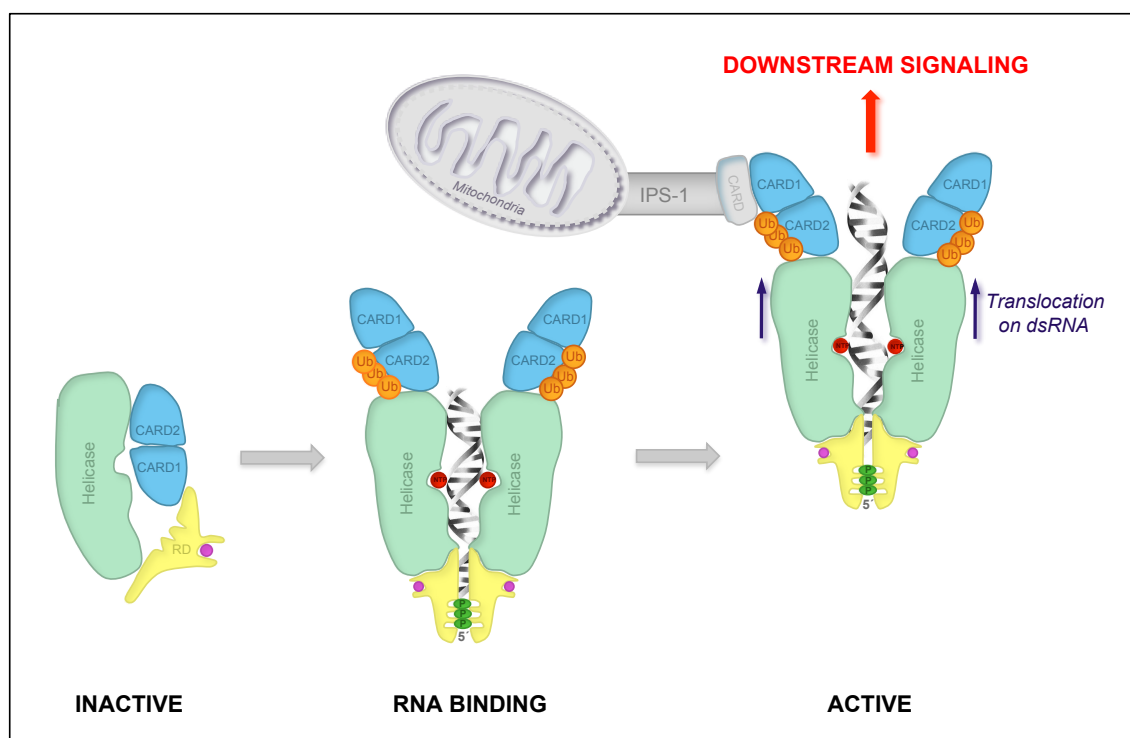


**Figure 28.** *Proposed model for RIG-I activation by 5'-triphosphate RNA-induced dimer formation*

Schematic representation of events leading to RIG-I activation. In the inactive state, RIG-I resides as monomer in an inactive form, where the CARDS are autoinhibited by the C-terminal regulatory domain (RD, illustrated in yellow with the zinc-coordination site depicted as magenta sphere) and mask the helicase domain. Binding of 5'-triphosphate RNA (triphosphates illustrated as green oval) to the RD induces dimerization and conformational changes that expose the CARDS to downstream signaling factors. Furthermore ubiquitination (Ub) of the CARDS is required for full activity of RIG-I. Binding of 5'-triphosphate RNA also stimulates the ATPase activity of the helicase domain, which mediates ATP-dependent translocation on double-stranded RNA regions.

The dsRNA translocation activity on dsRNA containing a 5'-triphosphate seems to function as a signal verification mechanism by activating the ATPase activity only when the RNA features both PAMPs, the 5'-triphosphate and the double-stranded nature. In summary, the current view suggests not only a functional connection between

the apparently different PAMPs but also indicates that the integration of more than one PAMP in a single activation mechanism might be important for the selective distinction of host viral RNA (Myong *et al.*, 2009). However, the molecular function of the translocase activity is not completely understood. One explanation might be that translocation displaces viral RNA-binding proteins from the RNA, thereby actively demasking viral patterns, interfering with viral replication and triggering a robust antiviral response. On the other hand, the signal strength is likely to be related to the time spent in the translocation mode and therefore to the length of the RNA.

## **5.2 The C-terminal cysteine-rich domain of MDA5 mediates ligand specificity**

MDA5 was shown to preferentially recognize long dsRNA since the synthetic dsRNA poly(I:C) specifically activates MDA5 in its long form of more than 1 Kb (Kato *et al.*, 2008). *In vivo* experiments revealed that MDA5 is essential for the induction of an innate immune response to infection with picornaviruses (Gitlin *et al.*, 2006; Hornung *et al.*, 2006; Kato *et al.*, 2006). Although recent studies demonstrated that MDA5 is also activated by murine norovirus-1 and murine hepatitis virus, as well as WNV and dengue virus (Fredericksen *et al.*, 2008; Loo *et al.*, 2007), the defined molecular structure that is responsible for MDA5 induction had not been identified yet.

Sequence alignment demonstrated that the C-terminus of MDA5 contains a cysteine-rich region homologous to the C-terminal domain identified in RIG-I. In an independent study, Saito *et al.* (2007) also described the existence of a C-terminal domain in MDA5. As for RIG-I, mutation of the invariant cysteine residues in MDA5 abolished activation of the IFN- $\beta$  promoter in response to poly(I:C), demonstrating that the C-terminal domain of MDA5 is involved in ligand binding as well. Since the CTD of MDA5 does not bind 5'-triphosphate RNA, it is likely that the C-terminal domain confers ligand specificity or it has a completely different functional role in MDA5 signaling. In contrast to the CTD of RIG-I, the corresponding domain in MDA5 does not exhibit repressor function (Saito *et al.*, 2007). During this thesis, a crystal structure of the MDA5 CTD was published in the protein data bank (PDB entry 3GA3). Analysis of this structure revealed a highly conserved fold similar to the structure of the CTD of RIG-I, which is also stabilized by a zinc ion that is coordinated by the invariant cysteine

residues (Li *et al.*, 2009a). In addition, this study shows that the C-terminal domain of MDA5 is characterized by the presence of a leucine-rich basic cleft that mediates binding of dsRNA through electrostatic interactions. Thus, the C-terminal domains of RIG-I and MDA5 share a common RNA-binding surface. Ligand specificity might be controlled by specific amino acid residues that are involved in formation of the respective binding pocket. While in the RIG-I CTD residue K858, which is located at the center of the 5'-triphosphate binding site, is critically required for triphosphate binding, MDA5 either contains a threonine or an isoleucine at this position, which might account for ligand specificity.

Since MDA5 is essentially involved in the recognition of picornaviruses, it was expected that during infection, naturally occurring agonists are generated which in turn trigger MDA5-dependent IFN- $\beta$  promoter activation in a reporter assay. This idea was further supported by the observation that total RNA isolated from VSV-infected cells potently activated RIG-I, suggesting the accumulation of RIG-I specific RNA signatures in the course of infection and virus replication. However, in MDA5 expressing HEK293 cells only a weak IFN response was observed upon both EMCV infection as well as transfection of RNA obtained from EMCV-infected cells.

There has been accumulating evidence that MDA5 might not function alone but rather in cooperation with LGP2 (Pippig *et al.*, 2009; Satoh *et al.*, 2010; Venkataraman *et al.*, 2007). Several independent studies demonstrated that LGP2, like its RLR relatives RIG-I and MDA5, contains a C-terminal domain, which is similar to the other two CTD with regard to the fold and the presence of the zinc-binding cluster (Li *et al.*, 2009b; Pippig *et al.*, 2009; Saito *et al.*, 2007). It was shown that the CTD of LGP2 binds to dsRNA (Saito *et al.*, 2007; Pippig *et al.*, 2009). Furthermore, the LGP2 CTD was shown to be necessary and sufficient for inhibition of RIG-I, but not MDA5 signaling, although it formed a complex with either protein (Saito *et al.*, 2007). With regard to the difficulties to activate MDA5 upon EMCV infection and the failure to respond to RNA isolated from EMCV-infected cells, it seemed likely that LGP2 by forming a complex with MDA5 acts as cofactor in this branch of innate immune signaling. However, cotransfection of LGP2 had no synergistic effect on the response of MDA5 expressing cells to both EMCV infection and transfection of EMCV RNA. Interestingly, cotransfection of LGP2 markedly increased the IFN response to VSV-M51R infection. A possible explanation for this effect is that LGP2, which selectively binds dsRNA (Li

*et al.*, 2009b; Pippig *et al.*, 2009), might detect dsRNA generated during VSV replication, which subsequently leads to stimulation of MDA5 activation by complex formation. *In vivo* studies using *Mda5* KO mice unambiguously demonstrated that LGP2 acts as positive regulator of MDA5 (Sato *et al.*, 2010; Venkataraman *et al.*, 2007), but with regard to the obtained *in vitro* data it cannot be excluded that a yet unidentified cofactor bridges or stabilizes a functional MDA5/LGP2 heterocomplex leading to its full activity. Thus, it is likely that due to the lack of this putative factor, cotransfection of MDA5 and LGP2 did not trigger a ligand-specific IFN response in the reporter assay.

In summary, our study (Cui *et al.*, 2008) together with the findings of other groups revealed that the C-terminal domains of all three RIG-I like helicases represent a RNA-binding element with a common core RNA-binding site but specific adaptation to their respective pattern that confers ligand specificity to each RLR.

### **5.3 *Helicobacter pylori* RNA is recognized by RIG-I**

A study by Rad and colleagues demonstrated that different TLRs contribute to the recognition of *Helicobacter pylori* in DCs (Rad *et al.*, 2007). However, microarray analysis indicated that a MyD88- and Trif-independent (thus TLR-independent) pathway plays a role in the *H. pylori*-mediated induction of type I IFN and ISGs in DCs (Rad *et al.*, 2009). In line with this, in previous studies it was already observed that bacterial DNA induces cell-type specific DNA-dependent type I IFN responses that are TLR-independent (Hochrein *et al.*, 2004; Ishikawa and Barber, 2008; Takaoka *et al.*, 2007). Moreover, the observation that B-DNA derived from *Legionella pneumophila* potentially triggered an innate immune response that did not require TLRs supported the idea that a cytoplasmic DNA receptor cooperates with TLR9 in the recognition of bacterial DNA in a cell-type specific manner (Stetson and Medzhitov, 2006). The existence of this alternative DNA recognition pathway was further confirmed by the identification of a protein designated as STING (also known as MITA, ERIS and MPYS) that seems to function downstream of the putative DNA receptor (Ishikawa and Barber, 2008; Ishikawa *et al.*, 2009; Jin *et al.*, 2008; Sun *et al.*, 2009; Zhong *et al.*, 2008). Cells lacking STING lost their ability to mount an efficient IFN- $\beta$  response upon infection with *Listeria monocytogenes* (Ishikawa *et al.*, 2009). Finally, screening for

IFN-inducible genes that contain DNA-binding sites revealed a candidate sensor, which was designated as DAI (DNA-dependent activator of IRFs) (Takaoka *et al.*, 2007). Thus, it was of particular interest, if the RLR family might be involved in TLR-independent recognition of bacterial RNA similar to cooperation of different PRRs in sensing DNA upon bacterial infection. Due to the observation by Rad and colleagues (2007) that different PRRs contribute to the activation of DCs in response to *H. pylori* infection, *H. pylori* was used to investigate this issue.

### 5.3.1 *Rig-I* mRNA is upregulated in *H. pylori*-infected BMDCs

Initially, analysis of the mRNA expression levels of IFN- $\beta$  (*Ifnb1*) as well as several IFN- $\beta$  induced genes (*Ifi204*, *Isg15*) in WT and *Trif* mutant BMDCs in response to *H. pylori* infection revealed that the *Trif* pathway downstream of TLR3 and TLR4 is not essential for the *H. pylori*-dependent activation of type I IFN. Moreover, compared to cells that remained uninfected, activation of WT and *Trif* mutant BMDCs upon infection with *H. pylori* was accompanied by the induction of *Rig-I* mRNA expression. This result provided the first evidence that RIG-I might actually play a role in the recognition of *H. pylori*. In line with this, RIG-I expression was shown to be upregulated in response to *Listeria monocytogenes* *in vivo* and *in vitro* (Imaizumi *et al.*, 2006). In addition, transfection of BMDCs with RNA isolated from *H. pylori*, led to increased IFN- $\beta$  levels in the supernatant of the stimulated cells, compared to the IFN- $\beta$  concentration that was measured after infection with *H. pylori*. This observation also implicated a possible role for RLRs in the TLR-independent IFN induction in response to *H. pylori*. However, transfection of BMDCs with the RIG-I-specific ligand 5'-triphosphate RNA resulted in the highest production of IFN- $\beta$ . These differences might be explained by the different nature of the ligands. The RIG-I-specific ligand 5'-triphosphate RNA is generated by *in vitro* transcription and bears a triphosphate moiety at the 5' end of the RNA, but despite the 5'-triphosphate signature IVT-RNA preparations are rather heterogenous, containing unexpected by-products such as hairpins and RNAs of different length (Schlee *et al.*, 2009; Schmidt *et al.*, 2009). In contrast, RNA isolated from *H. pylori* is a physiological agonist of yet undefined structure that might activate RIG-I or MDA5. Thus, although stimulation of DCs with *H. pylori* RNA led to lower IFN- $\beta$  protein levels compared to that induced by 5'-triphosphate RNA, RNA isolated from *H. pylori* presumably possesses the capacity to

trigger RLR-dependent IFN induction or at least contains a RNA fraction that has the potential to activate either RIG-I or MDA5.

### **5.3.2 *H. pylori* RNA activates RIG-I in a 5'-triphosphate-dependent manner**

The possible RLR-dependent IFN stimulatory potential of RNA isolated from *H. pylori* was further examined by IFN- $\beta$  promoter luciferase assay in HEK293 cells. Stimulation of RIG-I expressing cells by transfection of *H. pylori* RNA strongly increased the induction of IFN- $\beta$  promoter activation, whereas MDA5 expressing cells failed to activate the IFN- $\beta$  promoter in response to this ligand. Moreover, activation of the IFN- $\beta$  promoter by *H. pylori* RNA in HEK293 cells overexpressing RIG-I was comparable to the induction that was observed with VSV-M51R infection. Additionally, removal of the 5'-triphosphates completely abolished this IFN-inducing capacity. Taken together, these findings clearly demonstrate that RIG-I is activated by *H. pylori* RNA in a 5'-triphosphate-dependent manner.

With this regard, it was shown that prokaryotic messenger RNA, which is generated by bacterial RNA polymerase contains 5'-triphosphates like viral RNA (Bieger and Nierlich, 1989). Recently, it was shown that the 5'-triphosphate in prokaryotic mRNAs fulfills a protective function similar to that of the cap structure in eukaryotes (Celesnik *et al.*, 2007). Furthermore, mutant RIG-I that bears a point mutation in the K858 residue, which is critically involved in binding of the 5'-triphosphate structure (Cui *et al.*, 2008), did not elicit IFN- $\beta$  promoter activation in response to *H. pylori* RNA suggesting a common RNA binding mechanism of viral and bacterial RNA that subsequently activates RIG-I. In addition, inhibition of the *H. pylori* RNA-mediated induction of the IFN- $\beta$  promoter by LGP2 demonstrates that LGP2 acts as shared repressor for RIG-I activation by both viral and bacterial RNA.

Interestingly RNA from *E. coli* failed to induce IFN- $\beta$  promoter activation in RIG-I expressing cells, indicating that RNAs derived from different bacterial strains might bear distinct molecular features which are recognized by different PRRs. Another possibility might be that messenger RNAs of different bacterial strains possess distinct half-lives and are degraded more rapidly. Thus, dependent on the growth phase or life cycle of a given bacterium, the respective bacterial RNA might show differences in the

distribution of 5'-triphosphates, reflecting differences in their ability to activate RIG-I. Therefore, the inability of *E. coli* RNA to trigger a RIG-I-dependent IFN response presumably reflects the lack of a RNA pool containing the 5'-triphosphate signature. However, a recent study also demonstrated that the bacterial enzyme RppH, a prokaryotic functional homolog of a decapping enzyme, removes a diphosphate from the mRNA 5' end to generate a 5'-monophosphate mRNA in *E. coli* (Deana *et al.*, 2008). Thus, modification of the 5' end by this intrinsic enzyme suggests a possible mechanism how *E. coli* escapes the recognition by RIG-I and might reflect the massive invasiveness and pathogenicity of some bacteria (Deana *et al.*, 2008). Isolation of bacterial RNA at different time points as well as enzymatic treatment of bacterial RNA could be applied to further investigate this issue and to gain more insight how different bacterial RNAs activate a TLR-independent IFN response.

### **5.3.3 *H. pylori* virulence factors might contribute to the recognition of its RNA in the cytosol**

However, although this study provided unambiguous evidence that RIG-I is activated by *H. pylori* RNA in a 5'-triphosphate RNA-dependent manner similar to viral RNA, it is unclear how *H. pylori* RNA gains access to the cytoplasmic compartment where it can interact with RIG-I.

*H. pylori* is a Gram-negative microaerophilic bacterium that infects human gastric epithelial cell surfaces and the overlaying gastric mucin. When *H. pylori* colonizes the gastric mucosa, effector molecules are injected into gastric epithelial cells or the submucosal area through the type IV secretion system (Covacci *et al.*, 1999), which is encoded by the *cag* pathogenicity island and injects the CagA effector into the host cells (Covacci and Rappuoli, 2000). CagA has emerged as an extremely versatile effector protein that interferes with multiple host cell functions (Backert and Selbach, 2008). Several studies demonstrated that the type IV secretion system is involved in the transport of either protein or DNA-protein complexes (Cascales and Christie, 2003) from the bacterial cytoplasm directly into the cytoplasm of the infected cell. Thus, it seems likely that the type IV secretion system also mediates translocation of bacterial RNA into the cytoplasm where it could directly engage with RIG-I. In line with this, the activation of the type I IFN response during *Chlamydia pneumoniae* infection was mediated by intracellular-sensing RLRs, which seem to operate through a mechanism

dependent on the bacterial type 3 secretion system (Chiliveru *et al.*, 2010). Translocation of bacterial RNA was also related to the activation of RIG-I by *Legionella pneumophila* RNA (Monroe *et al.*, 2009). In addition, by demonstrating that *Legionella pneumophila* encodes a secreted bacterial protein, SdhA, that suppresses the RIG-I/MDA5 pathway, Monroe and colleagues clearly provided evidence that bacterial RNA in fact is an agonist of the RLR pathway and that bacteria like viruses have evolved mechanisms to evade this recognition. Delivery of bacterial products into the cytosol of the host cell is also applied by Gram-positive bacteria, such as *Listeria monocytogenes*, which use the pore-forming toxin streptolysin O for the injection of bacterial molecules into the host cell cytosol (Madden *et al.*, 2001). This suggests that by gaining access to the cytosolic compartment, bacteria might be exposed to the recognition by RLRs, which is reflected by upregulation of RIG-I upon *Listeria monocytogenes* infection (Imaizumi *et al.*, 2006). In line with this, it was shown that BMDCs are capable of ingesting *H. pylori* (Rad *et al.*, 2007) and that after 6 hrs, coinciding with the presence of intracellular bacteria, RIG-I mRNA expression levels were elevated.

Furthermore, another effector molecule, VacA, causes massive vacuolar degradation of epithelial cells, thus disrupting the gastric epithelial barrier. VacA-induced pore formation (Czajkowsky *et al.*, 1999) seems to be directly related to the formation of *H. pylori*'s intracellular niche (Terebiznik *et al.*, 2006). However, the intracellular localization of the bacterium might also contribute to its recognition by cytoplasmic PRRs and the induction of type I IFN.

In addition to VacA, *H. pylori* urease is involved in megasome formation and intracellular survival of the bacteria. It was shown that unopsonized *H. pylori* bacteria are engulfed by macrophages and neutrophils, but only 50 % of ingested organisms are killed (Allen *et al.*, 2000), since *H. pylori* phagosomes undergo clustering and homotypic fusion leading to the formation of megasomes, which in turn support bacterial survival for at least 24 hrs (Allen *et al.*, 2000). However, it was recently shown that VacA also promotes autophagosome formation (Terebiznik *et al.*, 2009). Autophagy can function as innate defense mechanism by killing intracellular microorganisms attempting to establish a replicative niche in the host cytoplasm (Levine and Deretic, 2007; Munz, 2009). These degradation products or components of pathogens might in turn be sensed by intracellular receptors to activate the innate

immune system. Thus, by inducing VacA-dependent autophagy *H. pylori* might deliver its RNA into the cytoplasm of the infected cell, where it activates RIG-I in a 5'-triphosphate-dependent manner leading to the induction of downstream signaling and the production of type I IFN.

Taken together, several bacterial factors might account for the cytosolic recognition of *H. pylori* RNA. Although this study provided the first evidence that *H. pylori* RNA activates RIG-I in a 5'-triphosphate RNA-dependent manner, further investigations are necessary to unravel the mechanisms that are involved in the TLR-independent recognition of bacterial RNA by cytosolic PRRs.

## **5.4 A novel RIG-I variant negatively regulates its own pathway**

Virus infection and transfection of 5'-triphosphate RNA were shown to be highly specific and effective in activating a RIG-I-dependent IFN response. However, unbalanced and excessive production of type I IFNs and proinflammatory cytokines could have deleterious effects on the immunity of the host, such as allergy, necrosis or the development of autoimmune diseases (Theofilopoulos *et al.*, 2005). Thus, RIG-I-mediated innate immunity is tightly regulated at different steps of the signaling pathway.

One of the most important regulatory mechanisms in biology is ubiquitination, which is extensively used to orchestrate an appropriate immune response (Bhoj and Chen, 2009). Various studies provided evidence that ubiquitination in fact plays a key role in the negative as well as positive regulation of the RIG-I pathway (Arimoto *et al.*, 2007a; Arimoto *et al.*, 2007b; Gack *et al.*, 2007; Gao *et al.*, 2009; Oshiumi *et al.*, 2008; Zeng *et al.*, 2010). In addition, alternative splicing of the RIG-I molecule itself was described to negatively regulate the pathway (Gack *et al.*, 2008). RIG-I splice variant, which is induced upon type I IFN treatment and virus infection, carries a short deletion (AA 36-80) within CARD1 that again interferes with ubiquitination and downstream signaling. Furthermore, by formation of RIG-I wildtype/splice variant-heterocomplexes, RIG-I splice variant robustly inhibits ligand-induced RIG-I multimerization and interaction with IPS-1.

#### 5.4.1 Type I IFN treatment and 5'-triphosphate RNA stimulation reveals the presence of three RIG-I variants

Immunoblotting revealed a novel variant of RIG-I, designated as RIG-I short form (approximately 95 kDa), which is induced in addition to RIG-I splice variant (101 kDa) upon type I IFN treatment. Furthermore, RIG-I short form was induced in a time- and dose-dependent manner and exhibited a different expression kinetics compared to RIG-I splice variant. Whereas weak induction of RIG-I splice variant was detectable within 9 hrs after type I IFN treatment with a further increase after 12 hrs, expression of RIG-I short form was barely detectable after 12 hrs and dramatically increased until 72 hrs after type I IFN treatment. Interestingly, the levels of RIG-I splice variant seemed to decline between 48 hrs and 72 hrs of type I IFN treatment compared to the strong induction of RIG-I short form, suggesting that RIG-I short form exerts its function or activity in a delayed manner compared to RIG-I splice variant. Interestingly, RIG-I short form was also induced in a dose-dependent manner by 5'-triphosphate RNA, while poly(I:C) stimulation failed to induce this novel RIG-I variant. This result might be explained by the higher IFN inducing capacity of 5'-triphosphate RNA as compared to poly(I:C), which was also observed in IFN- $\beta$  promoter reporter assay. Although short poly(I:C) is a RIG-I ligand (Kato *et al.*, 2008), luciferase assay revealed that it has a much lower IFN inducing capacity compared to 5'-triphosphate RNA stimulation (data not shown) or virus infection. Thus, it seems likely that an IFN-induced positive feedback loop which is activated by 5'-triphosphate RNA leads to the induction of RIG-I short form, whereas poly(I:C) lacks this stimulatory potential.

Due to the striking similarity that like RIG-I splice variant, RIG-I short form is absent in the steady state but rapidly induced when RIG-I is upregulated by type I IFN or activated by its specific ligand 5'-triphosphate RNA upon virus infection, it seems likely that RIG-I short form resembles an additional regulator of the RIG-I pathway that might control RIG-I by a different mechanism than RIG-I splice variant and at later time points.

Mass spectrometry analysis clearly revealed that type I IFN treatment in fact leads to the induction of three endogenous RIG-I variants in HEK293 cells, RIG-I full-length, RIG-I splice variant and RIG-I short form. Furthermore, alignment of the identified peptides indicated that RIG-I short form presumably comprises AA 155 to 925 (771 AA) of RIG-I full-length. Thus, RIG-I short form represents a N-terminally truncated variant of

RIG-I that completely lacks CARD1 but possesses the C-terminal 18 amino acids of CARD2 as well as the helicase and regulatory domain. However, analysis of a broad range of cell lines and/or primary cells is necessary to confirm the presence of RIG-I short form. Moreover, *in vivo* experiments will provide further information on the physiological relevance of RIG-I short form. Thus, it needs to be determined if for example injection of 5'-triphosphate RNA or virus infection leads to the induction of this RIG-I variant in mice.

According to the ENSEMBL genome browser, there are three transcripts within the human RIG-I gene (ENSEMBL entry ENSG00000107201) designated as DDX58-001 (encoding RIG-I full-length, 925 AA), DDX58-002 (encoding a variant of 722 AA in length, no physiological function described in literature), and DDX58-201 (encoding RIG-I splice variant, 880 AA). The primary transcript of the human RIG-I gene contains 18 exons. RIG-I splice variant completely lacks exon 2 (Gack *et al.*, 2008), whereas the identified sequence of RIG-I short form reflects a complete lack of exon 1 to exon 5 as well as parts of exon 6. Furthermore, although DDX58-002 represents a truncated form of RIG-I, it does not match with the novel RIG-I short form, which was identified in this study. Since RIG-I splice variant is generated by alternative splicing when RIG-I is activated, it needs to be elucidated which process is involved in the modification of the primary transcript that finally leads to RIG-I short form.

During alternative splicing, which occurs in humans in over 80 % of the genes, the exons of primary transcripts are reconnected in multiple ways, resulting in different mRNAs that are translated into different protein isoforms (Matlin *et al.*, 2005). Thus, it seems rather unlikely that RIG-I short form is generated by alternative splicing, since in contrast to RIG-I splice variant, where exon 1 is reconnected to exon 3, RIG-I short form completely lacks the first five exons and parts of exon 6, thereby excluding the formation of a new mRNA sequence by fusion of the neighbouring exons after splicing. However, further analysis is needed to accurately map the location of the translational start site of RIG-I short form. According to mass spectrometry analysis, translation would be initiated at L155, indicating an alternative translational start from a non-AUG codon, rather than generation of a different mRNA by alternative splicing. It is known that a number of mammalian mRNAs initiate translation from alternative codons, like leucine or valine, resulting in different isoforms of the respective protein, which then show a different subcellular localization and/or exhibit distinct biological functions

(Touriol *et al.*, 2003). For instance, the alternatively spliced variants of NOD2 and MyD88 display a different molecular function compared to their full-length counterparts, acting as dominant-negative inhibitors of the NOD2 pathway and TLR-mediated signaling, respectively (Janssens *et al.*, 2002; Rosenstiel *et al.*, 2006). However, the presence of two methionine residues further upstream of L155 at position 148 and 149 implicates that the use of a classical AUG start might be possible, as well. But, at the moment the mechanism that leads to a different mRNA and/or different protein isoform is elusive.

Thus, investigation of the N-terminus of RIG-I short form, for example by 5'-RACE PCR or N-terminal sequencing, will provide further information on the sequence that encodes RIG-I short form. Moreover, determination of the N-terminus of RIG-I short form could ultimately reveal, which molecular mechanism in fact plays a role in the generation of the novel RIG-I short form. So far, it seems likely that one of the mechanisms discussed above rather than proteolytic cleavage of full-length RIG-I leads to this short variant of RIG-I, since analysis of the amino acid sequence of RIG-I did not predict potential protease cleavage sites, which could account for the lack of CARD1 and parts of CARD2 observed in RIG-I short form.

#### **5.4.2 RIG-I short form acts as inhibitor of the RIG-I-mediated IFN response**

With regard to its structure, containing only a small part of CARD2 but a functional helicase and regulatory domain, RIG-I short form resembles the artificial construct RIG-I C (Yoneyama *et al.*, 2004), which inhibits RIG-I-mediated IFN signaling, suggesting that like RIG-I splice variant RIG-I short form might act as an endogenous inhibitor of the RIG-I pathway. IFN- $\beta$  promoter reporter assay revealed that RIG-I short form itself is not able to respond to 5'-triphosphate RNA as well as virus infection, reflecting the lack of CARD1 and the inability to interact with IPS-1. However, cotransfection of RIG-I full-length and increasing amounts of RIG-I short form suppressed the RIG-I-induced activation of the IFN- $\beta$  promoter upon stimulation with 5'-triphosphate RNA and VSV-M51R in a dose-dependent manner. Similarly, RIG-I splice variant acts as dominant inhibitor of RIG-I signaling (Gack *et al.*, 2008). RIG-I short form is absent in the steady state and was strongly upregulated by type I IFN and 5'-triphosphate RNA with a different kinetics to RIG-I splice variant, suggesting that

these two isoforms of RIG-I negatively regulate RIG-I activation at different time points.

### **5.4.3 Proposed mechanism of RIG-I regulation by RIG-I short form**

As already mentioned, due to its nature as IFN-induced gene, expression of RIG-I is markedly induced by type I IFN treatment. RIG-I short form is absent in the steady state but strongly upregulated by type I IFN and 5'-triphosphate RNA with a different kinetics compared to RIG-I splice variant, indicating that both exert their negative regulatory function on RIG-I-mediated antiviral signaling in a mechanistically and/or temporally different fashion. Moreover, since poly(I:C) stimulation only led to low level activation of the IFN- $\beta$  promoter in the reporter assay and failed to induce detectable levels of RIG-I short form in the western blot, it was suggested that RIG-I short form presumably controls the levels of endogenous RIG-I to prevent excessive IFN production. One possible explanation is that by blocking the IFN response, RIG-I short form could interfere with the unbalanced upregulation of RIG-I by the IFN feedback loop. With regard to the structure of RIG-I short form, consisting of an intact helicase domain and regulatory domain, the regulatory function of RIG-I short form might be achieved by two different modes of action.

The first scenario involves competitive binding of 5'-triphosphate RNA by the regulatory domain of RIG-I short form to prevent ligand-induced activation of RIG-I full-length. ATPase assay and RNA binding assay will provide evidence whether RIG-I short form in fact binds 5'-triphosphate RNA, if there is competition for the RNA ligand or if RIG-I short form exhibits higher binding affinities for 5'-triphosphate RNA. Another possibility implicates the binding of RIG-I short form to RIG-I full-length to form a multimeric RIG-I full-length/short form-complex, as described for RIG-I splice variant. Interaction studies using recombinant RIG-I full-length and RIG-I short form as well as immunoprecipitation studies with overexpressed proteins will be used to demonstrate this possible interaction. There are several mechanisms by which a RIG-I full-length/short form-heterocomplex is likely to regulate the RIG-I pathway. On the one hand, this multimeric complex could inhibit the interaction with IPS-1, thereby blocking the initiation of downstream signaling and subsequent IFN induction. On the

---

other hand, by interacting with RIG-I full-length, RIG-I short form might promote proteasome-dependent degradation of this complex.

Activation of RIG-I is mediated by delivery of Lys63-linked ubiquitination to the N-terminal CARDS of RIG-I (Gack *et al.*, 2007; Gao *et al.*, 2009; Oshiumi *et al.*, 2008; Zeng *et al.*, 2010). However, several molecules have been identified that promote degradation of RIG-I by interfering with its ubiquitination state (Arimoto *et al.*, 2007a; Arimoto *et al.*, 2007b; Kim *et al.*, 2008; Zhao *et al.*, 2005). Due to the lack of CARD1 that abolishes TRIM25 binding and subsequent Lys63-linked ubiquitination of RIG-I splice variant, it seems likely that RIG-I short form also lacks this activating modification. In addition, the RIG-I full-length/short form-heterocomplex might acquire Lys48-polyubiquitin chains that target this putative complex for degradation by the proteasome. In line with this hypothesis, ubiquitin-specific immunoprecipitation revealed that type I IFN treatment actually leads to ubiquitination of RIG-I short form. Since RIG-I splice variant completely lacks ubiquitination this result raises the possibility that RIG-I short form could bear a Lys48-linked ubiquitin modification. Thus, immunoprecipitation using specific antibodies for the respective ubiquitination types (Lys63- and Lys48-linked ubiquitination) will elucidate the ubiquitination patterns of RIG-I short form as well as RIG-I full-length upon induction of RIG-I short form and together with the binding studies will define the regulatory function of RIG-I short form in more detail.

## 6 SUMMARY

Cell-type specific activation of distinct sets of pattern recognition receptors provides maximum protection of the host from invading pathogens, such as viruses and bacteria. Whereas in plasmacytoid dendritic cells (DCs), recognition of viral RNAs is mediated by endosomal TLR7, the retinoic acid-inducible gene (RIG-I) like receptor (RLR) family is the key player for viral RNA recognition in the cytoplasm of infected conventional DCs, hepatocytes as well as fibroblasts. The RLR family comprises three members, RIG-I, melanoma differentiation-associated gene 5 (MDA5) and laboratory of genetics and physiology 2 (LGP2), each exerting a distinct function. RIG-I and MDA5 are activated upon viral infection and initiate downstream signaling by CARD-CARD (caspase recruitment domain) interactions with interferon- $\beta$  promoter stimulator protein 1 (IPS-1), leading to the induction of type I interferon (IFN) and proinflammatory cytokines. In contrast, LGP2 has a dual regulatory role by inhibiting RIG-I signaling on the one hand, but synergistically enhancing MDA5-dependent innate immune signaling on the other hand. RIG-I was shown to specifically recognize various viruses, such as vesicular stomatitis virus (VSV), Sendai Virus (SeV), Newcastle disease virus (NDV), influenza A virus, Japanese encephalitis virus and hepatitis C virus (HCV), whereas MDA5 is essential for IFN induction upon picornavirus infection. Activation of RIG-I requires a triphosphate structure at the 5'-end of the viral RNA, whereas a defined molecular feature that triggers MDA5 has not been identified to date. However at the outset of this study, it was unknown, which structures and molecular mechanisms facilitate the specific recognition of the 5'-triphosphate signature by RIG-I. Moreover, due to the lack of a natural agonist, so far, investigation of MDA5 in the context of viral infection was limited to *in vivo* studies. Furthermore, it was of particular interest if the RLR family is involved in recognition of other pathogens, such as bacteria, rather than exclusively sensing viral infection. The presence of the cytoplasmic DNA receptor DAI (DNA-dependent activator of interferon regulatory factors), that is involved in the TLR9/MyD88 (myeloid differentiation response protein 88)-independent recognition of intracellular dsDNA and the finding that intracellular bacteria that have a cytoplasmic phase in their life cycle, such as *Listeria monocytogenes*, still evoke DNA-dependent type I IFN responses, further supported the hypothesis that recognition of bacterial RNA by the RLRs might also contribute to bacterial recognition.

In the first part of this study, the structural and molecular mechanisms of 5'-triphosphate recognition by RIG-I were elucidated. Analysis of the amino acid sequence as well as the predicted protein structure of RIG-I revealed the presence of a putative, so far uncharacterized domain at the C-terminus of RIG-I. Overexpression of this putative domain, which comprises amino acids 802 to 925 of human RIG-I, suppressed the RIG-I-mediated IFN- $\beta$  promoter activation upon stimulation with 5'-triphosphate RNA and VSV-M51R infection in a dose-dependent manner. Thus, due to identification of this functional domain the structure of the RIG-I molecule needs to be revised, now comprising N-terminal CARDs, a central helicase domain and the C-terminal domain (CTD). Furthermore, structural analysis of the C-terminal domain unveiled the presence of two key structural features, a zinc-binding site, which is coordinated by four invariant cysteine residues, which are present in the entire RLR family, as well as a 5'-triphosphate binding site that is located in a positively charged groove of high sequence conservation. Subsequently, site directed mutagenesis of the respective residues and analysis of the generated mutants by IFN- $\beta$  promoter reporter assay, coimmunoprecipitation studies or *in vitro* RNA binding assay revealed that the disruption of the zinc-binding site is accompanied by the inability of RIG-I to respond to stimulation with either 5'-triphosphate RNA or virus infection and to bind its RNA ligand. In addition, RIG-I-triggered IFN induction in response to 5'-triphosphate RNA and virus infection was abolished when specific amino acids in the positively charged patch were mutated. Thus, this study provides evidence that the C-terminal domain has a dual function. First, in the steady state it regulates RIG-I activation by autoinhibition of the CARDs to prevent interaction with IPS-1 and induction of constitutive downstream signaling in the absence of RNA ligand. Secondly, the positively charged binding groove within the C-terminal domain directly binds 5'-triphosphate RNA with high affinity, leading to a conformational change and dimerization of RIG-I that is essential for full activation of RIG-I and subsequent induction of downstream signaling. Taken together, this newly identified C-terminal domain acts as a regulatory domain.

Since the role of MDA5 in recognition of picornaviruses was limited to *in vivo* studies and studies in primary cells, *in vitro* IFN- $\beta$  promoter reporter assays were established in HEK293 cells overexpressing MDA5. Stimulation of these cells with the synthetic dsRNA analogue poly(I:C) led to a strong activation of the IFN- $\beta$  promoter. Furthermore, it was observed that site-directed mutagenesis of residues homologous to those in the CTD of RIG-I, abolished this MDA5-dependent response to poly(I:C),

suggesting that the integrity of the C-terminal domain is also crucial for MDA5 signaling. However, infection of MDA5 expressing HEK293 cells with either encephalomyocarditis virus (EMCV), the prototypic picornavirus, or stimulation with RNA isolated from EMCV-infected cells failed to induce activation of the IFN- $\beta$  promoter. Cotransfection of LGP2 together with MDA5, which was shown to be indispensable for eliciting an MDA5-dependent virus response *in vivo*, also did not rescue the IFN induction by EMCV. Thus, it was not successful to reconstitute the MDA5 signaling cascade in transfectable cell lines *in vitro*, suggesting that other factors in addition to MDA5 and LGP2 might participate in the recognition of picornaviruses by MDA5 *in vivo*.

Moreover, this study provided the first evidence that apart from being activated by viral RNA, RIG-I also mediates IFN induction in response to *Helicobacter pylori* bacterial RNA. Upon transfection of RNA isolated from *H. pylori*, a strong activation of the IFN- $\beta$  promoter comparable to the induction triggered by VSV-M51R infection, was observed in cells overexpressing RIG-I, but not MDA5. Moreover, transfection of dephosphorylated *H. pylori* RNA completely abrogated this response, suggesting that bacterial RNA bears a 5'-triphosphate signature that activates RIG-I. Analysis of the IFN response of mutant RIG-I bearing a point mutation in the newly identified 5'-triphosphate binding site, provided further evidence that *H. pylori* RNA activates RIG-I by the same molecular mechanism like viral 5'-triphosphate containing RNA. Interestingly, RNA isolated from *E. coli* failed to induce IFN- $\beta$  promoter activation in RIG-I expressing cells, suggesting that RNAs derived from different bacterial strains might bear distinct molecular features, which are recognized by different sets of PRRs.

Finally, stimulation of HEK293 cells with type I IFN and 5'-triphosphate RNA indicated the existence of a yet unknown IFN-inducible short form of RIG-I. Mass spectrometry analysis revealed that this RIG-I short form probably comprises AA 155 to 925 of human full-length RIG-I. This RIG-I variant is induced by the IFN feedback loop and it was assumed that it functions as negative regulator of its own pathway to prevent uncontrolled IFN induction. IFN- $\beta$  promoter reporter assay provided evidence that overexpression of this short form of RIG-I in fact inhibits RIG-I-mediated IFN- $\beta$  promoter activation in response to 5'-triphosphate RNA as well as virus infection. Taken together, these results indicate that in addition to RIG-I splice variant, RIG-I short form is involved in balancing RIG-I-dependent IFN responses by negatively

regulating its own pathway. Further investigations are necessary to fully characterize this protein and to completely understand the molecular mechanisms that underlie this mode of regulation.

## 7 REFERENCES

- Ablasser, A., Bauernfeind, F., Hartmann, G., Latz, E., Fitzgerald, K.A., and Hornung, V. (2009). RIG-I-dependent sensing of poly(dA:dT) through the induction of an RNA polymerase III-transcribed RNA intermediate. *Nat. Immunol.* *10*, 1049-1051.
- Ahel, I., Ahel, D., Matsusaka, T., Clark, A.J., Pines, J., Boulton, S.J., and West, S.C. (2008). Poly(ADP-ribose)-binding zinc finger motifs in DNA repair/checkpoint proteins. *Nature* *451*, 81-85.
- Akira, S., and Takeda, K. (2004). Toll-like receptor signalling. *Nat. Rev. Immunol.* *4*, 499-511.
- Akira, S., Uematsu, S., and Takeuchi, O. (2006). Pathogen recognition and innate immunity. *Cell* *124*, 783-801.
- Akwa, Y., Hassett, D.E., Eloranta, M.L., Sandberg, K., Masliah, E., Powell, H., Whitton, J.L., Bloom, F.E., and Campbell, I.L. (1998). Transgenic expression of IFN-alpha in the central nervous system of mice protects against lethal neurotropic viral infection but induces inflammation and neurodegeneration. *J. Immunol.* *161*, 5016-5026.
- Alarcon-Riquelme, M.E. (2006). Nucleic acid by-products and chronic inflammation. *Nat. Genet.* *38*, 866-867.
- Alff, P.J., Sen, N., Gorbunova, E., Gavrilovskaya, I.N., and Mackow, E.R. (2008). The NY-1 Hantavirus Gn Cytoplasmic tail Co-precipitates TRAF3 and Inhibits Cellular Interferon Responses by Disrupting TBK1-TRAF3 Complex Formation. *J. Virol.* *18*, 9115-9122.
- Allen, L.A., Schlesinger, L.S., and Kang, B. (2000). Virulent strains of *Helicobacter pylori* demonstrate delayed phagocytosis and stimulate homotypic phagosome fusion in macrophages. *J. Exp. Med.* *191*, 115-128.
- Alwin, S., Gere, M.B., Guhl, E., Effertz, K., Barbas, C.F., 3rd, Segal, D.J., Weitzman, M.D., and Cathomen, T. (2005). Custom zinc-finger nucleases for use in human cells. *Mol. Ther.* *12*, 610-617.
- Andrejeva, J., Childs, K.S., Young, D.F., Carlos, T.S., Stock, N., Goodbourn, S., and Randall, R.E. (2004). The V proteins of paramyxoviruses bind the IFN-inducible RNA helicase, mda-5, and inhibit its activation of the IFN-beta promoter. *Proc.Natl.Acad.Sci.U.S.A* *101*, 17264-17269.
- Arimoto, K., Konishi, H., and Shimotohno, K. (2007a). Ubch8 regulates ubiquitin and ISG15 conjugation to RIG-I. *Mol. Immunol.* *45*, 1078-1084.
- Arimoto, K., Takahashi, H., Hishiki, T., Konishi, H., Fujita, T., and Shimotohno, K. (2007b). Negative regulation of the RIG-I signaling by the ubiquitin ligase RNF125. *Proc.Natl.Acad.Sci.U.S.A.* *104*, 7500-7505.
- Arinze, I.J., and Kawai, Y. (2005). Transcriptional activation of the human Galphai2 gene promoter through nuclear factor-kappaB and antioxidant response elements. *J. Biol. Chem.* *280*, 9786-9795.
- Backert, S., and Selbach, M. (2008). Role of type IV secretion in *Helicobacter pylori* pathogenesis. *Cell. Microbiol.* *10*, 1573-1581.
- Barral, P.M., Morrison, J.M., Drahos, J., Gupta, P., Sarkar, D., Fisher, P.B., and Racaniello, V.R. (2007). MDA-5 Is Cleaved in Poliovirus-Infected Cells. *J. Virol.* *81*, 3677-3684.
- Barral, P.M., Sarkar, D., Fisher, P.B., and Racaniello, V.R. (2009). RIG-I is cleaved during picornavirus infection. *Virology* *391*, 171-176.
- Bartenschlager, R., and Lohmann, V. (2001). Novel cell culture systems for the hepatitis C virus. *Antiviral Res.* *52*, 1-17.
- Bartenschlager, R., and Pietschmann, T. (2005). Efficient hepatitis C virus cell culture system: what a difference the host cell makes. *Proc.Natl.Acad.Sci.U.S.A* *102*, 9739-9740.
- Baum, A., Sachidanandam, R., and Garcia-Sastre, A. (2010). Preference of RIG-I for short viral RNA molecules in infected cells revealed by next-generation sequencing. *Proc.Natl.Acad.Sci.U.S.A* *107*, 16303-16308.
- Bhoj, V.G., and Chen, Z.J. (2009). Ubiquitylation in innate and adaptive immunity. *Nature* *458*, 430-437.

- Bick, M.J., Carroll, J.W., Gao, G., Goff, S.P., Rice, C.M., and MacDonald, M.R. (2003). Expression of the zinc-finger antiviral protein inhibits alphavirus replication. *J. Virol.* *77*, 11555-11562.
- Bieger, C.D., and Nierlich, D.P. (1989). Distribution of 5'-triphosphate termini on the mRNA of *Escherichia coli*. *J. Bacteriol.* *171*, 141-147.
- Bouchard, L., Vohl, M.C., Deshaies, Y., Rheaume, C., Daris, M., and Tchernof, A. (2007). Visceral adipose tissue zinc finger protein 36 mRNA levels are correlated with insulin, insulin resistance index, and adiponectinemia in women. *Eur. J. Endocrinol.* *157*, 451-457.
- Bowie, A.G., and Unterholzner, L. (2008). Viral evasion and subversion of pattern-recognition receptor signalling. *Nat. Rev. Immunol.* *12*, 911-922.
- Bushati, N., and Cohen, S.M. (2007). microRNA functions. *Annu. Rev. Cell Dev. Biol.* *23*, 175-205.
- Cascales, E., and Christie, P.J. (2003). The versatile bacterial type IV secretion systems. *Nat. Rev. Microbiol.* *1*, 137-149.
- Cayrol, C., Lacroix, C., Mathe, C., Ecochard, V., Ceribelli, M., Loreau, E., Lazar, V., Dessen, P., Mantovani, R., Aguilar, L., and Girard, J.P. (2007). The THAP-zinc finger protein THAP1 regulates endothelial cell proliferation through modulation of pRB/E2F cell-cycle target genes. *Blood* *109*, 584-594.
- Celesnik, H., Deana, A., and Belasco, J.G. (2007). Initiation of RNA decay in *Escherichia coli* by 5' pyrophosphate removal. *Mol. Cell* *27*, 79-90.
- Chang, G.T., Steenbeek, M., Schippers, E., Blok, L.J., van Weerden, W.M., van Alewijk, D.C., Eussen, B.H., van Steenbrugge, G.J., and Brinkmann, A.O. (2000). Characterization of a zinc-finger protein and its association with apoptosis in prostate cancer cells. *J. Natl. Cancer Inst.* *92*, 1414-1421.
- Chang, H.W., Watson, J.C., and Jacobs, B.L. (1992). The E3L gene of vaccinia virus encodes an inhibitor of the interferon-induced, double-stranded RNA-dependent protein kinase. *Proc. Natl. Acad. Sci. U.S.A.* *89*, 4825-4829.
- Chiliveru, S., Birkelund, S., and Paludan, S.R. (2010). Induction of interferon-stimulated genes by *Chlamydia pneumoniae* in fibroblasts is mediated by intracellular nucleotide-sensing receptors. *PLoS ONE* *5*, e10005.
- Chiu, Y.H., Macmillan, J.B., and Chen, Z.J. (2009). RNA polymerase III detects cytosolic DNA and induces type I interferons through the RIG-I pathway. *Cell* *138*, 576-591.
- Covacci, A., and Rappuoli, R. (2000). Tyrosine-phosphorylated bacterial proteins: Trojan horses for the host cell. *J. Exp. Med.* *191*, 587-592.
- Covacci, A., Telford, J.L., Del Giudice, G., Parsonnet, J., and Rappuoli, R. (1999). *Helicobacter pylori* virulence and genetic geography. *Science* *284*, 1328-1333.
- Crow, Y.J., Leitch, A., Hayward, B.E., Garner, A., Parmar, R., Griffith, E., Ali, M., Semple, C., Aicardi, J., Babul-Hirji, R., *et al.* (2006). Mutations in genes encoding ribonuclease H2 subunits cause Aicardi-Goutieres syndrome and mimic congenital viral brain infection. *Nat. Genet.* *38*, 910-916.
- Crow, Y.J., and Rehwinkel, J. (2009). Aicardi-Goutieres syndrome and related phenotypes: linking nucleic acid metabolism with autoimmunity. *Hum. Mol. Genet.* *18*, R130-136.
- Cui, S., Eisenacher, K., Kirchofer, A., Brzozka, K., Lammens, A., Lammens, K., Fujita, T., Conzelmann, K.K., Krug, A., and Hopfner, K.P. (2008). The C-terminal regulatory domain is the RNA 5'-triphosphate sensor of RIG-I. *Mol. Cell* *29*, 169-179.
- Czajkowsky, D.M., Iwamoto, H., Cover, T.L., and Shao, Z. (1999). The vacuolating toxin from *Helicobacter pylori* forms hexameric pores in lipid bilayers at low pH. *Proc. Natl. Acad. Sci. U.S.A.* *96*, 2001-2006.
- Deana, A., Celesnik, H., and Belasco, J.G. (2008). The bacterial enzyme RppH triggers messenger RNA degradation by 5' pyrophosphate removal. *Nature* *451*, 355-358.
- Diao, F., Li, S., Tian, Y., Zhang, M., Xu, L.G., Zhang, Y., Wang, R.P., Chen, D., Zhai, Z., Zhong, B., *et al.* (2007). Negative regulation of MDA5- but not RIG-I-mediated innate antiviral signaling by the dihydroxyacetone kinase. *Proc. Natl. Acad. Sci. U.S.A.* *104*, 11706-11711.
- Dixit, E., Boulant, S., Zhang, Y., Lee, A.S., Odendall, C., Shum, B., Hacohen, N., Chen, Z.J., Whelan, S.P., Fransen, M., *et al.* (2010). Peroxisomes are signaling platforms for antiviral innate immunity. *Cell* *141*, 668-681.
- Dong, J., Park, J.S., and Lee, S.H. (1999). In vitro analysis of the zinc-finger motif in human replication protein A. *Biochem. J.* *337* (Pt 2), 311-317.

- Doyle, S., Vaidya, S., O'Connell, R., Dadgostar, H., Dempsey, P., Wu, T., Rao, G., Sun, R., Haberland, M., Modlin, R., and Cheng, G. (2002). IRF3 mediates a TLR3/TLR4-specific antiviral gene program. *Immunity* *17*, 251-263.
- Drahos, J., and Racaniello, V.R. (2009). Cleavage of IPS-1 in cells infected with human rhinovirus. *J. Virol.* *83*, 11581-11587.
- Duchmann, R., Kaiser, I., Hermann, E., Mayet, W., Ewe, K., and Meyer zum Buschenfelde, K.H. (1995). Tolerance exists towards resident intestinal flora but is broken in active inflammatory bowel disease (IBD). *Clin. Exp. Immunol.* *102*, 448-455.
- Ebert, O., Harbaran, S., Shinozaki, K., and Woo, S.L. (2005). Systemic therapy of experimental breast cancer metastases by mutant vesicular stomatitis virus in immune-competent mice. *Cancer Gene Ther.* *12*, 350-358.
- Ebert, O., Shinozaki, K., Huang, T.G., Savontaus, M.J., Garcia-Sastre, A., and Woo, S.L. (2003). Oncolytic vesicular stomatitis virus for treatment of orthotopic hepatocellular carcinoma in immune-competent rats. *Cancer Res.* *63*, 3605-3611.
- Flanegan, J.B., Petterson, R.F., Ambros, V., Hewlett, N.J., and Baltimore, D. (1977). Covalent linkage of a protein to a defined nucleotide sequence at the 5'-terminus of virion and replicative intermediate RNAs of poliovirus. *Proc.Natl.Acad.Sci.U.S.A* *74*, 961-965.
- Foy, E., Li, K., Sumpter, R., Jr., Loo, Y.M., Johnson, C.L., Wang, C., Fish, P.M., Yoneyama, M., Fujita, T., Lemon, S.M., and Gale, M., Jr. (2005). Control of antiviral defenses through hepatitis C virus disruption of retinoic acid-inducible gene-I signaling. *Proc.Natl.Acad.Sci.U.S.A* *102*, 2986-2991.
- Fredericksen, B.L., Keller, B.C., Fornek, J., Katze, M.G., and Gale, M., Jr. (2008). Establishment and maintenance of the innate antiviral response to West Nile Virus involves both RIG-I and MDA5 signaling through IPS-1. *J. Virol.* *82*, 609-616.
- Friedman, C.S., O'Donnell, M.A., Legarda-Addison, D., Ng, A., Cardenas, W.B., Yount, J.S., Moran, T.M., Basler, C.F., Komuro, A., Horvath, C.M., *et al.* (2008). The tumour suppressor CYLD is a negative regulator of RIG-I-mediated antiviral response. *EMBO Rep.* *9*, 930-936.
- Fu, H.W., Moomaw, J.F., Moomaw, C.R., and Casey, P.J. (1996). Identification of a cysteine residue essential for activity of protein farnesyltransferase. Cys299 is exposed only upon removal of zinc from the enzyme. *J. Biol. Chem.* *271*, 28541-28548.
- Fujita, T. (2009). A nonself RNA pattern: tri-p to panhandle. *Immunity* *31*, 4-5.
- Furuichi, Y., and Shatkin, A.J. (2000). Viral and cellular mRNA capping: past and prospects. *Adv. Virus Res.* *55*, 135-184.
- Gack, M.U., Kirchhofer, A., Shin, Y.C., Inn, K.S., Liang, C., Cui, S., Myong, S., Ha, T., Hopfner, K.P., and Jung, J.U. (2008). Roles of RIG-I N-terminal tandem CARD and splice variant in TRIM25-mediated antiviral signal transduction. *Proc.Natl.Acad.Sci.U.S.A* *105*, 16743-16748.
- Gack, M.U., Shin, Y.C., Joo, C.H., Urano, T., Liang, C., Sun, L., Takeuchi, O., Akira, S., Chen, Z., Inoue, S., and Jung, J.U. (2007). TRIM25 RING-finger E3 ubiquitin ligase is essential for RIG-I-mediated antiviral activity. *Nature* *446*, 916-920.
- Gao, D., Yang, Y.K., Wang, R.P., Zhou, X., Diao, F.C., Li, M.D., Zhai, Z.H., Jiang, Z.F., and Chen, D.Y. (2009). REUL is a novel E3 ubiquitin ligase and stimulator of retinoic-acid-inducible gene-I. *PLoS ONE.* *4*, e5760.
- Gitlin, L., Barchet, W., Gilfillan, S., Cella, M., Beutler, B., Flavell, R.A., Diamond, M.S., and Colonna, M. (2006). Essential role of mda-5 in type I IFN responses to polyriboinosinic:polyribocytidylic acid and encephalomyocarditis picornavirus. *Proc.Natl.Acad.Sci.U.S.A* *103*, 8459-8464.
- Goutieres, F. (2005). Aicardi-Goutieres syndrome. *Brain Dev.* *27*, 201-206.
- Gutierrez, M.G., Master, S.S., Singh, S.B., Taylor, G.A., Colombo, M.I., and Deretic, V. (2004). Autophagy is a defense mechanism inhibiting BCG and Mycobacterium tuberculosis survival in infected macrophages. *Cell* *119*, 753-766.
- Heyninck, K., and Beyaert, R. (1999). The cytokine-inducible zinc finger protein A20 inhibits IL-1-induced NF-kappaB activation at the level of TRAF6. *FEBS Lett.* *442*, 147-150.

- Heyninck, K., De Valck, D., Vanden Berghe, W., Van Crielinge, W., Contreras, R., Fiers, W., Haegeman, G., and Beyaert, R. (1999). The zinc finger protein A20 inhibits TNF-induced NF-kappaB-dependent gene expression by interfering with an RIP- or TRAF2-mediated transactivation signal and directly binds to a novel NF-kappaB-inhibiting protein ABIN. *J. Cell Biol.* *145*, 1471-1482.
- Hochrein, H., Schlatter, B., O'Keeffe, M., Wagner, C., Schmitz, F., Schiemann, M., Bauer, S., Suter, M., and Wagner, H. (2004). Herpes simplex virus type-1 induces IFN-alpha production via Toll-like receptor 9-dependent and -independent pathways. *Proc.Natl.Acad.Sci.U.S.A* *101*, 11416-11421.
- Hoebe, K., Du, X., Georgel, P., Janssen, E., Tabet, K., Kim, S.O., Goode, J., Lin, P., Mann, N., Mudd, S., *et al.* (2003). Identification of Lps2 as a key transducer of MyD88-independent TIR signalling. *Nature* *424*, 743-748.
- Holm, L., and Sander, C. (1993). Protein structure comparison by alignment of distance matrices. *J. Mol. Biol.* *233*, 123-138.
- Hopfner, K.P., and Tainer, J.A. (2003). Rad50/SMC proteins and ABC transporters: unifying concepts from high-resolution structures. *Curr. Opin. Struct. Biol.* *13*, 249-255.
- Hornung, V., Ellegast, J., Kim, S., Brzozka, K., Jung, A., Kato, H., Poeck, H., Akira, S., Conzelmann, K.K., Schlee, M., *et al.* (2006). 5'-Triphosphate RNA is the ligand for RIG-I. *Science* *314*, 994-997.
- Hyoty, H., and Taylor, K.W. (2002). The role of viruses in human diabetes. *Diabetologia* *45*, 1353-1361.
- Imaizumi, T., Sashinami, H., Mori, F., Matsumiya, T., Yoshida, H., Nakane, A., Wakabayashi, K., Oyama, C., and Satoh, K. (2006). *Listeria monocytogenes* induces the expression of retinoic acid-inducible gene-I. *Microbiol. Immunol.* *50*, 811-815.
- Imaizumi, T., Tanaka, H., Tajima, A., Tsuruga, K., Oki, E., Sashinami, H., Matsumiya, T., Yoshida, H., Inoue, I., and Ito, E. (2010). Retinoic acid-inducible gene-I (RIG-I) is induced by IFN-gamma in human mesangial cells in culture: possible involvement of RIG-I in the inflammation in lupus nephritis. *Lupus* *19*, 830-836.
- Inaba, K., Inaba, M., Romani, N., Aya, H., Deguchi, M., Ikehara, S., Muramatsu, S., and Steinman, R.M. (1992). Generation of large numbers of dendritic cells from mouse bone marrow cultures supplemented with granulocyte/macrophage colony-stimulating factor. *J. Exp. Med.* *176*, 1693-1702.
- Inoue, A., Seidel, M.G., Wu, W., Kamizono, S., Ferrando, A.A., Bronson, R.T., Iwasaki, H., Akashi, K., Morimoto, A., Hitzler, J.K., *et al.* (2002). Slug, a highly conserved zinc finger transcriptional repressor, protects hematopoietic progenitor cells from radiation-induced apoptosis in vivo. *Cancer Cell* *2*, 279-288.
- Ishikawa, H., and Barber, G.N. (2008). STING is an endoplasmic reticulum adaptor that facilitates innate immune signalling. *Nature* *455*, 674-678.
- Ishikawa, H., Ma, Z., and Barber, G.N. (2009). STING regulates intracellular DNA-mediated, type I interferon-dependent innate immunity. *Nature* *461*, 788-792.
- IUBMB (1992). *Biochemical Nomenclature and Related Documents - A compendium, 2<sup>nd</sup> Vol* (London and Chapel Hill: Portland Press).
- Janssens, S., Burns, K., Tschopp, J., and Beyaert, R. (2002). Regulation of interleukin-1 and lipopolysaccharide-induced NF-kappaB activation by alternative splicing of MyD88. *Curr. Biol.* *12*, 467-471.
- Jin, L., Waterman, P.M., Jonscher, K.R., Short, C.M., Reisdorph, N.A., and Cambier, J.C. (2008). MPYS, a novel membrane tetraspanner, is associated with major histocompatibility complex class II and mediates transduction of apoptotic signals. *Mol. Cell Biol.* *28*, 5014-5026.
- Jounai, N., Takeshita, F., Kobiyama, K., Sawano, A., Miyawaki, A., Xin, K.Q., Ishii, K.J., Kawai, T., Akira, S., Suzuki, K., and Okuda, K. (2007). The Atg5 Atg12 conjugate associates with innate antiviral immune responses. *Proc.Natl.Acad.Sci.U.S.A* *104*, 14050-14055.
- Karin, M., and Ben-Neriah, Y. (2000). Phosphorylation meets ubiquitination: the control of NF-kappaB activity. *Annu. Rev. Immunol.* *18*, 621-663.
- Kato, H., Sato, S., Yoneyama, M., Yamamoto, M., Uematsu, S., Matsui, K., Tsujimura, T., Takeda, K., Fujita, T., Takeuchi, O., and Akira, S. (2005). Cell type-specific involvement of RIG-I in antiviral response. *Immunity* *23*, 19-28.

- Kato, H., Takeuchi, O., Mikamo-Satoh, E., Hirai, R., Kawai, T., Matsushita, K., Hiiragi, A., Dermody, T.S., Fujita, T., and Akira, S. (2008). Length-dependent recognition of double-stranded ribonucleic acids by retinoic acid-inducible gene-I and melanoma differentiation-associated gene 5. *J. Exp. Med.* *205*, 1601-1610.
- Kato, H., Takeuchi, O., Sato, S., Yoneyama, M., Yamamoto, M., Matsui, K., Uematsu, S., Jung, A., Kawai, T., Ishii, K.J., *et al.* (2006). Differential roles of MDA5 and RIG-I helicases in the recognition of RNA viruses. *Nature* *441*, 101-105.
- Kawai, T., Takahashi, K., Sato, S., Coban, C., Kumar, H., Kato, H., Ishii, K.J., Takeuchi, O., and Akira, S. (2005). IPS-1, an adaptor triggering RIG-I- and Mda5-mediated type I interferon induction. *Nat. Immunol.* *6*, 981-988.
- Kayagaki, N., Phung, Q., Chan, S., Chaudhari, R., Quan, C., O'Rourke, K.M., Eby, M., Pietras, E., Cheng, G., Bazan, J.F., *et al.* (2007). DUBA: a deubiquitinase that regulates type I interferon production. *Science* *318*, 1628-1632.
- Kim, M.J., Hwang, S.Y., Imaizumi, T., and Yoo, J.Y. (2008). Negative feedback regulation of RIG-I-mediated antiviral signaling by interferon-induced ISG15 conjugation. *J. Virol.* *82*, 1474-1483.
- Komuro, A., and Horvath, C.M. (2006). RNA- and virus-independent inhibition of antiviral signaling by RNA helicase LGP2. *J. Virol.* *80*, 12332-12342.
- Kovacsovics, M., Martinon, F., Micheau, O., Bodmer, J.L., Hofmann, K., and Tschopp, J. (2002). Overexpression of Helicard, a CARD-containing helicase cleaved during apoptosis, accelerates DNA degradation. *Curr. Biol.* *12*, 838-843.
- Krishna, S.S., Majumdar, I., and Grishin, N.V. (2003). Structural classification of zinc fingers: survey and summary. *Nucleic Acids Res.* *31*, 532-550.
- Kumar, H., Kawai, T., Kato, H., Sato, S., Takahashi, K., Coban, C., Yamamoto, M., Uematsu, S., Ishii, K.J., Takeuchi, O., and Akira, S. (2006). Essential role of IPS-1 in innate immune responses against RNA viruses. *J. Exp. Med.* *203*, 1795-1803.
- Lad, S.P., Yang, G., Scott, D.A., Chao, T.H., Correia, J.S., de la Torre, J.C., and Li, E. (2008). Identification of MAVS splicing variants that interfere with RIG-I/MAVS pathway signaling. *Mol. Immunol.* *45*, 2277-2287.
- Lademann, U., Kallunki, T., and Jaattela, M. (2001). A20 zinc finger protein inhibits TNF-induced apoptosis and stress response early in the signaling cascades and independently of binding to TRAF2 or 14-3-3 proteins. *Cell Death Differ.* *8*, 265-272.
- Laudes, M., Christodoulides, C., Sewter, C., Rochford, J.J., Considine, R.V., Sethi, J.K., Vidal-Puig, A., and O'Rahilly, S. (2004). Role of the POZ zinc finger transcription factor FBI-1 in human and murine adipogenesis. *J. Biol. Chem.* *279*, 11711-11718.
- Lebon, P., Badoual, J., Ponsot, G., Goutieres, F., Hemeury-Cukier, F., and Aicardi, J. (1988). Intrathecal synthesis of interferon-alpha in infants with progressive familial encephalopathy. *J. Neurol. Sci.* *84*, 201-208.
- Lemaitre, B., Nicolas, E., Michaut, L., Reichhart, J.M., and Hoffmann, J.A. (1996). The dorsoventral regulatory gene cassette spatzle/Toll/cactus controls the potent antifungal response in *Drosophila* adults. *Cell* *86*, 973-983.
- Levine, B., and Deretic, V. (2007). Unveiling the roles of autophagy in innate and adaptive immunity. *Nat. Rev. Immunol.* *7*, 767-777.
- Li, X., Lu, C., Stewart, M., Xu, H., Strong, R.K., Igumenova, T., and Li, P. (2009a). Structural Basis of Double-stranded RNA Recognition by the RIG-I like Receptor MDA5. *Arch. Biochem. Biophys.* *488*, 23-33.
- Li, X., Ranjith-Kumar, C.T., Brooks, M.T., Dharmaiyah, S., Herr, A.B., Kao, C., and Li, P. (2009b). The RIG-I-like receptor LGP2 recognizes the termini of double-stranded RNA. *J. Biol. Chem.* *284*, 13881-13891.
- Lin, R., Lacoste, J., Nakhaei, P., Sun, Q., Yang, L., Paz, S., Wilkinson, P., Julkunen, I., Vitour, D., Meurs, E., and Hiscott, J. (2006). Dissociation of a MAVS/IPS-1/VISA/Cardif-IKKepsilon molecular complex from the mitochondrial outer membrane by hepatitis C virus NS3-4A proteolytic cleavage. *J. Virol.* *80*, 6072-6083.
- Lin, Y., Robbins, J.B., Nyannor, E.K., Chen, Y.H., and Cann, I.K. (2005). A CCCH zinc finger conserved in a replication protein a homolog found in diverse Euryarchaeotes. *J. Bacteriol.* *187*, 7881-7889.
- Liu, X.Y., Wei, B., Shi, H.X., Shan, Y.F., and Wang, C. (2010). Tom70 mediates activation of interferon regulatory factor 3 on mitochondria. *Cell Res.* *20*, 994-1011.

- Liu, Y., Costantino, M.E., Montoya-Durango, D., Higashi, Y., Darling, D.S., and Dean, D.C. (2007). The zinc finger transcription factor ZFX1A is linked to cell proliferation by Rb-E2F1. *Biochem. J.* 408, 79-85.
- Livak, K.J., and Schmittgen, T.D. (2001). Analysis of relative gene expression data using real-time quantitative PCR and the 2(-Delta Delta C(T)) Method. *Methods* 25, 402-408.
- Loo, Y.M., Fornek, J., Crochet, N., Bajwa, G., Perwitasari, O., Martinez-Sobrido, L., Akira, S., Gill, M.A., Garcia-Sastre, A., Katze, M.G., and Gale, M., Jr. (2007). Distinct RIG-I and MDA5 signaling by RNA viruses in innate immunity. *J. Virol.* 82, 335-345.
- Loo, Y.M., Owen, D.M., Li, K., Erickson, A.K., Johnson, C.L., Fish, P.M., Carney, D.S., Wang, T., Ishida, H., Yoneyama, M., *et al.* (2006). Viral and therapeutic control of IFN-beta promoter stimulator 1 during hepatitis C virus infection. *Proc.Natl.Acad.Sci.U.S.A* 103, 6001-6006.
- Lu, C., Xu, H., Ranjith-Kumar, C.T., Brooks, M.T., Hou, T.Y., Hu, F., Herr, A.B., Strong, R.K., Kao, C.C., and Li, P. (2010). The Structural Basis of 5' Triphosphate Double-Stranded RNA Recognition by RIG-I C-Terminal Domain. *Structure* 18, 1032-1043.
- Lu, L.L., Puri, M., Horvath, C.M., and Sen, G.C. (2008). Select paramyxoviral V proteins inhibit IRF3 activation by acting as alternative substrates for inhibitor of kappaB kinase epsilon (IKKe)/TBK1. *J. Biol. Chem.* 283, 14269-14276.
- Madden, J.C., Ruiz, N., and Caparon, M. (2001). Cytolysin-mediated translocation (CMT): a functional equivalent of type III secretion in gram-positive bacteria. *Cell* 104, 143-152.
- Malathi, K., Dong, B., Gale, M., Jr., and Silverman, R.H. (2007). Small self-RNA generated by RNase L amplifies antiviral innate immunity. *Nature* 448, 816-819.
- Marques, J.T., Devosse, T., Wang, D., Zamanian-Daryoush, M., Serbinowski, P., Hartmann, R., Fujita, T., Behlke, M.A., and Williams, B.R. (2006). A structural basis for discriminating between self and nonself double-stranded RNAs in mammalian cells. *Nat. Biotechnol.* 24, 559-565.
- Matlin, A.J., Clark, F., and Smith, C.W. (2005). Understanding alternative splicing: towards a cellular code. *Nat. Rev. Mol. Cell Biol.* 6, 386-398.
- Matsumiya, T., Imaizumi, T., Yoshida, H., Satoh, K., Topham, M.K., and Stafforini, D.M. (2009). The levels of retinoic acid-inducible gene I are regulated by heat shock protein 90-alpha. *J. Immunol.* 182, 2717-2725.
- Mazur, D.J., and Perrino, F.W. (2001). Structure and expression of the TREX1 and TREX2 3' → 5' exonuclease genes. Characterization of the recombinant proteins. *J. Biol. Chem.* 276, 14718-14727.
- McCartney, S.A., Thackray, L.B., Gitlin, L., Gilfillan, S., Virgin, H.W., and Colonna, M. (2008). MDA-5 recognition of a murine norovirus. *PLoS Pathog.* 4, e1000108.
- Meylan, E., Curran, J., Hofmann, K., Moradpour, D., Binder, M., Bartenschlager, R., and Tschopp, J. (2005). Cardif is an adaptor protein in the RIG-I antiviral pathway and is targeted by hepatitis C virus. *Nature* 437, 1167-1172.
- Michallet, M.C., Meylan, E., Ermolaeva, M.A., Vazquez, J., Rebsamen, M., Curran, J., Poeck, H., Bscheider, M., Hartmann, G., Konig, M., *et al.* (2008). TRADD Protein Is an Essential Component of the RIG-like Helicase Antiviral Pathway. *Immunity* 28, 651-661.
- Mink, M.A., Stec, D.S., and Collins, P.L. (1991). Nucleotide sequences of the 3' leader and 5' trailer regions of human respiratory syncytial virus genomic RNA. *Virology* 185, 615-624.
- Minoda, Y., Saeki, K., Aki, D., Takaki, H., Sanada, T., Koga, K., Kobayashi, T., Takaesu, G., and Yoshimura, A. (2006). A novel Zinc finger protein, ZCCHC11, interacts with TIFA and modulates TLR signaling. *Biochem Biophys. Res. Commun.* 344, 1023-1030.
- Monroe, K.M., McWhirter, S.M., and Vance, R.E. (2009). Identification of host cytosolic sensors and bacterial factors regulating the type I interferon response to *Legionella pneumophila*. *PLoS Pathog.* 5, e1000665.
- Muller, S., Moller, P., Bick, M.J., Wurr, S., Becker, S., Gunther, S., and Kummerer, B.M. (2007). Inhibition of filovirus replication by the zinc finger antiviral protein. *J. Virol.* 81, 2391-2400.
- Munz, C. (2009). Enhancing immunity through autophagy. *Annu. Rev. Immunol.* 27, 423-449.
- Myong, S., Cui, S., Cornish, P.V., Kirchhofer, A., Gack, M.U., Jung, J.U., Hopfner, K.P., and Ha, T. (2009). Cytosolic Viral Sensor RIG-I Is a 5'-Triphosphate-Dependent Translocase on Double-Stranded RNA. *Science* 323, 1070-1074.

- Nejentsev, S., Walker, N., Riches, D., Egholm, M., and Todd, J.A. (2009). Rare variants of IFIH1, a gene implicated in antiviral responses, protect against type 1 diabetes. *Science* *324*, 387-389.
- Nieto, M.A. (2002). The snail superfamily of zinc-finger transcription factors. *Nat. Rev. Mol. Cell Biol.* *3*, 155-166.
- Okabe, Y., Sano, T., and Nagata, S. (2009). Regulation of the innate immune response by threonine-phosphatase of Eyes absent. *Nature* *460*, 520-524.
- Oshiumi, H., Matsumoto, M., Hatakeyama, S., and Seya, T. (2008). Riplet/RNF135, a RING-finger protein, ubiquitinates RIG-I to promote interferon-beta induction during the early phase of viral infection. *J. Biol. Chem.* *284*, 807-817.
- Park, J.S., Wang, M., Park, S.J., and Lee, S.H. (1999). Zinc finger of replication protein A, a non-DNA binding element, regulates its DNA binding activity through redox. *J. Biol. Chem.* *274*, 29075-29080.
- Pichlmair, A., Schulz, O., Tan, C.P., Naslund, T.I., Liljestrom, P., Weber, F., and Reis e Sousa, C. (2006). RIG-I-mediated antiviral responses to single-stranded RNA bearing 5'-phosphates. *Science* *314*, 997-1001.
- Pippig, D.A., Hellmuth, J.C., Cui, S., Kirchhofer, A., Lammens, K., Lammens, A., Schmidt, A., Rothenfusser, S., and Hopfner, K.P. (2009). The regulatory domain of the RIG-I family ATPase LGP2 senses double-stranded RNA. *Nucleic Acids Res.* *37*, 2014-2025.
- Plotch, S.J., Bouloy, M., Ulmanen, I., and Krug, R.M. (1981). A unique cap(m7GpppXm)-dependent influenza virion endonuclease cleaves capped RNAs to generate the primers that initiate viral RNA transcription. *Cell* *23*, 847-858.
- Publicover, J., Ramsburg, E., Robek, M., and Rose, J.K. (2006). Rapid pathogenesis induced by a vesicular stomatitis virus matrix protein mutant: viral pathogenesis is linked to induction of tumor necrosis factor alpha. *J. Virol.* *80*, 7028-7036.
- Rad, R., Ballhorn, W., Volland, P., Eisenacher, K., Mages, J., Rad, L., Ferstl, R., Lang, R., Wagner, H., Schmid, R.M., *et al.* (2009). Extracellular and intracellular pattern recognition receptors cooperate in the recognition of *Helicobacter pylori*. *Gastroenterology* *136*, 2247-2257.
- Rad, R., Brenner, L., Krug, A., Volland, P., Mages, J., Lang, R., Schwendy, S., Reindl, W., Dossumbekova, A., Ballhorn, W., *et al.* (2007). Toll-like receptor-dependent activation of antigen-presenting cells affects adaptive immunity to *Helicobacter pylori*. *Gastroenterology* *133*, 150-163.
- Regl, G., Kasper, M., Schnidar, H., Eichberger, T., Neill, G.W., Ikram, M.S., Quinn, A.G., Philpott, M.P., Frischauf, A.M., and Aberger, F. (2004). The zinc-finger transcription factor GLI2 antagonizes contact inhibition and differentiation of human epidermal cells. *Oncogene* *23*, 1263-1274.
- Rehwinkel, J., Tan, C.P., Goubau, D., Schulz, O., Pichlmair, A., Bier, K., Robb, N., Vreede, F., Barclay, W., Fodor, E., and Reis e Sousa, C. (2010). RIG-I detects viral genomic RNA during negative-strand RNA virus infection. *Cell* *140*, 397-408.
- Remington, M.C., Tarle, S.A., Simon, B., and Merchant, J.L. (1997). ZBP-89, a Kruppel-type zinc finger protein, inhibits cell proliferation. *Biochem. Biophys. Res. Commun.* *237*, 230-234.
- Rice, G.I., Bond, J., Asipu, A., Brunette, R.L., Manfield, I.W., Carr, I.M., Fuller, J.C., Jackson, R.M., Lamb, T., Briggs, T.A., *et al.* (2009). Mutations involved in Aicardi-Goutieres syndrome implicate SAMHD1 as regulator of the innate immune response. *Nat. Genet.* *41*, 829-832.
- Rosenstiel, P., Huse, K., Till, A., Hampe, J., Hellmig, S., Sina, C., Billmann, S., von Kampen, O., Waetzig, G.H., Platzer, M., *et al.* (2006). A short isoform of NOD2/CARD15, NOD2-S, is an endogenous inhibitor of NOD2/receptor-interacting protein kinase 2-induced signaling pathways. *Proc.Natl.Acad. Sci.U.S.A* *103*, 3280-3285.
- Saito, T., Hirai, R., Loo, Y.M., Owen, D., Johnson, C.L., Sinha, S.C., Akira, S., Fujita, T., and Gale, M., Jr. (2007). Regulation of innate antiviral defenses through a shared repressor domain in RIG-I and LGP2. *Proc.Natl.Acad.Sci.U.S.A* *104*, 582-587.
- Saito, T., Owen, D.M., Jiang, F., Marcotrigiano, J., and Gale, M. (2008). Innate immunity induced by composition-dependent RIG-I recognition of hepatitis C virus RNA. *Nature* *454*, 523-527.
- Saitoh, T., Yamamoto, M., Miyagishi, M., Taira, K., Nakanishi, M., Fujita, T., Akira, S., Yamamoto, N., and Yamaoka, S. (2005). A20 is a negative regulator of IFN regulatory factor 3 signaling. *J. Immunol.* *174*, 1507-1512.

- Samanta, M., Iwakiri, D., Kanda, T., Imaizumi, T., and Takada, K. (2006). EB virus-encoded RNAs are recognized by RIG-I and activate signaling to induce type I IFN. *EMBO J.* *25*, 4207-4214.
- Sambrook, J., and Russel, D.W. (2001). *Molecular cloning - a laboratory manual*. (Cold Spring Harbor, New York, Cold Spring Harbor Laboratory Press).
- Sanada, T., Takaesu, G., Mashima, R., Yoshida, R., Kobayashi, T., and Yoshimura, A. (2008). FLN29 deficiency reveals its negative regulatory role in the Toll-like receptor (TLR) and retinoic acid-inducible gene I (RIG-I)-like helicases signaling pathway. *J. Biol. Chem.* *283*, 33858-33864.
- Sato, M., Suemori, H., Hata, N., Asagiri, M., Ogasawara, K., Nakao, K., Nakaya, T., Katsuki, M., Noguchi, S., Tanaka, N., and Taniguchi, T. (2000). Distinct and essential roles of transcription factors IRF-3 and IRF-7 in response to viruses for IFN- $\alpha$ /beta gene induction. *Immunity* *13*, 539-548.
- Satoh, T., Kato, H., Kumagai, Y., Yoneyama, M., Sato, S., Matsushita, K., Tsujimura, T., Fujita, T., Akira, S., and Takeuchi, O. (2010). LGP2 is a positive regulator of RIG-I- and MDA5-mediated antiviral responses. *Proc.Natl.Acad.Sci.U.S.A* *107*, 1512-1517.
- Sazinsky, M.H., Mandal, A.K., Arguello, J.M., and Rosenzweig, A.C. (2006). Structure of the ATP binding domain from the *Archaeoglobus fulgidus* Cu<sup>+</sup>-ATPase. *J. Biol. Chem.* *281*, 11161-11166.
- Schiff, L.A., Nibert, M.L., Co, M.S., Brown, E.G., and Fields, B.N. (1988). Distinct binding sites for zinc and double-stranded RNA in the reovirus outer capsid protein sigma 3. *Mol. Cell Biol.* *8*, 273-283.
- Schlee, M., Roth, A., Hornung, V., Hagmann, C.A., Wimmenauer, V., Barchet, W., Coch, C., Janke, M., Mihailovic, A., Wardle, G., *et al.* (2009). Recognition of 5' triphosphate by RIG-I helicase requires short blunt double-stranded RNA as contained in panhandle of negative-strand virus. *Immunity* *31*, 25-34.
- Schmidt, A., Schwerd, T., Hamm, W., Hellmuth, J.C., Cui, S., Wenzel, M., Hoffmann, F.S., Michallet, M.C., Besch, R., Hopfner, K.P., *et al.* (2009). 5'-triphosphate RNA requires base-paired structures to activate antiviral signaling via RIG-I. *Proc.Natl.Acad.Sci.U.S.A* *106*, 12067-12072.
- Schmitz, G., Heimerl, S., and Langmann, T. (2004). Zinc finger protein ZNF202 structure and function in transcriptional control of HDL metabolism. *Curr. Opin. Lipidol.* *15*, 199-208.
- Schnell, M.J., Buonocore, L., Kretzschmar, E., Johnson, E., and Rose, J.K. (1996). Foreign glycoproteins expressed from recombinant vesicular stomatitis viruses are incorporated efficiently into virus particles. *Proc.Natl.Acad. Sci.U.S.A* *93*, 11359-11365.
- Seth, R.B., Sun, L., Ea, C.K., and Chen, Z.J. (2005). Identification and characterization of MAVS, a mitochondrial antiviral signaling protein that activates NF- $\kappa$ B and IRF3. *Cell* *122*, 669-682.
- Sharif-Askari, E., Vassen, L., Kosan, C., Khandanpour, C., Gaudreau, M.C., Heyd, F., Okayama, T., Jin, J., Rojas, M.E., Grimes, H.L., *et al.* (2010). Zinc finger protein Gfi1 controls the endotoxin-mediated Toll-like receptor inflammatory response by antagonizing NF- $\kappa$ B p65. *Mol. Cell. Biol.* *30*, 3929-3942.
- Shingai, M., Ebihara, T., Begum, N.A., Kato, A., Honma, T., Matsumoto, K., Saito, H., Ogura, H., Matsumoto, M., and Seya, T. (2007). Differential Type I IFN-Inducing Abilities of Wild-Type versus Vaccine Strains of Measles Virus. *J. Immunol.* *179*, 6123-6133.
- Shiraishi, A., Joko, T., Higashiyama, S., and Ohashi, Y. (2007). Role of promyelocytic leukemia zinc finger protein in proliferation of cultured human corneal endothelial cells. *Cornea* *26*, S55-58.
- Soucy-Faulkner, A., Mukawera, E., Fink, K., Martel, A., Jouan, L., Nzengue, Y., Lamarre, D., Vande, V.C., and Grandvaux, N. (2010). Requirement of NOX2 and reactive oxygen species for efficient RIG-I-mediated antiviral response through regulation of MAVS expression. *PLoS Pathog.* *6*, e1000930.
- Spiropoulou, C.F., Ranjan, P., Pearce, M.B., Sealy, T.K., Albarino, C.G., Gangappa, S., Fujita, T., Rollin, P.E., Nichol, S.T., Ksiazek, T.G., and Sambhara, S. (2009). RIG-I activation inhibits ebolavirus replication. *Virology* *392*, 11-15.
- Steinberg, C., Eisenacher, K., Gross, O., Reindl, W., Schmitz, F., Ruland, J., and Krug, A. (2009). The IFN regulatory factor 7-dependent type I IFN response is not essential for early resistance against murine cytomegalovirus infection. *Eur. J. Immunol.* *39*, 1007-1018.
- Stetson, D.B., Ko, J.S., Heidmann, T., and Medzhitov, R. (2008). Trex1 prevents cell-intrinsic initiation of autoimmunity. *Cell* *134*, 587-598.
- Stetson, D.B., and Medzhitov, R. (2006). Recognition of cytosolic DNA activates an IRF3-dependent innate immune response. *Immunity* *24*, 93-103.

- Sumpter, R., Jr., Loo, Y.M., Foy, E., Li, K., Yoneyama, M., Fujita, T., Lemon, S.M., and Gale, M., Jr. (2005). Regulating intracellular antiviral defense and permissiveness to hepatitis C virus RNA replication through a cellular RNA helicase, RIG-I. *J. Virol.* **79**, 2689-2699.
- Sun, Q., Sun, L., Liu, H.H., Chen, X., Seth, R.B., Forman, J., and Chen, Z.J. (2006). The specific and essential role of MAVS in antiviral innate immune responses. *Immunity* **24**, 633-642.
- Sun, W., Li, Y., Chen, L., Chen, H., You, F., Zhou, X., Zhou, Y., Zhai, Z., Chen, D., and Jiang, Z. (2009). ERIS, an endoplasmic reticulum IFN stimulator, activates innate immune signaling through dimerization. *Proc.Natl.Acad.Sci.U.S.A* **106**, 8653-8658.
- Sun, Y.W. (1997). RIG-I, a human homolog gene of RNA helicase, is induced by retinoic acid during differentiation of acute promyelocytic leukemia cells. (Thesis, Shanghai Second Medical University, Shanghai).
- Suzuki, K., Imaizumi, T., Tsugawa, K., Ito, E., and Tanaka, H. (2007). Expression of retinoic acid-inducible gene-I in lupus nephritis. *Nephrol. Dial. Transplant.* **22**, 2407-2409.
- Takaoka, A., Wang, Z., Choi, M.K., Yanai, H., Negishi, H., Ban, T., Lu, Y., Miyagishi, M., Kodama, T., Honda, K., *et al.* (2007). DAI (DLM-1/ZBP1) is a cytosolic DNA sensor and an activator of innate immune response. *Nature* **448**, 501-505.
- Takeuchi, O., and Akira, S. (2010). Pattern recognition receptors and inflammation. *Cell* **140**, 805-820.
- Tanner, N.K., and Linder, P. (2001). DExD/H box RNA helicases: from generic motors to specific dissociation functions. *Mol. Cell* **8**, 251-262.
- Terebiznik, M.R., Raju, D., Vazquez, C.L., Torbricki, K., Kulkarni, R., Blanke, S.R., Yoshimori, T., Colombo, M.I., and Jones, N.L. (2009). Effect of *Helicobacter pylori*'s vacuolating cytotoxin on the autophagy pathway in gastric epithelial cells. *Autophagy* **5**, 370-379.
- Terebiznik, M.R., Vazquez, C.L., Torbicki, K., Banks, D., Wang, T., Hong, W., Blanke, S.R., Colombo, M.I., and Jones, N.L. (2006). *Helicobacter pylori* VacA toxin promotes bacterial intracellular survival in gastric epithelial cells. *Infect. Immun.* **74**, 6599-6614.
- Theofilopoulos, A.N., Baccala, R., Beutler, B., and Kono, D.H. (2005). Type I interferons (alpha/beta) in immunity and autoimmunity. *Annu. Rev. Immunol.* **23**, 307-336.
- Tijms, M.A., van Dinten, L.C., Gorbalenya, A.E., and Snijder, E.J. (2001). A zinc finger-containing papain-like protease couples subgenomic mRNA synthesis to genome translation in a positive-stranded RNA virus. *Proc.Natl.Acad.Sci.U.S.A* **98**, 1889-1894.
- Touriol, C., Bornes, S., Bonnal, S., Audigier, S., Prats, H., Prats, A.C., and Vagner, S. (2003). Generation of protein isoform diversity by alternative initiation of translation at non-AUG codons. *Biol. Cell* **95**, 169-178.
- Tsugawa, K., Oki, E., Suzuki, K., Imaizumi, T., Ito, E., and Tanaka, H. (2008). Expression of mRNA for functional molecules in urinary sediment in glomerulonephritis. *Pediatr. Nephrol.* **23**, 395-401.
- Vaughn, D.E., Rodriguez, J., Lazebnik, Y., and Joshua-Tor, L. (1999). Crystal structure of Apaf-1 caspase recruitment domain: an alpha-helical Greek key fold for apoptotic signaling. *J. Mol. Biol.* **293**, 439-447.
- Venkataraman, T., Valdes, M., Elsbey, R., Kakuta, S., Caceres, G., Saijo, S., Iwakura, Y., and Barber, G.N. (2007). Loss of DExD/H Box RNA Helicase LGP2 Manifests Disparate Antiviral Responses. *J. Immunol.* **178**, 6444-6455.
- Wagner, S., Hess, M.A., Ormonde-Hanson, P., Malandro, J., Hu, H., Chen, M., Kehrer, R., Frodsham, M., Schumacher, C., Beluch, M., *et al.* (2000). A broad role for the zinc finger protein ZNF202 in human lipid metabolism. *J. Biol. Chem.* **275**, 15685-15690.
- Walker, J.E., Saraste, M., Runswick, M.J., and Gay, N.J. (1982). Distantly related sequences in the alpha- and beta-subunits of ATP synthase, myosin, kinases and other ATP-requiring enzymes and a common nucleotide binding fold. *EMBO J.* **1**, 945-951.
- Wang, L., Wildt, K.F., Castro, E., Xiong, Y., Feigenbaum, L., Tessarollo, L., and Bosselut, R. (2008). The zinc finger transcription factor Zbtb7b represses CD8-lineage gene expression in peripheral CD4+ T cells. *Immunity* **29**, 876-887.
- Wang, S.Z., Dulin, J., Wu, H., Hurlock, E., Lee, S.E., Jansson, K., and Lu, Q.R. (2006). An oligodendrocyte-specific zinc-finger transcription regulator cooperates with Olig2 to promote oligodendrocyte differentiation. *Development* **133**, 3389-3398.
- Wang, Y., Ludwig, J., Schuberth, C., Goldeck, M., Schlee, M., Li, H., Juranek, S., Sheng, G., Micura, R., Tuschl, T., *et al.* (2010). Structural and functional insights into 5'-ppp RNA pattern recognition by the innate immune receptor RIG-I. *Nat. Struct. Mol. Biol.* **17**, 781-787.

- Wang, Y., Zhang, H.X., Sun, Y.P., Liu, Z.X., Liu, X.S., Wang, L., Lu, S.Y., Kong, H., Liu, Q.L., Li, X.H., *et al.* (2007). Rig-I(-/-) mice develop colitis associated with downregulation of Galphai2. *Cell Res.* *17*, 858-868.
- Winkler, C., Denker, K., Wortelkamp, S., and Sickmann, A. (2007). Silver- and Coomassie-staining protocols: detection limits and compatibility with ESI MS. *Electrophoresis* *28*, 2095-2099.
- Wu, Y., Qian, X., He, Y., Moya, I.A., and Luo, Y. (2005). Crystal structure of an ATPase-active form of Rad51 homolog from *Methanococcus voltae*. Insights into potassium dependence. *J. Biol. Chem.* *280*, 722-728.
- Xu, L., Xiao, N., Liu, F., Ren, H., and Gu, J. (2009). Inhibition of RIG-I and MDA5-dependent antiviral response by gC1qR at mitochondria. *Proc.Natl.Acad.Sci.U.S.A.* *106*, 1530-1535.
- Xu, L.G., Wang, Y.Y., Han, K.J., Li, L.Y., Zhai, Z., and Shu, H.B. (2005). VISA is an adapter protein required for virus-triggered IFN-beta signaling. *Mol. Cell* *19*, 727-740.
- Yagi, H., Kajiwara, N., Tanaka, H., Tsukihara, T., Kato-Yamada, Y., Yoshida, M., and Akutsu, H. (2007). Structures of the thermophilic F1-ATPase epsilon subunit suggesting ATP-regulated arm motion of its C-terminal domain in F1. *Proc.Natl.Acad.Sci.U.S.A* *104*, 11233-11238.
- Yanai, H., Ban, T., Wang, Z., Choi, M.K., Kawamura, T., Negishi, H., Nakasato, M., Lu, Y., Hangai, S., Koshiba, R., *et al.* (2009). HMGB proteins function as universal sentinels for nucleic-acid-mediated innate immune responses. *Nature* *462*, 99-103.
- Yang, Y., Liang, Y., Qu, L., Chen, Z., Yi, M., Li, K., and Lemon, S.M. (2007a). Disruption of innate immunity due to mitochondrial targeting of a picornaviral protease precursor. *Proc.Natl.Acad.Sci.U.S.A* *104*, 7253-7258.
- Yang, Y.G., Lindahl, T., and Barnes, D.E. (2007b). Trex1 exonuclease degrades ssDNA to prevent chronic checkpoint activation and autoimmune disease. *Cell* *131*, 873-886.
- Yoneyama, M., and Fujita, T. (2007). RIG-I family RNA helicases: Cytoplasmic sensor for antiviral innate immunity. *Cytokine Growth Factor Rev.* *18*, 545-551.
- Yoneyama, M., and Fujita, T. (2009). RNA recognition and signal transduction by RIG-I-like receptors. *Immunol. Rev.* *227*, 54-65.
- Yoneyama, M., and Fujita, T. (2010). Recognition of viral nucleic acids in innate immunity. *Rev. Med. Virol.* *20*, 4-22.
- Yoneyama, M., Kikuchi, M., Matsumoto, K., Imaizumi, T., Miyagishi, M., Taira, K., Foy, E., Loo, Y.M., Gale, M., Jr., Akira, S., *et al.* (2005). Shared and unique functions of the DExD/H-box helicases RIG-I, MDA5, and LGP2 in antiviral innate immunity. *J. Immunol.* *175*, 2851-2858.
- Yoneyama, M., Kikuchi, M., Natsukawa, T., Shinobu, N., Imaizumi, T., Miyagishi, M., Taira, K., Akira, S., and Fujita, T. (2004). The RNA helicase RIG-I has an essential function in double-stranded RNA-induced innate antiviral responses. *Nat. Immunol.* *5*, 730-737.
- Yount, J.S., Gitlin, L., Moran, T.M., and Lopez, C.B. (2008). MDA5 participates in the detection of paramyxovirus infection and is essential for the early activation of dendritic cells in response to Sendai Virus defective interfering particles. *J. Immunol.* *180*, 4910-4918.
- Zeng, W., Sun, L., Jiang, X., Chen, X., Hou, F., Adhikari, A., Xu, M., and Chen, Z.J. (2010). Reconstitution of the RIG-I pathway reveals a signaling role of unanchored polyubiquitin chains in innate immunity. *Cell* *141*, 315-330.
- Zhang, T., Wang, H., Saunee, N.A., Breslin, M.B., and Lan, M.S. (2010). Insulinoma-associated antigen-1 zinc-finger transcription factor promotes pancreatic duct cell trans-differentiation. *Endocrinology* *151*, 2030-2039.
- Zhang, X., Wang, C., Schook, L.B., Hawken, R.J., and Rutherford, M.S. (2000). An RNA helicase, RHIV-1, induced by porcine reproductive and respiratory syndrome virus (PRRSV) is mapped on porcine chromosome 10q13. *Microb. Pathog.* *28*, 267-278.
- Zhao, C., Denison, C., Huijbregtse, J.M., Gygi, S., and Krug, R.M. (2005). Human ISG15 conjugation targets both IFN-induced and constitutively expressed proteins functioning in diverse cellular pathways. *Proc.Natl.Acad.Sci.U.S.A* *102*, 10200-10205.
- Zhao, T., Yang, L., Sun, Q., Arguello, M., Ballard, D.W., Hiscott, J., and Lin, R. (2007). The NEMO adaptor bridges the nuclear factor-kappaB and interferon regulatory factor signaling pathways. *Nat. Immunol.* *8*, 592-600.
- Zhong, B., Yang, Y., Li, S., Wang, Y.Y., Li, Y., Diao, F., Lei, C., He, X., Zhang, L., Tien, P., and Shu, H.B. (2008). The adaptor protein MITA links virus-sensing receptors to IRF3 transcription factor activation. *Immunity* *29*, 538-550.

## 8 APPENDIX

### 8.1 Equipment

<b>Device</b>	<b>Manufacturer/Distributor</b>
Agarose gel electrophoresis system	Bio-Rad (München, D)
Analytical balance	Ohaus (Pine Brook, NJ, USA)
Autoradiography cassette	Amersham GE Healthcare (München, Germany)
Bacterial incubator	Binder (Tuttlingen, Germany)
Balance	Ohaus (Pine Brook, NJ, USA)
Centrifuge Biofuge Fresco	Heraeus (Hanau, Germany)
Centrifuge 5810R	Eppendorf (Hamburg, Germany)
Centrifuge 5418	Eppendorf (Hamburg, Germany)
Centrifuge Sorvall RC26 plus	Kendro (Langenselbold, Germany)
Centrifuge Avanti J-20xp	Beckman Coulter (Krefeld, Germany)
Centrifuge L8-55M	Beckman Coulter (Krefeld, Germany)
Centrifuge Optima XL-100K	Beckman Coulter (Krefeld, Germany)
Electrophoresis power supply EV202	Consort (Turnhout, Belgium)
Electrophoresis power supply PowerPac 300	Bio-Rad (München, Germany)
Electrophoresis system Hoefer SE 400	Amersham GE Healthcare (München, Germany)
Electrophoresis system Mini Protean II	Bio-Rad (München, Germany)
Film processor Hyperprocessor	Amersham GE Healthcare (München, Germany)
Freezer -20 °C	Siemens (München, Germany)
Freezer -80 °C	Kendro (Langenselbold, Germany)
Fridge	Liebherr (Bulle, Switzerland)

<b>Device</b>	<b>Manufacturer/Distributor</b>
Gel documentation system GelDocXR	Bio-Rad (München, Germany)
Glass homogenizer	Brand (Wertheim, Germany)
Ice machine	Ziegra (Isernhagen, Germany)
Incubator Hera Cell 240	Heraeus (Hanau, Germany)
Laminar flow Hera Safe	Kendro (Langenselbold, Germany)
Luminometer Single Tube	Turner Biosystems (Sunnyvale, CA, USA)
Magnetic stirrer	Heidolph (Schwabach, Germany)
Microwave	Siemens (München, Germany)
Microscope Optech IB	Exacta Optech (München, Germany)
Multipipette plus	Eppendorf (Hamburg, Germany)
Nanodrop ND-1000 Spectrophotometer	Peqlab (Erlangen, Germany)
Neubauer counting chamber	Roth (Karlsruhe, Germany)
Nitrogen freezing tank MVE 6000	MVE (Marietta, GA, USA)
PCR cycler Mastercycler	Eppendorf (Hamburg, Germany)
pH-meter	WTW (Weilheim, Germany)
Pipetboy acu	Integra Biosciences (Fernwald, Germany)
Pipettes	Gilson (Middleton, WI, USA)
Rocking platform ST5	CAT (Staufen, Germany)
Roller wheel	Snijders Scientific (Tilburg, Netherlands)
Rotor F-34-6-38	Eppendorf (Hamburg, Germany)
Rotor Ti100	Beckman Coulter (Krefeld, Germany)
Sealing apparatus Folio	Severin (Sundern, Germany)
Semidry Blotter HEP-1 Panther	Owl Scientific (Portsmouth, NH, USA)
Shaking incubator	Edmund Bühler GmbH (Tübingen, Germany)
Spectrophotometer Smart Spec	Bio-Rad (München, Germany)

<b>Device</b>	<b>Manufacturer/Distributor</b>
Thermomixer	Eppendorf (Hamburg, Germany)
Trans-Blot Electrophoretic Transfer cell	Bio-Rad (München, Germany)
Vortexer Genie 2	Scientific Industries (Bohemia, NY, USA)
Water Bath	GFL (Burgwedel, Germany)

## 8.2 Consumables

<b>Item</b>	<b>Manufacturer/Distributor</b>
Aspiration pipette	BD Falcon (Franklin Lakes, NJ, USA)
Bottle Top filter	Corning (Lowell, MA, USA)
Cell culture flask with vented screw (25 cm <sup>2</sup> and 75 cm <sup>2</sup> )	BD Falcon (Franklin Lakes, NJ, USA)
Cell culture plates (6- and 24-well)	BD Falcon (Franklin Lakes, NJ, USA)
Cell scraper	Sarstedt (Nümbrecht, Germany)
CL-X Posure film	Thermo (Rockford, IL, USA)
Combitips	Eppendorf (Hamburg, Germany)
Conical Tubes (15 ml and 50 ml)	BD Falcon (Franklin Lakes, NJ, USA)
Cryotubes 1 ml	Corning (Lowell, MA, USA)
Filter tips	Greiner Bio-One (Frickenhausen, Germany)
Hyperfilm ECL	Amersham GE Healthcare (München, Germany)
Maxi-Sorp ELISA plate (96-well)	Nunc (Wiesbaden, Germany)
Nitrocellulose membrane	Schleicher & Schüll (Dassel, Germany)
Needles (20 G, 27 G)	Braun (Melsungen, Germany)
Parafilm	Roth (Karlsruhe, Germany)
PCR tubes (8-strip)	Brand (Wertheim, Germany)

<b>Item</b>	<b>Manufacturer/Distributor</b>
Petri dish	Peske (Aindlingen, Germany)
Petri dish (100 mm x15 mm)	BD Falcon (Franklin Lakes, NJ, USA)
PVDF membrane Immobilon-P	Millipore (Schwalbach, Germany)
Round Bottom Tube (14 ml)	BD Falcon (Franklin Lakes, NJ, USA)
Safe lock microcentrifuge tubes (1,5 ml)	Eppendorf (Hamburg, Germany)
Safe lock microcentrifuge tubes (2 ml)	Sarstedt (Nümbrecht, Germany)
Scalpel (disposable)	Feather (Osaka, Japan)
Serological pipettes (5 ml, 10 ml, 25 ml)	BD Falcon (Franklin Lakes, NJ, USA)
Slide-A-Lyzer dialysis cassettes	Pierce (Rockford, IL, USA)
Spreading spatula (sterile)	Roth (Karlsruhe, Germany)
Syringe filter (0,2 µm)	Corning (Lowell, MA, USA)
Syringe Luer-Lok sterile (5 ml, 10 ml)	BD (Franklin Lakes, NJ, USA)
Syringe sterile (5 ml, 10 ml, 20 ml)	BD (Franklin Lakes, NJ, USA)
Tissue culture dish (60 mm and 100 mm)	BD Falcon (Franklin Lakes, NJ, USA)
Whatman 3 mm blotting paper	Whatman (Dassel, Germany)
Whatman blotting paper GB005	Whatman (Dassel, Germany)

### **8.3 Reagents**

<b>Name</b>	<b>Manufacturer/Distributor</b>
2-Propanol	J.T. Baker (Deventer, Netherlands)
ABTS	Roche (Mannheim, Germany)
Acetic acid	Merck (Darmstadt, Germany)
Agarose	Biozym (Hess.-Oldendorf, Germany)
Ammonium persulphate (APS)	Sigma-Aldrich (Seelze, Germany)

<b>Name</b>	<b>Manufacturer/Distributor</b>
Ampicillin	Roth (Karlsruhe, Germany)
Anti-Flag M2 Affinity Gel	Sigma-Aldrich (Seelze, Germany)
$\beta$ -Mercaptoethanol	Sigma-Aldrich (Seelze, Germany)
Bacto Tryptone	BD (Franklin Lakes, NJ, USA)
Biotin-16-UTP	Roche (Mannheim, Germany)
Bovine serum albumin (BSA)	Sigma-Aldrich (Seelze, Germany)
Bradford Reagent	Bio-Rad (München, Germany)
Bromophenol blue	Sigma-Aldrich (Seelze, Germany)
Chloroform	Merck (Darmstadt, Germany)
Citric acid	Roth (Karlsruhe, Germany)
Complete Protease Inhibitor Mix	Roche (Mannheim, Germany)
Crystal violet	Fluka (Seelze, Germany)
D-(+)-Glucose	Roth (Karlsruhe, Germany)
Dimethyl sulfoxide (DMSO)	Sigma-Aldrich (Seelze, Germany)
Disodium phosphate	Fluka (Seelze, Germany)
D-MEM	ATCC LGC Promochem (Wesel, Germany)
D-MEM (with L-)Glutamine	Invitrogen (Karlsruhe, Germany)
DNA Ladder (100 bp and 1 Kb)	NEB (Frankfurt am Main, Germany)
dNTP mix	Promega (Mannheim, Germany)
DOTAP	Roth (Karlsruhe, Germany)
DTT	Roth (Karlsruhe, Germany)
EDTA (0,5 M, pH 8,0)	Invitrogen (Karlsruhe, Germany)
EDTA (EDTA-si-sodium-salt x 2 H <sub>2</sub> O)	Sigma-Aldrich (Seelze, Germany)
Ethanol absolute (EtOH)	J.T. Baker (Deventer, Netherlands)
Ethanol (for use in molecular biology)	Merck (Darmstadt, Germany)

<b>Name</b>	<b>Manufacturer/Distributor</b>
Ethidiumbromide (10 mg/ml)	Invitrogen (Karlsruhe, Germany)
Fetal Calf Serum (FCS)	Biochrom (Berlin, Germany)
Formaldehyde (37 %)	Roth (Karlsruhe, Germany)
Glacial acetic acid	Roth (Karlsruhe, Germany)
Glutamax-I (100 x)	Invitrogen (Karlsruhe, Germany)
Glycerol	Roth (Karlsruhe, Germany)
Glycin	Roth (Karlsruhe, Germany)
GM-CSF	own production
G-MEM	Invitrogen (Karlsruhe, Germany)
Hepes	Sigma-Aldrich (Seelze, Germany)
Hepes buffer solution (1 M)	Invitrogen (Karlsruhe, Germany)
Hydrochloric acid (HCl)	Merck (Darmstadt, Germany)
Hydrogen peroxide (30 %)	Sigma-Aldrich (Seelze, Germany)
Isofluran (Forene 100 % (v/v))	Abbott (Wiesbaden, Germany)
Kanamycin	Invitrogen (Karlsruhe, Germany)
Laemmli sample buffer	Bio-Rad (München, Germany)
LB Agar	Roth (Karlsruhe, Germany)
Lipofectamine2000	Invitrogen (Karlsruhe, Germany)
Magnesium chloride ( $\text{MgCl}_2 \times 6 \text{H}_2\text{O}$ )	Roth (Karlsruhe, Germany)
Magnesium sulphate ( $\text{MgSO}_4 \times 7 \text{H}_2\text{O}$ )	Roth (Karlsruhe, Germany)
Methanol	J.T. Baker (Deventer, Netherlands)
MEM- $\alpha$	PAA (Pasching, Austria)
M-PER mammalian extraction buffer	Pierce (Rockford, IL, USA)
NEAA (100 x)	PAA (Pasching, Austria)
NP-40	Sigma-Aldrich (Seelze, Germany)

<b>Name</b>	<b>Manufacturer/Distributor</b>
Opti-MEM I reduced serum medium	Invitrogen (Karlsruhe, Germany)
PBS powder (w/o Ca and Mg)	Invitrogen (Karlsruhe, Germany)
PBS (w/o Ca and Mg) solution	PAA (Pasching, Austria)
Penicillin/Streptomycin (100 x)	PAA (Pasching, Austria)
Phenol	Roth (Karlsruhe, Germany)
Poly(I:C)	Amersham GE Healthcare (München, Germany)
Phenylmethylsulfonylfluoride (PMSF)	Roth (Karlsruhe, Germany)
Potassium acetate	Sigma-Aldrich (Seelze, Germany)
Potassium chloride	Roth (Karlsruhe, Germany)
Prestained Protein Ladder	Fermentas (St. Leon-Rot, Germany)
Protein G sepharose (PGS)	Biovision (Mountain View, CA, USA)
Red Blood Cell Lysis Buffer	Sigma-Aldrich (Seelze, Germany)
Restore Western Blot Stripping Buffer	Pierce (Rockford, IL, USA)
RIPA buffer	Sigma-Aldrich (Seelze, Germany)
Rotiphorese Gel 30	Roth (Karlsruhe, Germany)
RPMI 1640	Invitrogen (Karlsruhe, Germany)
Silver nitrate	Sigma-Aldrich (Seelze, Germany)
Skim Milk Powder	Fluka (Seelze, Germany)
Sodium acetate ( $C_2H_3NaO_2 \times 3 H_2O$ )	Roth (Karlsruhe, Germany)
Sodium carbonate	Merck (Darmstadt, Germany)
Sodium chloride	Roth (Karlsruhe, Germany)
Sodium hydroxide solution (NaOH)	Merck (Darmstadt, Germany)
Sodium dihydrogen phosphate	Fluka (Seelze, Germany)
Sodium orthovanadate	Sigma-Aldrich (Seelze, Germany)
Sodium pyruvate solution (100 mM)	Invitrogen (Karlsruhe, Germany)

---

<b>Name</b>	<b>Manufacturer/Distributor</b>
Sodium thiosulphate ( $\text{Na}_2\text{S}_2\text{O}_3 \times 5 \text{H}_2\text{O}$ )	Sigma-Aldrich (Seelze, Germany)
Streptavidin Agarose (SA)	Sigma-Aldrich (Seelze, Germany)
TEMED	Fluka (Seelze, Germany)
Tris	Roth (Karlsruhe, Germany)
Triton X-100	Sigma-Aldrich (Seelze, Germany)
Trizol reagent	Invitrogen (Karlsruhe, Germany)
Trypsin/EDTA solution (1 x)	PAA (Pasching, Austria)
Tryptose broth (1 x)	Invitrogen (Karlsruhe, Germany)
Tween-20	Sigma-Aldrich (Seelze, Germany)
Universal Type I Interferon	PBL (Piscataway, NJ, USA)
Yeast Extract	BD (Franklin Lakes, NJ, USA)

## 8.4 Kits and enzymes

Name	Manufacturer/Distributor
Alkaline Phosphatase, Calf Intestinal	NEB (Frankfurt am Main, Germany)
Ampliscribe Flash T7 Kit	Epicentre Biotechnologies (Madison, WA, USA)
Dual Luciferase Assay System	Promega (Mannheim, Germany)
DNase I	Fermentas (St. Leon-Rot, Germany)
Endofree Plasmid Maxi Kit	Qiagen (Hilden, Germany)
<i>Pfu</i> Ultra Polymerase	Stratagene (La Jolla, CA, USA)
QIAprep Spin Miniprep Kit	Qiagen (Hilden, Germany)
QIAquick PCR purification Kit	Qiagen (Hilden, Germany)
QIAquick Gel Extraction Kit	Qiagen (Hilden, Germany)
Restriction endonucleases	NEB (Frankfurt am Main, Germany); Fermentas (St. Leon-Rot, Germany)
RNA protect cell reagent	Qiagen (Hilden, Germany)
RNase inhibitor	Fermentas (St. Leon-Rot, Germany)
RNeasy Mini Kit	Qiagen (Hilden, Germany)
Superscript II reverse transcriptase	Invitrogen (Karlsruhe, Germany)
Super Signal West Pico Chemiluminescent detection Kit	Pierce (Rockford, IL, USA)
SYBR Green Mastermix	Applied Biosystems (Darmstadt, Germany)
T4 DNA ligase	NEB (Frankfurt am Main, Germany)
<i>Taq</i> DNA Polymerase	Invitrogen (Karlsruhe, Germany)
Quick Change Site-directed Mutagenesis Kit	Stratagene (La Jolla, CA, USA)
Quick ligation Kit	NEB (Frankfurt am Main, Germany)

## **8.5 Primers**

**Table 8. Oligonucleotide primers for cloning**

Sequences shown in bold and italics indicate the restriction sites that were used for cloning of the amplified PCR product into an expression vector bearing either a HA or Flag-tag (Ben2-HA, Ben2-Flag). Each forward primer (for) contains an *EcoRV* site, the reverse primer (rev) a *NotI* site, respectively. Primer binding sites refer to Genbank accession numbers NM\_020746 (human IPS-1) and AF038963 (human RIG-I).

Name	Position	Accession number	Sequence
<b>scIPS-1_for</b>	1 – 24 bp	NM_020746	5' – CTA <b>GAT ATC</b> ATG CCG TTT GCT GAA GAC AAG ACC – 3'
<b>scIPS-1_rev</b>	2589 – 2600 bp	NM_020746	5' – TAT AAA <b>GCG GCC GCT</b> CAT GCC CTC AG – 3'
<b>scRIG-I (AA 802-925)_for</b>	2561 – 2581 bp	AF038963	5' – GGG CTA TTT <b>GAT ATC</b> GAT AAG GAA AAT AAA AAA CTG – 3'
<b>scRIG-I (AA 802-925)_rev</b>	2919 – 2935 bp	AF038963	5' – AAA <b>GCG GCC GCT</b> CAT TTG GAC ATT TCT G – 3'
<b>scRIG-I short form_for</b>	621 – 643 bp	AF038963	5' – GGT ATG <b>ATA TCT</b> TGG TGG AAT GCC TTC TCA GAT C – 3'
<b>scRIG-I short form_rev</b>	2919 – 2935 bp	AF038963	5' – AAA <b>GCG GCC GCT</b> CAT TTG GAC ATT TCT – 3'

Table 9. *Oligonucleotide primers for analytical PCR and sequencing*

Name	Application	Sequence
<b>MycA</b>	Mycoplasma PCR	5' - GGC GAA TGG GTG AGT AAC ACG - 3'
<b>MycB</b>		5' - CGG ATA ACG CTT GCG ACC TAT G - 3'
<b>Seq_RIG-I_for</b>	Sequencing of RIG-I mutants	5' - ATT GAC TGG ACG TGG CAA AA - 3'
<b>Seq_RIG-I_rev</b>		5' - GGA CAT TTC TGC TGG ATC AAA TG - 3'
<b>Seq_MDA5_for</b>	Sequencing of MDA5 mutants	5' - TAC GTC CTG GTT GCT CAC AGT GG - 3'
<b>Seq_MDA5_rev</b>		5' - CTC ATC ACT AAA TAA ACA GCA TTC TGA ATA G - 3'
<b>M13R2</b>	Sequencing of newly generated expression plasmids (Ben2 vector backbone)	5' - GGA AAC AGC TAT GAC CAT G - 3'
<b>T7</b>		5' - TAA TAC GAC TCA CTA TAG GG - 3'

**Table 10. Oligonucleotide primers for generation of PCR products comprising the leader RNA of VSV**

pVSV-GFP encodes the full-length antigenomic VSV RNA under control of a T7 promoter and was used to generate a PCR product which in turn can be used as template for *in vitro* transcription to generate VSV specific 5'-triphosphate RNA. To make sure that suitable templates for *in vitro* transcription are obtained, PCR was performed using a T7 promoter specific forward primer in combination with four different reverse primers designated as VSV-R1 to VSV-R4.

Name	Sequence
<b>T7Prom_for</b>	5' - TAA TAC GAC TCA CTA TAG GGA GAA CGA AG - 3'
<b>VSV-R1</b>	5' - TAA CAG ACA TTT TGA TTA CTG TTG ATT ACT GT - 3'
<b>VSV-R2</b>	5' - CAA TGA TTC TCT TGA CTG TAA CAG ACA T - 3'
<b>VSV-R3</b>	5' - GAT TAC TGT TGA TTA CTG TTA AAG TTT CTC - 3'
<b>VSV-R4</b>	5' - GTT GAT TAC TGT TAA AGT TTC TCC TGA GCC - 3'

**Table 11. Oligonucleotide primers for site-directed mutagenesis of the conserved RIG-I cysteines into arginine (C→R)**

Underlined sequences indicate the mutation of cysteines (Cys, C) into arginine (Arg, R). Positions of the mutated cysteine residues refer to UniProtKB/Swiss-Prot accession number O95786 (human RIG-I). Mutation of cysteines at AA position 829 and 841 served as control.

RIG-I mutant	Position of mutation	Sequence
<b>C810R</b>	for	5' - GTC CCT GAT AAG GAA AAT AAA AAA CTG CTC <u>CGC</u> AGA AAG TGC AAA GCC TTG GC - 3'
	rev	3' - CAG GGA CTA TTC CTT TTA TTT TTT GAC GAG GCG TCT TTC ACG TTT CGG AAC CG - 5'
<b>C813R</b>	for	5' - CTG CTC TGC AGA AAG <u>CGC</u> AAA GCC TTG GCA TGT TAC ACA GCT GAC G - 3'
	rev	3' - GAC GAG ACG TCT TTC <u>GCG</u> TTT CGG AAC CGT ACA ATG TGT CGA CTG C - 5'
<b>C818R</b>	for	5' - GAA AGT GCA AAG CCT TGG <u>CAA</u> GAT ACA CAG CTG ACG TAA GAG TGA TAG AGG - 3'
	rev	3' - CTT TCA CGT TTC GGA ACC <u>GTT</u> CTA TGT GTC GAC TGC ATT CTC ACT ATC TCC - 5'
<b>C864R</b>	for	5' - GAA AAA AGA GCA AAG ATA TTC <u>AGA</u> GCC CGA CAG AAC TGC AGC CAT G - 3'
	rev	3' - CTT TTT TCT CGT TTC TAT AAG <u>TCT</u> CGG GCT GTC TTG ACG TCG GTA C - 5'
<b>C869R</b>	for	5' - CGA CAG AAC <u>CGC</u> AGC CAT GAC TGG GGA ATC CAT GTG - 3'
	rev	3' - GCT GTC TTG <u>GCG</u> TCG GTA CTG ACC CCT TAG GTA CAC - 5'
<b>C829R</b>	for	5' - TGA CGT AAG AGT GAT AGA GGA ACG <u>CCA</u> TTA CAC TGT GCT TGG AG - 3'
	rev	3' - ACT GCA TTC TCA CTA TCT CCT TGC <u>GGT</u> AAT GTG ACA CGA ACC TC - 5'
<b>C841R</b>	for	5' - GCT TTT AAG GAA <u>CGC</u> TTT GTG AGT AGA CCA CAT CCC AAG CCA AAG C - 3'
	rev	3' - CGA AAA TTC CTT <u>GCG</u> AAA CAC TCA TCT GGT GTA GGG TTC GGT TTC G - 5'

**Table 12. Oligonucleotide primers for site-directed mutagenesis of conserved RIG-I cysteines residues into alanine (C→A)**

Underlined sequences indicate the mutation of cysteines (Cys, C) into alanine (Ala, A). Positions of the mutated cysteine residues refer to UniProtKB/Swiss-Prot accession number O95786 (human RIG-I). Mutation of cysteines at AA position 829 and 841 served as control.

RIG-I mutant	Position of mutation	Sequence
<b>C810A</b>	for	5' - GTC CCT GAT AAG GAA AAT AAA AAA CTG CTC <u>GCC AGA</u> AAG TGC AAA GCC TTG GC - 3'
	rev	3' - CAG GGA CTA TTC CTT TTA TTT TTT GAC GAG <u>CGG</u> TCT TTC ACG TTT CGG AAC CG - 5'
<b>C813A</b>	for	5' - CTG CTC TGC AGA AAG <u>GCC AAA</u> GCC TTG GCA TGT TAC ACA GCT GAC G - 3'
	rev	3' - GAC GAG ACG TCT TTC <u>CGG</u> TTT CGG AAC CGA ACA ATG TGT CGA CTG C - 5'
<b>C864A</b>	for	5' - GAA AAA AGA GCA AAG ATA TTC <u>GCA</u> GCC CGA CAG AAC TGC AGC CAT G - 3'
	rev	3' - CTT TTT TCT CGT TTC TAT AAG <u>CGT</u> CGG GCT GTC TTG ACG TCG GTA C - 5'
<b>C869A</b>	for	5' - CGA CAG AAC <u>GCC AGC</u> CAT GAC TGG GGA ATC CAT GTG - 3'
	rev	3' - GCT GTC TTG <u>CGG</u> TCG GTA CTG ACC CCT TAG GTA CAC - 5'
<b>C829A</b>	for	5' - TGA CGT AAG AGT GAT AGA GGA <u>AGC CCA</u> TTA CAC TGT GCT TGG AG - 3'
	rev	3' - ACT GCA TTC TCA CTA TCT CCT TCG <u>GGT</u> AAT GTG ACA CGA ACC TC - 5'
<b>C841A</b>	for	5' - GCT TTT AAG GAA <u>GCC</u> TTT GTG AGT AGA CCA CAT CCC AAG CCA AAG C - 3'
	rev	3' - CGA AAA TTC CTT <u>CGG</u> AAA CAC TCA TCT GGT GTA GGG TTC GGT TTC G - 5'

**Table 13. Oligonucleotide primers for site-directed mutagenesis of the triphosphate-binding groove in the CTD of RIG-I**

Underlined sequences indicate the mutation of AA residues, involved in formation of the triphosphate-binding groove, to either alanine (A) or glutamate (E). AA positions of the mutations refer to UniProtKB/Swiss-Prot accession number O95786 (human RIG-I).

RIG-I mutant	Position of mutation	Sequence
<b>H830A</b>	AA 830	for 5' - GTA AGA GTG ATA GAG GAA TGC <u>GCT</u> TAC ACT GTG CTT GGA GAT G - 3'
		rev 3' - CAT TCT CAC TAT CTC CTT ACG <u>CGA</u> ATG TGA CAC GAA CCT CTA C - 5'
<b>H830E</b>	AA 830	for 5' - GTA AGA GTG ATA GAG GAA TGC <u>GAA</u> TAC ACT GTG CTT GGA GAT G - 3'
		rev 3' - CAT TCT CAC TAT CTC CTT ACG <u>CTT</u> ATG TGA CAC GAA CCT CTA C - 5'
<b>K858A</b>	AA 858	for 5' - GCA GTT TTC AAG TTT TGA <u>AGC</u> AAG AGC AAA GAT ATT CTG TG - 3'
		rev 3' - CGT CAA AAG TTC AAA ACT TCG TTC TCG TTT CTA TAA GAC AC - 5'
<b>K858E</b>	AA 858	for 5' - GCA GTT TTC AAG TTT TGA <u>AGA</u> AAG AGC AAA GAT ATT CTG TG - 3'
		rev 3' - CGT CAA AAG TTC AAA ACT <u>TCT</u> TTC TCG TTT CTA TAA GAC AC - 5'
<b>K888A</b>	AA 888	for 5' - CAT TTG AGA TTC CAG TTA TAG <u>CAA</u> TTG AAA GTT TTG TGG TGG - 3'
		rev 3' - GTA AAC TCT AAG GTC AAT ATC <u>GTT</u> AAC TTT CAA AAC ACC ACC - 3'
<b>K888E</b>	AA 888	for 5' - CAT TTG AGA TTC CAG TTA TAG <u>AAA</u> TTG AAA GTT TTG TGG TGG - 3'
		rev 3' - GTA AAC TCT AAG GTC AAT ATC <u>TTT</u> AAC TTT CAA AAC ACC ACC - 5'

**Table 14. Oligonucleotide primers for site-directed mutagenesis of conserved cysteines residues in MDA5 (C→R)**

Underlined sequences indicate the mutation of the conserved cysteines (Cys, C) to arginine (Arg, R). AA positions of the mutations refer to UniProtKB/Swiss-Prot accession number Q9BYX4 (human MDA5). To generate mutant MDA5 in which all cysteine residues are changed to arginine, cysteine residues that are located at AA 907, 910 and 915 were mutated in a first round of mutagenesis to generate MDA5 Cys1-3R, which was then used as template for a second round of mutagenesis together with primer Cys4-5R.

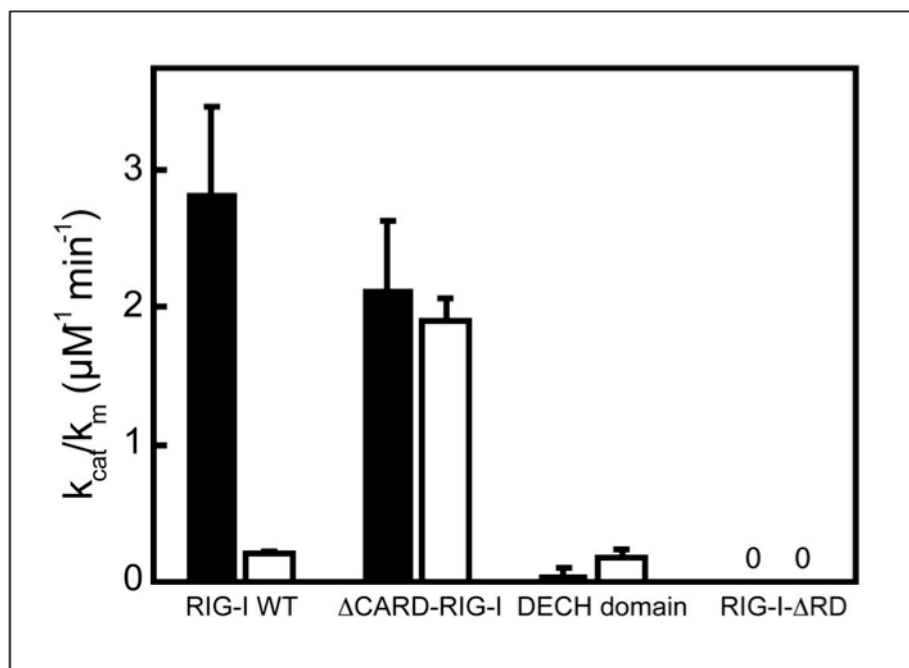
MDA5 mutant	Position of mutation	Sequence
<b>Cys1-3R</b>	AA 907, 910, 915	for 5' - CCC ATC ACT AAT AAC TTT CCT TCG CAA AAA CCG CAG TGT GCT AGC CAG ATC TGG GGA AGA TAT CC -3'
		rev 3' - GGG TAG TGA TTA TTG AAA GGA AGC GTT TTT GGC GAC ACA CGA TCG GTC TAG ACC CCT TCT ATA GG - 5'
<b>Cys4-5R</b>	AA 962, 964	for 5' - GGT GAA ATC ATC CGC AAA AGA GGC CAG GCT TGG GGA ACA ATG ATG G - 3'
		rev 3' - CCA CTT TAG TAG GCG TTT TCT CCG GTC CGA ACC CCT TGT TAC TAC C - 5'

Table 15. Oligonucleotide primers for quantitative real time PCR

Name	Accession number (product size) Reference	Sequence
<b>Cyclophilin A_for</b>	NM_004644.1 (100 bp)	5' - ATG GTC AAC CCC ACCGTG T - 3'
<b>Cyclophilin A_rev</b>		5' - TTC TGC TGT CTT TGG AAC TTT GTC - 3'
<b>IFN-<math>\beta</math>_for</b>	NM_010510.1 (99 bp)	5' - AGC CCT CTC CAT CAA CTA TAA G - 3'
<b>IFN-<math>\beta</math>_rev</b>		5' - GAG GTT GAT CTT TCC ATT CAG - 3'
<b>IFI204_for</b>	NM_00839.2 (81 bp) (Doyle <i>et al.</i> , 2002)	5' - TTG GCT GCA ATG GGT TCA T - 3'
<b>IFI204_rev</b>		5' - AGT GGG ATA TTC ATT GGT TCG C - 3'
<b>ISG15_for</b>	U58202.1 (82 bp) (Doyle <i>et al.</i> , 2002)	5' - CAG GAC GGT CTT ACC CTT TCC - 3'
<b>ISG15_rev</b>		5' - CAG GAC GGT CTT ACC CTT TCC - 3'
<b>RIG-I_for</b>	NM_172689.3 (250 bp) (Rothenfusser <i>et al.</i> , 2005)	5' - AGA GAA TTC GGC ACC CAG AA - 3'
<b>RIG-I_rev</b>		5' - AGC TCT CGC TCG GTC TCA TC - 3'

## **8.6 Supplemental figures**

These figures provide additional information on data obtained by our collaborators Sheng Cui and Karl-Peter Hopfner throughout this study, which were used in the discussion section to complete the overall picture on the function of the newly identified C-terminal domain of RIG-I. All figures are part of the article by Sheng Cui and myself (Molecular Cell, 2008) „The C-terminal regulatory domain is the RNA 5'-triphosphate sensor of RIG-I“, which was prepared from this study. The reproduction of these figures in this thesis is in agreement with Sheng Cui and Karl-Peter Hopfner.



**Figure 29.** *Biochemical analysis of RIG-I variants*

Catalytic efficiency ( $k_{\text{cat}}/K_m$ ) of RIG-I WT and  $\Delta\text{CARD-RIG-I}$ , RIG-I- $\Delta\text{RD}$  (lacking the regulatory domain) and the DECH domain (helicase domain) for 5'-triphosphate RNA (black bars) and nonphosphorylated RNA (white bars). Error bars represent standard errors of the nonlinear regression analysis. For determination of the  $k_{\text{cat}}$  (catalytic constant, turnover number) and the  $K_m$  (Michaelis-Menten kinetics) values please see (Cui *et al.*, 2008).

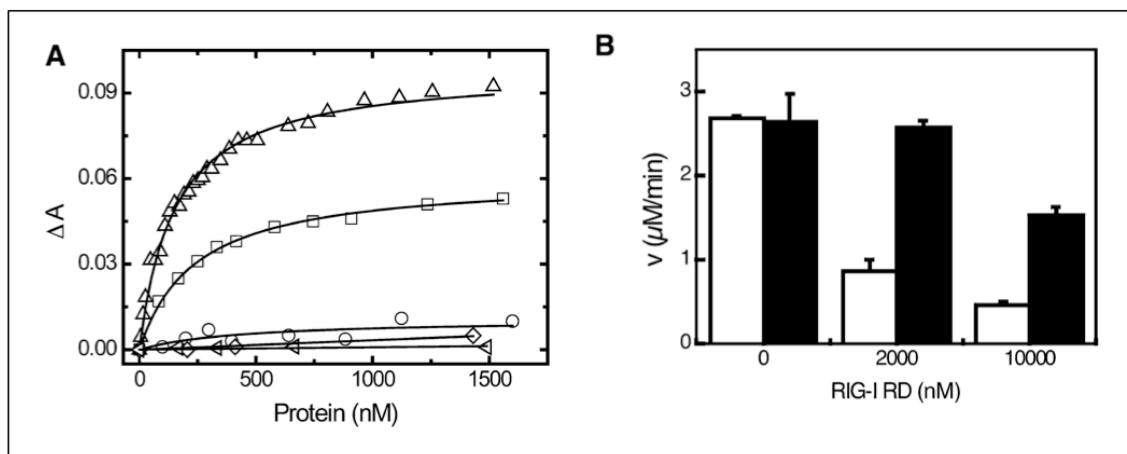


**Figure 30.** *The RIG-I regulatory domain (RD) binds RNA 5'-triphosphates*

(A) Fluorescence anisotropy changes ( $\Delta A$ ) measured by titrating RIG-I WT ( $\Delta$ ) or RD ( $\square$ ) into a solution containing fluorescently labeled 5'-triphosphate RNA. Nonlinear regression against single site binding isotherms (solid lines) reveals dissociation constants of  $151 \pm 8$  nM for RIG-I WT and  $217 \pm 11$  nM for the RD. Titration of RD into dephosphorylated RNA ( $\circ$ ) or dsRNA ( $\triangleleft$ ) did not result in significant changes in the anisotropy, suggesting that the 5'-triphosphate confers much of the binding affinity of 5'-triphosphate RNA to the RD. The RD of MDA5 ( $\diamond$ ) also did not result in anisotropy changes for 5'-triphosphate RNA.

(B) Dose-dependent inhibition of ATPase activity of 20 nM  $\Delta$ CARD-RIG-I by adding indicated amounts of RD in the presence of 200 nM 5'-triphosphate RNA (white bars) or 200 nM dsRNA (black bars). Data represent mean and SD of three independent measurements.

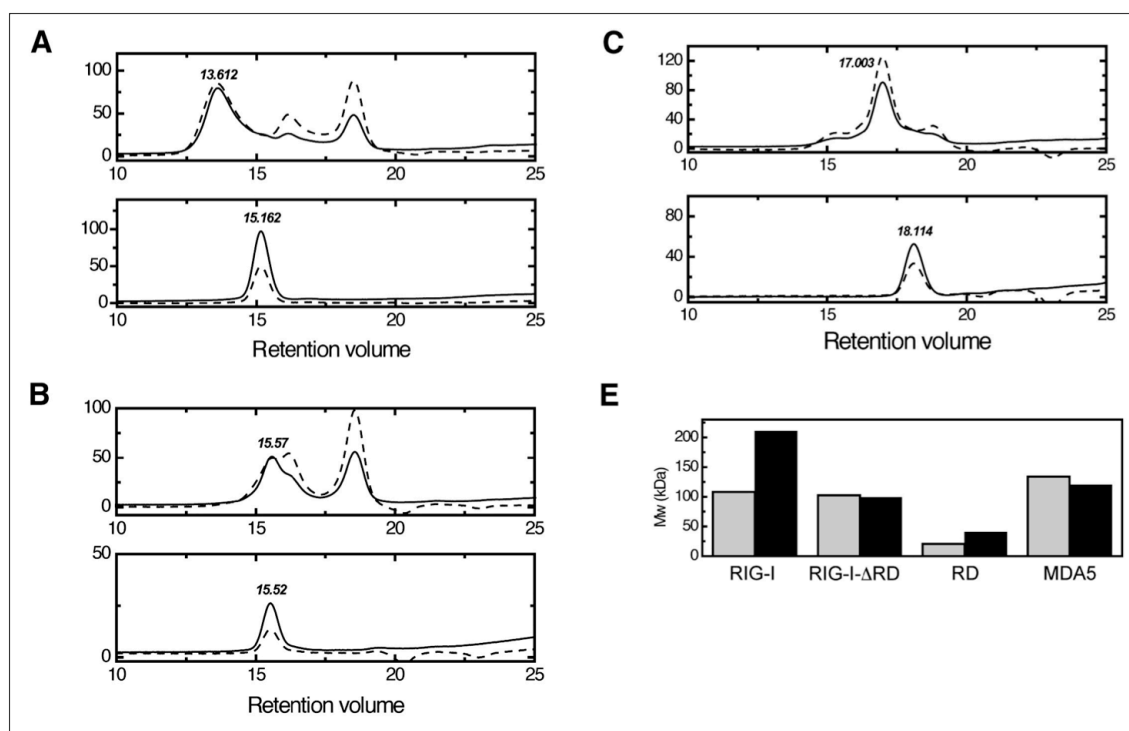


**Figure 31.** *The regulatory domain promotes 5'-triphosphate RNA-dependent RIG-I dimerization*

Gel filtration of 5'-triphosphate RNA-dependent dimerization of RIG-I (A), RIG-I- $\Delta$ RD (B) and RD (C) in the presence (upper panels) and absence (lower panels) of 5'-triphosphate RNA. Plotted are UV absorption profiles (260 nm, dashed lines; 280 nm, solid lines). The retention volume maxima of the proteins (verified by gel electrophoresis) are indicated. Additional peaks with increased 260 nm over 280 nm absorption stem from free RNA. The molecular weight of the protein fractions was analyzed by light scattering (E). RIG-I and RD form dimers in the presence of 5'-triphosphate RNA, while RIG-I- $\Delta$ RD and MDA5 are still monomeric.

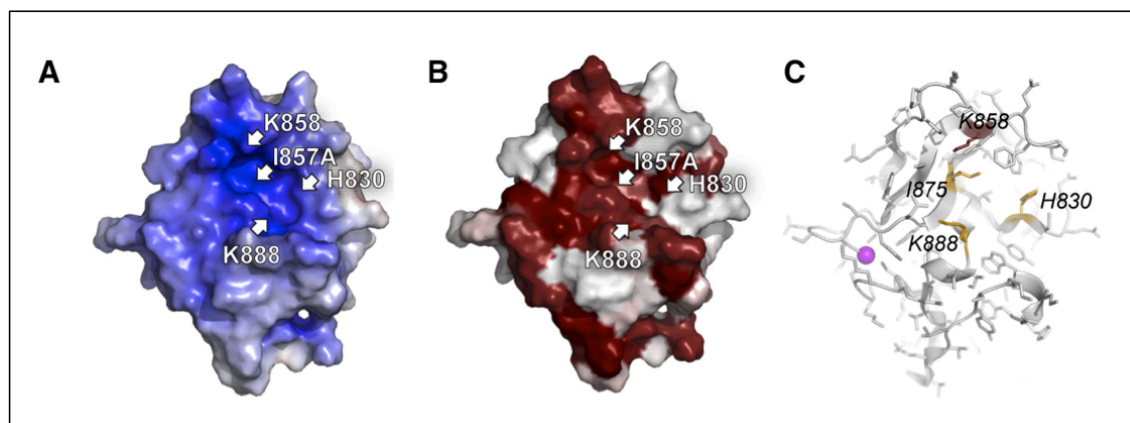


**Figure 32.** *Localization of the RNA 5'-triphosphate-binding site on the RIG-I CTD*  
(A) Electrostatic surface potential. Dark blue indicates a highly positively charged region.  
(B) Surface conservation of RIG-I RD ranging from dark red (invariant) to white (unconserved). A patch of high sequence conservation colocalizes with the positively charged groove (A).  
(C) Localization of the mutations, shown in a ribbon model with added side chains. The magenta sphere indicates the zinc-coordination site.

## ACKNOWLEDGEMENT

First of all I would like to thank Dr. Anne Krug for giving me the opportunity to carry out my PhD thesis in her laboratory. In particular, I am thankful for her confidence in my scientific skills, even at the very beginning of the project, as well as her belief that I will be able to newly establish all the molecular biology techniques required for this project in the lab. I am grateful for the stimulating discussions, for initiating interesting collaborations and the possibility to work so independently.

I want to thank Prof. Michael Schemann for external supervision of my PhD thesis and Prof. Hannelore Daniel for chairing the thesis committee.

Many thanks go to Dr. Wolfgang Reindl for all the discussions, his mental support in times when the experiments were disappointing and last but not least for his friendship. I further want to thank Laurence Reindl and her family for their support.

I want to thank Sheng Cui and Prof. Karl-Peter Hopfner for the fruitful collaboration on the structure and function of RIG-I. Many thanks also go to Simon Rothenfusser, Frank Schmitz, Hendrik Poeck and Zsolt Ruzsics for providing material, technical assistance and helpful discussions.

Wibke, Christian, Annika, Daniela, Jakob, Yvonne, Andreas and Alex: thank you for all the fun we had in the lab.

And this is for you Krishna, my dearest friend. The time we spent in Nepal together was the best I could ever imagine. I am deeply grateful for showing me how to see the world through different eyes.

Alex, when you entered the lab, we soon became friends, now you are the most important part of my life.

Last Last but not least I want to thank my family for their continuous support and patience, their persistent interest and confidence. Ich weiss, Ihr wollt das nicht hören, weil diese Dinge selbstverständlich für Euch sind, aber trotzdem DANKE, für alles!

